WHY DOES IRON OVERLOAD ASSOCIATED WITH INSULIN RESISTANCE OCCUR?

Thesis submitted to

THE TAMIL NADU DR. M.G.R. MEDICAL UNIVERSITY

CHENNAI

for the degree of

DOCTOR OF PHILOSOPHY

By

JOE VARGHESE

DEPARTMENT OF BIOCHEMISTRY

CHRISTIAN MEDICAL COLLEGE

VELLORE – 632002, INDIA

DECEMBER 2017

TABLE OF CONTENTS **Page no.**

1. Introduction …….. 4
2. Aims and objectives ……. 9
3. Review of literature …….. 10
   3.1. Review of current understanding of systemic iron homeostasis …… 10
   3.2. Hepcidin, the central regulator of iron homeostasis …….. 18
   3.3. Insulin, the central regulator of energy homeostasis ……. 29
   3.4. Diabetes mellitus …… 41
   3.5. Role of insulin resistance in the pathogenesis of type 2 diabetes mellitus …… 47
   3.6. Role of beta cell dysfunction in the pathogenesis of type 2 diabetes mellitus ….. 53
   3.7. Role of iron in the pathogenesis of type 2 diabetes mellitus ……. 55
4. Scope and plan of work …… 66
5. Materials and methods ……. 69
   5.1. Equipment used ……. 69
   5.2. Materials ……... 70
   5.3. Methodology ……. 72
      Study 1 …… 78
      Study 2 …… 126
      Study 3 …… 192
      Study 4 …… 245
6. Results and discussion
   6.1. Study 1 ……... 75
      Abstract …… 75
      Introduction ……. 76
      Methodology ……... 78
      Results ……. 92
      Discussion …… 115
      Summary and conclusions …… 121
   6.2. Study 2 …… 122
      Abstract …… 122

Introduction …….. 123
Methodology …… 126
Results …….. 139
Discussion …… 172
Summary and conclusions …… 185
6.3. Study 3 …… 187
Abstract …… 187
Introduction …….. 188
Methodology …… 192
Results …….. 207
Discussion …… 234
Summary and conclusions …… 240
6.4. Study 4 …… 241
Abstract …… 241
Introduction …….. 242
Methodology …… 245
Results …….. 253
Discussion …… 273
Summary and conclusions …… 279
7. Summary of results ……. 280
8. Conclusions …… 284
9. Recommendations and future directions ……286
10. Bibliography ……... 288
11. Appendix
Appendix I: MIQE checklist …… 323
Appendix II: qPCR validation data …….. 327
Appendix III and IV: Composition of control diet and high-fat diet…… 330
Appendix V and VI: Patient information sheet and consent form (English) …….. 332
Appendix VII and VIII: Patient information sheet and consent form (Tamil) …… 334
12. Publications ……338

1. INTRODUCTION

Diabetes mellitus is one of the most prevalent non-communicable diseases in India and the world over. It is estimated that there are over 60 million diabetics in India and this number is expected to increase significantly over the next few decades (1).

Insulin resistance (IR) is the hallmark of type 2 diabetes mellitus (T2DM), which is the most common type of diabetes. The pathogenesis of IR is complex and multi-factorial. A number of risk factors, including obesity and genetic predisposition, have been shown to be associated with IR. However, the molecular mechanisms involved have not been fully elucidated (2).

Iron is a transition metal and an essential micronutrient. It is required for the synthesis of hemoglobin and is therefore essential for erythropoiesis. Approximately 25 mg of iron is required every day for normal erythropoiesis in the bone marrow. More than 95% of this is provided by the recycling of iron derived from senescent erythrocytes. The macrophages that form the reticuloendothelial system, especially in the spleen, play a major role in this process. The rest of the daily iron requirement is derived from absorption of dietary iron, which occurs in the duodenum. Duodenal absorption of iron is a highly regulated process. Any increase in iron absorption in excess of the requirement results in iron overload, as the body has no physiologically regulated mechanisms to excrete iron. Such iron overload has been shown to be associated with tissue damage seen in conditions like hereditary hemochromatosis and thalassemia (3).

A large number of epidemiological studies have shown a strong association between serum ferritin levels, an indicator of body iron stores, and IR. For example, the National Health and

Nutrition Education Survey (NHANES) done among 9486 adults in USA, showed that the odds ratio for newly developed T2DM was 4.94 in males and 3.61 in females who had serum ferritin that exceeded 300 µg/L (4). This and a number of other studies have shown that this association remains strong even after adjusting for age, sex, race, body mass index (BMI), smoking and C-reactive protein (CRP) levels (5–9). In addition, the "normal" range of serum ferritin (15-300 µg/L in males and 15-200 µg/L in females) is quite wide and values at either end of this range may be associated with health risks that currently remain unknown (10).

Although a strong association exists between increased body iron stores and T2DM, the molecular interactions between processes involved in iron homeostasis and insulin sensitivity are not known. There is some evidence that supports the view that iron overload may play a causal role in the pathogenesis of diabetes mellitus. For example, the incidence of diabetes is higher is conditions characterized by iron overload, viz. hereditary hemochromatosis (11) and thalassemia (12,13). Decreasing body iron stores, by iron chelation or phlebotomy in these conditions, tends to improve insulin sensitivity (14–16). These findings are supported by results from research using animal models of T2DM, where dietary iron overload was associated with insulin resistance (17) and iron restriction/phlebotomy was associated with improved insulin sensitivity (18,19).

Insulin acts by binding to its cell surface receptor and triggering multiple intracellular signaling cascades. The phosphorylation and activation of Akt is a key event in this pathway (20). Activated Akt phosphorylates several downstream targets, which mediate the effects of insulin on metabolism, cell growth and proliferation (21). Although iron overload is thought to be

associated with insulin resistance, very little is known about the effects of increased intracellular iron on the insulin signaling pathway.

The mechanism(s) by which iron accumulates in the body in diabetes is not known. It has been hypothesized that inappropriately low levels of hepcidin, the chief regulator of systemic iron homeostasis, may play a key role in mediating increased iron stores in T2DM (22). Hepcidin is a small-molecular-weight peptide (25 amino acids) secreted mainly by hepatocytes (23). It binds to ferroportin (the only known transporter in mammalian cells that exports iron) and triggers its internalization and degradation (24). Since ferroportin is expressed on the basolateral surface of enterocytes and also on macrophages, hepcidin decreases duodenal iron absorption and also inhibits iron recycling by macrophages.

Studies on hepcidin in patients with T2DM have reported variable findings, with some studies showing increased serum hepcidin levels in diabetics (25,26), while others show decreased levels (27–29); still others show no significant differences (30). The reasons for these varying reports are unclear. A number of factors regulate hepatic hepcidin synthesis. It is known that hepcidin expression is induced in response to increased liver iron levels, increased transferrin saturation and inflammatory mediators such as interleukin-6 (IL-6). On the other hand, hepcidin expression is decreased in response to iron-deficiency anemia, hypoxia and erythropoiesis (31). The effects of IR *per se* on hepatic hepcidin expression and on factors that regulate it are not known.

Among the factors that regulate hepatic hepcidin expression, inhibitory signals from the bone marrow, mediated by certain regulators secreted by erythroid precursors ("erythroid regulators of hepcidin"), play a very important role (32). Although the identity of these erythroid regulators is not clearly known, growth differentiation factor 15 (GDF15) (33), twisted gastrulation factor

(TWSG1) (34) and erythroferrone (ERFE) (35) have been proposed to be potential candidates. It is known that T2DM is associated with hyperinsulinemia and that insulin is a growth factor for erythropoiesis (36–38). However, the effects of insulin resistance on erythropoiesis or on the expression of GDF15, TWSG1 and ERFE in erythroid precursors are not clearly known.

In summary, a number of epidemiological studies have shown that raised serum ferritin, a marker of body iron stores, is associated with insulin resistance. There is evidence to suggest that iron overload may play a causal role in the pathogenesis of insulin resistance, although the molecular mechanisms are not known. Dysregulation of hepcidin (the chief regulator of systemic iron homeostasis) has been reported in some studies on patients with diabetes. However, there is very little information available on the effects of insulin resistance on factors that regulate hepcidin expression, especially the erythroid regulators. Several critical questions remain unanswered: Is iron-overload a cause or a consequence of IR? Does increased intracellular iron impair insulin signaling? What are the effects of IR on regulation of hepatic hepcidin expression? Do these changes affect expression levels of proteins involved in iron homeostasis? The studies carried out and described in this thesis attempt to answer these questions.

HYPOTHESIS OF THE PROPOSED STUDY

Increased intracellular iron levels may impair insulin signaling in hepatocytes, thus contributing to insulin resistance (IR) in these cells. Insulin resistance may affect expression of hepcidin and other iron-related proteins in the liver, resulting in dysregulation of systemic iron homeostasis. One of the ways in which IR may affect hepatic hepcidin expression may be through its effects on erythropoiesis. This may result in suppression of hepatic hepcidin expression (via up-regulation of the erythroid regulators of hepcidin in the bone marrow) and increased intestinal iron absorption, leading to iron overload. Iron accumulation within cells may further exacerbate insulin resistance, thus constituting a vicious cycle.

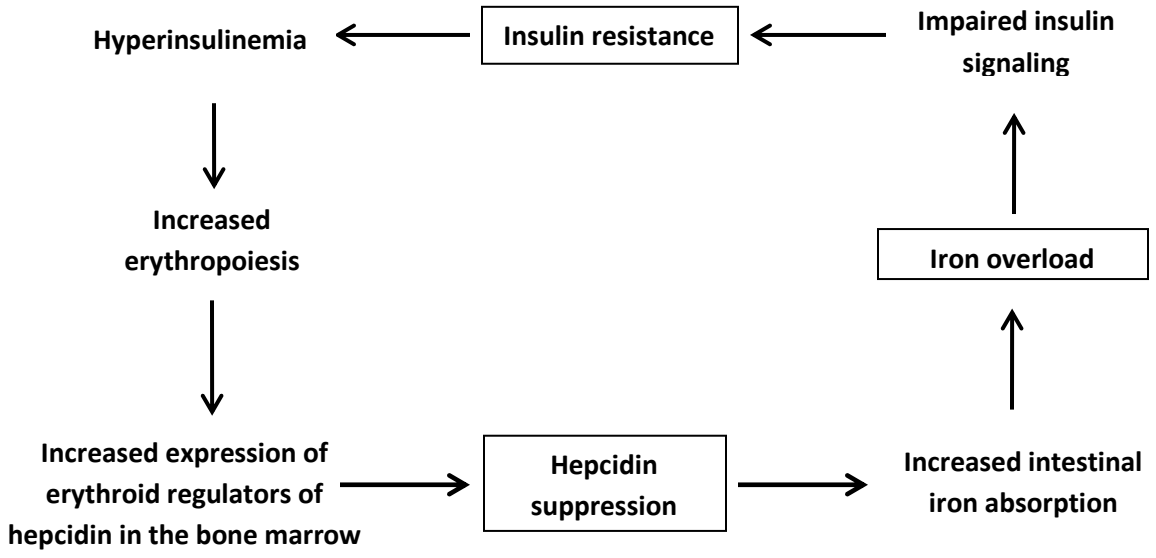

2. AIMS AND OBJECTIVES

The overall aim of this study was to systematically investigate the interactions between iron and insulin at the molecular level, and to elucidate possible mechanisms by which events involved in iron homeostasis and insulin resistance are linked.

The specific objectives of this study were:

1. To study the effects of iron on insulin signaling in mouse primary hepatocytes *in vitro.*
2. To study the time-course of development of, and interactions between, insulin resistance and alterations in iron metabolism, in a mouse model of type 2 diabetes mellitus (T2DM).
3. To study the effects of insulin resistance on terminal erythroid differentiation in the bone marrow and the expression of putative erythroid regulators of hepcidin, in a mouse model of T2DM.
4. To study links between insulin resistance and iron metabolism in patients newly diagnosed to have diabetes mellitus or pre-diabetes by determining
    a. serum hepcidin levels and markers of iron status in these patients
    b. expression of erythroid regulators of hepcidin in reticulocytes in peripheral blood, isolated from these patients

3. REVIEW OF LITERATURE

Iron is an essential micronutrient that plays multiple roles in the body. As a constituent of heme, it is present is several important proteins, including hemoglobin, myoglobin, cytochrome P450 enzymes and in components of the electron transport chain in the mitochondria. Iron is also part of iron-sulfur clusters, which are critical components of proteins involved in redox reactions, especially in the mitochondrial electron transport chain. In addition, iron acts as a cofactor for several enzymes that play important roles in cellular metabolism (39)

3.1. Review of current understanding of systemic iron homeostasis

On average, an adult has about 3–4 grams of total body iron, which is mainly present in hemoglobin (~2500mg), ferritin (~1000mg) and myoglobin (~300mg). The body guards its iron zealously and there is very little loss of iron, usually less than 1 mg per day in males and slightly more in pre-menstrual females due to menstrual blood loss. This loss is replaced by intestinal absorption of dietary iron. Iron released by breakdown of senescent RBCs in the reticuloendothelial system (chiefly in the spleen), is recycled; about 25 mg of iron is supplied to the bone marrow for erythropoiesis from this source each day. Iron is stored as ferritin in various organs, chiefly the liver. A small amount of iron (3-4 mg) circulates in blood bound to transferrin, which is the iron transport protein (39) (Fig. 3.1).

3.1.1. Duodenal absorption of dietary iron

Since there are no physiological mechanisms for iron excretion from the body, iron entry by absorption of dietary iron, is strictly regulated (32).

Figure 3.1

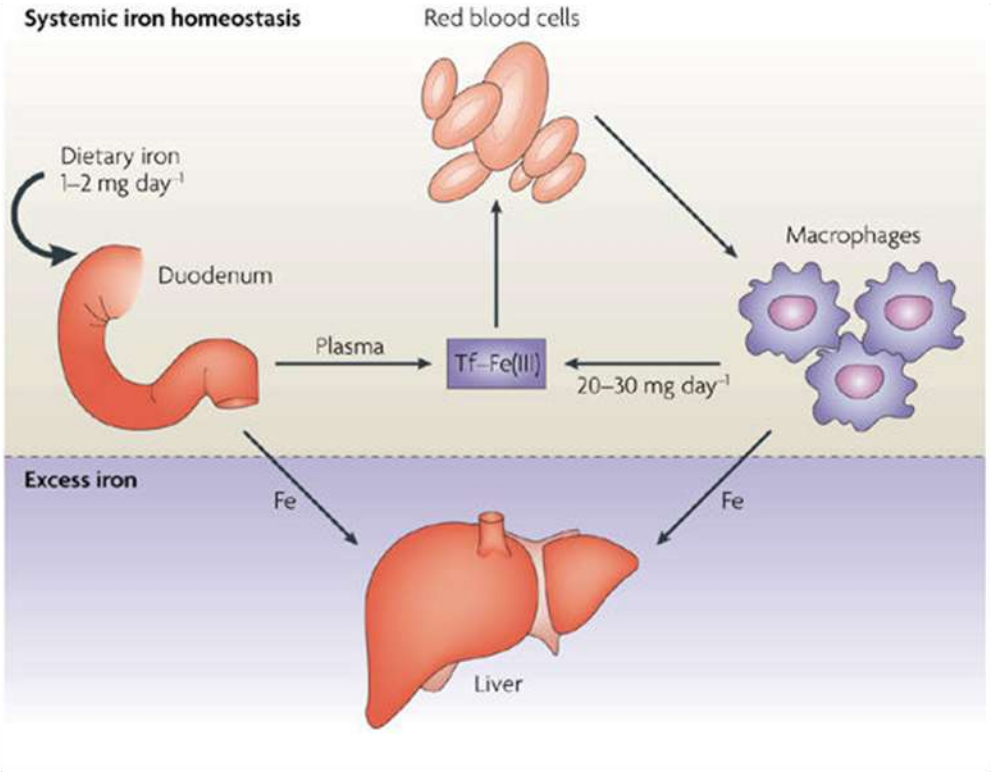

Figure 3.1: General outline of iron metabolism

Iron present in the diet is absorbed in the duodenum and circulates in blood bound to transferrin (Tf). Transferrin-bound iron is taken up by various tissues, especially the erythroid precursor cells in the bone marrow. Senescent RBCs are phagocytosed by macrophages (mainly in the spleen) and iron that is released re-enters the circulation. Excess iron is stored as ferritin in various tissues, especially the liver.

Source of image: De Domenico I, McVey Ward D, Kaplan J. Regulation of iron acquisition and storage: consequences for iron-linked disorders. *Nat Rev Mol Cell Biol*. 2008 Jan;9(1):72-81.

Iron absorption chiefly occurs in the duodenum. The apical membrane of duodenal enterocytes expresses divalent metal transporter 1 (DMT1 or Nramp2), which transports non-heme iron (and other divalent cations to a lesser extent) across the luminal membrane into the enterocyte (40). DMT1 transports iron in its ferrous (Fe^{2+}) form; however, the majority of dietary iron is in the ferric form (Fe^{3+}). A number of factors help in the reduction of ferric iron to its ferrous form. The enterocytes express on its apical membrane several enzymes (called brush-border ferrireductases) that catalyze the conversion of Fe^{3+} to Fe^{2+}. The physiologically most important ferrireducatase is the duodenal cytochrome b (dcytb) (41). In addition, gastric acid and other reducing agents found in food (like ascorbic acid) also aid iron absorption by facilitating reduction of Fe^{3+} to Fe^{2+}. Dietary heme is taken up duodenal enterocytes by independent mechanisms. The intestinal heme transporter has not been definitively identified (42). Once transported into the enterocyte, heme is catabolized by the microsomal enzyme, heme oxygenase, to release iron in the cytosol (43).

Inside the enterocyte, iron can either be stored or transported into circulation across the basolateral membrane. Iron stored as ferritin in the cytosol is lost when enterocytes turnover (every 2-5 days in humans) and is therefore not absorbed into systemic circulation. Iron export from the cell is mediated by ferroportin (or Ireg1) which is the only known cellular iron export protein (44,45). Iron transported into systemic circulation is tightly bound to the plasma protein, transferrin. Transferrin binds iron in its Fe^{3+} form, and this requires a membrane-bound ferroxidase on enterocytes, a copper-containing protein called hephaestin. Hephaestin catalyzes the conversion of Fe^{2+} to Fe^{3+} (46) (Fig. 3.2).

Figure 3.2

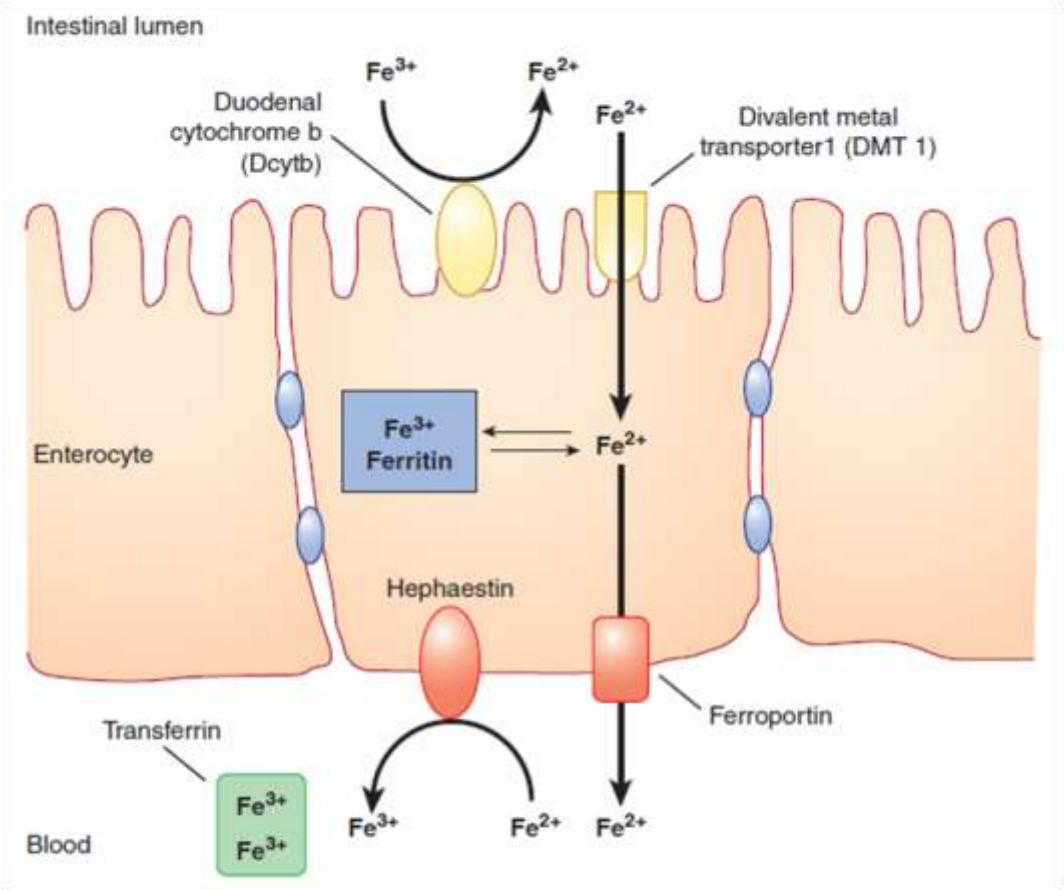

Figure 3.2: Duodenal absorption of non-heme iron

Non-heme iron present in the diet mainly as Fe^{3+} is reduced Fe^{2+} by the ferri-reductase, duodenal cytochrome b (dcytb). Fe^{2+} is transported across the apical membrane by divalent metal transporter-1 (DMT-1). Inside the enterocyte, iron is either stored in the form of ferritin, or transported across the basolateral membrane by ferroportin. Fe^{2+} is oxidized to Fe^{3+} by the ferroxidase, hephaestin. Fe^{3+} is bound to transferrin in blood and transported to various sites in the body.

Source of image: Murray R, Rodwell V, Weil A, Bender D, Botham K. Plasma Proteins and Immunoglobulins. In: Harpers Illustrated Biochemistry, 29th Edition. McGraw Hill Professional; 2012.

3.1.2. Iron transport in the blood

Free iron is toxic due to its ability to catalyze redox reactions, resulting in oxidative damage of tissues. Therefore, iron is transported in blood tightly bound to the protein, transferrin. Transferrin has two high-affinity sites for binding Fe^{3+}. The plasma concentration of transferrin is about 300 mg/dL. This amount of transferrin can potentially bind a total of about 300 µg of iron (per deciliter of plasma) and is referred to as the total iron-binding capacity (TIBC) of blood. However, serum iron levels are normally only about 50-150 µg/dL; this is because, under normal conditions, transferrin is saturated with iron only to an extent of about 25 to 45%. Transferrin saturation (Tfsat) decreases under conditions of iron deficiency (< 15% indicates severe iron deficiency), and increases under conditions of iron overload (>45%) (39).

Most of the iron found in circulation is bound to transferrin. However, a very small amount of iron is also found in circulation loosely complexed with citrate, acetate or albumin. This is referred to as non-transferrin bound iron (NTBI). This form of iron is toxic; its levels increase in plasma when transferrin saturation approaches 75 – 80%. This is seen in conditions of iron overload. Significant tissue damage can occur under these conditions (47).

3.1.3. Cellular uptake of plasma iron

All cells express transferrin receptors (TfR1) on their surface to take up iron from the circulation. Erythroid precursor cells in the bone marrow, which are the largest consumers of iron, show very high expression levels of TfR1. This receptor has a high affinity for holo-transferrin (transferrin to which iron is bound). Once transferrin is bound to TfR1, the complex undergoes internalization, by receptor-mediated endocytosis (Fig. 3.3).

Figure 3.3

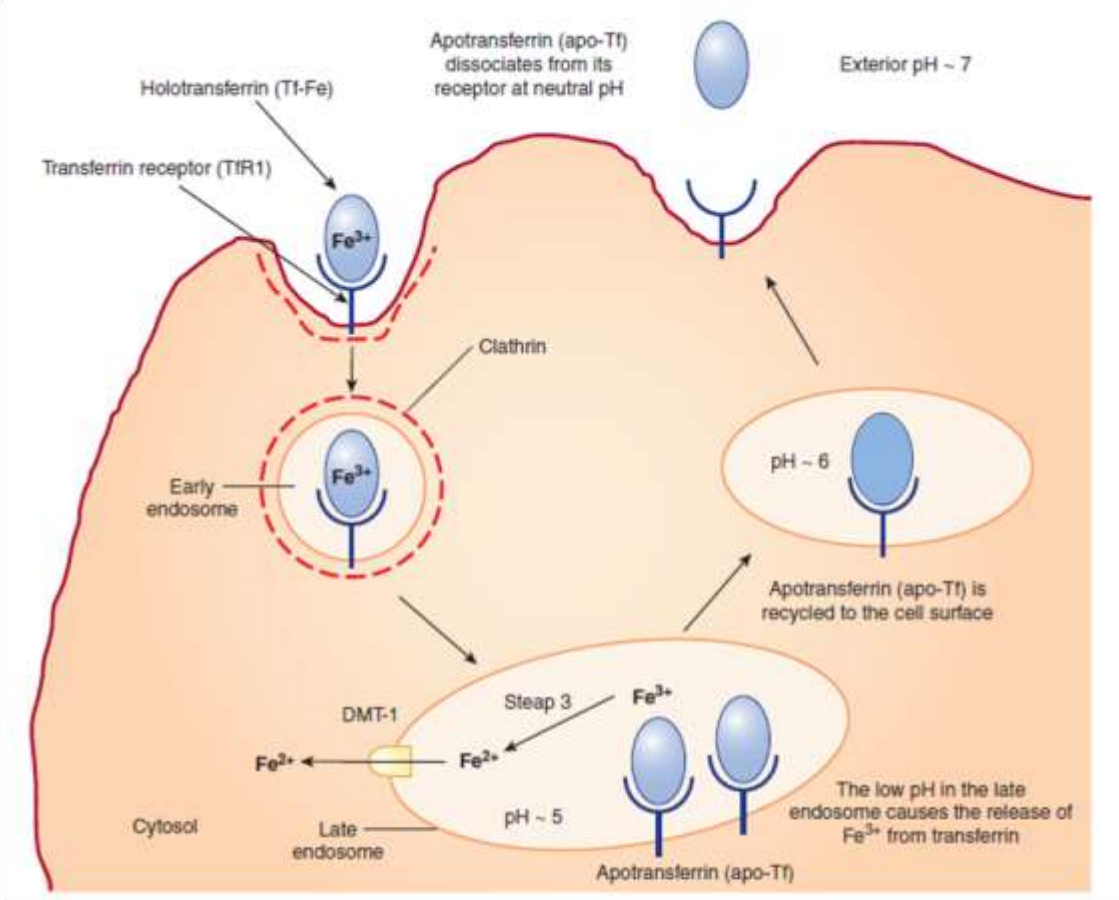

Figure 3.3: The transferrin cycle

Transferrin (Tf) bound to iron (holo-transferrin) binds to its receptor, transferrin receptor 1 (TfR1), present on the cell membrane. The ligand-receptor complex undergoes endocytosis. Iron is released from its binding sites on transferrin in the acidic conditions present in the late endosome. Fe^{3+} is reduced to Fe^{2+} by the ferri-reductase, Steap 3, and transported into the cytosol by DMT-1. The TfR1-Tf complex is recycled back to the cell membrane where Tf is released. (

Source of image: Murray R, Rodwell V, Weil A, Bender D, Botham K. Plasma Proteins and Immunoglobulins. In: Harpers Illustrated Biochemistry, 29th Edition. McGraw Hill Professional; 2012.

Within the acidic environment of the endosome that is formed, iron is released and transported into the cytosol via DMT-1. TfR1 bound to apo-transferrin (transferrin devoid of iron) is recycled back to the cell surface. Apo-transferrin is then released into the circulation, where it becomes available to bind more iron. This process is called the transferrin cycle; it occurs several times a day (39) (Fig. 3.3).

3.1.4. Iron recycling by macrophages

RBCs have an average lifespan of 120 days. Following this, macrophages (especially in the spleen) take up senescent RBCs (erythrophagocytosis) and break them down in order to release heme from hemoglobin. Heme is transported into the cytosol form the endosome by the heme transporter, HRG1 (heme responsive gene – 1) (48). In the cytosol, heme is catabolized by the enzyme, heme oxygenase 1 (HO-1), which releases free iron while converting heme into biliverdin. Iron is either stored within the macrophages as ferritin or transported out via the iron exporter, ferroportin (Fig. 3.4). This iron, which is in its ferrous form, is oxidized to its ferric form by the plasma protein, ceruloplasmin, which has ferroxidase activity. Ferric iron then binds to transferrin and is transported to other cells, chiefly the bone marrow. About 25 mg of iron is recycled each day in this manner (39).

3.1.5. Cellular iron storage

Ferritin is the cytoplasmic iron storage protein; it forms spherical structures consisting of 24 subunits, which can store 3000-4500 ferric atoms in its core. Ferritin is made up of two types of subunits – H (heavy) and L (light).

Figure 3.4

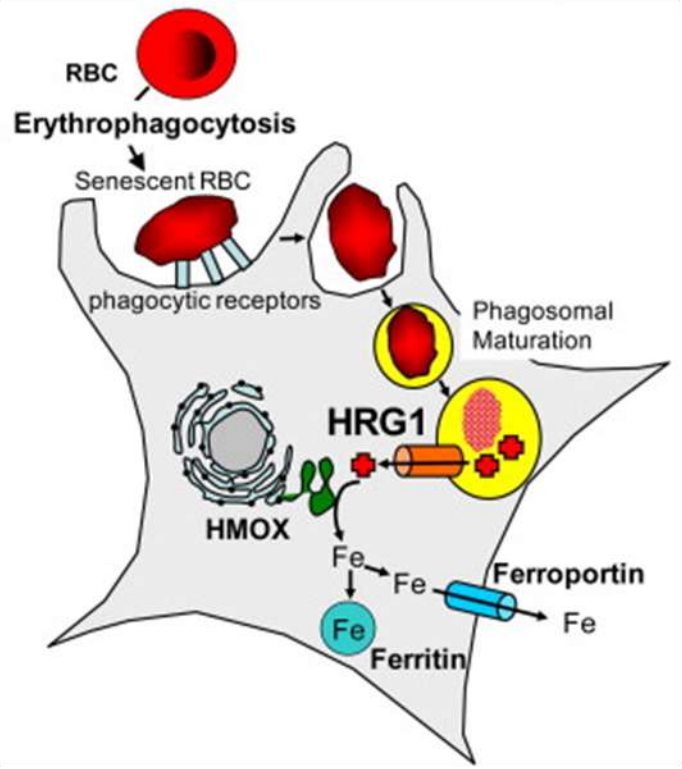

Figure 3.4: Iron recycling by macrophages

Senescent RBCs are phagocytosed by splenic macrophages (erythrophagocytosis) and heme is released from hemoglobin. The heme transporter, HRG1, transports heme from the erythrophagolysosome to the cytosol. Here, heme is degraded by heme oxygenase 1 (HMOX) to release iron. Iron is either stored in the macrophage as ferritin, or transported out of the cell (via ferroportin).

Source of image: White, C., Yuan, X., Schmidt, P.J., Bresciani, E., Samuel, T.K., Campagna, D., et al. 2013. HRG1 is essential for heme transport from the phagolysosome of macrophages during erythrophagocytosis. *Cell metabolism*, 17(2), pp.261-270 (graphical abstract).

The H subunit of ferritin has intrinsic ferroxidase activity that facilitates the uptake of cytosolic Fe into the ferritin core (31). Ferrous iron is made available for storage in ferritin by the cytoplasmic chaperone protein, poly (rC) binding protein – 1 (PCBP-1) (49).

Ferritinophagy, a specialized form of autophagy, is the process by which ferritin is degraded in lysosomes in order to release iron (50). The cargo receptor, nuclear receptor coactivator 4 (NCOA4), plays a key role in mediating the induction of ferritinophagy in response to decreased intracellular iron (51).

A soluble form of ferritin is present in the plasma and is commonly considered a marker of body iron stores. Plasma ferritin is mainly made up of L-ferritin, is poorly glycosylated and contains very little iron. In mice, it has been shown that serum ferritin is derived mainly from macrophages (52). Serum levels of ferritin have also been shown to increase in response to inflammation (53).

3.2. Hepcidin, the central regulator of iron homeostasis

Iron homeostasis is characterized by the coordinated regulation of iron absorption in the duodenum, iron utilization in the bone marrow, iron recycling in the macrophages and iron storage in the liver and spleen. Hepcidin, a peptide synthesized and secreted primarily by the liver, is the chief hormone that regulates iron homeostasis (32). In humans, it is coded by a single gene on chromosome 19. In mice, two genes (*Hamp1* and *Hamp2*) code for hepcidin, however, only *Hamp1* is involved in regulation of hepcidin levels in blood (54). It is synthesized as a preprohormone of 84 amino-acids. It undergoes proteolytic cleavage to remove a 24-amino acid signal sequence to form prohepcidin, which is then cleaved by a furin-like prohormone

convertase to generate a 25-amino acid (2.7 kDa) peptide, which is the mature form of hepcidin (55) (Fig. 3.5). Hepcidin circulates mostly free in plasma with a small proportion (<0.3%) weakly bound to albumin and α_2-macroglobulin (56,57).

3.2.1. Mechanism of action of hepcidin

Hepcidin acts by binding to ferroportin, the only known iron exporter, and inducing its internalization and proteasomal degradation (24). It therefore decreases intestinal iron absorption and also release of iron from macrophages, resulting in hypoferremia. Hepcidin excess (as seen in chronic inflammatory conditions) is characterized by decreased circulating iron levels and resultant anemia; on the other hand, hepcidin deficiency (as seen in hemochromatosis) results in tissue iron overload (32).

The 6 amino acids at the N-terminal of hepcidin are highly conserved; they are critical for its interaction with the extracellular loop of ferroportin (58,59). Alterations, either in the N-terminal sequence of hepcidin or in critical amino acids that constitute the extracellular loop of ferroportin (e.g., C326S in ferroportin), result in disruption of the hepcidin-ferroportin interaction (60–62). Binding of hepcidin to ferroportin results in rapid induction of ubiquitination of critical lysine residues in the intracellular domains of ferroportin, resulting in proteasomal degradation of the protein (63,64). Hepcidin is also known to induce alterations in gene expression of ferroportin and other iron-related proteins, especially in the duodenum (65). However, the mechanisms involved are not clear.

Figure 3.5

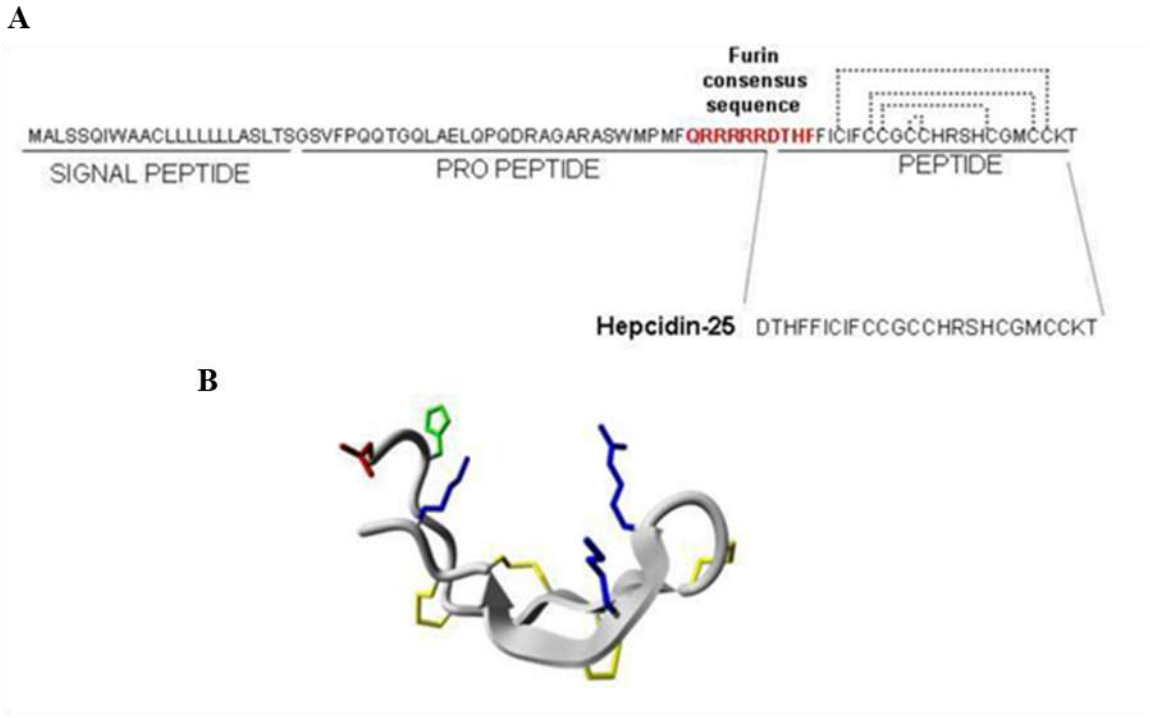

Figure 3.5: Post-translational processing and structure of hepcidin

A: Hepcidin is synthesized as a pre-propeptide (84 amino acids). Removal of the signal sequence results in formation of pro-hepcidin. Pro-hepcidin is then cleaved by a furin-like convertase to form the mature hepcidin (25 amino acids).

B: Hepcidin consists of 2 short beta-strands that are stabilized by 4 inter-strand disulphide bonds.

Source of image: Poli M, Asperti M, Ruzzenenti P, Regoni M, Arosio P. Hepcidin antagonists for potential treatments of disorders with hepcidin excess. *Front Pharmacol*. 2014 Apr 28;5:86.

3.2.2. Regulation of hepcidin

Transcriptional regulation is the only well-established mechanism by which hepcidin is regulated. There are a number of factors that are known to regulate it, with some increasing and others decreasing its expression in the liver (Fig. 3.6). Signaling through the bone morphogenetic protein–SMA/Mothers Against Decapentaplegic (BMP-SMAD) pathway is the predominant transcriptional regulator of hepcidin (Fig. 3.7). BMPs can powerfully induce hepcidin gene expression (66). The hepatic BMP receptor (BMPR) is a heterodimer consisting of type I (Alk2 or Alk3) and type II (ActRIIA) subunits (67,68). Binding of BMPs to its receptor, results in phosphorylation-mediated activation of receptor-regulated SMADs (R-SMADs or SMAD1/5/8). Phosphorylated R-SMADs heterodimerize with co-SMAD (SMAD4); the complex translocates to the nucleus where it binds to BMP-response elements (BMPRE) in the hepcidin promoter (69–71). Although multiple BMPs have been shown to activate hepcidin, in mice the most important *in vivo* regulators of hepcidin are BMP6 (72) and probably BMP2 (73). Hemojuvelin (HJV) is a membrane GPI-anchored BMP co-receptor that is expressed in hepatocytes and skeletal muscle. In the hepatocytes, HJV is essential for BMP-BMPR interactions that regulate hepcidin (74–76).

Matriptase-2, a membrane-associated serine protease (TMPRSS6), regulates hepcidin expression by down-regulating signaling via the BMP-SMAD pathway (77,78). It has been suggested that matriptase-2 acts by cleaving HJV, the BMP co-receptor, thus decreasing BMP-induced hepcidin expression (79). Neogenin is a membrane receptor that is also known to increase hepcidin expression via the BMP-SMAD pathway (80). It has been shown to interact with HJV (81) as well as matriptase-2 (82); however the exact mechanisms and significance of neogenin-mediated hepcidin regulation are not clear.

Figure 3.6

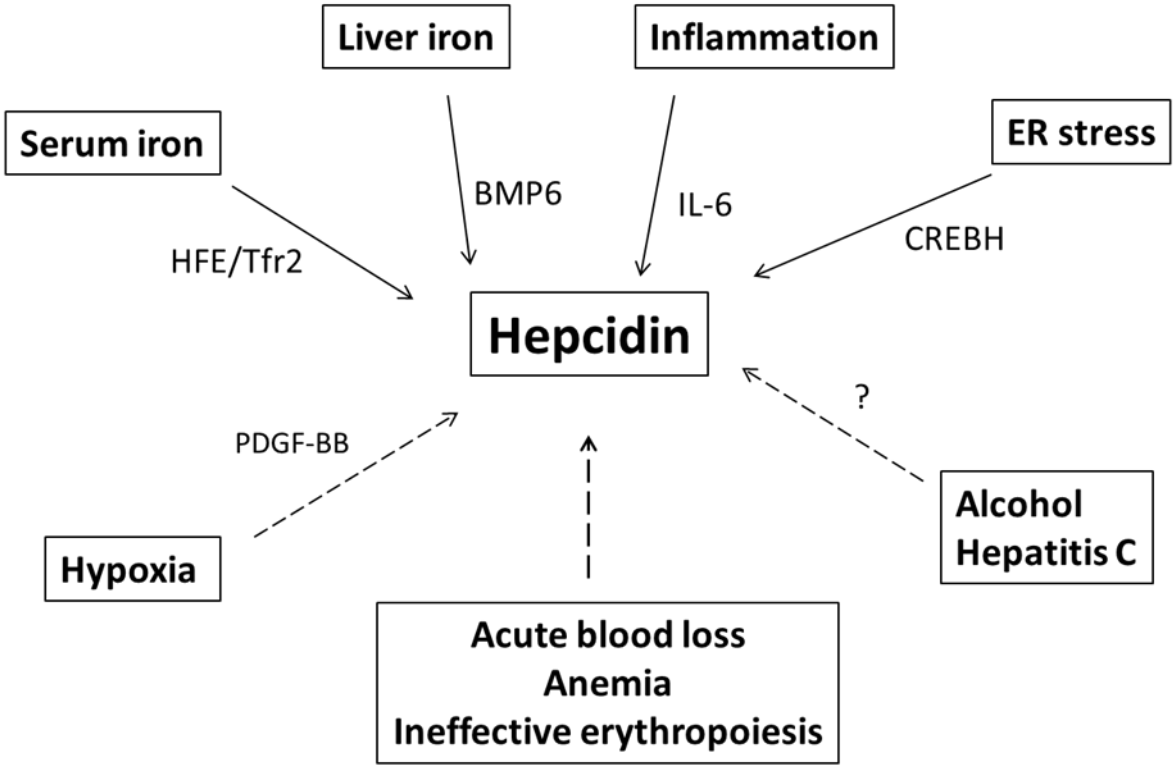

Figure 3.6: Factors that regulate hepcidin

A variety of factors regulate hepcidin. Factors known to increase hepcidin include serum iron, liver iron stores, inflammation and endoplasmic reticulum (ER) stress. On the other hand, hypoxia, anemia, acute blood loss, ineffective erythropoiesis (e.g., thalassemia), chronic alcohol abuse and hepatitis C infection are known to down-regulate hepcidin.

BMP6, bone morphogenetic protein 6; IL-6, interleukin-6; CREBH, cAMP-responsive element-binding protein; HFE, classical hemochromatosis protein; TfR2, transferrin receptor 2; PDGF-BB, platelet-derived growth factor – BB.

Figure 3.7

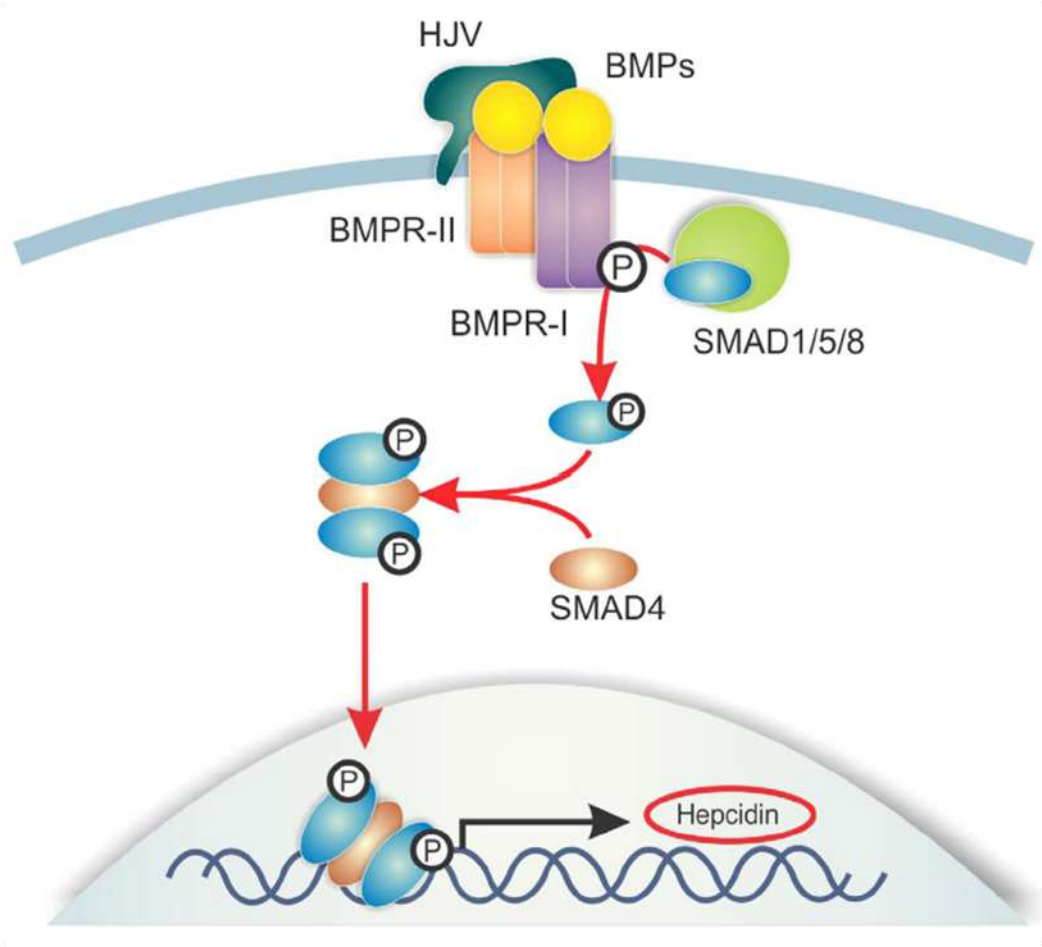

Figure 3.7: BMP-SMAD pathway of hepcidin regulation

The hepatic BMP receptor (BMPR) is a heterodimer consisting of type I and type II subunits. Hemojuvelin (HJV) is a BMP co-receptor. Binding of BMPs to its receptor, results in phosphorylation-mediated activation of receptor-associated SMADs (SMAD1/5/8). Phosphorylated SMAD1/5/8 hetero-dimerize with SMAD4 and translocate to the nucleus where it binds to BMP-response elements in the hepcidin promoter

Source of image: Modified from: Goh JB, Wallace DF, Hong W, Subramaniam VN. Endofin, a novel BMP-SMAD regulator of the iron-regulatory hormone, hepcidin. *Sci Rep*. 2015 Sep 11;5:13986

.

3.2.2.1 Regulation of hepcidin expression by plasma iron levels

Hepcidin expression is regulated by changes in plasma iron levels. Although the mechanisms involved have not been clearly elucidated, it is hypothesized that transferrin receptor 2 (TfR2), the classical hemochromatosis-associated protein (HFE) and HJV may play important roles (83,84). The model that has been proposed, based on current evidence, is shown in Fig. 3.8. On the hepatocyte sinusoidal (basolateral) membrane, holo-transferrin competes with HFE for binding to TfR1 (as they have overlapping binding sties on TfR1) (85). Binding of holo-transferrin to TfR1, results in displacement of HFE from TfR1; free HFE then interacts with holo-transferrin-bound TfR2 on the cell surface. This trigger an intracellular signaling pathway (probably the BMP-SMAD pathway) that induces hepcidin (86,87)

3.2.2.2 Regulation of hepcidin by liver iron stores

Hepatic hepcidin expression is known to be regulated by liver iron stores. It has been shown that liver *Bmp6* mRNA expression in mice is strongly correlated with liver iron stores, as well as with hepcidin expression, suggesting that BMP6 may be the "stores regulator" of hepcidin (88,89). Mice lacking the BMP6 gene (*Bmp6*$^{-/-}$) have very low levels of hepcidin and develop massive iron overload (90). However, the association between BMP6 and liver iron stores has not yet been demonstrated in humans. In addition, the site of BMP6 synthesis in response to iron overload is not clear. It has been shown that *Bmp6* expression increases in response to iron overload in non-parenchymal cells of the liver, but not in the parenchymal cells (91). BMP6 released from liver sinusoidal cells act on the neighboring hepatocytes in a paracrine manner, to increase hepcidin expression via the BMP-SMAD pathway (92).

Figure 3.8

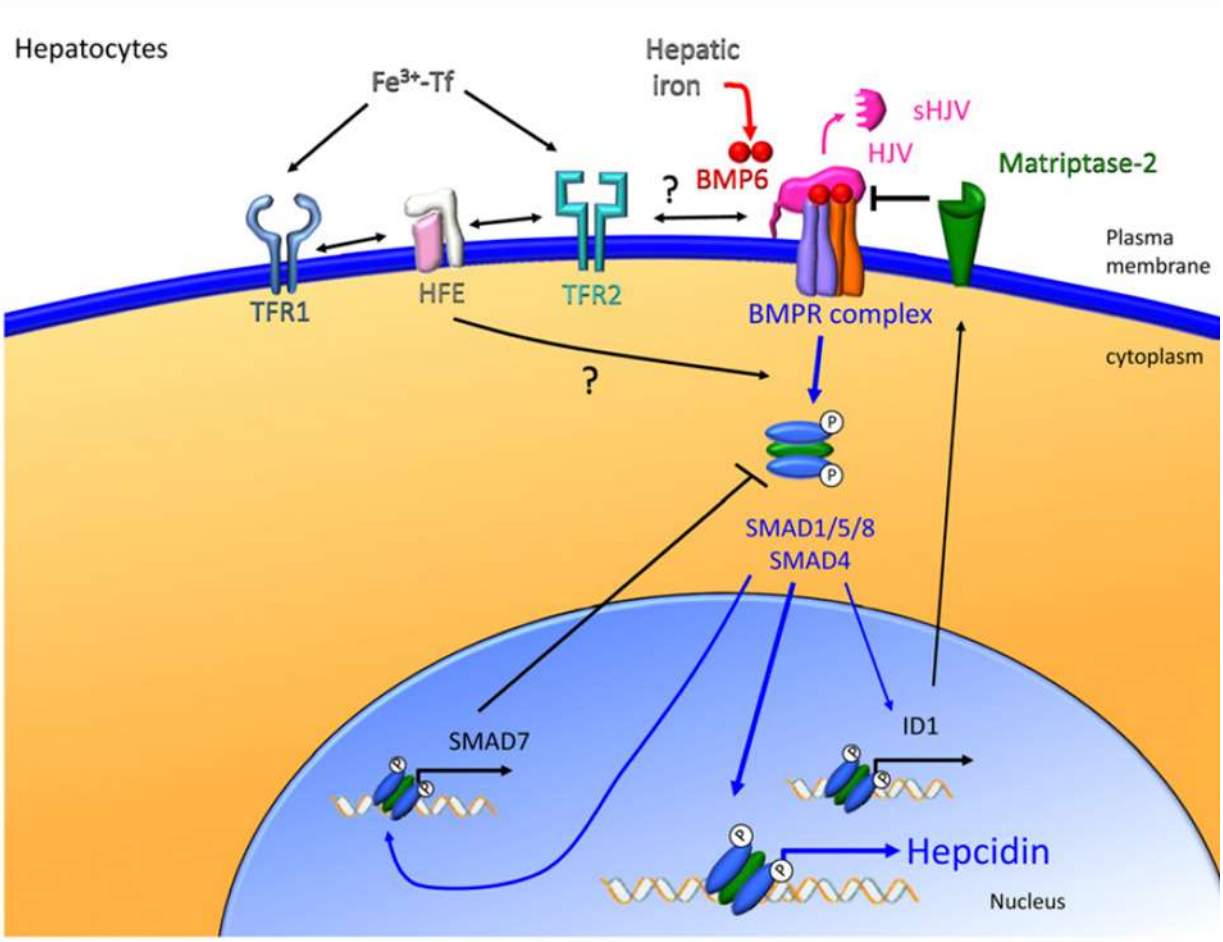

Figure 3.8: Proposed mechanism for regulation of hepcidin by iron levels in the blood

Circulating holo-transferrin (Fe^{3+} - Tf) binds to TfR1 on the cell surface which causes the displacement of HFE from its binding site on TfR1. HFE interacts with TfR2 (which also binds to holo-transferrin) and activates the SMAD signaling pathway by interacting with the BMP receptor (BMPR) complex or via other signaling mechanisms.

Source of image: Meynard D, Babitt JL, Lin HY.
The liver: conductor of systemic iron balance. *Blood.* 2014 Jan 9;123(2):168-76.

It has also been shown that liver sinusoidal cells take up ferritin and regulate expression of *Bmp6* and hepcidin in response to ferritin-derived iron (93). The molecular mechanisms that regulate *Bmp6* expression in these cells are not known. It has also been shown that hepatic iron stores can regulate *Hamp1* expression by modulating *Tmprss6* expression (94).

3.2.2.3 Regulation of hepcidin by erythropoietic signals

Increased erythropoiesis is associated with suppression of hepatic hepcidin expression and increased duodenal iron absorption (95–97). This ensures iron availability to support erythropoiesis. In pathological conditions, such as thalassemia (which is characterized by ineffective erythropoiesis), erythropoiesis-mediated hepcidin suppression contributes to iron overload and tissue damage (98,99). Factors secreted by the erythroid precursors in the bone marrow, called the "erythroid regulators" of hepcidin, are known to be potent suppressors of hepatic hepcidin expression (Fig. 3.9). The identities of these factors are not clearly known (100). Growth differentiation factor–15 (GDF-15), twisted gastrulation factor 1 (TWSG-1) and erythroferrone (ERFE) have been identified as putative erythroid regulators of hepcidin.

Among the erythroid regulators of hepcidin that have been identified, ERFE (or erythroferrone), a member of the tumor necrosis factor superfamily, has been reported to be the most promising candidate (35,101). Mice lacking the gene for ERFE showed impaired suppression of hepcidin in response to phlebotomy and erythropoietin (EPO) administration (35). Its expression in the marrow was increased during iron deficiency and acute hemolysis (101). In addition, it was shown to play role in suppression of hepcidin in thalassemic mice and during recovery from anemia of inflammation (102,103).

Figure 3.9

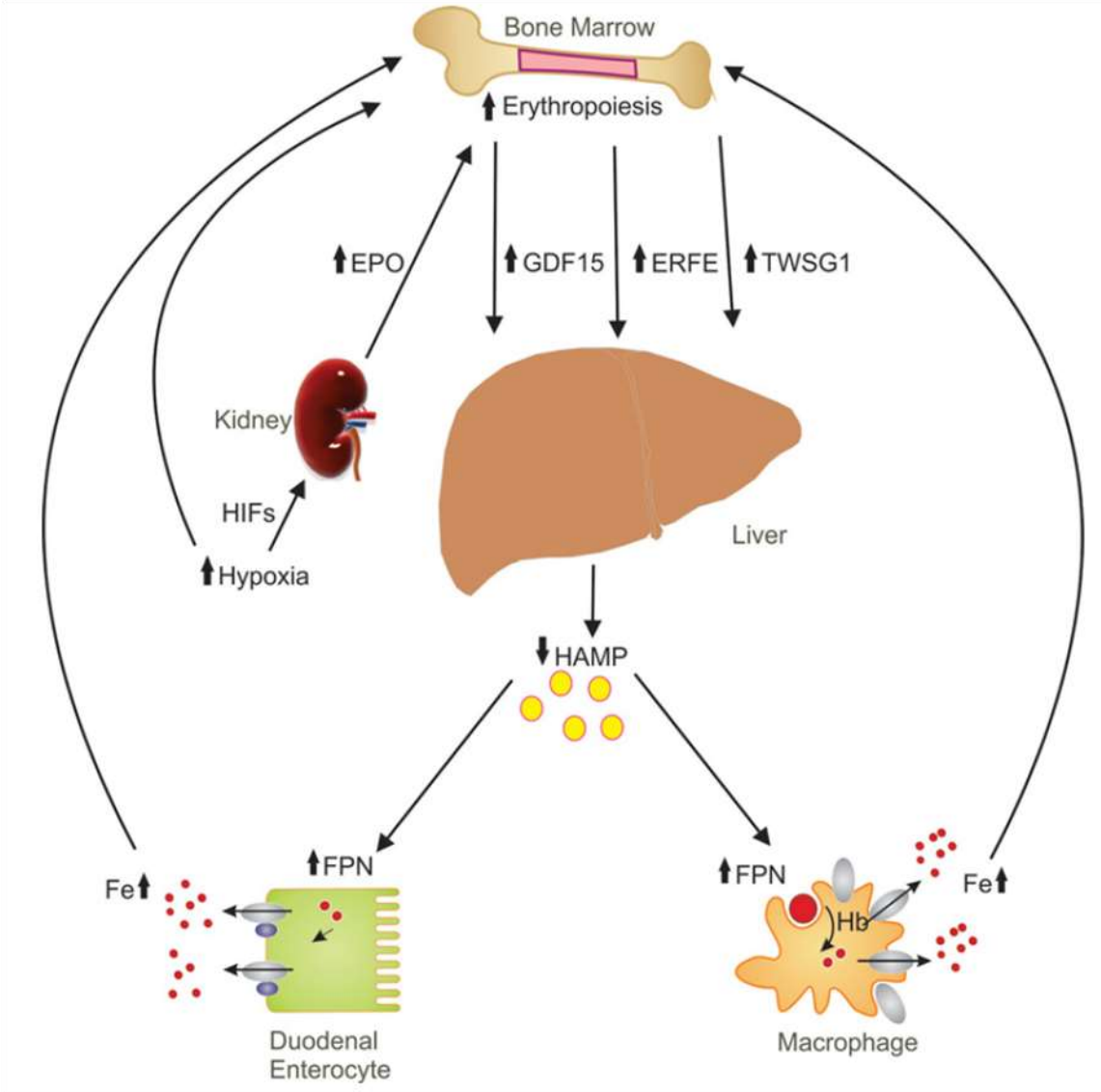

Figure 3.9 Regulation of hepcidin by factors secreted by erythroid progenitor cells (erythroid regulators of hepcidin)

Factors such as hypoxia, anemia and blood loss increase the secretion of erythropoietin (EPO) from the kidney. EPO acts upon the bone marrow to stimulate erythropoiesis and also increase the secretion of factors (erythroid regulators) that suppress hepcidin expression in the liver. Decreased hepcidin increases the release of iron from macrophages and iron absorption from the diet, thus making iron available for erythropoiesis. The putative erythroid regulators of hepcidin are ERFE, GDF-15 and TWSG-1.

Source of image: Rishi G, Subramaniam VN.
The relationship between systemic iron homeostasis and erythropoiesis. *Biosci Rep*. 2017 Nov 29;37(6).

GDF-15 is a divergent member of the TGF-β family and is highly expressed by late erythroid precursors (104). Serum GDF-15 is markedly elevated in patients with thalassemia and other causes of ineffective erythropoiesis (105,106); it has been shown to inhibit hepcidin expression *in vitro* at these high levels (33). However, mice lacking the gene for GDF-15 were able suppress hepcidin in response to acute blood loss (105). In addition, its levels were not increased in a mouse model of thalassemia (35,70), thus questioning its pathophysiological importance as a regulator of hepcidin.

TWSG1 is a modulator of the BMP-SMAD signaling pathway; it is highly expressed in early erythroblasts. Treatment of hepatocytes with TWSG1 *in vitro* has been shown to suppress hepcidin expression (34). As with GDF-15, it has been shown that phlebotomy did not increase expression of TWSG1 in mouse bone marrow (35). In addition, TWSG1 levels were not modulated by iron deficiency or in response to blood loss (101). Therefore, the current evidence suggests that TWSG1 may not play an important role as a physiological regulator of hepcidin.

3.2.2.4 Regulation of hepcidin by hypoxia

Hepcidin expression is suppressed in response to hypoxia and this response is thought to be mediated by hypoxia-inducible factors (HIFs) (107,108). Although it has been shown that HIFs can directly suppress hepcidin expression in hepatocytes (107), it is now known that hypoxia-induced hepatic hepcidin suppression is mediated by increased erythropoiesis in response to erythropoietin (108,109). Hypoxia may also increase blood levels of platelet-derived growth factor–BB (PGDF-BB), which suppresses hepcidin via the cAMP response element binding protein–H (CREB-H (110).

3.2.2.5 Regulation of hepcidin by inflammation and other stress signals

Hepcidin expression is increased in response to inflammation. This response may be part of the innate immune mechanism aimed at decreasing the availability of iron to invading pathogens (111). The pro-inflammatory cytokine, interleukin-6 (IL-6), has been shown to induce hepcidin by signaling through the Janus kinase 2–signal transducer and activator of transcription 3 (Jak2-STAT3) pathway (112–114). The BMP-SMAD pathway also plays a role in hepcidin induction by IL-6 (115). Other mediators of inflammation, like Activin B, may also play a role by activating the BMP-SMAD pathway (116,117).

In addition to these, it is known that hepcidin expression can be increased in response to endoplasmic reticulum stress (118,119) and gluconeogenic signals (120) acting via CREB-H/SMAD and PGC-1α/CREB-3l3 respectively.

3.3. Insulin, the central regulator of energy homeostasis

Insulin was discovered in 1921 by Banting and Best, who extracted from pancreatic tissue "an islet cell factor that had potent hypoglycemic activity". Insulin was the first protein that was proven to have hormonal action. In addition, it was the first protein to be crystallized, sequenced and synthesized by chemical methods. It was also the first protein to be synthesized by recombinant DNA technology for commercial use.

Insulin is a low-molecular weight protein (5.7 kDa), which consists of two polypeptide chains (A and B) linked to each other by two inter-chain disulphide bonds. The A and B chains have 21 and 30 amino acids respectively. Insulin is synthesized in pancreatic beta cells as a preprohormone. Following removal of the 23 amino acid leader sequence in the endoplasmic

reticulum, it forms proinsulin. Proinsulin undergoes a series of proteolytic cleavages to form equimolar amounts of C-peptide and mature insulin. Mature insulin is packaged into granules in the Golgi apparatus and stored in the cytosol.

3.3.1. Insulin secretion

On average, the human pancreas secretes about 40 to 50 units of insulin per day. Glucose is the most potent insulin secretogogue. Apart from glucose, amino acids (arginine and leucine), ketone bodies and certain gastrointestinal peptides (such as glucagon-like peptide 1 and cholecystokinin) can stimulate insulin release. In response to glucose stimulation, insulin release occurs in two phases. The first phase release is swift and short-lasting, while the second phase is slow and occurs over a period of 2 to 4 hours. A reduction in the first-phase release of insulin is one of the earliest signs of beta cell failure in type 2 diabetes.

The process of glucose-induced insulin secretion in beta cells is shown in Fig 3.10. Glucose enters beta cells via glucose transport protein 2 (GLUT2). Inside the beta cell, glucose is phosphorylated by glucokinase. This is considered the rate-limiting step in the process of insulin secretion. Further metabolism of glucose-6-phosphate by glycolysis, the citric acid cycle and finally oxidative phosphorylation, results in formation of ATP. ATP binds to and inhibits the ATP-sensitive K^+ channels, resulting in depolarization. Membrane depolarization activates voltage-sensitive calcium channels, which results in calcium influx into the cell. Increased levels of intracellular calcium trigger exocytosis of insulin-containing granules. Glucose-induced insulin secretion can be augmented by incretins (such as glucagon-like peptide 1) secreted from neuroendocrine cells in the intestine following ingestion of food.

Figure 3.10

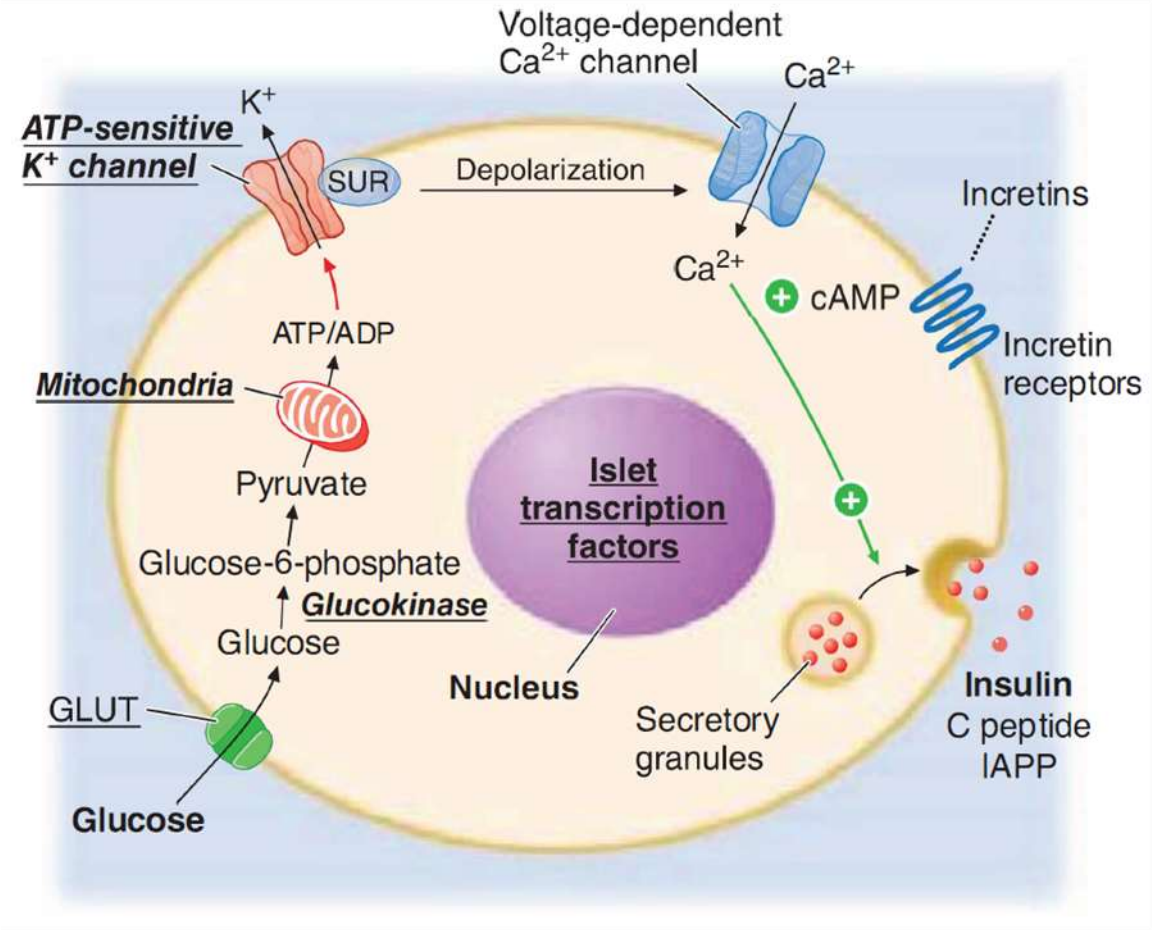

Figure 3.10: Glucose-stimulated secretion of insulin from pancreatic beta cells

Glucose is transported into the beta cell via GLUT transporters on the cell membrane. Inside the beta cells, glucose is phosphorylated by glucokinase and further metabolized to produced ATP. ATP binds to and inhibits the ATP-sensitive K^+ channels resulting in depolarization of the cell. Consequently, voltage-gated calcium channels are activated resulting in exocytosis of insulin-containing secretory granules.

Source of image: Kasper DL, Jameson JL, Hauser S, Loscalzo J, Fauci AS, Longo D. Harrison's Principles of Internal Medicine 19/E (Vol.1 & Vol.2). McGraw-Hill Education; 2015. (Figure 417-5, page 2402).

Once secreted into the portal vein, about 50% of insulin is rapidly degraded in a single pass through the liver. Consequently, insulin has a very short half-life of 3-5 minutes.

3.3.2 Overview of the insulin signaling pathway (121,122)

Insulin binds to its receptor on insulin-sensitive tissues, such as the liver, skeletal muscle and adipose tissue. This receptor is a dimer of dimers; it consists of 2 extracellular α subunits and 2 transmembrane β subunits, which are held together by disulphide bonds (Fig. 3.11). Binding of insulin to the α subunits results in phosphorylation of tyrosine residues on the β subunits. These are recognized by phosphotyrosine-binding domains of adaptor proteins, such as insulin receptor substrates 1 and 2 (IRS 1/2). Phosphorylation of IRS 1 and 2 at specific tyrosine residues provides docking sites for binding of phosphoinositol-3-kinase (PI3K) via src homology 2 (SH2) domains. PI3K catalyzes the conversion of the membrane phospholipid, phosphatidylinositol (4,5)-bisphosphate (PIP_2) to phosphatidylinositol (3,4,5)-trisphosphate ($PIP_{3).}$ PIP_3 forms a docking site for phosophoinositide-dependent protein kinase–1 (PDK-1), which then recruits and phosphorylates protein kinase B or Akt at two key residues, Thr 308 and Ser 473.

The phosphorylation and activation of Akt lies at the heart of the insulin signaling pathway. In the liver, activated Akt phosphorylates glycogen synthase kinase 3 β (Gsk3β) at Ser9, thus inactivating it. Gsk3β, in its active state, phosphorylates and inactivates glycogen synthase kinase, thus inhibiting glycogenesis. Insulin-induced inactivation of Gsk3β, thus, activates glycogenesis.

Figure 3.11

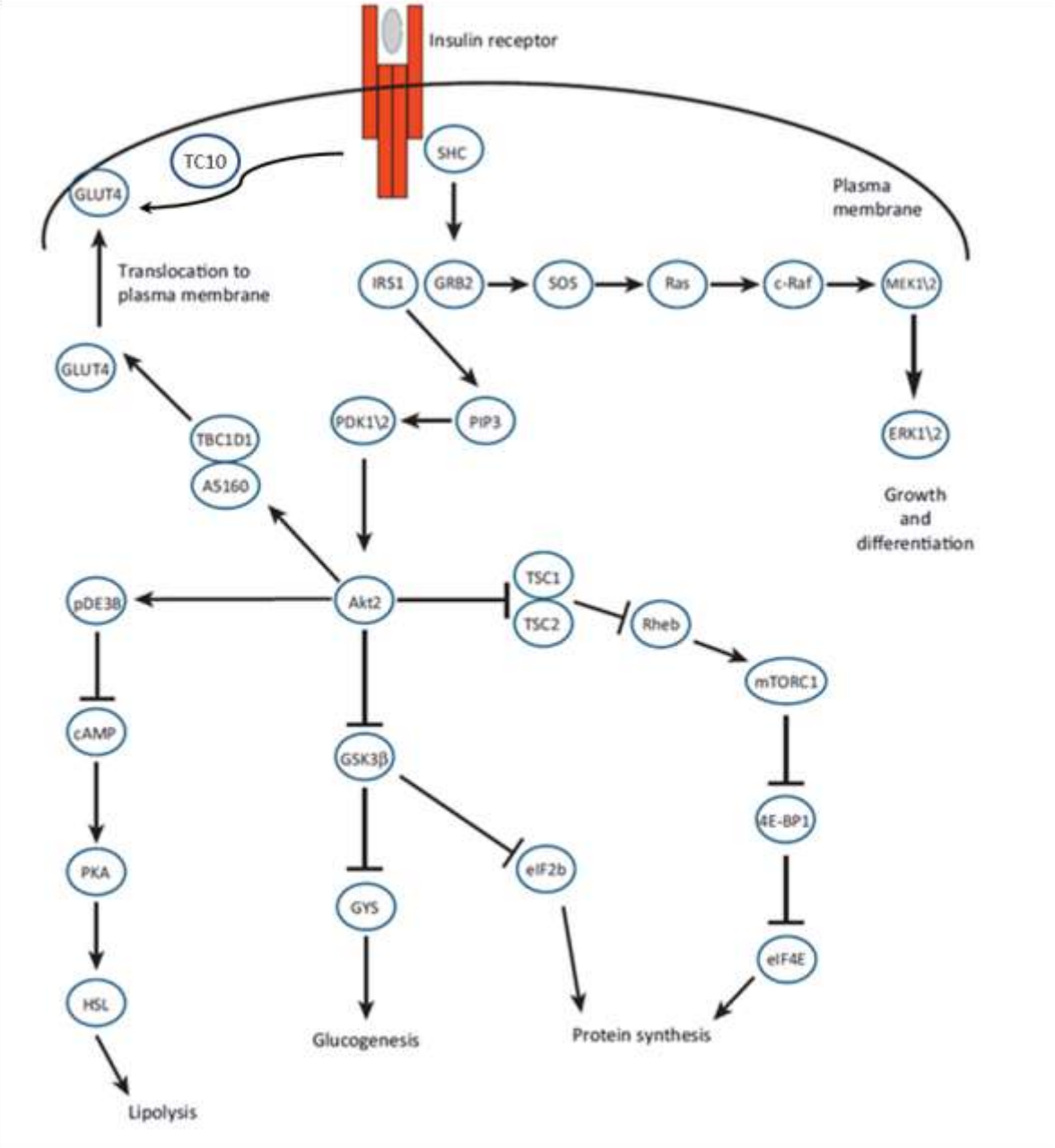

Figure 3.11. The intracellular insulin signaling pathway

Source of image: Cildir G, Akıncılar SC, Tergaonkar V. Chronic adipose tissue inflammation: all immune cells on the stage. *Trends Mol Med*. 2013 Aug;19(8):487-500.

Akt also phosphorylates and induces the nuclear exclusion of the key gluconeogenic transcription factor, forkhead box O1 (FoxO1). FoxO1 is an important transcription factor that activates the transcription of gluconeogenic genes, glucose-6-phosphatase (G6Pase) and phosphoenolpyruvate carboxykinase (PEPCK). FoxO1 inactivation by Akt (in response to insulin) thus decreases expression of gluconeogenic genes. In addition, insulin also phosphorylates and inactivates peroxisome proliferator-activated receptor gamma co-activator 1-alpha (PGC-1α), which (along with FoxO1) plays an important role in the regulation of G6Pase and PEPCK.

In the skeletal muscle and adipose tissue, an important effect of insulin is to induce translocation of the insulin-sensitive glucose transporter (GLUT4) from intracellular storage vesicles to the cell membrane. The translocation of GLUT4 is mediated by both Akt-dependent and independent mechanisms. The Akt independent pathway involves insulin receptor-mediated activation of the Cbl-CAP complex, which translocates to lipid rafts on the membrane to interact with the adaptor protein Crk and the guanine nucleotide exchange factor, C3G. C3G, in turn, activates the GTP-binding protein, TC10, which induces the translocation of GLUT4 to the membrane.

Insulin also increases uptake of amino acids by tissue and stimulates protein synthesis. Gsk3β phosphorylates and inactivates the translation initiation factor eIF2B. Insulin, by inactivating Gsk3β, promotes protein synthesis by activating eIF2b. Akt also activates the mammalian target of rapamycin (mTOR) pathway, which increases protein synthesis by inactivating eIF4B-binding protein. In the adipose tissue and liver, insulin increases the mRNA expression of the transcription factor, sterol regulatory element-binding protein 1c (SREBP-1C). SREBP-1c is the

master regulator of lipid metabolism and increases the transcription of genes involved in synthesis of fatty acids, triacylglycerol and cholesterol. Insulin, acting via the adapter protein Grb2, can activate the mitogen-activated protein kinase (MAPK) pathway. In this way, insulin has growth-stimulatory and mitogenic properties, in addition to its profound effects on intermediary metabolism.

3.3.3 Metabolic effects of insulin

Insulin has profound effects on the metabolism of glucose, lipids and proteins. The principal metabolic effect of insulin is to decrease blood glucose levels. It does so by increasing the peripheral cellular uptake of glucose (in the skeletal muscle and adipose tissue) and by decreasing hepatic glucose output (Fig. 3.12).

3.3.3.1 Effect of insulin on glucose uptake from blood

Under normal conditions, the skeletal muscle is responsible for more than 80% of insulin-induced decrease in blood glucose levels. In the skeletal muscle and in adipose tissue, insulin induces the rapid translocation of glucose transporters (GLUT4) to the cell membrane. This mainly involves signaling via the Cbl-CAP-TC10 pathway (described in section 3.3.2) (123–125). Increase in cell surface GLUT4 levels results in increase glucose uptake into cells from the circulation, resulting in a rapid decrease in blood glucose levels.

Figure 3.12

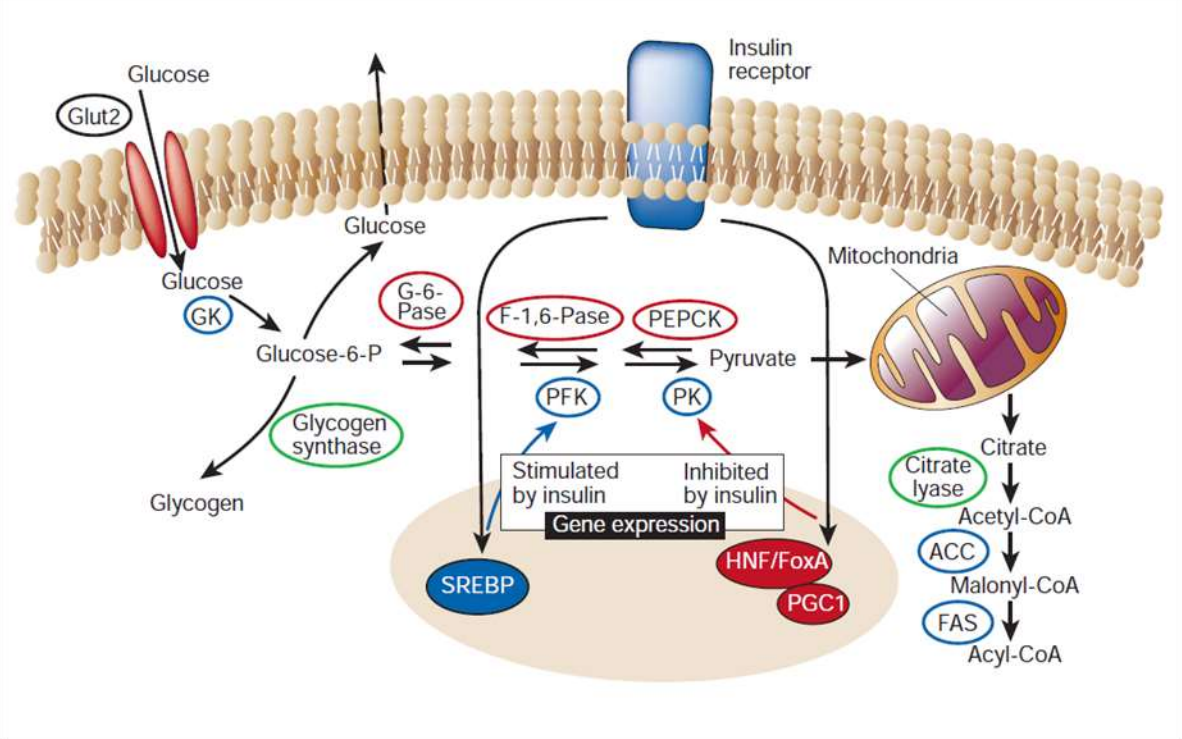

Figure 3.12. Role of insulin in hepatic glucose metabolism

In hepatocytes, insulin stimulates glycolysis and promotes its storage as glycogen and lipids. At the same time it decreases glucose production by inhibiting glycogenolysis and gluconeogenesis. It does so by increasing the activity of glycogen synthase and citrate lyase (green circles), and increasing the transcription of glucokinase (GK), phosphofructokinase (PFK), pyruvate kinse (PK), acetyl CoA carboxylase (ACC) and fatty acid synthase (FAS) (blue circles). It also decreases the transcription of phosphoenolpyruvate carboxykinase (PEPCK), fructose-1,6-bisphosphatase (F-1,6-Pase) and glucose-6-phosphatase (G6Pase) (red circles). These effects are mediated by inhibition of the transcription factors, FoxO1 (or FoxA), HNF and PGC1 (red ovals) and activation of SREBP (blue oval).

Source of image: Saltiel AR, Kahn CR. Insulin signalling and the regulation of glucose and lipid metabolism. *Nature*. 2001 Dec 13;414(6865):799-806.

Insulin also increases glucose uptake in the liver, but the mechanism does not involve GLUT transporter. Insulin induces glucokinase (126), which phosphorylates glucose transported into hepatocytes via GLUT2. Increased phosphorylation of glucose maintains a glucose concentration gradient across the cell membrane, which facilitates the movement of glucose into the cell.

3.3.3.2 Effect of insulin on glucose utilization

Insulin increases glycolysis in the liver, skeletal muscle and adipose tissue, both by increasing the activity and transcription of glucokinase/hexokinase, phosphofructokinase (PFK1) and pyruvate kinase. In addition, it increases lipogenesis by increasing the activities of pyruvate dehydrogenase, acetyl CoA carboxylase and fatty acid synthase. These effects require signaling via $SREBP_{1C}$ (126) (Fig 3.12).

3.3.3.3 Effect of insulin on hepatic glucose production (HGP)

Insulin decreases HGP by inhibiting glycogenolysis and gluconeogenesis. The mechanisms involved are complex and not fully understood. It brings about this effect through a combination of direct effects on the liver and indirect effects (through its effects on extra-hepatic tissues). The indirect effects are mediated by inhibitory effects on lipolysis in the adipose tissue, modulation of vagal activity mediated by the effects of insulin on the hypothalamus in the brain (demonstrated in mice) and by decreasing substrate availability for gluconeogenesis (127)

In the liver, insulin increases glycogen synthesis by activating glycogen synthase, the rate-limiting enzyme in glycogenesis. It does so by phosphorylating and inhibiting Gsk3β (as described in section 3.3.2). In addition, insulin also activates phospho-protein phosphatase 1

(PP1). PP1 dephosphorylates glycogen synthase (activating it) and glycogen phosphorylase (inhibiting it), thus coordinately activating glycogenesis synthesis and inhibiting glycogenolysis (128).

Increased hepatic glucose production (HGP), driven primarily by increased gluconeogenesis, is a characteristic feature of diabetes (129). Regulation of HGP is a complex process, with glucagon and insulin being the primary hormonal regulators. Glucagon stimulates HGP by increasing the phosphorylation of the bi-functional enzyme, phosphofructokinase-2/fructose bisphophatase-2, thus increasing the gluconeogenic flux. It also increases the transcription of key gluconeogenic genes, phosphoenolpyruvate carboxykinase (PEPCK, *Pck1)* and glucose-6-phosphatase *(G6pc)*, by activating cAMP-response element binding protein (CREB), which is a transcription factor (130). While glucagon sets the basal tone for HGP, insulin can powerfully suppress it by acting through multiple mechanisms. Insulin, acting via its receptors on the cell surface, phosphorylates and activates Akt (protein kinase B) (20). Activated Akt phosphorylates several downstream targets, including glycogen synthase kinase 3β (Gsk3β) and forkhead box O1 (FoxO1), both of which are inactivated by Akt-catalyzed phosphorylation (at Ser9 and Ser256 respectively). Inactivation of Gsk3β inhibits glycogenolysis, while that of FoxO1 results in suppression of gluconeogenesis (21).

The effects of insulin on HGP *in vivo* are apparent within minutes of its secretion from the pancreas. It is therefore thought that these acute effects of insulin are not mediated by its effects on transcriptional regulation of gluconeogenic genes (131). Although the direct effects of insulin on the liver are important for HGP regulation *in vivo* (132), studies have shown that insulin can regulate HGP even in the absence of direct insulin signaling in the liver (133,134). For example,

mice lacking insulin receptors (133) or Akt (135) specifically in the liver were able suppress HGP in response to insulin. These studies show that the indirect effects of insulin (mediated by its effects on extra-hepatic tissues) play an important role in short-term regulation of HGP.

Insulin-induced inhibition of lipolysis in the adipose tissue has been shown to play a key role in HGP regulation. The mechanism that has been proposed is as follows: insulin induces a decrease in NEFA in the blood by suppressing lipolysis in the adipose tissue. This results in decreased hepatic acetyl CoA levels. Low acetyl CoA decreases the allosteric activation of pyruvate carboxylase resulting in decreased substrate flux through the gluconeogenic pathway (136).

Insulin decreases the availability of gluconeogenic substrates by decreasing the release of glucogenic amino acids (such as alanine) and lactate from the muscle. In mice, it has been shown that the central effect of insulin (on the hypothalamus) can suppress HGP by decreasing flux through G6Pase (137,138). The mechanisms involved are not clear; however it involves the orexigenic (appetite-promoting) NPY/AgRP neurons and anorexigenic POMC neurons in the brain and IL-6-STAT3 signaling in the liver (139,140). It is not clear whether similar mechanisms are operational in humans as well.

3.3.4 Role of AMP-activated protein kinase (AMPK) in energy metabolism in the liver

AMP-activated protein kinase (AMPK) is an important intracellular energy sensor (141). AMPK activation results in inhibition of anabolic pathways (which consume ATP) and stimulation of catabolic pathways (which increase ATP production). The insulin-sensitizing hormone adiponectin and the anti-diabetic drug metformin bring about their effects, at least in part, by activating the AMPK pathway (142,143).

Figure 3.13

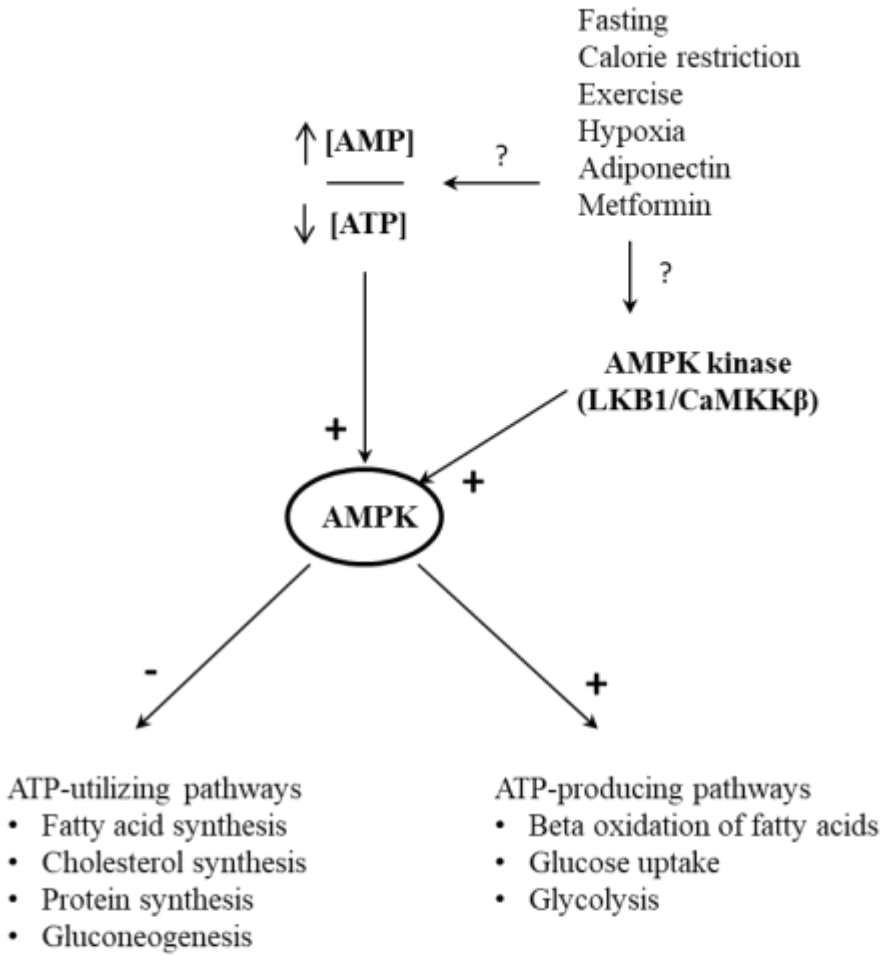

Figure 3.13. Role of AMP-activated protein kinase in metabolism in the liver

The AMPK pathway is activated by an increase in the AMP / ATP ratio and/or by activation of AMPK-kinases such as liver kinase B1 (LKB1) or (Ca^{2+}/calmodulin-dependent protein kinase kinase β (CaMMK- β). Factors such as fasting, calorie restriction and exercise, as well as adiponectin and the anti-diabetic drug, metformin activate AMPK by mechanisms that are not completely understood. Activation of AMPK results in inhibition of ATP-consuming pathways and activation of ATP-producing pathways.

AMPK, adenosine monophosphate activated kinase; AMP, adenosine monophosphate; ATP, adenosine triphosphate; LKB1, liver kinase B1; CaMMK, Ca^{2+}/calmodulin-dependent protein kinase kinase.

AMPK is activated when the AMP/ATP ratio in the cell increases, indicating an energy-depleted state. Binding of AMP to the γ subunit of AMPK induces a conformational change that exposes the Thr172 residue on the α-subunit. Subsequent phosphorylation at Thr172 by AMPK kinases (AMPKK) is required for full activation of AMPK. Liver kinase B1 (LKB1) is a key AMPKK involved in phosphorylation of AMPK at Thr172 (144).

Activation of AMPK results in initiation of a metabolic program the involves inhibition of anabolic pathways, such as fatty acid and protein synthesis, activation of catabolic pathways, such as fatty acid oxidation, and increased mitochondrial biogenesis and cellular glucose uptake (141) (Fig. 3.13). AMPK decreases HGP by inducing the phosphorylation and inactivation of CREB-regulated transcription co-activator 2 (CRTC2), a key transcriptional co-activator involved in induction of gluconeogenic genes by glucagon (145). In addition, AMPK also inhibits glucagon-induced increase in gluconeogenesis, by activating phosphodiesterase-mediated cAMP degradation (146).

3.4. Diabetes mellitus

Diabetes mellitus refers to a heterogeneous group of conditions characterized by hyperglycemia. Depending on the specific type of diabetes, hyperglycemia may result from impaired insulin secretion, resistance to insulin-induced uptake of glucose, increased hepatic glucose production or a combination of all these factors (147). Chronic hyperglycemia results in secondary pathophysiological changes that can result in damage to multiple organ systems. Diabetes is the leading cause of chronic renal failure, adult blindness and lower limb amputations due to non-traumatic causes. In addition, it increases the risk of cardiovascular, cerebrovascular and

peripheral vascular disease. Overall, diabetes is one of the leading causes of morbidity and mortality world-wide (148).

3.4.1. Diabetes, a global epidemic

The International Diabetes Federation reports that, in 2017, there were more than 425 million people with diabetes. This figure was projected to go up to 642 million in the year 2040 (149). While the prevalence of diabetes has remained more-or-less static in the developed world, it has risen rapidly in developing countries. There has also been an epidemiological shift, with diabetes no longer being a disease of the affluent in urban areas. In the urban areas, diabetes is now more common among the poorer sections of society, while in rural regions world-wide the prevalence of diabetes has increased from 5.7% in 1985–89 to 8.7% in 2005–11 (150).

3.4.2. Diabetes, the Indian scenario

Recent data from India shows an overall prevalence of 7.3% for diabetes and 10.3% for pre-diabetes (151). There were marked inter-state differences, which is reflective of the socio-economic, ethnic and racial diversity in the country. Overall, the prevalence was higher among economically disadvantaged populations in urban areas. The prevalence was lower in rural areas compared to urban areas; however the differences were less marked, when compared to data from the early 2000s (151).

3.4.3. Classification of diabetes

Diabetes is classified broadly into 4 types as shown in Table 3.1. The two major types are type 1 and type 2 diabetes mellitus. Type 1 diabetes mellitus (T1DM) is characterized by an absolute deficiency in insulin secretion. On the other hand, type 2 diabetes mellitus (T2DM) has a more complex pathogenesis characterized by variable degrees of insulin resistance (IR) and impaired insulin secretion. These are discussed in detail in section 3.5 and 3.6.

Apart from T1DM and T2DM, a heterogeneous group of conditions, such as those associated with abnormal beta cell development or function, defective insulin action, disorders of the pancreas, endocrinopathies and other genetic diseases, are grouped under the third class called "other specific types of diabetes" (Table 3.1). Gestational diabetes refers to diabetes mellitus that is diagnosed for the first time during pregnancy. Most women with GDM revert to normal glucose tolerance after child-birth; however, they have significantly increased risk of developing T2DM over the next 10- 20 years (152).

Table 3.1: Classification of diabetes mellitus

I. Type 1 diabetes mellitus (characterized by beta cell destruction leading to absolute insulin deficiency)
   a. immune-mediated
   b. idiopathic

II. Type II (characterized by varying degrees of insulin resistance and insulin secretory defect)

III. Other specific types of diabetes:
   a. Mutations in specific genes resulting in genetic defects in beta cell development and function.
      i. Hepatocyte nuclear factor (HNF)-4α (MODY 1)
      ii. Glucokinase (MODY 2)
      iii. HNF-1α (MODY 3)
      iv. Insulin promoter factor-1 (MODY 4)
      v. HNF-1β (MODY 5)
      vi. NeuroD1 (MODY 6)
      vii. Mitochondrial DNA
      viii. Subunits of the ATP-sensitive K^+ channel
      ix. Proinsulin or insulin
      x. Pancreatic islet regulatory proteins
   b. Genetic defects in insulin action
      i. Type A insulin resistance
      ii. Leprechaunism
      iii. Rabson-Mendenhall syndrome
      iv. Lipodystrophy syndromes
   c. Disease of the exocrine pancreas
   d. Endocriopathies – acromegaly, Cushing's syndrome, pheochromocytoma etc.
   e. Other genetic syndromes

IV. Gestational diabetes mellitus

Source: Kasper DL, Jameson JL, Hauser S, Loscalzo J, Fauci AS, Longo D. Harrison's Principles of Internal Medicine 19/E (Vol.1 & Vol.2). McGraw-Hill Education; 2015. (Table 417-1, page 2399).

3.4.4. Diagnosis of diabetes and pre-diabetes

As per the criteria of the American Diabetes Association (2017), a diagnosis of normal glucose tolerance, pre-diabetes or diabetes can be based on fasting plasma glucose levels, plasma glucose 2 h after a glucose challenge (oral glucose tolerance test [OGTT]) or glycated hemoglobin (HbA_{1c}) levels (153). Normal glucose tolerance is defined as:

- fasting plasma glucose < 100 mg/dL (<5.6 mmol/L)
- plasma glucose 2 h-post glucose challenge in an OGTT < 140 mg/dL (7.8 mmol/L)
- HbA_{1c} < 5.7% (< 39 mmol/mol)

Pre-diabetes is defined as:

- fasting plasma glucose 100 – 125 mg/dL (5.6 to 6.9 mmol/L) or
- plasma glucose 2 h-post glucose challenge in an OGTT 140 – 199 mg/dL (7.8 - 11.1 mmol/L) or
- HbA_{1c} 5.7 % – 6.4 % (39 – 47 mmol/mol)

Diabetes mellitus is defined as:

- fasting plasma glucose ≥ 126 mg/dL (7.0 mmol/L) or
- plasma glucose 2 h-post glucose challenge in an OGTT ≥ 200 mg/dL (11.1 mmol/L) or
- HbA_{1c} ≥ 6.5% (< 48 mmol/mol) or
- random blood glucose ≥ 200 mg/dL (11.1 mmol/L) in a patient with classic symptoms of hyperglycemia, or hyperglycemic crisis

3.4.5. Pathophysiology of diabetes mellitus

3.4.5.1 Type 1 diabetes mellitus (T1DM)

T1DM is characterized by autoimmune destruction of pancreatic beta cells resulting in insulin deficiency. Most, but not all, people with T1DM have a genetic predisposition and develop overt hyperglycemia at a relative young age (< 20 years) (147). Such patients are born with normal beta cell mass; however, an autoimmune process (probably triggered by an infectious or environmental factor) results in progressive loss of beta cells. Patients become overtly diabetic when more than 70 – 80% of beta cells are destroyed (154).

The factors that trigger the autoimmune process are poorly understood. Although beta cells are embryologically and functionally similar to other islet cells (such as the alpha [glucagon-producing], delta [somatostatin-producing] and PP [pancreatic polypeptide-producing] cells), the autoimmune process specifically targets the beta cells (154). Infiltration of islets by activated T lymphocytes (‘insulitis’) is a characteristic feature of T1DM and occurs early in the pathogenesis of the condition (155). In many cases, auto-antibodies targeted against insulin, ICA512/IA-2, glutamic acid decarboxylase and the zinc transporter, ZnT-8, are detectable (156). However, these are not beta cell-specific and are unlikely to mediate beta cell destruction in this condition. Overall, the pathogenesis of autoimmune beta cell destruction is poorly understood.

3.4.5.2 Type 2 diabetes mellitus (T2DM)

The pathogenesis of T2DM involves both IR as well as impaired insulin secretion. Although the primary abnormality is not clearly known, it is generally held that IR precedes onset of impaired insulin secretion by several years (157).

Most of our current knowledge regarding the pathogenesis of T2DM comes from studies done on Caucasians. Obesity is one of the most important risk factors for T2DM in this group (158). Factors such as a sedentary lifestyle, consumption of high-calorie diet and lack of exercise, have led to an increase in the global prevalence of obesity. World-wide, the prevalence of obesity has tripled between 1975 and 2016. About 39% of the world's population is estimated to be overweight (BMI of 25-30) and, of these, 13% are obese (BMI > 30) (159).

Increase in adipose tissue, especially visceral fat, is associated with the development of a chronic inflammatory state (160). This results in the development of IR (discussed in detail in section 3.5.1). Early in the course of the disease, a compensatory increase in insulin secretion by pancreatic beta cells maintains glucose tolerance at or near normal levels. However, with progressive increase in IR, combined with decreased insulin secretion ('beta cell failure'), hyperglycemia ensues. Initially, hyperglycemia is mainly post-prandial (impaired glucose tolerance). However, increasing beta cell failure coupled with increased hepatic glucose production, results in fasting hyperglycemia (impaired fasting glycemia). With further increase in IR and decrease in beta cell function, the patient eventually develops diabetes (147). These events are summarized in Fig. 3.14.

3.5 Role of insulin resistance in the pathogenesis of T2DM

Insulin resistance (IR) refers to a condition where tissues (mainly liver, skeletal muscle and adipose tissue) respond sub-optimally to the metabolic effects of insulin. Decreased uptake of glucose especially by the skeletal muscle results in post-prandial hyperglycemia, while increased hepatic glucose production contributes to fasting hyperglycemia (147).

Figure 3.14

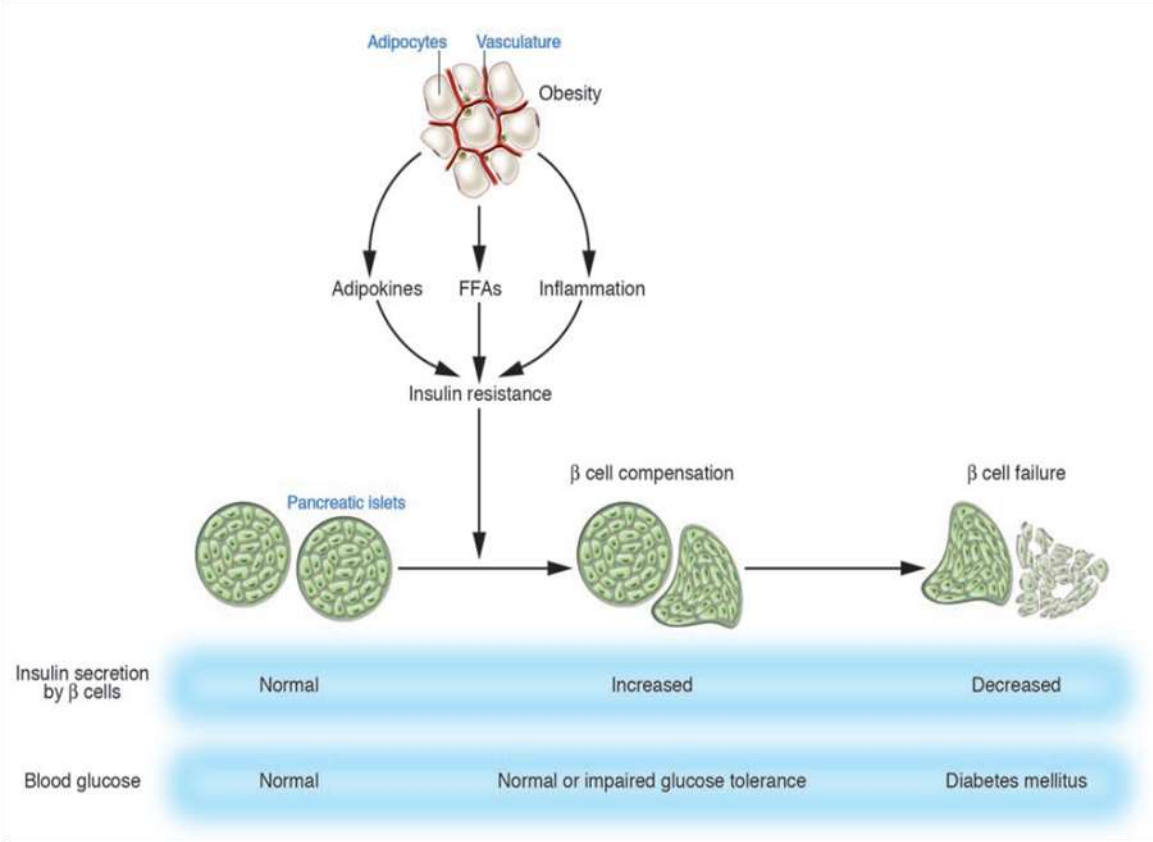

Figure 3.14. Pathogenesis of type 2 diabetes mellitus

Obesity-associated inflammation in the adipose tissue, release of free fatty acids (FFAs) and secretion of adipokines results in insulin resistance. Pancreatic beta cells compensate for insulin resistance by increasing insulin secretion. Onset of beta cell failure results in insulin secretion that is insufficient to maintain normal glucose tolerance. This results in pre-diabetes and, finally, over diabetes mellitus.

Source of image: Kasuga M. Insulin resistance and pancreatic beta cell failure. *J Clin Invest*. 2006 Jul;116(7):1756-60.

3.5.1 Role of adipose tissue in the pathogenesis of IR

3.5.1.1 Adipose tissue inflammation and IR

Adipose tissue inflammation associated with obesity is probably the most important factor in the pathogenesis of IR (158,161–163). The mechanisms involved in initiation of inflammation in the adipose tissue are not clearly delineated. However, adipocyte hypoxia and death resulting in activation of resident macrophages has been proposed to play an important role (164). Once initiated, secretion of pro-inflammatory cytokines, such as monocyte chemo-attractant protein 1 (MCP1), tumor necrosis factor alpha (TNFα) and interleukin-6 (IL-6), by adipocytes and macrophages plays an important role in recruiting additional macrophages and initiating a feed-forward cycle (165,166) (Fig. 3.15).

Adipose tissue macrophages (ATMs) play an important role in sustaining and exacerbating adipose tissue inflammation. The resident ATMs have an anti-inflammatory (or M2) profile, while macrophages recruited to the adipose tissue by inflammation have a pro-inflammatory (or M1) phenotype (167). The pro-inflammatory macrophages secrete a variety of inflammatory mediators, which induce IR in adipocytes, stimulate lipolysis and release non-esterified fatty acids (NEFA) into the circulation (168).

Figure 3.15

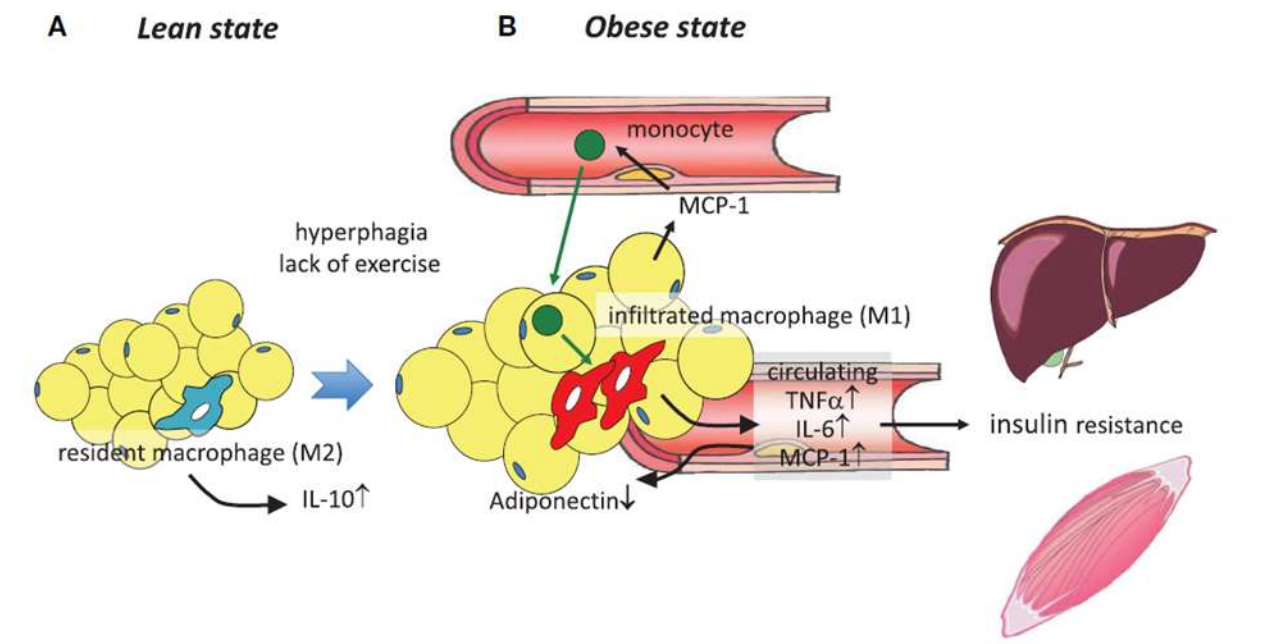

Figure 3.15. Role of adipose tissue in the pathogenesis of insulin resistance

A: In the lean state, resident macrophages in the adipose tissue are in the anti-inflammatory (M2) state.

B: In the obese state, inflammation in the adipose tissue results in recruitment of macrophages which are pro-inflammatory (M1). These macrophages secrete pro-inflammatory cytokines, such as TNF-α, IL-6 and MCP-1, which exacerbate inflammation by recruiting additional macrophages to the adipose tissue. Lipolysis induced by these cytokines, as well altered secretion of adipokines (e.g., decrease in adiponectin and increase in resistin) results in insulin resistance in the liver and skeletal muscle.

.

Source of image: Tateya S, Kim F, Tamori Y. Recent advances in obesity-induced inflammation and insulin resistance. *Front Endocrinol* (Lausanne). 2013 Aug 8;4:93.

3.5.1.2 Subcutaneous and visceral adipose tissue

The distribution of fat in the body can have a major influence on insulin sensitivity. It is well-recognized that people with peripheral (subcutaneous or gluteofemoral) distribution of fat (fat distributed predominantly around the buttocks and thighs) have better insulin sensitivity than those with central (visceral or intra-abdominal) distribution of fat (omental and mesenteric fat) (169,170).

There are several factors that may account for this. Intra-abdominal (visceral) fat is metabolically more active; it expresses adipokines and pro-inflammatory cytokines to a greater extent than subcutaneous fat (171). It also has a larger proportion of immune cells like macrophages and lymphocytes.

Intra-abdominal fat is also more lipolytic and resistant to the anti-lipolytic effects of insulin. On the other hand, subcutaneous fat has higher capacity to take up and esterify fatty acids from circulation (172). In addition, blood from intra-abdominal fat drains directly to the liver, exposing the liver to high concentrations of NEFA and pro-inflammatory cytokines (especially 1L-6). This may explain why IR develops initially in the liver, while the peripheral tissues are still insulin-sensitive (173).

3.5.1.3 Gonadal adipose tissue in mice

In mice, intra-abdominal fat depots include the peri-gonadal (or gonadal), peri-renal (or retroperitoneal) and mesenteric (intestinal) adipose tissue. The mesenteric fat pad is most analogous to human visceral adipose tissue as it drains directly into the portal vein (174).

However, it is not commonly used for experimental purposes due to its limited quantity and difficulty associated with surgically accessing and manipulating it. The peri-gonadal fat pad (called epididymal fat pad in males and peri-ovarian fat pad in females) is used most commonly in animal experiments because it is the largest intra-abdominal fat depot in mice and is easily accessible. In addition, it shares many of the metabolic features that are characteristic of visceral fat in humans, such as increased metabolic capacity, development of inflammation and infiltration of immune cells in response to obesity (or high-fat feeding), secretion of adipokines and inflammatory cytokines, etc. (174). However, humans do not have fat pads that are analogous to the perigonadal fat pads of mice. Therefore, it has been suggested that these are "peri-visceral" in nature and not truly visceral adipose tissue. Nevertheless, most studies done in mice have used the peri-gonadal adipose depot as a source of visceral fat (175)

3.5.2 Role of ectopic lipid accumulation in IR

Adipose tissue lipolysis and increased NEFA in the blood is associated with deposition of lipids in the muscle as well as the liver (ectopic lipid accumulation). In the muscle, IR is strongly correlated with intramyocellular lipid content. Lipid-induced IR results in decreased translocation of GLUT4 to the membrane in response to insulin, resulting in impaired glucose uptake (176–178). Ectopic lipid accumulation in the liver is referred to as non-alcoholic fatty liver disease (NAFLD). NAFLD is strongly associated with hepatic insulin resistance and is an important component of the metabolic syndrome (179,180).

The mechanisms by which intracellular lipid induces IR ('lipotoxicity') are not fully understood. It is generally believed that fatty acid metabolites such as diacylglycerol (DAG), fatty acid CoA

and ceramides are important mediators in lipotoxicity (181). DAG can activate novel protein kinase C (PKC) isoforms, such as PKCθ, PKCε and PKCδ, which mediate phosphorylation of specific serine residues on IRS1 and IRS2, thus inhibiting signaling via the Akt pathway (182). Ceramides, acting through multiple mechanisms, including activation of PKCζ, can inhibit insulin-induced activation of the Akt pathway (183).

3.6 Role of beta cell dysfunction in the pathogenesis of T2DM

It is now known that normal glucose tolerance can be maintained in individuals who have a high degree of IR, if beta cell function is preserved. More than 75% of the functional capacity of beta cells is lost in patients who are diabetic (184,185). Studies done on Pima Indians have shown that irrespective of the degree of IR, only those patients who have a pre-existing defect in beta cell function progress to develop diabetes (186). The nature of the beta cell defect is not known; it is probably mediated by genetic or environmental mechanisms.

The beta-cell centric view of pathogenesis of diabetes is shown in Fig 3.16. Impaired or inadequate insulin secretion can result in increased lipolysis in the adipose tissue and release of NEFA into circulation. Increased release of NEFA results in exacerbation of IR and further deterioration in beta cell function, thus constituting a feed-forward cycle. In addition, decreased insulin also results in hyperglycemia by decreased peripheral uptake of glucose in muscles and increasing hepatic glucose output. Hyperglycemia can itself decrease beta cell function (glucotoxicity). In addition, the lack of insulin, acting via the hypothalamus, can increase food intake resulting in obesity and exacerbation of IR (158,185).

Figure 3.16

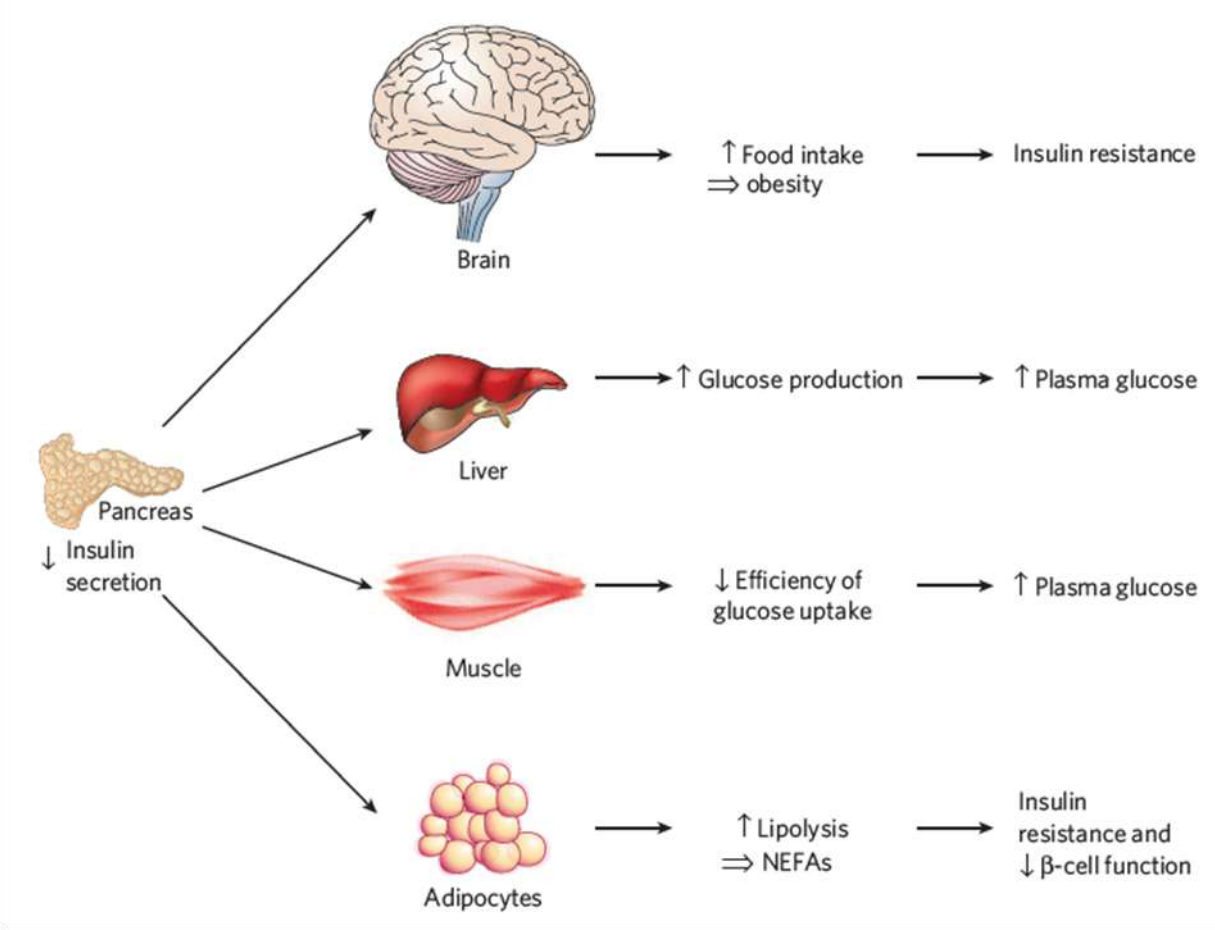

Figure 3.16. Role of beta cell dysfunction in the pathogenesis of insulin resistance

Impaired or inadequate insulin secretion can result in increased lipolysis in the adipose tissue. Increased release of non-esterified fatty acids (NEFA) results, not only in exacerbation of IR, but also in further deterioration in beta cell function, thus constituting a feed-forward cycle. In addition, decrease insulin results in hyperglycemia by decreased peripheral uptake of glucose in muscles and increasing hepatic glucose output. Hyperglycemia can itself decrease beta cell function (glucotoxicity). In addition, the lack of insulin, acting via the hypothalamus, can increase food intake resulting in obesity and exacerbation of IR.

Source of image: Kahn SE, Hull RL, Utzschneider KM. Mechanisms linking obesity to insulin resistance and type 2 diabetes. *Nature*. 2006 Dec 14;444(7121):840-6.

3.7 Role of iron in the pathogenesis of T2DM

In recent years, there has been an increase in interest in the association between elevated body iron stores and diabetes mellitus (10,187). A relationship between increased body iron stores and diabetes mellitus was first shown in patients with hereditary hemochromatosis (188). Subsequently, it was shown that patients who develop iron overload secondary to other causes, such as repeated blood transfusions in thalassemia, were also predisposed to develop diabetes mellitus (98). In addition, reports from a number of epidemiological studies have shown a strong association between body iron stores and risk of diabetes mellitus (described in section 3.7.1).

The interest in the role of iron in the pathogenesis of diabetes stems from the fact that body iron stores can be manipulated either by dietary means, phlebotomy or by pharmacological chelation of iron. Currently, the mainstay of treatment of T2DM consists mainly of controlling blood glucose at or near physiological levels in efforts to delay/prevent the chronic complication of diabetes. There are very few effective strategies aimed at primary prevention of IR in genetically-predisposed individuals.

3.7.1 Serum ferritin levels and the risk of diabetes mellitus

Serum ferritin levels in healthy individuals are generally considered to be a marker of body iron stores (189–191). A number of epidemiological studies have shown an association between increased serum ferritin levels and increased risk of developing diabetes mellitus (192,193). For example, the National Health and Nutrition Education Survey (NHANES), showed that the odds ratio for T2DM in males and females with serum ferritin > 300 µg/L was 4.94 and 3.61,

respectively (4). Even across the reference range of ferritin in apparently healthy women, the positive correlation between ferritin and diabetes risk remained strong (26).

Ferritin levels are known to be elevated in conditions characterized by inflammation. Since inflammation plays an important role in the pathogenesis of diabetes, it is possible that elevated ferritin in this condition may be due to inflammation. However, multiple studies have shown that the association between ferritin and risk of diabetes remains strong after adjusting for potential confounding factors, including inflammation (5–9). These studies, therefore, suggest that elevated ferritin that is associated with diabetes is representative of increased body iron stores in this condition, and not of inflammation.

Recently, the EPIC-InterAct study (194) studied serum levels of ferritin, iron and transferrin, as well as transferrin saturation, in 11,052 cases of incident diabetes and compared them to a random cohort of 15,182 individuals. The results of this large study confirmed the reported association between serum ferritin and diabetes; however, the other markers of iron status studied (serum iron, transferrin and transferrin saturation) did not show a positive association. In fact, among women, transferrin saturation > 45% was associated with a significant protective effect. These results were interpreted to suggest that "the underlying relationship between iron stores and T2DM is more complex than the simple link suggested by the association of ferritin with T2DM" (194).

3.7.2. Hereditary hemochromatosis and diabetes

Hereditary hemochromatosis (HH) refers to a group of conditions characterized by decreased hepcidin secretion. Most patients with HH are homozygous for the C282Y substitution mutation in the HFE protein (classical or type 1 hemochromatosis). Classical hemochromatosis is highly prevalent in people of northern European ancestry. Other causes of hemochromatosis, like those associated with defects in hemojuvelin or hepcidin (type 2 or juvenile hemochromatosis), transferrin receptor 2 (type 3) and ferroportin (type 4) are relatively uncommon and are characterized by a more severe iron overload phenotype (195).

HH was described initially as a triad of cirrhosis, skin pigmentation and diabetes mellitus ('bronze diabetes'). The prevalence of diabetes among patients with HH has been reported to be highly variable (196,197). Earlier studies, which were based on a clinical diagnosis of HH, found a very high prevalence of diabetes in HH. However, newer studies, which are based on a definitive genetic diagnosis of HH, have found a lower prevalence of 13-22% for diabetes and 18-30% for pre-diabetes (11,198). Nevertheless, these rates are much higher than the background prevalence rates of diabetes / pre-diabetes in this population (~5 – 10%).

Diabetes associated with HH has a complex pathogenesis (199,200). McClain et al (2006) showed that among patients with HH who had pre-diabetes, the major metabolic defect was an impaired insulin secretory capacity (11). However, these patients were found to display insulin sensitivity, rather than IR. Most patients with HH who eventually developed overt diabetes were obese, an independent cause for IR. Similar results were obtained in a mouse model of hemochromatosis (*Hfe*$^{-/-}$) where an insulin secretory defect was shown; these mice, however,

were insulin sensitive (19). Based on these findings, the authors have suggested that the primary defect in HH is impaired insulin secretion. Patients with HH seem to be unable to increase insulin secretion to compensate for IR induced by independent risk factors, such as obesity; they are therefore pre-disposed to develop diabetes. In support of these findings, it has been shown that patients with HH who underwent phlebotomy to reduce body iron stores, showed an improvement in insulin secretory capacity, but not in insulin sensitivity (198,201).

3.7.3 Iron-loading anemias and diabetes

Conditions characterized by ineffective erythropoiesis are associated with increased body iron stores and increased prevalence of diabetes. An example of such a condition is thalassemia where impaired production of globin chains results in severe anemia. These patients receive multiple blood transfusions, which eventually result in massive iron overload. It is also known that thalassemics who are not transfusion-dependent also develop iron overload, due to increased intestinal iron absorption (99,202).

Patients with thalassemia have a high prevalence of diabetes (203,204). Multiple studies have shown that both insulin secretory defects and IR co-exist in these patients (12,205–207). Unlike in hereditary hemochromatosis, where a tendency towards improved insulin sensitivity has been demonstrated, IR is pre-dominant in thalassemia and precedes the development of diabetes by several years (206,207). In addition, decreasing body iron stores through chelation therapy significantly improved insulin sensitivity in these patients (14,208). These findings suggest that iron plays a role in the pathogenesis of IR associated with iron-loading anemias, such as thalassemia.

It is not clearly known why iron overload in HH is associated with increased insulin sensitivity, while iron overload in thalassemia results in IR. One possible explanation is that this may be related to the differences in distribution of iron in the body in these two conditions. HH is characterized by a relative deficiency in hepcidin; hence, tissues that express the iron export protein ferroportin are relatively iron-depleted (209,210), while those that do not express ferroportin or take up non-transferrin bound iron (like the liver, pancreas and heart) are iron-overloaded (211). On the other hand, iron loading either due to multiple blood transfusions (as in thalassemia) results in induction of hepcidin. Increased hepcidin decreases ferroportin protein expression on the surface of cells, resulting in intracellular sequestration of iron (24). In this context, very little is known about iron levels in insulin-sensitive tissue, such as skeletal muscle and adipose tissue, in these two conditions.

3.7.4. Evidence to suggest that iron plays a causal role in the pathogenesis of IR

There is evidence to suggest that iron may play a causal role in the pathogenesis of IR. For example, incidence of diabetes in thalassemics has rapidly declined after aggressive iron chelation became a routine part of therapy in these patients (14). Insulin sensitivity has been shown to be improved by phlebotomy in patients with (15) or without T2DM (16). Phlebotomy or dietary iron restriction in Otsuka Long-Evans Tokushima Fatty (OLETF) rats, a model of T2DM, resulted in decreased average glycated hemoglobin levels (HbA1c) levels (18). Restriction of iron in diet or iron chelation was also shown to significantly protect leptin-deficient ob/ob mice against diabetes (19). High dietary iron, on the other hand, induced IR in mice (17). The above reports show that depletion of body iron stores can increase insulin sensitivity, suggesting that iron may play a causative role in diabetes.

3.7.5 Iron and obesity-associated IR

Inflammation in the adipose tissue plays a key role in the development of IR (161). Iron is important for adipocyte differentiation and adipose tissue hypertrophy/hyperplasia (212). Since inflammation is known to regulate systemic iron homeostasis, there is considerable amount of interest in elucidating the interplay between obesity, inflammation and iron homeostasis in adipose tissue.

3.7.5.1 Effect of obesity on iron homeostasis

Obesity can affect iron metabolism in a number of ways. For example, obesity is associated with a chronic, low-grade inflammatory state. Inflammation, acting via IL6-STAT3 signaling in hepatocytes, can increase hepcidin levels resulting in hypoferremia (112). In fact, multiple studies have shown that obesity is associated with anemia (213–215).

Obesity has also been shown to be associated with changes in tissue iron content. It has been shown that high-fat diet-induced obesity in mice decreased liver iron stores (216,217). Other studies have shown that diet-induced obesity resulted in decreased intestinal iron absorption in a hepcidin-independent manner, thus contributing to the iron-deficient phenotype seen in these mice (218).

3.7.5.2 Effect of iron on adipose tissue

Iron is known to be essential for adipocyte differentiation and adipose tissue hypertrophy/ hyperplasia (212). Treatment of primary adipocytes with iron resulted in increased lipolysis. In addition, iron decreased insulin-dependent glucose uptake in these cells (219). In mice, a high-

iron diet was shown to result in increased adipocyte iron stores and IR in the visceral adipose tissue (17). On the other hand, a low-iron diet was shown to improve insulin sensitivity in ob/ob mice (19). These results show that increased adipocyte iron can induce adipocyte IR. In addition, iron-induced lipolysis can increase free fatty acid release, ectopic lipid accumulation and systemic IR.

Iron is critical for mitochondrial function (220). It has been shown that depletion of iron in adipocytes results in reduction in the transcription factor, Tfam, which decreases mitochondrial biogenesis and adipogenesis. On the other hand, excess iron was also associated with impaired adipocyte differentiation (221). Therefore, precise control of adipocyte iron concentrations is required for mitochondrial function in adipocytes.

The adipose tissue is an endocrine organ that secretes a number of factors that play a critical role in maintaining whole-body energy homeostasis and insulin sensitivity (222,223). Of particular importance is the hormone, adiponectin. Adiponectin is an insulin-sensitizing hormone which is synthesized and secreted by adipocytes (224). It has been shown that mice fed a high-iron diet had decreased serum levels of adiponectin (225). Mice with adipocyte-specific iron overload (induced by adipocyte-specific deletion of ferroportin) show decreased mRNA expression of adiponectin (225). Similar findings were also seen in human studies where serum ferritin was shown to be inversely proportional to adiponectin levels (225–227). It has also been shown that serum ferritin levels correlated independently with increased adipocyte IR and decreased adiponectin after adjusting for a host of confounding factors (226).

Apart from adiponectin, adipocyte iron and serum ferritin levels are known to affect serum levels of other adipokines. For example, adipocyte-specific ferroportin knock-out mice were shown to have decreased levels of leptin, a hormone involved in regulation of whole-body energy homeostasis and food intake (228). Iron levels are also associated with alterations in resistin (17), visfatin (229) and retinol-binding protein-4 (230), all of which have been shown to play an important role in the development of IR. These results show that iron can play a role in the pathogenesis of IR by modulating the secretion of adipokines.

Adipose tissue macrophages (ATMs) play an important role in adipose tissue inflammation and IR (167). It has been shown that ATMs regulate adipose tissue iron homeostasis as well (231). A subset of ATMs, with an iron-recycling phenotype, appears to be important in regulating adipocyte iron levels. These ATMs have a M2 (anti-inflammatory) phenotype, which is altered in obesity. High-fat feeding resulted in a decrease iron content in ATMs and an increase in iron in the adipocytes, which resulted in whole-body IR (217,231).

3.7.6 Effect of iron on pancreatic beta cells and insulin secretory capacity

Pancreatic beta cells tend to accumulate iron due the high expression of DMT-1 (232). DMT-1 mediates the uptake of zinc, which is required for formation of insulin secretory vesicles. Increased iron in beta cells has been shown to impair its insulin secretory function. For example in hemochromatosis, glucose tolerance is primarily due to iron-induced decrease in insulin secretion. Both in humans with hemochromatosis as well as in $Hfe^{-/-}$ mice, beta cell function tended to improve following iron depletion by phlebotomy (113,117,130). Ob/ob mice, which

were fed a low-iron diet or treated with iron chelators, showed significantly improved beta cell function (19).

The mechanisms by which iron induces beta cell damage are not clearly known. Beta cells are highly susceptible to oxidative stress (233). It is possible that iron-induced oxidative stress may play a role in beta cell dysfunction (described in section 3.6). However, as mentioned above, beta cell dysfunction in humans with HH as well as in mouse models of this condition could be reversed by iron chelation or phlebotomy. It, therefore, appears that iron does not induce permanent damage in beta cells. However, the mechanisms involved and the relevance of iron in the pathogenesis of beta cell failure associated with T2DM requires further investigation.

3.7.7 Molecular mechanisms by which iron affects insulin sensitivity and beta cell function

Iron can affect insulin sensitivity and beta cell function in a number of ways (10).

3.7.7.1 Oxidative stress and reactive oxygen species (ROS)

Iron is a potent pro-oxidant. It can catalyze the formation of hydroxyl radicals through the Fenton reaction resulting in oxidative tissue damage. Both iron overload and iron deficiency has also been associated with oxidative stress (234).

ROS can induce IR by multiple mechanisms. For example, oxidative stress can activate intracellular stress-sensitive pathways like nuclear factor-κB, p38 mitogen-activated protein kinase and JNK resulting in inhibition of insulin signaling via IRS1 and 2 (235). In addition, oxidative stress-induced activation of FoxO1, can result in sustained gluconeogenesis even in the

presence of insulin (236). It has also been shown that oxidative modification of phenylalanine residues on insulin can decrease its binding affinity to insulin receptors (237).

Beta cells are prone to oxidative damage as they have low expression of anti-oxidant enzymes like catalase, glutathione peroxidase and superoxide dismutase (SOD) (238). Oxidative stress can impair glucose-induced insulin secretion and induce apoptosis in beta cells (239,240).

3.7.7.2 Hypoxia-inducible factors (HIFs)

Iron is required for prolyl hydroxylase-mediated hydroxylation of HIFs which results in its ubiquitination and proteasomal degradation (241). Iron overload is therefore characterized by decreased HIF levels. In beta cells, decreased HIF-1α levels result in decreased expression of its target genes, *Glut1* and *Glut2*. This results in impaired glucose-stimulated insulin secretion. On the other hand, stabilization of HIF-1α (by iron chelation) had the opposite effect (242).

HIFs are also involved in glucose metabolism by increasing the expression of glucose transporters and stimulating glycolytic flux (243). For example, iron depletion augmented glucose uptake in the liver by stabilizing HIF-1α (244).

3.7.7.3 AMP-activated protein kinase

AMP-activated protein kinase (AMPK) is a key cellular energy sensor (described in section 3.3.4). Iron is known to activate AMPK in the liver and in the muscle; however the mechanisms that are involved are not clear (245). Increased intracellular iron can induce mitochondrial dysfunction resulting in an increase in the AMP/ATP ratio. A high AMP/ATP ratio is known to activate AMPK (141). On the other hand, iron-induced oxidative stress can activate the upstream

kinase of AMPK, liver kinase B1 (LKB1). Phosphorylation of AMPK by LKB1 can also result in AMPK activation (245,246).

In addition to the above, iron can significantly affect insulin sensitivity through induction of epigenetic changes, modifying the activity of iron regulatory proteins (IRPS), regulation of circadian rhythms and by regulating the processing and maturation of microRNAs.

4. SCOPE AND PLAN OF WORK

Type 2 diabetes mellitus (T2DM) is a global epidemic that is a major cause of morbidity and mortality, all over the world and especially in India. Over the last two decades, there is accumulating evidence from epidemiological studies which have shown a close association between increased body iron stores and risk of T2DM. However, the molecular basis of the cross-talk between iron metabolism and insulin resistance (IR), the hallmark of T2DM, is not clear. This study was designed to attempt to systematically study this association. It was envisaged that the results of this study would provide a clearer understanding of the role of iron in the pathogenesis of IR and also the effects of IR on iron homeostasis in the body.

Currently, management of diabetes is primarily based on attempts to achieve adequate glycemic control in an effort to delay/prevent chronic complications of diabetes (such as nephropathy, neuropathy, and retinopathy). There are very few effective strategies aimed at primary prevention in genetically pre-disposed persons, other than measures to reduce body weight and increase physical activity. Iron stores in the body can be easily manipulated by dietary means, phlebotomy or by using iron chelators. A better understanding of the role of iron in the pathogenesis of diabetes will possibly provide newer therapeutic options, based on manipulation of body iron stores, in the management of diabetes.

The hypothesis of this study (based on evidence available at the time of designing the study) was that increased cellular iron stores may induce IR by inhibiting insulin signaling. Compensatory hyperinsulinemia (in an effort to overcome IR) may have a stimulatory effect on erythropoiesis in the bone marrow. Increased expression of the erythroid regulators of hepcidin (induced by

stimulated erythropoiesis) may down-regulate expression of hepcidin (the chief regulator of iron homeostasis) in the liver. This may lead to increased duodenal iron absorption and a consequent increase in body iron stores, thus constituting a feed-forward (vicious) cycle.

In order to test this hypothesis, we first studied the effect of increased intracellular iron on insulin signaling in mouse primary hepatocytes *in vitro* (Study 1). Hepatocytes are insulin-sensitive cells. These studies were carried out *in vitro* to avoid factors operational *in vivo* that could potentially confound the effects of iron, per se, on hepatocytes that were of interest.

In study 2, a time-course analysis of the interactions between IR and iron metabolism was carried out, using a mouse model of diabetes mellitus. The high-fat-feeding induced obesity model (in C57Bl/6 mice) is one of the most commonly used animal models for studies related to the pathogenesis of IR and T2DM. This model was used to study changes in systemic iron homeostasis that were induced by IR.

In study 3, the mouse model of diabetes mellitus (used in study 2) was used to study the effects of IR on maturation of erythroid precursors in the bone marrow. In addition, bone marrow erythroid precursor cells were used to study expression of putative erythroid regulators of hepcidin.

In study 4, patients newly diagnosed with diabetes or pre-diabetes and age-matched controls were recruited to study parameters associated with iron homeostasis. In addition, reticulocytes were isolated from blood obtained from these patients to study expression levels of the erythroid regulators of hepcidin.

In summary, an attempt was made to systematically study the inter-relationships between processes involved in iron homeostasis and IR, using *in vitro* (mouse primary hepatocytes in culture) and *in vivo* (high-fat diet induced IR in mice) models, as well as patients with diabetes/pre-diabetes.

5. MATERIALS AND METHODS

5.1. Equipment used

A. The following equipment available in the Basic Science Laboratory, Department of Biochemistry, Christian Medical College were used:

a. Spectrophotometer (Shimadzu UV-1800, Shimadzu, Japan)

b. Gel documentation system (Flourochem E system, ProteinSimple, USA)

c. Gel documentation system (Flourochem SP, Alpha Innotech, USA)

d. Conventional PCR thermocycler (2720 Thermocycler), Applied Biosystems, USA

e. Real-time PCR thermocycler (Chromo4 DNA Engine, Bio-Rad, USA)

f. NanoDrop spectrophotometer (NanoDrop 2000c, Thermo Fisher Scientific, USA)

g. Elix and Milli Q ultra-pure water system (Millipore, USA)

h. Horizontal electrophoresis system (Hoefer, Thermo Fisher Scientific, USA)

i. SDS-PAGE and western blotting apparatus (Mini-PROTEAN 3, Bio-Rad, USA)

j. Refrigerated table-top centrifuge (MPW R 350 R, MPW, Poland)

k. Refrigerated table-top centrifuge (Rota 4R V/FM) centrifuge (Plasto Craft, India)

l. Microplate reader (iMARK microplate reader, BioRad, USA)

m. Mechanical homogenizer (Remi, Mumbai, India)

n. pH meter (EasyFive Plus, Mettler Toledo, USA)

o. Analytical Balance (Analytical Plus, Ohaus, USA)

p. Test tube roller (250 RM, Tarsons, India)

B. The following equipment available in the Core Facility, Centre for Stem Cell Research, Christian Medial College, Vellore, was used:

   a. Flow cytometer (BD FACS Aria III, BD Biosciences, USA)

   b. Fluorescence microscope (Leica DMI6000B, Leica Camera AG, Germany)

5.2. Materials

A. The following chemicals were obtained from Sigma, India:

   Acrylamide, adenosine diphosphate, AEBSF, ammonium acetate, ammonium chloride, ammonium molybdate, ammonium persulfate, aprotinin, beta mercaptoethanol, bovine serum albumin (BSA), bromophenod blue, chloroform, diethyl pyrocarbonate, desferrioxamine, dithiotretol, ethylenediamine tetraacetic acid (EDTA) disodium, dimethyl sulfoxide (DMSO), Dulbecco's modified Eagle's medium (DMEM), ethylene glycol-bis(β-aminoethyl ether) tetraacetic acid, ferric ammonium citrate (FAC), formaldehyde, formamide, guanidium hydrochloride, HEPES, iron (standard), leupeptin, MOPS, sodium bicarbonate, isopropanol, sodium dodecyl sulphate, sodium metavanadate, PBS tablets, pepstatin, phenol red, phenylmethane sulfonyl fluoride (PMSF), sodium azide, sodium pyruvate, TEMED, tergitol (NP-40), thioglycollic acid, tris aminomethane, Trizma base, trypan blue and Tri-reagent.

B. The following chemicals were obtained from Sisco Research Laboratories, India:

   Butanol, Coomassie brilliant blue, calcium chloride, dextrose, dinitro phenyl phosphate, glycine, potassium dihydrogen phosphate, potassium chloride, magnesium chloride, sodium acetate, disodium hydrogen phosphate, nicotinamide adenine dihydrogen phosphate

(reduced) (NADPH), sodium dihydrogen phosphate, sodium hydroxide, paraformaldehyde, sodium carbonate, sodium chloride, trichloroacetic acid and triton – X

C. The following chemicals were obtained from Qualigens Fine Chemicals, Mumbai, India: Glacial acetic acid, sulphuric acid, hydrochloric acid, methanol and nitric acid

D. Others chemical used: absolute alcohol (Hayman, England), agarose (Genei, Bangalore, India)

E. All cell culture equipment/consumables (including plates, pipettes, scrapers etc.) were obtained from Eppendorf, Germany and Tarsons, India.

F. All PCR-related consumables (96-well plates, strip tubes, caps etc.) were obtained from Axygen Scientific, Thermo Scientific, USA.

G. All disposable microtubes, pipette tips etc. were obtained from Tarsons, India.

H. Details of oligonucleotides (used for qPCR) and antibodies (used for western blotting and flow cytometry) are given in the methodology section of each study.

5.3. Methodology

Study 1: Iron induces basal activation of Akt but decreases its activation in response to insulin in mouse primary hepatocytes

Mouse primary hepatocytes were loaded with iron *in vitro* by incubation with ferric ammonium citrate (FAC). To study the effects of insulin, FAC-treated hepatocytes were incubated with insulin (10nM) for 5 minutes (for study of intracellular signaling events) or 3 h (for gene expression studies). Hepatic glucose production assays were carried out to provide a functional read-out of the effects of iron, both in the presence and absence of insulin.

Details of all methods used are provided in the methodology section of study 1 (page 78).

Study 2: Interactions between insulin resistance and dysregulated iron homeostasis, produced by high-fat feeding in mice: a time-course study

Male C57Bl/6 mice were fed a high-fat diet (HFD) or control diet for various time periods (up to 24 weeks). Glucose and insulin tolerance tests were carried out to monitor development of glucose intolerance and IR. Subsets of mice were euthanized after 4, 8, 12, 16, 20 or 24 weeks of feeding. Western blot analyses and qPCR were done to determine expression levels of various iron-related parameters in the liver, adipose tissue and duodenum. Iron content of various tissues was visualized, using perfusion Perls' Prussian blue staining. Iron content was also measured in the liver, spleen, gonadal white adipose tissue (gWAT) and skeletal muscle. Serum levels of iron, hepcidin, ferritin, insulin, adiponectin, triglycerides, C-reactive protein and interleukin-6 (IL6) were estimated.

Details of all methods used are provided in the methodology section of study 2 (page 126).

Study 3: Effect of high-fat diet-induced insulin resistance on erythroid maturation and erythroid regulators of hepcidin in the bone marrow in mice

Terminal erythroid differentiation (TED) was studied in the bone marrow and spleen from mice fed a control diet or HFD for various durations (as detailed in Study 2), using flow cytometry. In addition, erythroid (TER119-positive) cells were isolated from the bone marrow and used to determine gene expression of the putative erythroid regulators of hepcidin (erythroferrone [ERFE], growth differentiation factor –15 [GDF-15] and twisted gastrulation factor –1 [TWSG-1]). Serum levels of hemoglobin, GDF-15 and erythropoietin were estimated.

Details of all methods used are provided in the methodology section of study 3 (page 192).

Study 4: Dysregulated iron homeostasis in patients newly diagnosed with diabetes mellitus or pre-diabetes

Adult males who were newly diagnosed to have diabetes mellitus (n=40) or pre-diabetes (n=40), based on fasting plasma glucose (FPG) levels (as per the criteria of the American Diabetic Association [ADA]), were the subjects of the study. Men, who were found to be normoglycemic, using the criteria of the ADA, were recruited as control subjects. Anthropometric measurements were made on all subjects. Blood samples were obtained for measurement of hematological parameters, markers of iron status (ferritin, hepcidin, iron, total iron-binding capacity and transferrin saturation), C-reactive protein (CRP) (marker of inflammation) and insulin. Homeostatic model assessment–insulin resistance (HOMA-IR) and HOMA-β (indices of insulin

resistance and pancreatic insulin secretory capacity respectively), were calculated. In addition, reticulocytes were isolated from peripheral venous blood obtained from a sub-set of control and diabetic patients to determine gene expression of erythroferrone, a factor known to regulate hepcidin levels.

Details of all subjects who were part of this study and the various methods used are provided in the methodology section of study 4 (page 245).

5.4. Statistical analysis

Statistical Package for Social Scientists (SPSS), version 16.0, was used for all statistical analyses. The Shapiro-Wilk test was used to test for normality of distribution of data. For normally distributed data, one-way ANOVA followed by pair-wise comparisons using Bonferroni test was done. For skewed data, the Kruskal –Wallis test followed by pair-wise comparisons using Mann Whitney test was done. For correlational analysis, Pearson's correlation was used for normally distributed data and Spearman's correlation for skewed data. Multivariate analysis was done using linear regression. A p-value less than 0.05 was taken to indicate statistical significance in all cases.

STUDY 1

Iron induces basal activation of Akt but decreases its activation in response to insulin in mouse primary hepatocytes

1. Abstract

An iron-overloaded state has been reported to be associated with insulin resistance. On the other hand, conditions where iron overload occurs primarily in the liver (such as classical hemochromatosis) have been reported to be associated with increased insulin sensitivity. The reasons for these contradictory finding are unclear. In this context, the effects of increased intracellular iron *per se* on insulin signaling in hepatocytes are not known. This study was designed to address this lacuna.

Mouse primary hepatocytes were loaded with iron *in vitro* by incubation with ferric ammonium citrate (FAC). To study the effects of insulin, FAC-treated hepatocytes were incubated with insulin (10nM) for 5 minutes (for study of intracellular signaling events) or 3 h (for gene expression studies). Hepatic glucose production assays were carried out to provide a functional read-out of the effects of iron, both in the presence and absence of insulin.

Iron-loading of hepatocytes *in vitro* resulted in phosphorylation-mediated activation of Akt (with accompanying downstream phosphorylation of glycogen synthase kinase 3β and forkhead box O1) and AMP-activated protein kinase. This was associated with decreased basal as well as forskolin-stimulated gluconeogenesis (forskolin being a glucagon agonist). Iron attenuated forskolin-mediated induction of the key gluconeogenic enzyme, glucose-6-phosphatase. It also

decreased activation of the Akt pathway in response to insulin, by decreasing protein levels of insulin receptor substrates 1 and 2, resulting in insulin resistance.

Overall, these results show that increased intracellular iron appeared to have dual effects on insulin sensitivity in hepatocytes. It increased basal activation of the Akt pathway (in the absence of insulin), but decreased activation of this pathway in response to insulin.

2. Introduction:

Insulin resistance (IR) is the hallmark of type 2 diabetes mellitus (T2DM). Several lines of evidence suggest that iron plays a role in the pathogenesis of IR (10). For example, children with thalassemia major, who are treated with repeated blood transfusions and have increased body iron stores, develop hyperinsulinemia and IR before they develop diabetes (205). Aggressive iron chelation in thalassemics has reduced the incidence of diabetes in such patients (14). Further evidence for the role of iron in IR is provided by improvements in insulin sensitivity following phlebotomy, both in patients with T2DM (15) and in healthy individuals (16). Iron-deficient rats show increased peripheral glucose uptake in response to insulin (247,248). Phlebotomy or dietary iron restriction, in a rat model of T2DM, resulted in decreased glycated hemoglobin levels (18). Iron chelation significantly protected *ob/ob* mice from diabetes (19) and improved insulin signaling in the rat liver (244). On the other hand, mice fed a high-iron diet have been shown to develop insulin resistance (17).

Hereditary hemochromatosis refers to a group of conditions characterized by increased body iron stores, which results from inappropriately low levels of hepcidin, the central iron regulatory hormone (249). Although raised iron stores are associated with IR (as described above), other studies have shown that insulin sensitivity (based on measurements of plasma glucose and

insulin in an OGTT) was increased in patients with classical hemochromatosis and in mouse models of the condition (*Hfe*$^{-/-}$ mice) (11,246). The reason(s) for these apparently contradictory findings are not clear; they may be related to the fact that iron overload in hemochromatosis is primarily seen in the liver and not in other insulin-sensitive tissues, such as skeletal muscle and adipose tissue. Such differences in iron levels in tissues may potentially affect results from studies done in humans and animal models of hemochromatosis, as glucose tolerance *in vivo* is determined by factors that regulate insulin sensitivity in the liver and peripheral tissues. For example, insulin has been shown to suppress HGP indirectly by inhibiting lipolysis in adipose tissue and not only by acting directly on the liver (133). In this context, the effect of increased levels of iron *per se* on hepatic insulin signaling and HGP is unclear. Similarly, it has been shown that in mice fed a high-iron diet, AMPK is activated in the liver and skeletal muscle; this was associated with decreased HGP (245). However, it is not known whether the decrease in HGP in this context was a direct effect of increased levels of hepatic iron or mediated by the effects of iron overload in extra-hepatic tissues.

In the current study, the effects of high intracellular iron levels on insulin signaling and HGP in mouse primary hepatocytes were determined. It was chosen to study these effects *in vitro* in order to avoid confounding factors that are operational *in vivo* that would influence the effects of interest in this study.

3. Methods:

3.1. Animals

Male C57Bl/6 mice, aged between 10 and 12 weeks, were used for all the experiments. These were carried out with the approval of the Institutional Animal Ethics Committee at Christian Medical College, Vellore, India (IAEC No. 14/2013), in accordance with the regulations of the Committee for the Purpose of Control and Supervision of Experiments on Animals (CPCSEA), Government of India.

3.2. Isolation of mouse primary hepatocytes

Primary hepatocytes were isolated from 8-12 weeks old, male C57Bl/6 mice, using a modified collagenase perfusion method, as described earlier (250), with some modifications (251,252). Under terminal anesthesia, the inferior vena cava (IVC) of the mouse was cannulated using a 26G butterfly cannula. After successful cannulation, the portal vain was cut to allow blood to drain out. The liver was then perfused with 50 mL Hanks's buffered salt solution (HBSS), containing 25mM HEPES and 0.5 mM EGTA, at a rate of 5-8 mL/min. This was followed by perfusion with 60-75 mL of digestion solution (DMEM with 5 mM glucose, 15mM HEPES and 100 CDU/mL collagenase type IV [Worthington, UK]). Following digestion, the liver was excised and hepatocytes were liberated by gently tearing the capsule. The hepatocytes were passed through a 100 μm sieve filter, in order to remove tissue debris. The cells were washed thrice by adding serum-free DMEM, followed by centrifugation at 50*g* for 2 min (in order to remove hepatic non-parenchymal cells). The hepatocytes obtained in the pellet at the end of the centrifugations were re-suspended in DMEM with 10% fetal calf serum (FCS). Viability of the

isolated cells (as determined by trypan blue exclusion) was consistently found to be more than 90%. The cells were seeded in 6 or 12-well collagen-coated plates at a density of 3 x 10^4 cells per cm^2 and allowed to adhere to the bottom of the wells for 2 h.

3.3. Treatment of hepatocytes with iron, insulin and/or forskolin

Two hours after seeding, cells were washed with PBS and maintained in serum-free DMEM. Ferric ammonium citrate (FAC) was added to each well. The concentrations used were 0, 7.5, 75 or 750 μM concentrations. Incubations were carried out for 16 h. This was done to increase the intracellular iron content (253). To study the effects of insulin on control and FAC-treated hepatocytes, cells were washed with PBS at the end of the 16 hours of incubation. They were then treated with insulin (10nM) for 5 minutes (for study of intracellular signaling events) or 3 h (for gene expression studies). In a sub-set of hepatocytes treated with FAC (at 75μM) for 16 h, the cells were washed at the end of the incubations and then treated with desferrioxamine (DFO) (250μM) for 6 h, in order to chelate iron.

3.4. Determination of cell viability

At the end of the incubations with FAC, the viability of the cells was determined by MTT assay, estimation of lactate dehydrogenase (LDH) activity in the medium and by ethidium homodimer-1 (EthD-1) staining.

3.4.1 MTT (3-[4,5-dimethylthiazol-2-yl]-2,5-diphenyltetrazolium bromide) assay

Metabolically active and viable cells reduce MTT (yellow) to insoluble formazan crystals (purple) which are solubilized in isopropanol. The absorbance at 570 nm is indicative of viability of cells (254).

For the MTT assay, hepatocytes were seeded in 12-well plates and incubated for 16 h, either with or without FAC at various doses (as described in sections 3.2 and 3.3). Following this, cells were washed twice with PBS; they were then incubated with 700 μL serum-free DMEM (without phenol red) containing MTT (0.5 mg/mL final conc.), for 4 h. After incubation, the medium was carefully removed and discarded. The MTT formazan formed was dissolved in 700 μL of isopropanol and its absorbance was measured at 570 nm. Results were expressed as fold-change compared to control cells that were not treated with FAC.

3.4.2 Lactate dehydrogenase (LDH) activity in the medium

LDH is a cytosolic enzyme that is released into the medium when the cell membrane is damaged. Hence, LDH activity in the medium is often used as a marker of cellular damage in cells in culture (255)

To estimate LDH activity in the medium, 0.1 mL of the medium was added to a reaction mixture, containing 2.7 mL of 0.2 M Tris (pH 7.3), 0.1 mL of 6.6 mM NADH and 0.1 mL of 30 mM sodium pyruvate. Changes in absorbance at 340 nm were recorded every minute for 5 minutes, using a UV- spectrophotometer (Shimadzu UV-1800, Japan). LDH activity was calculated using the molar absorptivity for NADH of $6.22 \times 10^3\ M^{-1}cm^{-1}$.

3.4.3 Ethidium homodimer-1 (EthD-1) staining

EthD-1 is a cell-impermeant dye, which is non-fluorescent when it remains extracellular in the absence of damage to cellular membranes. EthD-1 enters the cell under conditions where the cell membrane is damaged and binds to DNA in the nucleus, producing a bright red fluorescence. (255).

Primary hepatocytes (in 12-well plates), treated with various doses of FAC (as described in section 3.2 and 3.2), were washed twice with PBS to remove all traces of the medium. Cells were then treated with 250 μL of PBS containing EthD-1 at a final concentration of 4 μM, and incubated in the dark for 30 min. Following this, cells were washed with PBS and viewed under a fluorescence microscope (Leica DMI6000B) (excitation wavelength = 528 nm, emission wavelength = 617 nm). Cells treated with 70% methanol for 30 min (dead cells) were used as positive control; dead cells showed bright red fluorescence.

3.5. Calcein fluorescence quenching by intracellular labile iron

After treatment with or without FAC, cells were washed twice with PBS and incubated with calcein-AM (2 μM final concentration) for 30 min. Following this, cells were washed again with PBS. Fluorescence in the cells was visualized under a fluorescence microscope (Leica DMI6000B), using the standard fluorescein filter. Intracellular labile iron is known to quench calcein fluorescence (256); hence, a decrease in green fluorescence was taken to indicate increased intracellular labile iron.

3.6. Hepatocyte glucose production assay:

Hepatocyte glucose production assays were carried out as described earlier (251). Primary hepatocytes, incubated with or without FAC for 16 h, were washed twice with PBS and incubated in glucose and phenol red-free DMEM (D5030, Sigma-Aldrich, USA) for 1 hour (in order to deplete glycogen). Following this, cells were incubated in glucose production buffer, which consisted of glucose-free, phenol red-free DMEM supplemented with 44 mM $NaHCO_3$, 2 mM L-glutamine and 10 nM dexamethasone. Lactate/pyruvate (20mM/2mM) or glycerol (10mM), as appropriate, was added as the gluconeogenic substrate. In some subsets of wells, insulin (10 nM) and/or forskolin (activator of adenylyl cyclase and hence, mimics the action of glucagon) (25 μM) were added. The use of forskolin provided a positive control. After 3, 6, 9 and 12 hours, an aliquot of the medium (60 μL) was removed for estimation of glucose, by the glucose oxidase-peroxidase (GOD-POD) method. At the end of 12 h, cells were lysed with RIPA buffer. The protein content of the lysate was estimated, using the Pierce BCA protein assay kit (cat. no. 23225, Thermo Fisher Scientific, USA).

3.7. Determination of gene expression by quantitative real-time PCR (qPCR):

Quantitative RT-PCR was used to determine the mRNA expression of genes of interest.

3.7.1 RNA isolation

Primary hepatocytes, in 6-well plates, were homogenized in Tri-Reagent (Sigma) (0.5 mL per well) and transferred to RNAase-free microfuge tubes. RNA was isolated according to the manufacturer's instructions. Briefly, 0.1 mL of chloroform (0.2 mL per mL of Tri-Reagent) was added to each tube; the contents of each tube were mixed vigorously, using a vortex mixer. The

tubes were then incubated on ice for 15 min. They were then centrifuged at 12,000*g* at 4°C for 15 min. Following centrifugation, the samples separated into 3 distinct layers (lower red organic phase containing proteins, middle white interphase containing genomic DNA and upper colorless aqueous phase containing RNA). The upper aqueous phase was transferred into fresh tubes, and 0.25 mL of isopropanol (0.5 mL per mL of Tri-Reagent) was added to precipitate RNA. Samples were mixed well and incubated on ice for 5-10 min. After incubation, the samples were centrifuged at 12000*g* for 10 min at 4°C. The precipitated RNA settled at the bottom and on the sides of the tube. The supernatant was discarded; the RNA precipitate was washed by adding 0.5 mL of 75% ethanol (1 mL per mL of Tri-Reagent). The tubes were then centrifuged at 7500*g* for 5 min at 4°C. The supernatant was discarded and RNA was allowed to dry on ice for 10-15 min. Following this, it was dissolved in 30-50 µL of DEPC water (depending upon the size of the pellet). Samples were incubated at 60°C for 5 min to help the RNA dissolve.

3.7.2. Quantification of RNA and assessment of purity

RNA was quantified using a NanoDrop 2000c spectrophotometer (Thermo Fisher Scientific, USA). In order to do this, 1–1.5 µL of the dissolved RNA was placed on the pedestal of the instrument, to obtain the spectral output and to measure optical density at 260, 280 and 230 nm. Nucleic acids such as DNA and RNA absorb maximally at 260 nm. An optical density of 1.0 at 260 nm indicates RNA concentration of 40 µg/mL; the RNA content of each sample was calculated accordingly.

The purity of the isolated RNA was assessed based on the overall spectral output as well as the 260/280 and 260/230 ratios (257). Samples with a normal spectrum with a single peak at 260 nm as well as 260/280 and 260/230 ratios > 1.8 were considered to be of acceptable purity for

downstream applications (Fig 6.1.1-A). A low 260/280 ratio indicated contamination by phenol or protein. On the other hand, a low 260/230 ratio indicated contamination by constituents of the extraction reagent (such as guanidine).

In cases where the 260/280 and/or 260/230 ratio was lesser than 1.8, the samples were subjected to further purification by ethanol precipitation. For this, samples were made up to 100 µL with DEPC-water; to this, 10 µL of 3M sodium acetate and 220 µL of ice-cold 100% ethanol were added and mixed well. Samples were incubated at -20°C for 1-2 hours (or overnight). Following this, they were centrifuged at 12,000*g* for 10 min at 4°C. The supernatant was discarded and the RNA pellet obtained was washed with 0.5 mL of 75% ethanol. The samples were then centrifuged at 12000*g* for 10 min at 4°C. The RNA pellet was allowed to dry on ice for 5-10 min and re-dissolved in sufficient volume of DEPC-water. The quantity of RNA obtained was estimated using the NanoDrop spectrophotometer, and purity was assessed as described earlier.

3.7.3 Assessment of integrity of isolated RNA by agarose gel electrophoresis

The integrity of isolated RNA was assessed by denaturing RNA agarose gel electrophoresis (258). Intact RNA electrophoretically resolves into two distinct bands corresponding to 28S and l8S rRNAs. The appearance of these two bands, with the 28S band being approximately twice as dense as the 18S band, indicates that the RNA in the sample is intact (Fig 6.1.1-B). Degraded samples form a smear, rather than 2 distinct bands as described above. Presence of fluorescence within the well suggests contamination with genomic DNA. Such samples were subjected to DNAase treatment, using a commercially available kit as per manufacturer's instructions (cat. no. AM1907, Ambion Turbo DNA-free kit, Thermo Fisher Scientific, USA). RNA samples were either used immediately for cDNA construction or stored at -70°C till further use.

Figure 6.1.1

A

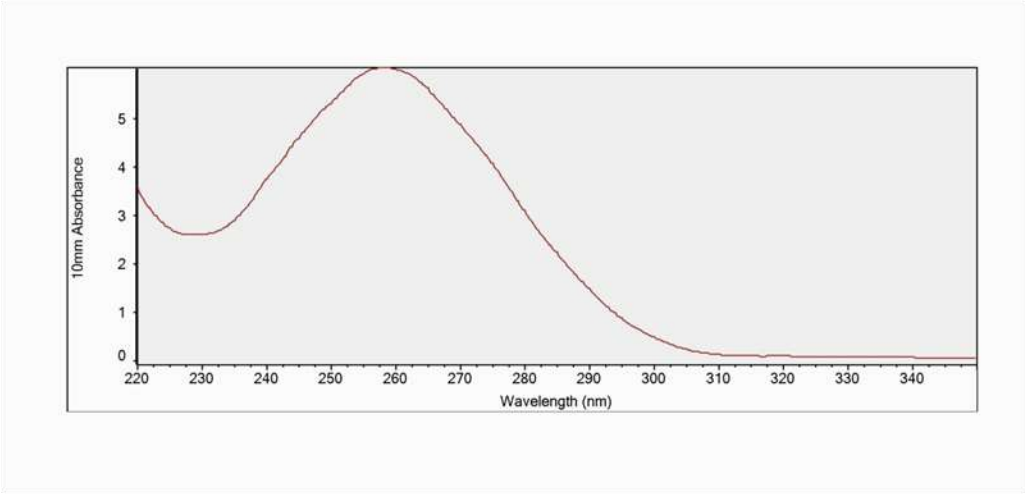

B

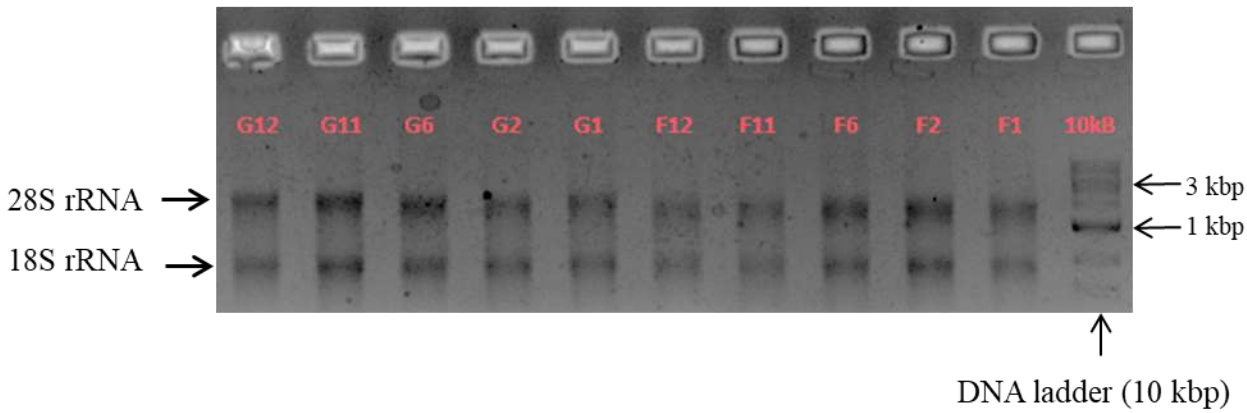

Figure 6.1.1

A: Representative image showing the spectral output of 'pure' RNA showing a single peak at 260 nm, with 260/280 and 260/230 ratios > 1.8.

B: Representative image of RNA gel showing two distinct bands corresponding to 28S and 18S rRNA. Presence of these bands indicate integrity of RNA in the sample. RNA samples shown here were isolated from primary hepatocytes.

3.7.4 Complementary DNA (cDNA) construction

The Reverse Transcriptase Core Kit (cat. no. RT-RTCK-03, Eurogentec, Belgium) was used for construction of cDNA, as per manufacturer's instructions. One microgram of the isolated RNA was added to a reaction mixture that consisted of 5 mM $MgCl_2$, 500 µM of each dNTP, 2.5 µM oligo d(T) primer, 0.4 U/µL RNAase inhibitor and 0.25 U/µL reverse transcriptase (EuroScript RT) in a total volume of 20 µL. Samples were incubated at 48°C for 30 minutes to complete the reverse transcription reaction. This was followed by incubation at 95°C for 5 minutes to inactivate the reverse transcriptase enzyme. cDNA samples were diluted 1:10, using DEPC-water, prior to the PCR assay. All samples were stored at -20C°.

3.7.5 Quantitative PCR reactions

Quantitative PCR reactions were carried out using the Takyon No ROX SYBR Master Mix dTTP Blue kit (cat. no. UF-NSMT-B0701, Eurogentec, Belgium), according to manufacturer's instructions. All PCR reactions were run in duplicate in 96-well plates. Two microliters of 1:10 diluted cDNA was added to a reaction mixture that consisted of the 2x Takyon master mix (5 µL) and forward and reverse primers (at a final concentration of 250 nM), in a total volume of 10 µL. The reactions were carried out on a BioRad Chromo4 thermal cycler. The conditions were: 95°C for 3 min (Takyon DNA polymerase activation) followed by 40 cycles of 95°C for 10 seconds (denaturation) and 60°C for 60 seconds (extension). The expression levels of the genes of interest were normalized to *Rpl19,* which was used as the reference gene. All primers were synthesized commercially and were purchased from Sigma, India. Sequences of all primers used are listed in Table 6.1.1. Primer pairs were standardized and melting curve analyses were done to validate the specificity and efficiency of qPCR reactions.

Table 6.1.1: Primers used for qPCR

Sl. No.	Gene	Accession number	Primer sequence	Amplicon size (bp)
1	Acaca1	NM_133360.2	5'-GCCTCTTCCTGACAAACGAG-3' 5'-TGACTGCCGAAACATCTCTG-3'	239
2	Fasn	NM_007988.3	5'-AAGGCTGGGCTCTATGGATT-3' 5'-TGAGGCTGGGTTGATACCTC-3'	177
3	G6pc	NM_008061.3	5'-TCTGTCCCGGATCTACCTTG-3' 5'-GTAGAATCCAAGCGCGAAAC-3'	172
4	Irs1	NM_010570.4	5'-CCAGCCTGGCTATTTAGCTG-3' 5'-CCCAACTCAACTCCACCACT-3'	174
5	Irs2	NM_001081212.1	5'-GTAGTTCAGGTCGCCTCTGC-3' 5'-CAGCTATTGGGACCACCACT-3'	190
6	Gck	NM_010292.4	5'-TTGCAACACTCAGCCAGACA-3' 5'-TGCTCTACCAGAGTCAACGAC-3'	147
7	Rpl19	NM_009078.2	5'- ATGAGTATGCTCAGGCTACAGA-3' 5'- GCATTGGCGATTTCATTGGTC-3'	104

The Minimum Information for Publication of Quantitative Real-Time PCR Experiments (MIQE) check-list and qPCR primer validation data has been provided in Appendix I and II.

3.8. Western blotting:

Primary hepatocytes were homogenized in ice-cold RIPA buffer (Tris-HCl 10mM, NaCl 140mM, EDTA 1.5mM, sodium deoxycholate 0.1%, Triton-X 1%, SDS 0.1%, pH 8.0), containing a cocktail of protease inhibitors (cat. no. 5872S, Cell Signaling Technology, USA). Homogenized samples were centrifuged at 14,000*g* for 20 min at 4°C to remove tissue debris. Protein content in the supernatant obtained was estimated using the Pierce BCA protein assay kit (cat. no. 23225, Thermo Fisher Scientific Inc., USA). The samples were stored at -70°C till further use.

For electrophoretic separation of proteins, samples were heated at 95°C for 5 minutes in Laemmli buffer. They were loaded on 10% SDS-PAGE gels (25 μg protein) and subjected to electrophoresis at 80V for 90-120 min. Separated proteins were transferred onto PVDF membrane (0.45 μm pore size, Immobilon-P, Millipore, Merck, Germany) at 80V over 2 h. After completion of transfer, the membrane was washed with TBS-T (25 mM Tris pH 7.4, 3 mM KCl, 140 mM NaCl, 0.02% Tween-20) and then blocked with 5% BSA (in TBS-T), at room temperature for 2 h. After blocking, the membrane was cut into strips based on the molecular weight of the proteins of interest and each strip was probed with the appropriate primary antibody, overnight at 4°C. Following incubation with the specific primary antibody, membranes were washed thrice (5 min per wash) with TBS-T and further probed with appropriate secondary antibody, over 2 hours at room temperature. After probing with the secondary antibody, the membrane was washed again with TBS-T. Bands obtained were detected using SuperSignal

West Dura Extended Duration chemiluminescence substrate kit (cat. no. 34075, Thermo Fisher Scientific, USA), according to the manufacturer's instructions. The intensities of the bands were quantified using ImageJ software (NIH, USA); they were normalized to that of β-actin, which was used as a loading control. Sources and dilutions of primary and secondary antibodies used are shown in Table 6.1.2.

3.9. Estimation of iron levels

The iron content in the hepatocytes was measured by a spectrophotometric assay, as described previously (259), with certain modifications. Hepatocytes were lysed in RIPA buffer and lysates were centrifuged at 14,000*g* for 20 minutes. Forty microlitres of each supernatant were added to 40 µL of acid reagent (3M hydrochloric acid and 10% trichloroacetic acid), mixed and incubated for 30 min at room temperature. Following acid digestion, samples were centrifuged at 10,000*g* for 10 min. Ten microlitres of the supernatant (acid extract) was mixed with 190 µL of chromogen reagent (4M sodium acetate containing 0.01% bathophenanthrolinedisulphonic acid and 0.1% thioglycollic acid). The absorbance of the reaction mixture was measured at 540 nm after an incubation period of 15 min, using iMark microplate reader (BioRad, USA), and compared to readings from a set of iron standards (Sigma, USA). The final results were normalized to the protein content of the RIPA lysates used.

3.10. Statistical analyses:

Statistical Package for Social Scientists (SPSS), version 16.0, was used for all statistical analyses. The Kruskal-Wallis test was used to look for effects of the various treatments on the parameters of interest. Pair-wise comparisons were done using the Mann-Whitney test.

Table 6.1.2: Primary and secondary antibodies

Sl. No.	Protein	Primary antibody (source and dilution)	Secondary antibody#
1	Phospho-AKT (Thr308)	CST* (#9275) 1: 1000	Anti-rabbit
2	Phospho-AKT (Ser473)	CST (#9271) 1: 1000	Anti-rabbit
3	AKT	CST (#9272) 1: 1000	Anti-rabbit
4	Phospho-GSK3β (Ser9)	CST (#5558) 1: 1000	Anti-rabbit
5	GSK3β	CST (#9315) 1: 1000	Anti-rabbit
6	Phospho-FoxO1 (Ser256)	CST (#9461) 1: 1000	Anti-rabbit
7	FoxO1	CST (#9454) 1: 1000	Anti-rabbit
8	Phospho-AMPKα (Thr172)	CST (#2531) 1: 1000	Anti-rabbit
9	AMPKα	CST (#2532) 1: 1000	Anti-rabbit
10	Phospho-ACC (Ser79)	CST (#11818) 1: 1000	Anti-rabbit
11	ACC	CST (#3662) 1: 1000	Anti-rabbit
12	IRS1	CST (#2390) 1: 1000	Anti-rabbit
13	Phospho-IRS1 (Ser307)	CST (#2381) 1: 1000	Anti-rabbit
14	Phospho-IRS1 (Ser789)	CST (#2389) 1: 1000	Anti-rabbit
15	IRS2	CST (#4502) 1: 500	Anti-rabbit
16	Phospho-SAPK/JNK (Thr183/Tyr185)	CST (#4668)1: 1000	Anti-rabbit
17	Ferritin (light chain)	Santa Cruz Biotechnology (sc-14420) 1:1000	Anti-goat
18	TfR1	Invitrogen (#13-6800) 1: 500	Anti-mouse
19	Beta-actin	Sigma-Aldrich (#A5316) 1: 5000	Anti-mouse

* CST – Cell Signaling Technology, USA, # All secondary antibodies were purchased from Pierce (Thermo Fisher Scientific, USA)

Correlation analysis was done by Spearman's correlation test. A p value of less than 0.05 was used to indicate statistical significance in all cases. Data was obtained from at least three independent experiments (primary hepatocytes isolated from at least 3 mice), with each done in duplicates or triplicates, under the specified conditions.

4. Results:

4.1. Treatment of hepatocytes with FAC increased intracellular iron content

Primary hepatocytes, treated with FAC, showed increases in cellular iron content (Fig. 6.1.2-A). This was associated with increased protein levels of ferritin (Fig. 6.1.2-B) and decreased levels of transferrin receptor 1 (TfR1) protein (Fig 6.1.2-C), both of which are indicative of increased iron levels in the cells. Intracellular labile iron quenches calcein fluorescence and the degree of quenching is indicative of the intracellular labile iron pool (LIP) (256). Fluorescence microscopic imaging showed a decrease in calcein fluorescence in hepatocytes treated with FAC, indicating an increase in the LIP (Fig.6.1.3). These results show that FAC treatment resulted in an increase in intracellular iron, with a concomitant increase in the LIP.

FAC treatment did not affect cell viability, as determined by the MTT assay (Fig. 6.1.4-A). Cell viability was also assessed by estimating LDH in the medium used for cell culture. There was a small, but significant, increase in LDH activity in the medium, at the highest dose of FAC used (750 μM) (Fig. 6.1.4.-B). Similarly, fluorescence microscopic imaging of cells stained with ethidium homodimer-1 showed a small increase in red fluorescence (indicative of cell damage) only in cells treated with 750 μM FAC (Fig. 6.1.5). There was, however, no change seen in cells treated with 7.5 and 75 μM FAC compared to untreated cells. These 2 concentrations (and not the 750 μM concentration) are the ones at which effects of interest were seen in the present study, as will be shown in the results described below.

Figure 6.1.2

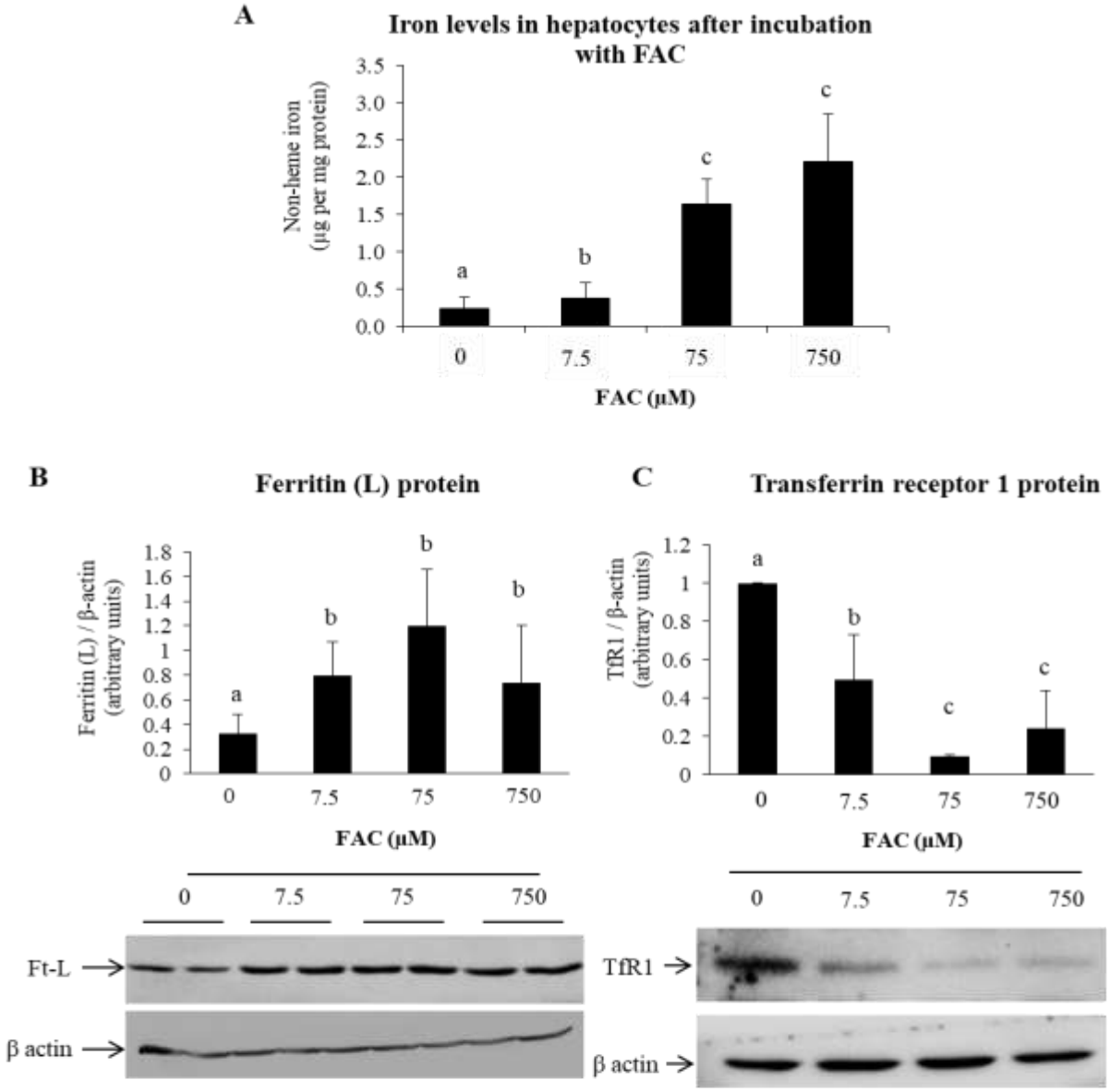

Figure 6.1.2: Effect of treatment with FAC on intracellular iron content

A: Intracellular iron levels estimated using a bathophenanthrolene-based colorimetric assay. B and C: Representative images and densitometric quantification of western blots for ferritin (light chain) (B) and TfR1 (C).

Data represents mean ± SD of results obtained from at least three independent experiments (primary hepatocytes isolated from at least 3 mice with each done in duplicates or triplicates, under the specified conditions. Bars in each panel, marked with dissimilar alphabets, indicate data that are significantly different from one another. A p value <0.05 was taken to indicate statistical significance in all cases.

Figure 6.1.3

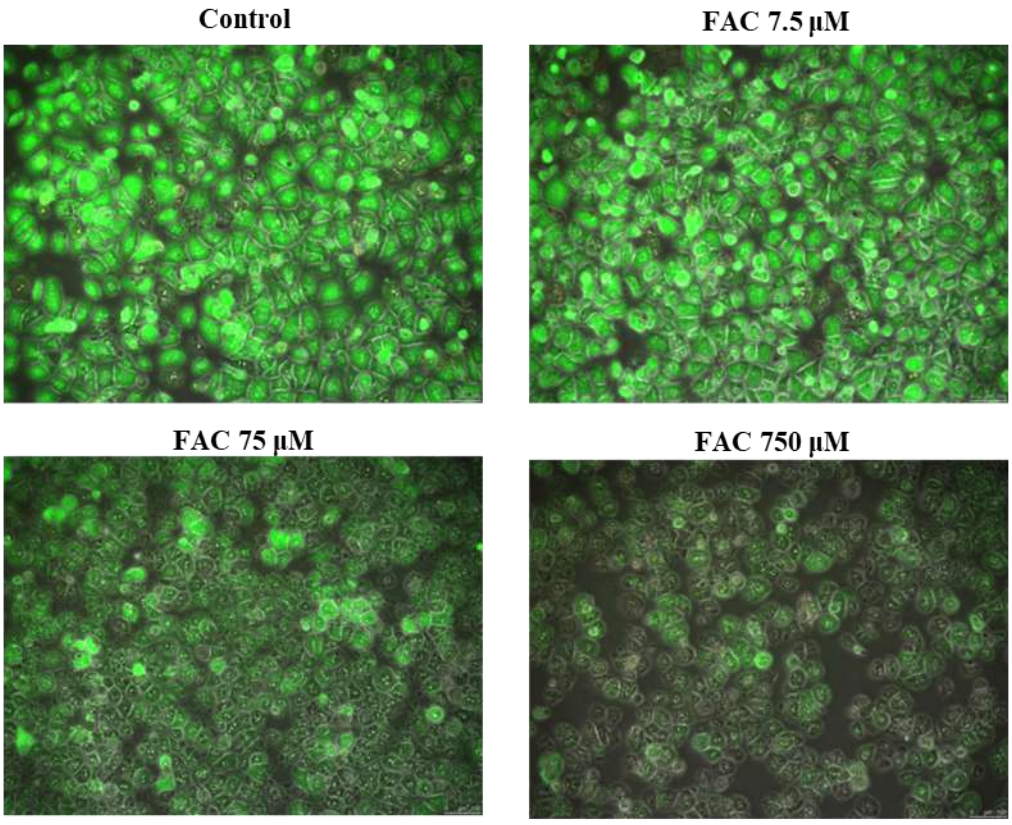

Figure 6.1.3 Effect of treatment with FAC on intracellular labile iron pool (LIP)

Representative images of primary hepatocytes treated with FAC (as indicated) for 16 h and then stained with green fluorescent calcein-AM to assess intracellular LIP. A decrease in green fluorescence indicates an increase in LIP.

Figure 6.1.4

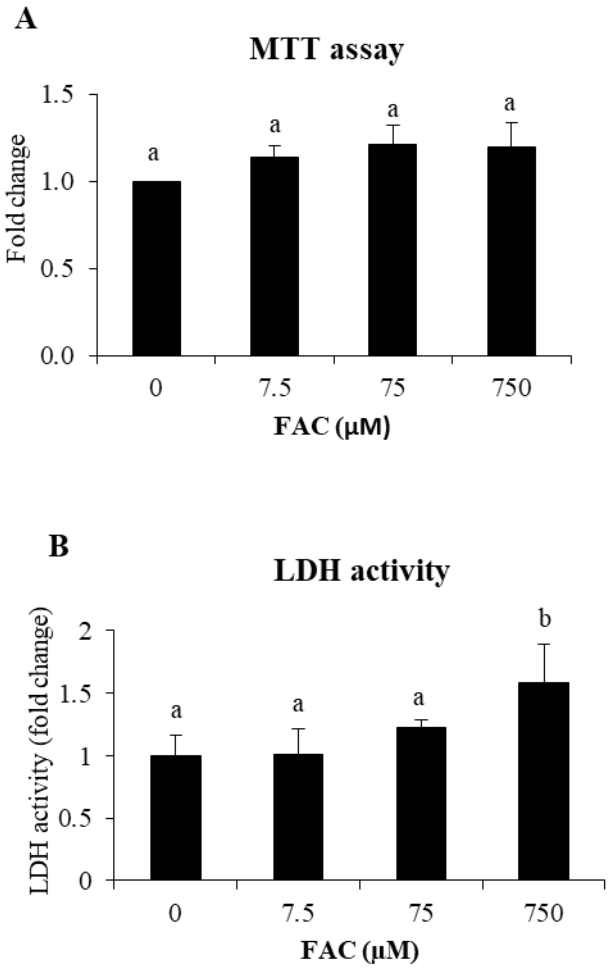

Figure 6.1.4: Effect of treatment with FAC on cell viability

A: MTT assay. B: LDH activity in the medium.

Data are shown as fold-change compared to control (hepatocytes not treated with FAC). Results obtained from three independent experiments (primary hepatocytes isolated from 3 mice), with each done in triplicates, under the specified conditions. Bars in each panel, marked with dissimilar alphabets, indicate data that are significantly different from one another. A p value <0.05 was taken to indicate statistical significance in all cases.

Figure 6.1.5

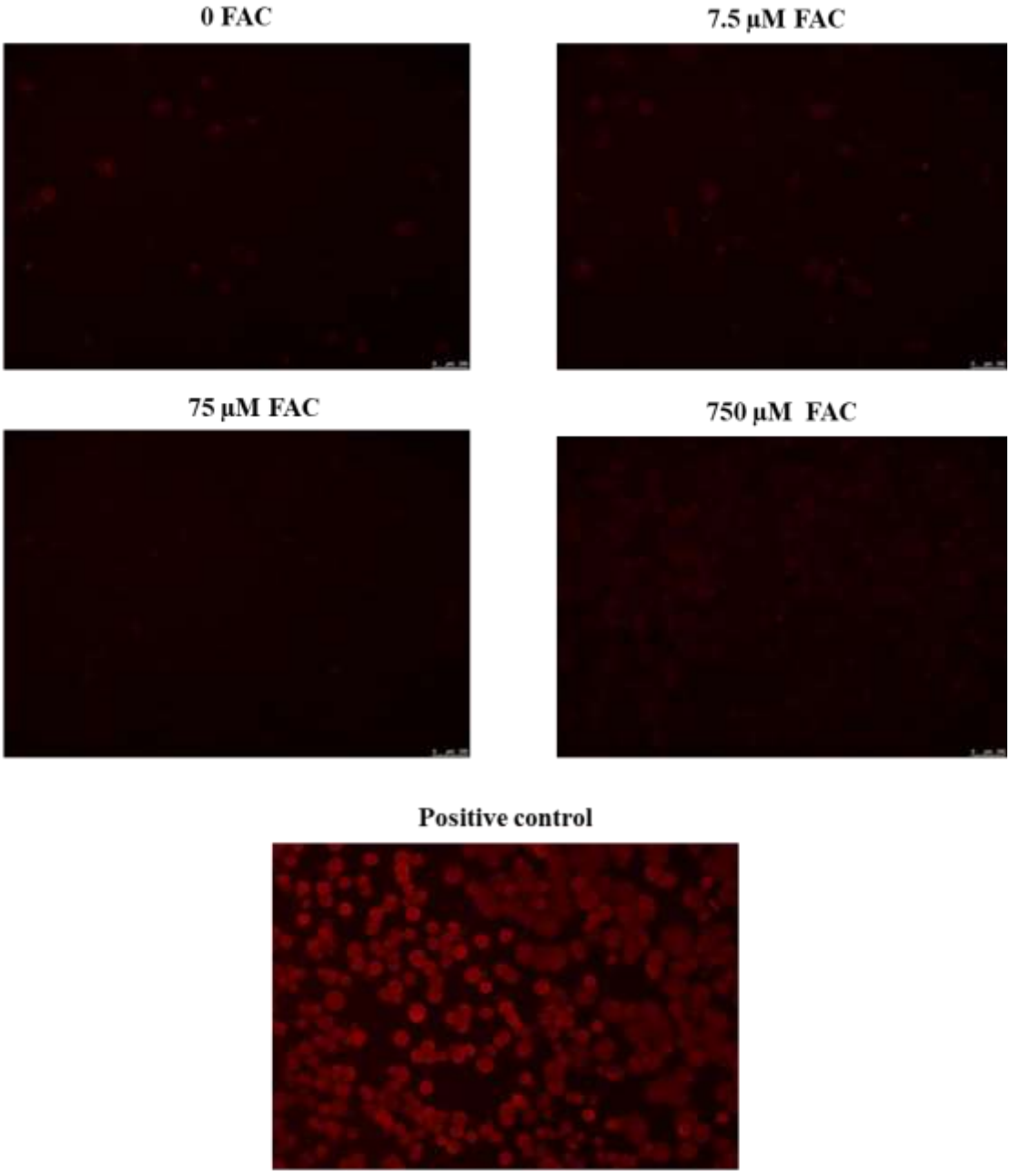

Figure 6.1.5: Effect of treatment with FAC on cell viability (ethidium homodimer-1 staining)

Representative images of primary hepatocytes treated with FAC (as indicated) for 16 h and then stained with red-fluorescent ethidium homodimer-1. An increase in red fluorescence indicates loss of plasma membrane integrity. Positive control consists of primary hepatocytes which were treated with 70% methanol for 30 min prior to staining.

4.2. Treatment with FAC increased phosphorylation of Akt and its downstream targets, Gsk3β and FoxO1

Activation of Akt involves phosphorylation at Thr308 and Ser473 (260). FAC treatment resulted in increases in phosphorylation of Akt at both Thr308 and Ser473, without affecting total Akt levels (Fig. 6.1.6-A, B). Increased phosphorylation of downstream targets of Akt activation, viz. Gsk3β (Fig. 6.1.7-A) and FoxO1 (Fig. 6.1.7-B), was also seen. Incubation of hepatocytes with DFO (250μM), an iron chelator, for 6 h after pre-treatment with FAC (for 16 h) resulted in significant decreases in intracellular iron content (Fig. 6.1.8-A) and was associated with attenuation of iron-induced Akt phosphorylation (Fig. 6.1.8-B).

4.3. Treatment with FAC activated AMP-activated kinase (AMPK)

Since AMPK activation is known to trigger the phosphorylation and activation of Akt and GSK3β in the liver (261), the effect of iron on AMPK was examined in the current study. Treatment with FAC induced an increase in phosphorylation of AMPK at Thr172 (Fig. 6.1.9-A). The downstream target of AMPK, acetyl CoA carboxylase (ACC), was also found to be phosphorylated (at Ser79) (Fig. 6.1.9-B). Activated AMPK is known to phosphorylate and inhibit sterol response element-binding protein 1c (SREBP-1c), resulting in suppression of lipogenesis, by decreasing mRNA levels of ACC (*Acaca*) and fatty acid synthase (*Fasn*) (262,263). In addition, SREBP-1c inhibition results in induction of *Irs2* but not of *Irs 1* (264). In keeping with these reported effects, in the present study treatment with FAC was found to reduce mRNA expression of *Acaca* and *Fasn*, and increase the expression of *Irs2* (Fig. 6.1.10–A, B and C). No significant changes were seen in *Irs1* expression (Fig. 6.1.10-D).

Figure 6.1.6

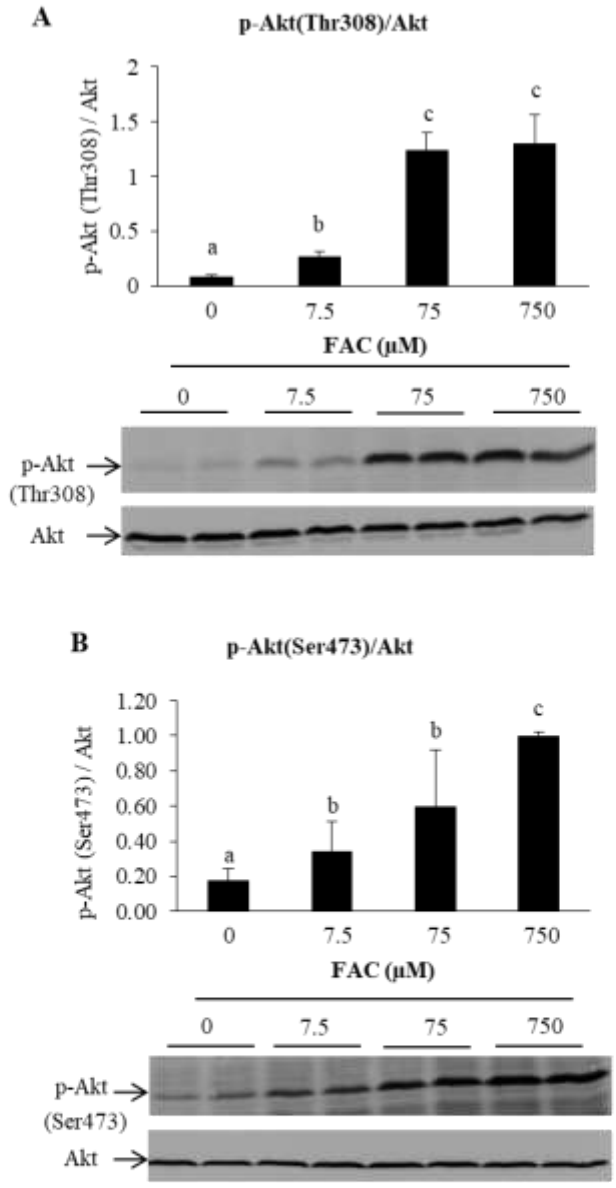

Figure 6.1.6: Effect of treatment with FAC on phosphorylation of Akt

Mouse primary hepatocytes were treated with FAC at various concentrations (as indicated) for 16 hours. Representative images for western blots and densitometric quantification of the bands obtained are shown for p-Akt [Thr308]/Akt (A) and p-Akt [Ser473]/Akt (B).

Data represents mean ± SD of results obtained from at least three independent experiments (primary hepatocytes isolated from at least 3 mice), with each done in duplicate, under the specified conditions. Bars in each panel, marked with dissimilar alphabets, indicate data that are significantly different from one another. A p value <0.05 was taken to indicate statistical significance in all cases.

Figure 6.1.7

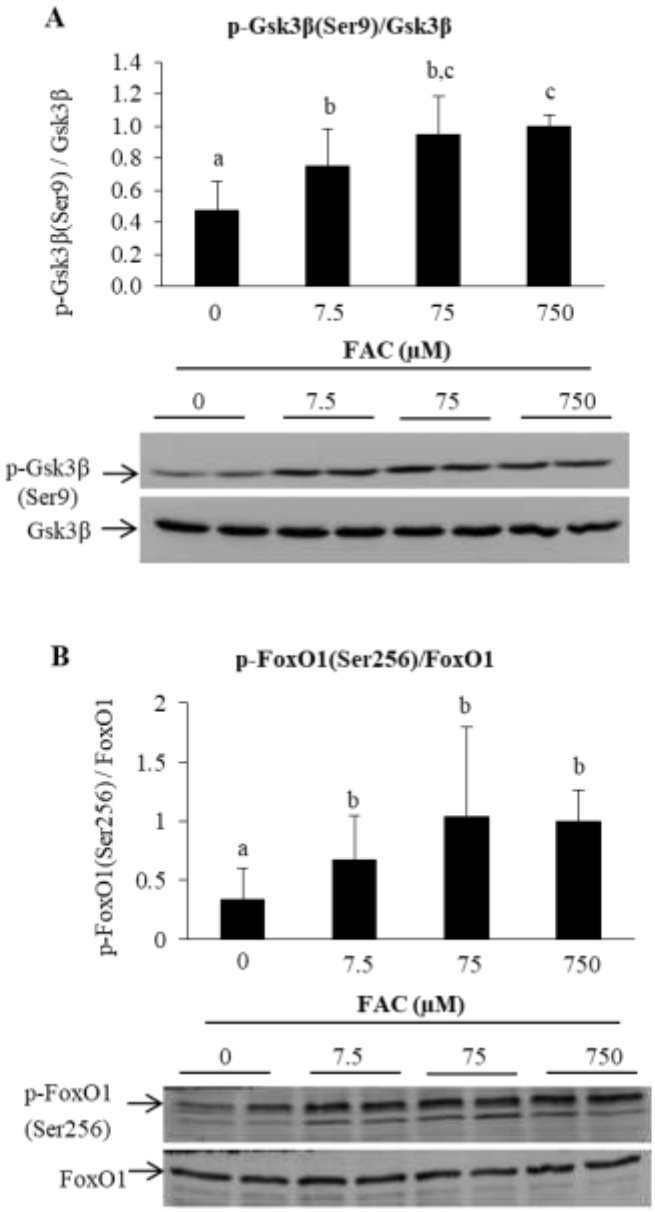

Figure 6.1.7: Effect of treatment with FAC on phosphorylation of Gsk3β and FoxO1

Mouse primary hepatocytes were treated with FAC at various concentrations (as indicated) for 16 hours. Representative images for western blots and densitometric quantification of the bands obtained are shown for p-Gsk3β [Ser9]/Gsk3β (A) and p-FoxO1 [Ser256]/FoxO1 (B).

Data represents mean ± SD of results obtained from at least three independent experiments (primary hepatocytes isolated from at least 3 mice), with each done in duplicate, under the specified conditions. Bars in each panel, marked with dissimilar alphabets, indicate data that are significantly different from one another. A p value <0.05 was taken to indicate statistical significance in all cases.

Figure 6.1.8

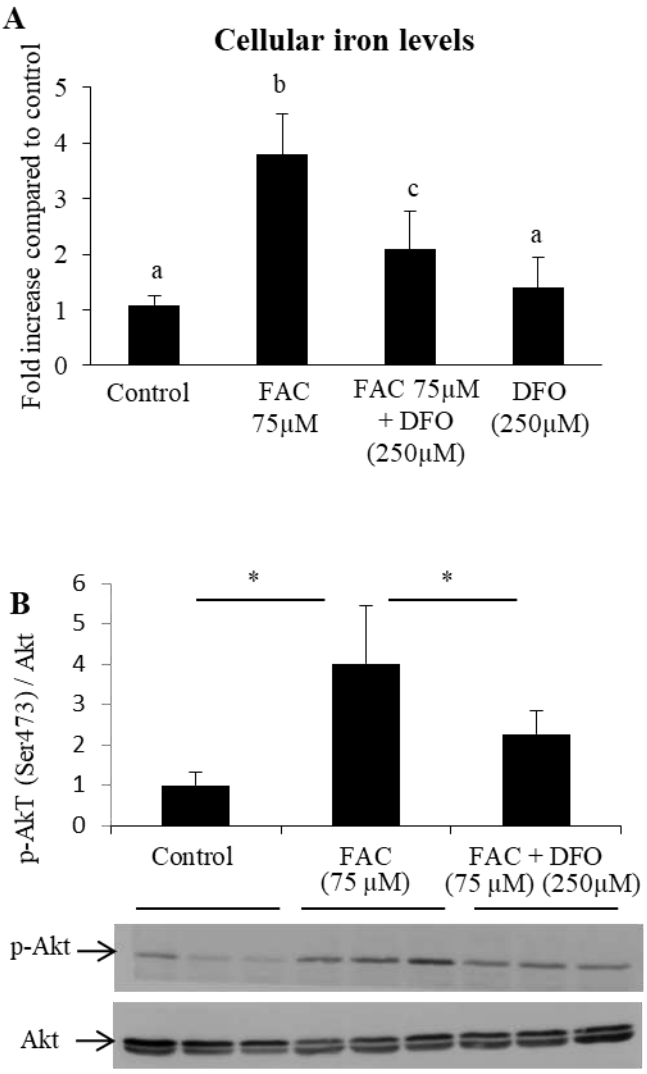

Figure 6.1.8: Effect of iron chelation in FAC-treated cells on cellular iron content and Akt phosphorylation

Hepatocytes treated with FAC (75 µM) for 16 hours were further treated with DFO (250 µM) for 6 hours. Intracellular iron content estimated at the end of the incubation periods (A) and representative images and densitometric quantification of the bands for p-Akt (Ser473)/Akt (B) are shown.

Data represents mean ± SD of results obtained from at least three independent experiments (primary hepatocytes isolated from at least 3 mice), with each done in duplicate, under the specified conditions. Bars in each panel, marked with dissimilar alphabets, indicate data that are significantly different from one another. A p value <0.05 was taken to indicate statistical significance in all cases.

Figure 6.1.9

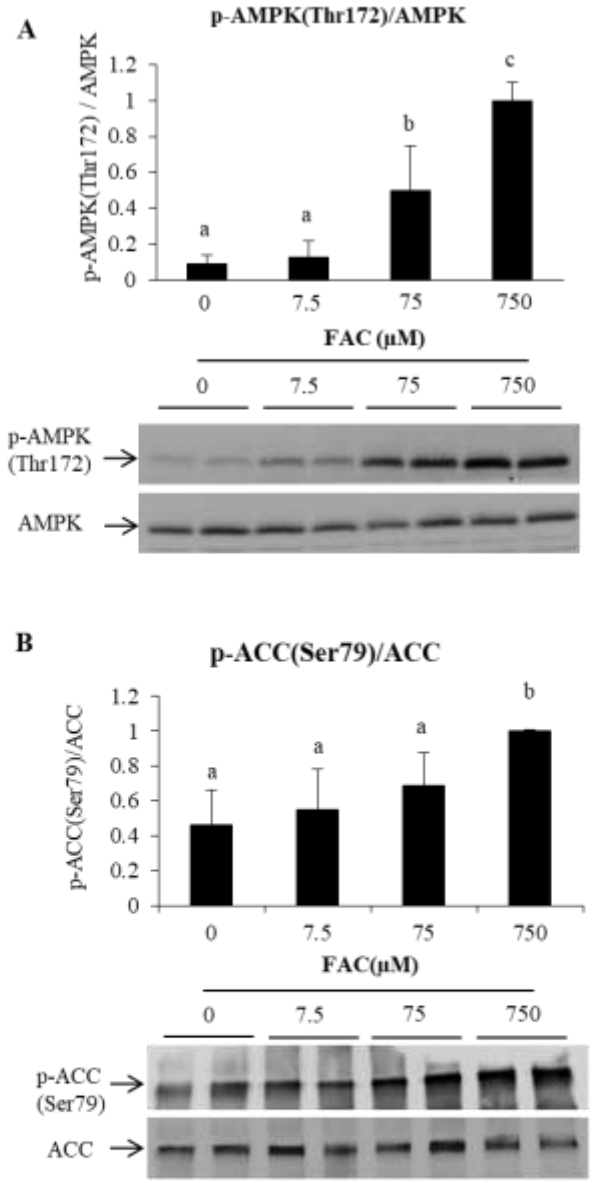

Figure 6.1.9: Effect of treatment with FAC on phosphorylation of AMPK and ACC

Mouse primary hepatocytes were treated with FAC at various concentrations (as indicated) for 16 hours. Representative images for western blots and densitometric quantification of the bands obtained are shown for p-AMPK (Thr172)/AMPK (A) and p-ACC (Ser79)/ACC (B).

Data represents mean ± SD of results obtained from at least three independent experiments (primary hepatocytes isolated from at least 3 mice), with each done in duplicate, under the specified conditions. Bars in each panel, marked with dissimilar alphabets, indicate data that are significantly different from one another. A p value <0.05 was taken to indicate statistical significance in all cases.

Figure 6.1.10

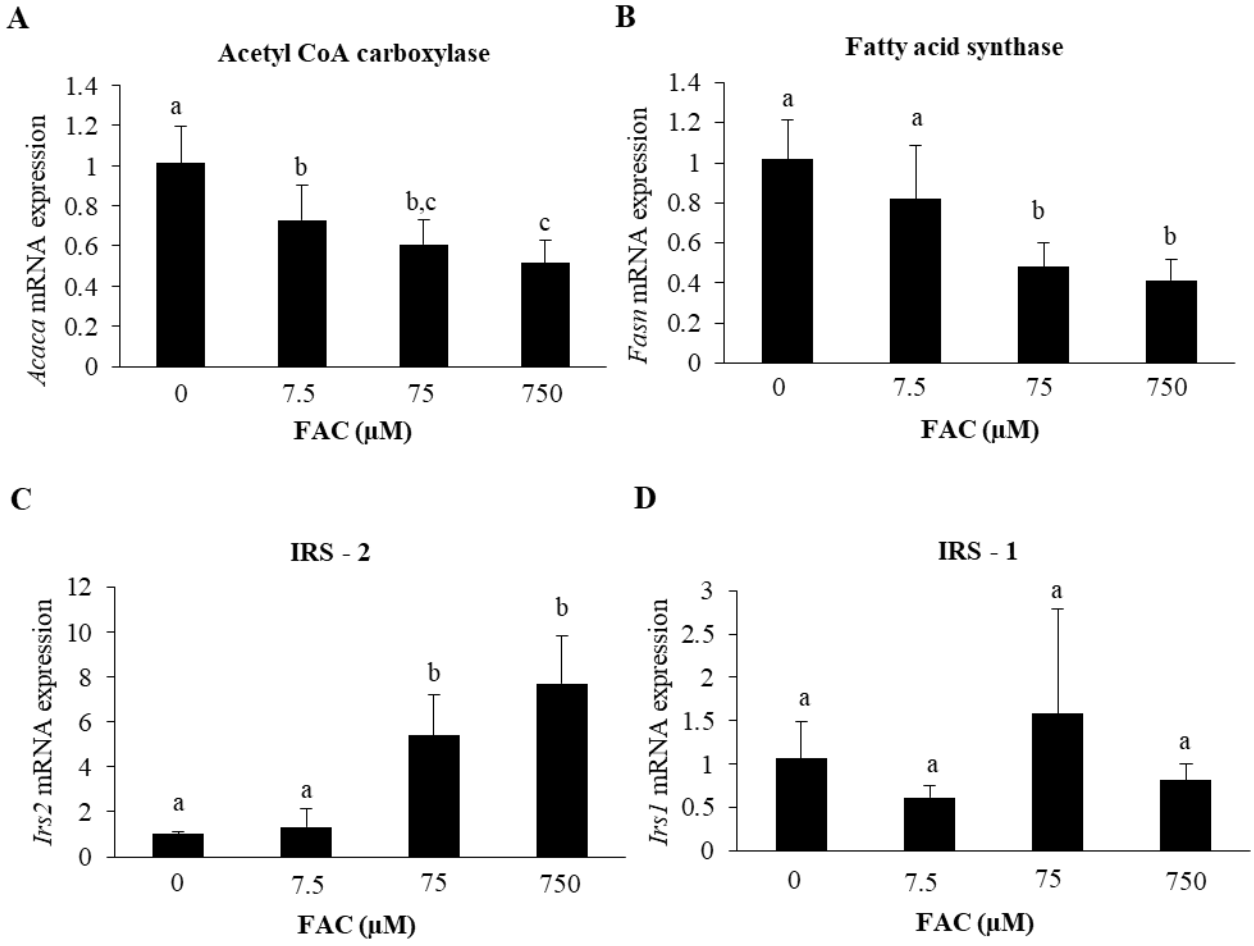

Figure 6.1.10: Effect of treatment with FAC on gene (mRNA) expression of Acaca, Fasn, Irs1 and Irs2

Mouse primary hepatocytes were treated with FAC at various concentrations (as indicated) for 16 hours. Gene expression (determined by qPCR) of acetyl CoA carboxylase (Acaca) (A), fatty acid synthase (Fasn) (B), IRS-2 (Irs2) (C) and IRS-1 (Irs1) (D).

Data represents mean ± SD of results obtained from at least three independent experiments (primary hepatocytes isolated from at least 3 mice), with each done in duplicate, under the specified conditions. Bars in each panel, marked with dissimilar alphabets, indicate data that are significantly different from one another. A p value <0.05 was taken to indicate statistical significance in all cases.

4.4. Treatment with FAC decreased hepatocyte glucose production

In order to assess the functional consequences of activation of the Akt and AMPK pathways by iron, hepatocyte glucose production (HGP) was measured, both in the presence and absence of FAC, using either lactate or glycerol as the gluconeogenic substrate. FAC was used at concentrations of 7.5 μM and 75 μM for these measurements, avoiding the concentration of 750 μM at which some extent of cell damage was observed (Fig. 6.1.4 and 6.1.5). Hepatocytes treated with FAC at 75 μM showed significantly lower HGP, when compared to control cells or those treated with FAC 7.5 μM; the effects seen were similar irrespective of the use of lactate or glycerol as the gluconeogenic substrate (Fig. 6.1.11-A and C). At 7.5 μM, FAC tended to lower glucose production, when compared to control cells, with the effects being statistically significant at 3 and 6 hrs (in the case of lactate-driven basal HGP) (Fig. 6.1.11-A). Forskolin, an adenylyl cyclase activator that mimics the effects of glucagon in hepatocytes (265), was used to induce HGP and served as a positive control. Forskolin-induced HGP was significantly attenuated by FAC (75 μM) treatment (Fig. 6.1.11-B and D). These results show that iron significantly decreased both basal and forskolin-induced HGP in hepatocytes. Addition of insulin (10 nM) to the medium did not significantly affect basal or forskolin-stimulated HGP induced by lactate or glycerol (Fig. 6.1.12), except for a significant decrease in HGP from lactate in the presence of FAC at 75 μM, after 12 hours of incubation (Fig. 6.1.12-A).

Since similar changes in HGP were seen, irrespective of lactate or glycerol being used as the gluconeogenic substrate, changes in gene expression of *G6pc*, an enzyme involved in gluconeogenesis from both of these substrates, was investigated. Glucagon, and other adenylyl cyclase activators such as forskolin, are known to induce the expression of *G6pc* in hepatocytes

(130). FAC treatment decreased forskolin-induced transcriptional activation of *G6pc* (Fig. 6.1.13). In the absence of forskolin, however, FAC treatment (at 75μM) resulted in a small but significant increase in expression of *G6pc* (Fig. 6.1.13).

4.5. Treatment with iron rendered hepatocytes less sensitive to insulin-induced activation of the Akt pathway

To assess the effect of iron on insulin-induced activation of the Akt pathway, hepatocytes were incubated with varying doses of FAC for 16 h, and then treated with insulin (10nM) for 5 min. Insulin-induced activation of Akt (Fig. 6.1.14-A), as well as Gsk3β (Fig. 6.1.14-B) (the downstream target of activated Akt), was significantly attenuated by treatment with iron. Consistent with this, insulin did not suppress *G6pc* (Fig. 6.1.15-A) or induce glucokinase (*Gck)* (Fig. 6.1.15-B) in FAC-treated hepatocytes. Both of these are known responses to insulin and were seen in the absence of FAC treatment (Fig. 6.1.15). These results suggest that increased intracellular iron rendered hepatocytes resistant to the effects of insulin.

4.6. Iron down-regulated protein levels of IRS1 and IRS2

Insulin receptor substrates 1 and 2 (IRS 1 and 2) are upstream of Akt in the insulin signaling pathway. FAC treatment induced decreases in protein levels of IRS1 and IRS2 (Fig. 6.1.16-A and B). Phosphorylation of IRS1 at Ser307 (Fig. 6.1.17-A) and Ser789 (Fig. 6.1.17-B), both of which are known to inhibit signaling via IRS-1, tended to increase progressively in response to increasing concentrations of FAC. However, there was no demonstrable activation of JNK (c-Jun N-terminal kinase), a stress-induced kinase known to phosphorylate IRS1 at Ser307 (Fig. 6.1.18).

Figure 6.1.11

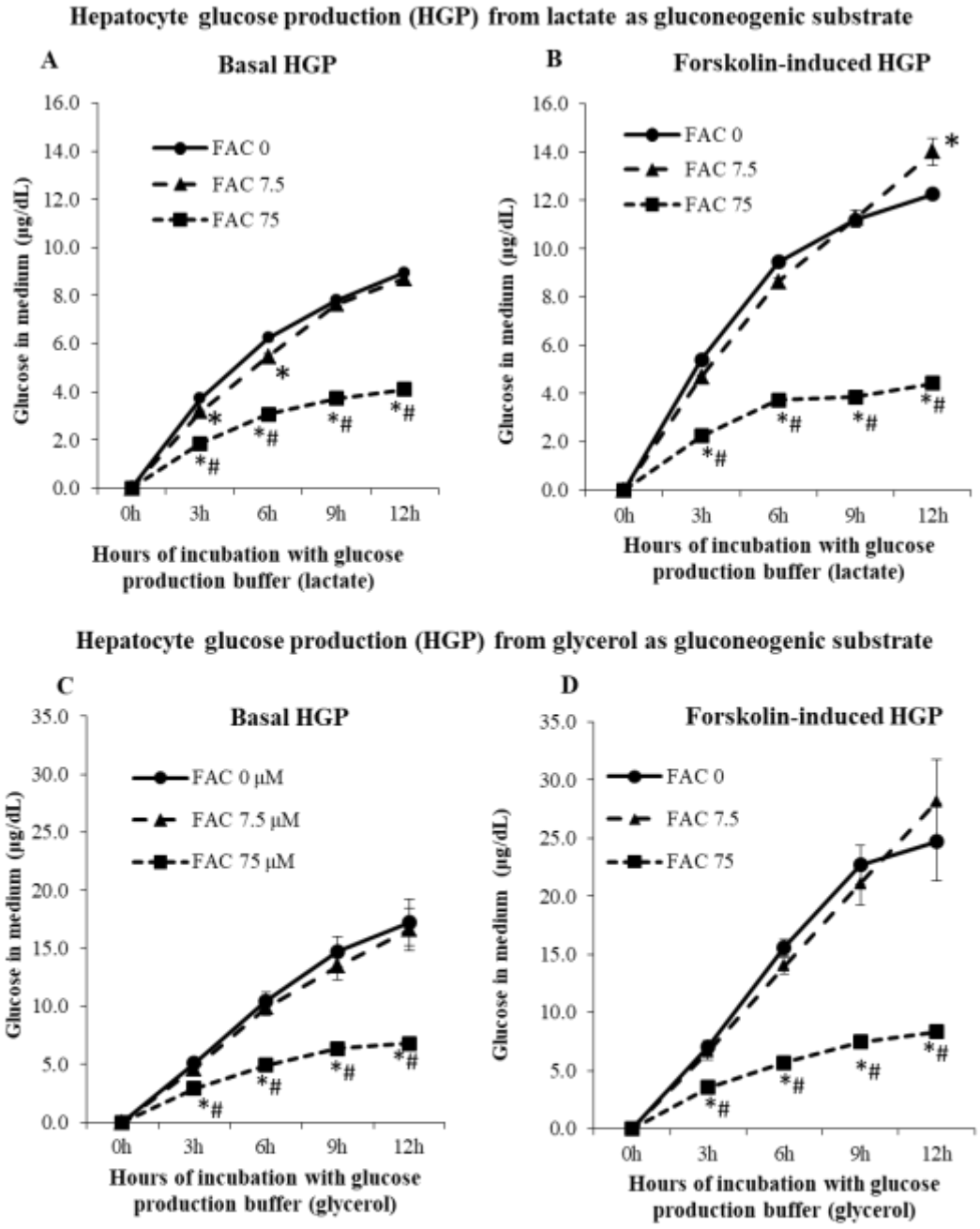

Figure 6.1.11: Effect of treatment with FAC on hepatocyte glucose production (HGP)

A and B: HGP assay using lactate as the gluconeogenic substrate in the presence (B) or absence (A) of forskolin (25 µM). C and D: HGP assay using glycerol as the gluconeogenic substrate in the presence (D) or absence (C) of forskolin (25 µM).

Data are shown as mean ± SE of results obtained from at least three independent experiments (primary hepatocytes isolated from at least 3 mice), with each done in triplicates, under the specified conditions. In A-D, * indicates $p<0.05$ compared to FAC 0 and # indicates $p<0.05$ when compared to FAC 7.5 µM.

Figure 6.1.12

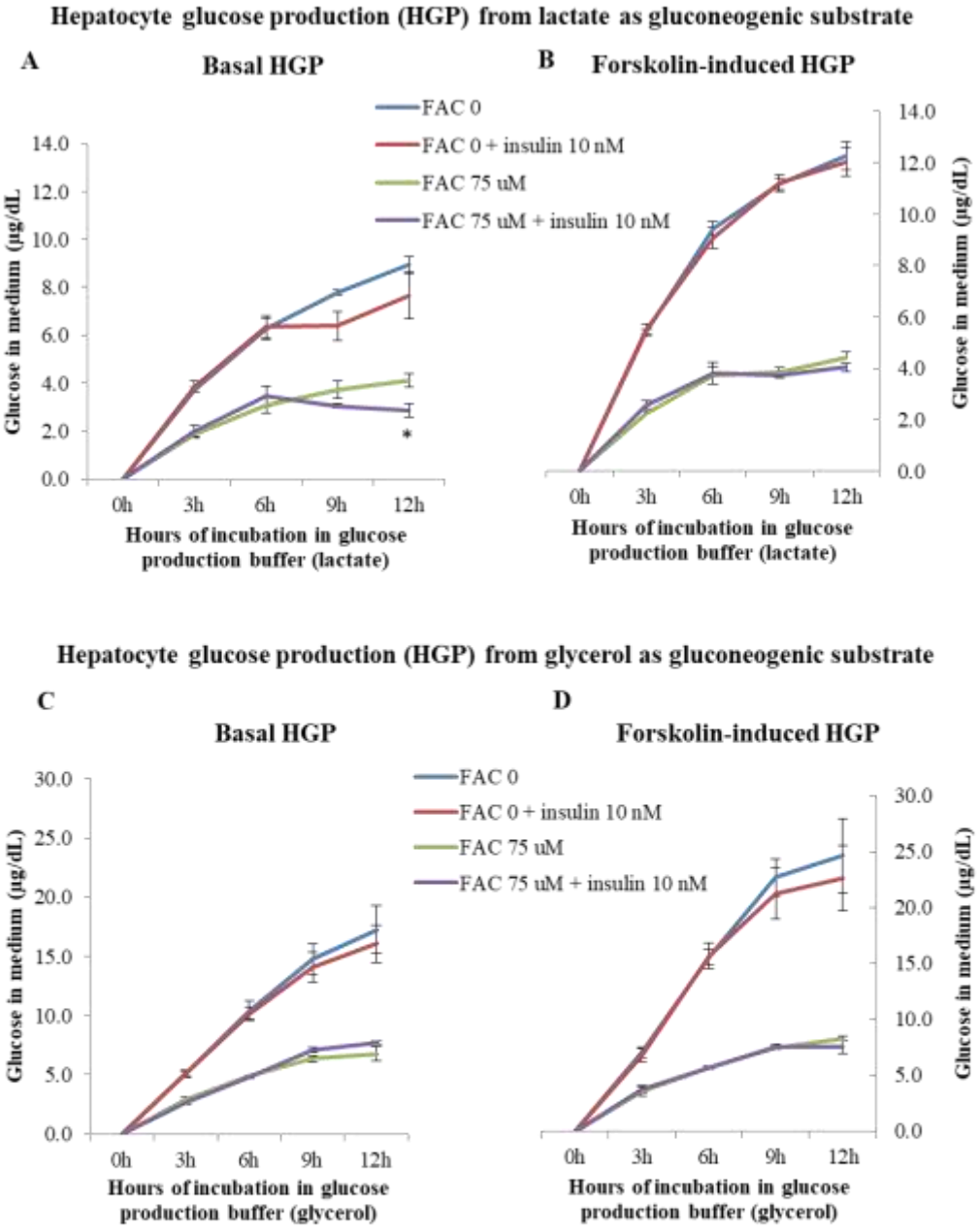

Figure 6.1.12: Effect of treatment with FAC on HGP in the presence and absence of insulin

A and B: HGP assay using lactate as the gluconeogenic substrate in the presence (B) or absence (A) of forskolin (25 µM). C and D: HGP assay using glycerol as the gluconeogenic substrate in the presence (D) or absence (C) of forskolin (25 µM). In each case, HGP was estimated in the presence and absence of insulin (10nM).

Data are shown as mean ± SE of results obtained from at least three independent experiments (primary hepatocytes isolated from at least 3 mice), with each done in triplicates, under the specified conditions. In A, * indicates $p<0.05$ when FAC 75µM + insulin 10 nM) was compared to FAC 75 µM alone.

Figure 6.1.13

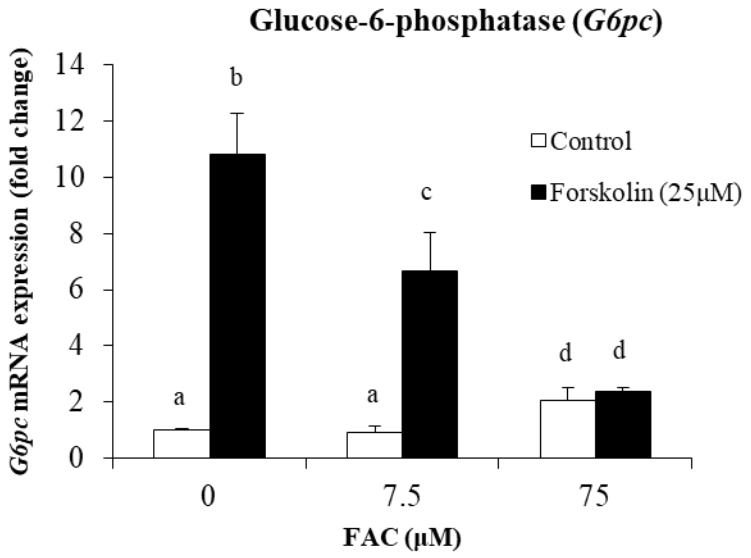

Figure 6.1.13: Effect of treatment with FAC on gene (mRNA) expression of G6pc in the presence and absence of forskolin

Mouse primary hepatocytes were treated with FAC at various concentrations (as indicated) for 16 h and then treated with forskolin (25 µM) or vehicle (DMSO) for 3 h. Gene expression of glucose-6-phosphatase was determined by qPCR.

Data represents mean ± SE of results obtained from three independent experiments (primary hepatocytes isolated from 3 mice), with each done in triplicate, under the specified conditions. Bars marked with dissimilar alphabets, indicate data that are significantly different from one another. A p value <0.05 was taken to indicate statistical significance in all cases.

Figure 6.1.14

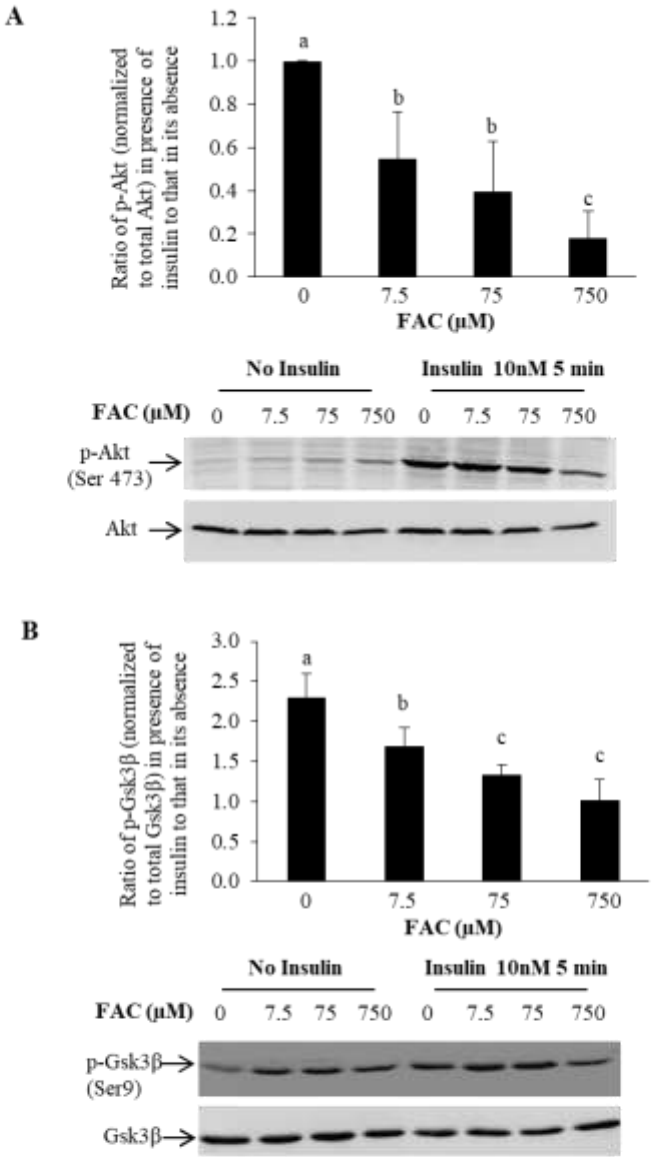

Figure 6.1.14: Effect of treatment with FAC on insulin-induced phosphorylation of Akt and Gsk3β

Hepatocytes were treated with FAC at various concentrations (as indicated) for 16 h and then treated with insulin (10nM) or normal saline for 5 min. The effect of insulin treatment on phosphorylation of Akt (A) or Gsk3β (B) was determined as a ratio of p-Akt or p-GSK3β levels in the presence of insulin to that in its absence.

Data represents mean ± SD of results obtained from at least three independent experiments (primary hepatocytes isolated from at least 3 mice), with each done in duplicates or triplicates, under the specified conditions. Bars in each panel, marked with dissimilar alphabets, indicate data that are significantly different from one another. A p value of less than 0.05 was taken to indicate statistical significance in all cases.

Figure 6.1.15

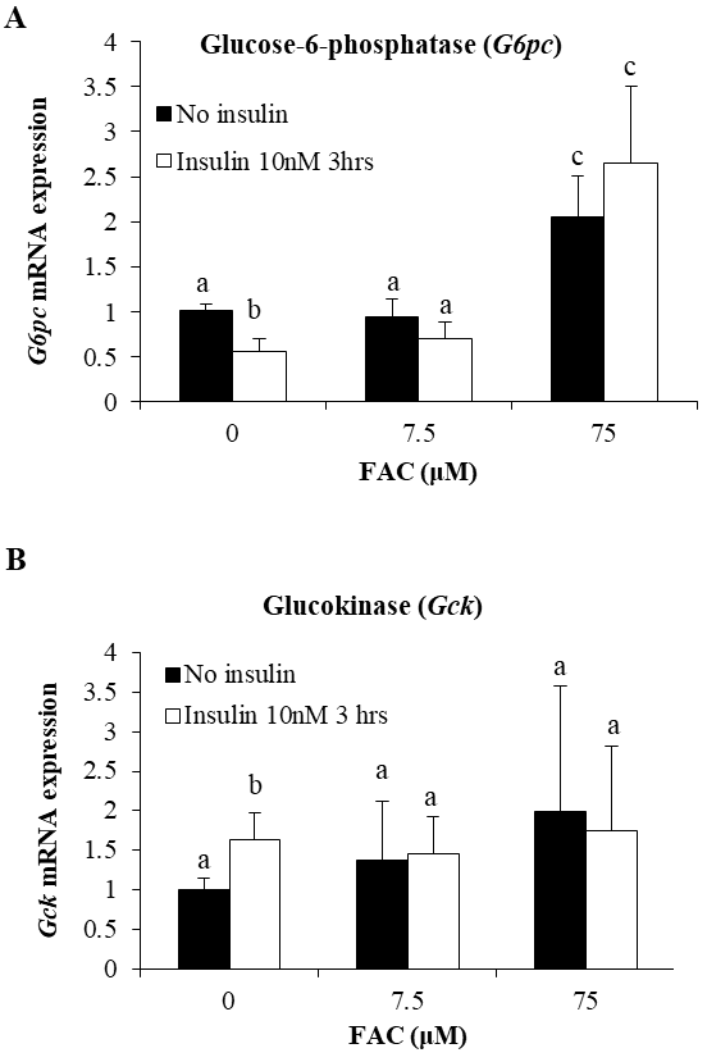

Figure 6.1.15: Effect of treatment with FAC on gene (mRNA) expression of G6pc and Gck, in the presence and absence of insulin

Mouse primary hepatocytes were treated with FAC at various concentrations (as indicated) for 16 h and then treated with insulin (10 nM) for 3 h. Gene expression of glucose-6-phosphatase (A) and glucokinase (B) were determined by qPCR.

Data represents mean ± SD of results obtained from three independent experiments (primary hepatocytes isolated from 3 mice), with each done in triplicate, under the specified conditions. Bars marked with dissimilar alphabets, indicate data that are significantly different from one another. A p value <0.05 was taken to indicate statistical significance in all cases.

Figure 6.1.16

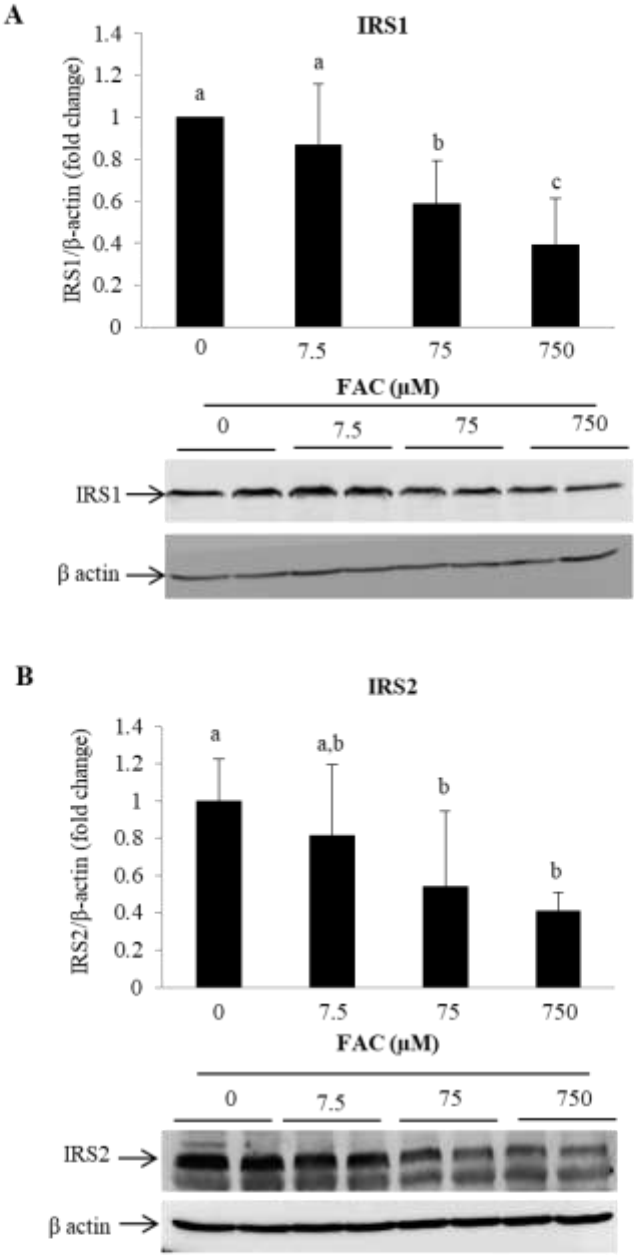

Figure 6.1.16: Effect of treatment with FAC on protein levels of IRS-1 and IRS-2 in hepatocytes

Hepatocytes were treated with FAC at various concentrations (as indicated) for 16 h. Representative images for western blots and densitometric quantification of the bands obtained are shown for IRS-1 (A) and IRS-2 (B) (normalized to β-actin).

Data represents mean ± SD of results obtained from at least three independent experiments (primary hepatocytes isolated from at least 3 mice), with each done in duplicates, under the specified conditions. Bars in each panel, marked with dissimilar alphabets, indicate data that are significantly different from one another. A p value of less than 0.05 was taken to indicate statistical significance in all cases.

Figure 6.1.17

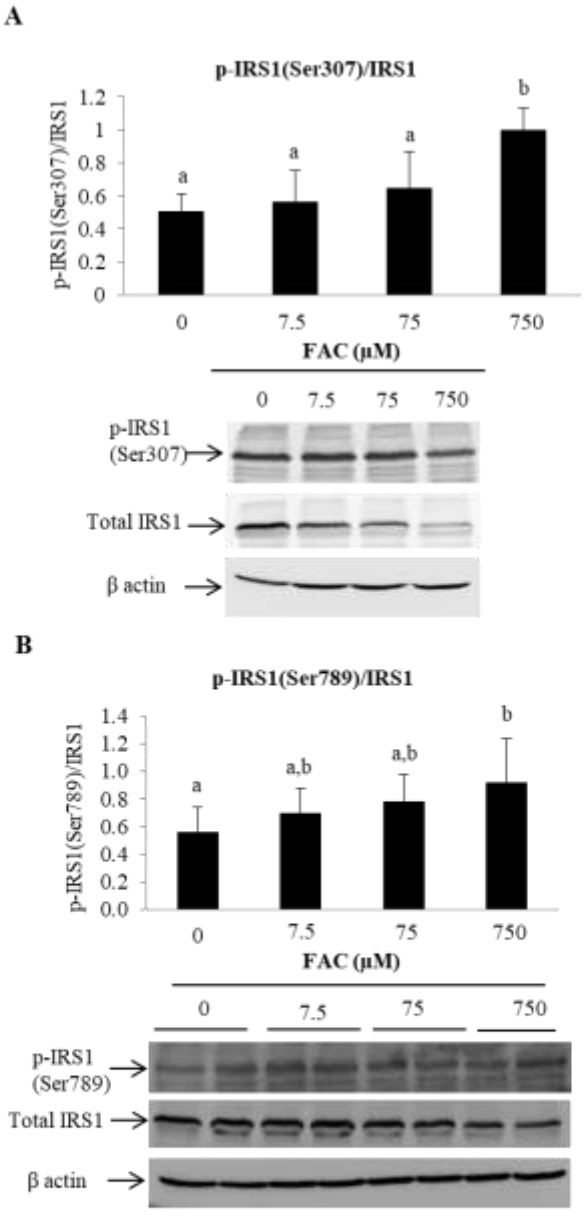

Figure 6.1.17: Effect of treatment with FAC on p-IRS-1(Ser307) and p-IRS-1(Ser789) in hepatocytes

Hepatocytes were treated with FAC at various concentrations (as indicated) for 16 h. Representative images for western blots and densitometric quantification of the bands obtained are shown for p-IRS-1 (Ser307) (A) and p-IRS-1 Ser789) (B) (normalized to total IRS-1 levels).

Data represents mean ± SD of results obtained from at least three independent experiments (primary hepatocytes isolated from at least 3 mice), with each done in duplicates, under the specified conditions. Bars in each panel, marked with dissimilar alphabets, indicate data that are significantly different from one another. A p value of less than 0.05 was taken to indicate statistical significance in all cases.

Figure 6.1.18

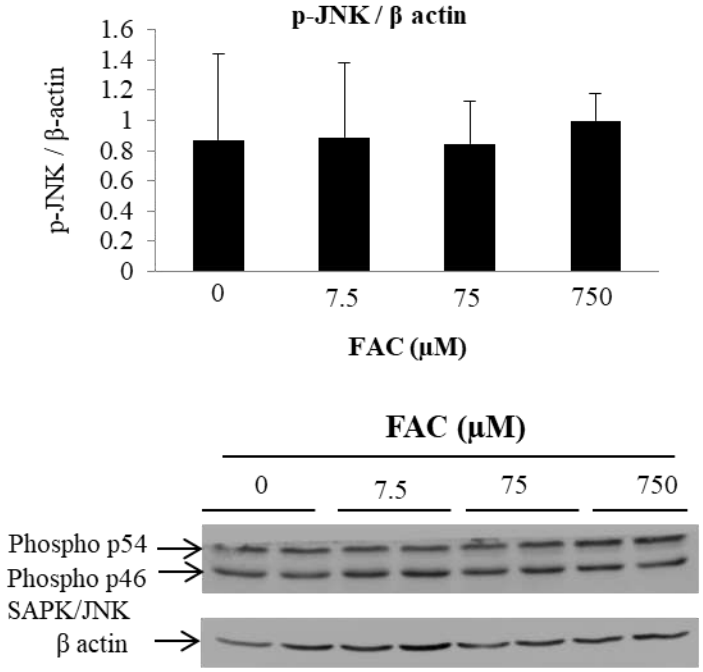

Figure 6.1.18: Effect of treatment with FAC on phosphorylation of JNK in hepatocytes

Hepatocytes were treated with FAC at various concentrations (as indicated) for 16 h. Representative images for western blots and densitometric quantification of the bands obtained are shown for p-JNK (normalized to β-actin).

Data represents mean ± SD of results obtained from at least three independent experiments (primary hepatocytes isolated from at least 3 mice), with each done in duplicates, under the specified conditions. Bars in each panel, marked with dissimilar alphabets, indicate data that are significantly different from one another. A p value of less than 0.05 was taken to indicate statistical significance in all cases.

4.7. Correlation analyses

Results of correlation analyses showed that, in FAC-treated hepatocytes, intracellular iron levels were significantly and positively correlated with p-Akt (Ser473), p-Akt (Thr308), p-Gsk3β (Ser9), p-FoxO1 (Ser256) and p-AMPK (Thr172), and negatively correlated with IRS1 and IRS2 protein levels. In addition, markers of insulin signaling (p-Akt [Ser473], p-Akt [Thr308], p-Gsk [Ser9] and p-FoxO1 [Ser256]) were significantly and positively correlated with one another and with p-AMPK (Thr172) (Table 6.1.3).

Table 6.1.3: Correlation analyses among parameters of interest in primary hepatocytes treated with FAC

Sl. no	Parameter	Parameter	Spearman's correlation coefficient	p-value
1	Intracellular iron level vs.	p-Akt (Ser473)	0.648	0.004
		p-Akt (Thr308)	0.843	<0.001
		p-Gsk3β (Ser9)	0.771	0.003
		p-FoxO1 (Ser256)	0.652	0.008
		p-AMPK (Thr172)	0.812	<0.001
		p-IRS1 (Ser307)	0.470	0.049
		Total IRS1	- 0.667	0.002
		Total IRS2	- 0.684	0.007
2	p-Akt (Ser473) vs.	p-Akt (Thr308)	0.671	0.004
		p-Gsk3β (Ser9)	0.638	0.025
		p-FoxO1 (Ser256)	0.574	0.020
		p-AMPK (Thr172)	0.649	0.001
3	p-Akt (Thr308) vs.	p-Gsk3β (Ser9)	0.997	<0.001
		p-FoxO1 (Ser256)	0.641	0.007
		p-AMPK (Thr172)	0.747	0.001
4	p-Gsk3β (Ser9) vs.	p-FoxO1 (Ser256)	0.713	0.009
		p-AMPK (Thr172)	0.716	0.009
5	p-FoxO1 (Ser256) vs.	p-AMPK (Thr172)	0.515	0.041

5. Discussion

Molecular interactions between insulin signaling and iron in hepatocytes, and their net effect on HGP have not been clearly elucidated, as far as is ascertainable from published literature. The present study was an attempt to address this lacuna. Mouse primary hepatocytes, which were iron-loaded *in vitro* by incubation with FAC at various concentrations, were used in the present study to investigate this. Studies that report findings from work done with primary hepatocytes usually report data obtained from at least three independent experiments (primary hepatocytes isolated from at least 3 mice), with each done in duplicates or triplicates, under the specified conditions (146,266,267). In keeping with this, the present study also shows data obtained from experiments done on hepatocytes isolated from at least three different mice.

The rationale for treating hepatocytes with FAC (a highly soluble form of iron) was to rapidly increase intracellular iron content. This model was not meant to mimic a physiological/pathological condition *in vivo,* where iron accumulation tends to occur over a prolonged period. The doses of FAC chosen were based on a previous publication, where primary hepatocytes treated with similar doses of FAC showed increases in intracellular iron levels, without a concomitant decrease in cell viability (253). In addition, FAC was chosen because ferric citrate is a physiologically relevant form of iron. It has been shown that non-transferrin bound iron (NTBI), which increases in blood in conditions of iron overload (such as hemochromatosis and thalassemia), is mainly found as ferric citrate (268,269).

Treatment of hepatocytes with FAC resulted in increases in intracellular iron content (Fig. 6.1.2). There was a concern about the viability of cells incubated with FAC in this study. The MTT assay showed no significant damage to the cells even at the highest dose of FAC used. There was

a small but significant increase in LDH activity in the medium and increased fluorescence of EthD-1 staining at the highest dose of FAC used (750 µM) (Fig 6.1.4-B and 6.1.5). This showed that FAC, at this dose, induced cell damage to a certain extent. However, all the effects of interest produced by treatment with FAC, which are reported in this study, were seen at 7.5 and 75 µM concentrations. No decrease in cell viability was seen at these doses (Fig 6.1.4 and 6.1.5).

The results of the present study are summarized in Fig 6.1.19. Overall, the results show that increases in intracellular iron had dual effects on insulin sensitivity in hepatocytes. On one hand, iron activated the Akt signaling pathway in hepatocytes in a ligand-independent manner, i.e., even in the absence of insulin (Fig. 6.1.6 and 6.1.7). In addition, iron activated AMPK, a key energy-sensing pathway, which inhibits gluconeogenesis (Fig. 6.1.9). Consequently, gluconeogenesis was down-regulated and HGP was decreased by increased levels of intracellular iron (Fig. 6.1.11). On the other hand, iron decreased activation of the Akt pathway in response to insulin (Fig. 6.1.14), by decreasing levels of IRS 1 and 2 (Fig. 6.1.16), resulting in insulin resistance. The findings of this study provide a plausible explanation for why iron overload, in general, is associated with insulin resistance, but why improved glucose tolerance and insulin sensitivity is seen in classical hemochromatosis (characterized by iron overload primarily in the liver) (11,246). As far as is ascertainable, these findings, in mouse primary hepatocytes, are novel and have not been reported earlier.

Figure 6.1.19

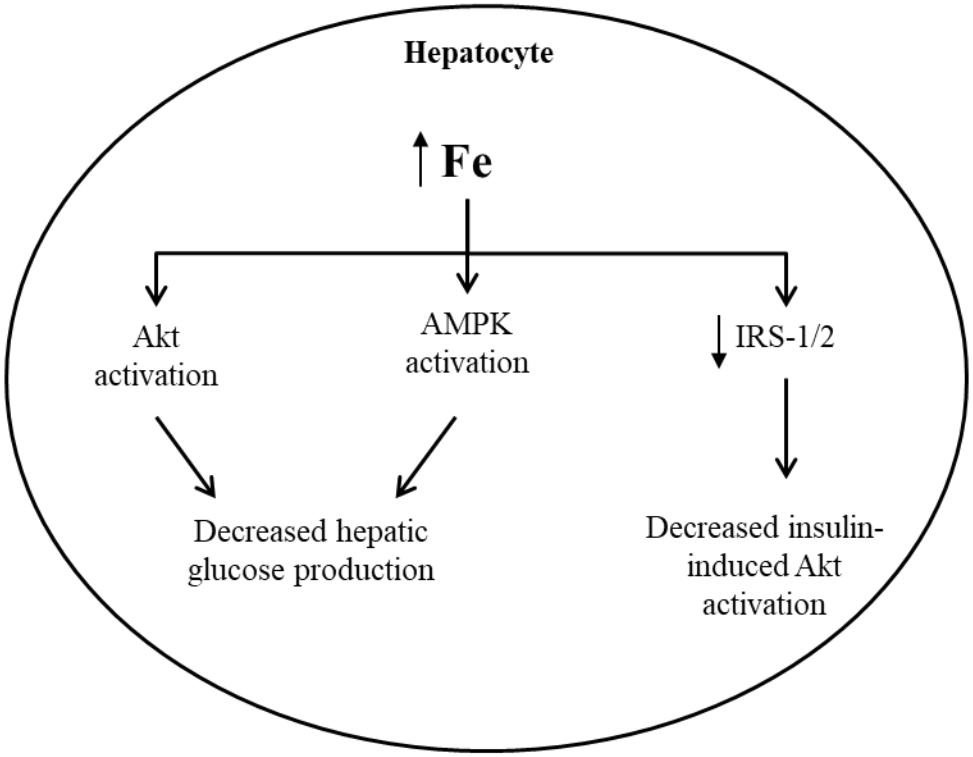

Figure 6.1.19: Schematic diagram of the proposed effect of intracellular iron on insulin signaling

Increased intracellular iron activated the Akt and AMPK pathways, resulting in decreased hepatic glucose output. In addition, iron decreased levels of IRS-1 and 2, which are upstream of Akt in the insulin signaling pathway, resulting in decreased insulin-stimulated activation of the Akt pathway.

AMPK is activated by its upstream kinase, liver kinase B1 (LKB1), by phosphorylation at Thr172 (141). It has been shown previously that LKB1 and AMPK were activated in the liver and skeletal muscle of mice fed a high-iron diet (245). Ligand-independent activation of the Akt pathway has been shown to occur in response to activation of AMPK (270,271), thus suggesting a likely mechanism by which Akt phosphorylation is induced by iron. FAC treatment resulted in activation of AMPK, which was highly correlated with phosphorylation of Akt at both Thr308 and Ser473 (Table 6.1.3). It is, therefore, possible that iron-induced activation of Akt may be mediated by AMPK activation. Additional studies with genetic knock-down or pharmacological inhibition of AMPK would be required to confirm this.

Iron decreased basal as well as forskolin-induced HGP (Fig. 6.1.11). Iron also decreased forskolin-induced mRNA expression of *G6pc* (Fig. 6.1.13). Activation of AMPK has been shown to decrease HGP by inducing the phosphorylation and inactivation of CREB-regulated transcription co-activator 2 (CRTC2), a key transcriptional co-activator involved in induction of gluconeogenic genes by glucagon (145). In addition, AMPK inhibits glucagon-induced increase in *G6pc* expression by activating phosphodiesterase-mediated cAMP degradation (146). Activation of the Akt pathway also results in suppression of gluconeogenesis by inhibiting FoxO1-induced expression of *G6pc* (272,273). Therefore, iron-induced activation of Akt and AMPK pathways can explain the decrease in HGP and *G6pc* expression in this setting.

In the absence of forskolin, despite the fact that iron inhibited HGP, expression of *G6pc* was not found to be decreased; in fact, iron induced a small but significant increase in the mRNA levels of these enzymes (Fig. 6.1.13). The reason(s) for decreased HGP in the absence of a decrease in *G6pc* is/are not totally clear; however, it has been shown that activation of AMPK can decrease

HGP by allosteric/covalent regulation of the gluconeogenic flux, even in the absence of significant decreases in mRNA levels of gluconeogenic genes (146). In fact, it is well established that HGP *in vivo* is regulated by post-translational mechanisms through the control of substrate flux, rather than exclusively by changes in gene expression (131). A possible explanation for the increase in *G6pc* expression induced by FAC treatment (at 75 μM) (Fig 6.1.13 and 6.1.15-A) may be iron-induced mitochondrial dysfunction, which has been shown to occur in response to iron overload and result in increased expression of gluconeogenic genes (274).

Although treatment with iron activated the Akt pathway, insulin-induced phosphorylation of Akt (and its downstream target, GSK3β) was significantly decreased in iron-loaded hepatocytes (Fig 6.1.14), suggesting that an iron-overloaded state results in resistance to the actions of insulin. The functional consequences of this observation were studied by investigating changes in HGP in response to insulin treatment. However, insulin did not have an effect on HGP, neither in the presence of forskolin nor in its absence (Fig 6.1.12). This is consistent with recent studies which have shown that direct insulin signaling in hepatocytes is dispensable for insulin-mediated down-regulation of HGP (133,134). Regulation of HGP by insulin *in vivo* has been suggested to be mediated by an intermediate extra-hepatic organ/tissue; this is possibly the adipose tissue, via changes in free fatty acid levels in blood (136).

In the present study, iron induced a progressive decrease in IRS1 and IRS2 protein levels (Fig. 6.1.16). Since IRS1 and IRS2 are up-stream of Akt in the insulin signaling cascade, a decrease in the levels of these proteins may account for the impaired phosphorylation and decreased activation of Akt induced by insulin in these cells. Phosphorylation of IRS1 at Ser307 and its subsequent degradation has been proposed to play a key role in the development of insulin

resistance (275). Stress-induced protein kinases, including JNK and mTOR, are known to increase phosphorylation of IRS1 at Ser307 (276,277). Treatment with iron induced an increase in the p-IRS1 (Ser307)/total IRS1 ratio (Fig. 6.1.17-A), but did not activate JNK (Fig. 6.1.18). It is possible that increased phosphorylation of IRS1 at Ser307 in this setting may be mediated by mTOR; this was not investigated in the present study and is a possibility that requires further exploration. In addition, iron induced IRS1 phosphorylation at Ser789 (Fig. 6.1.17-B), which is known to be mediated by AMPK, and to inhibit signal transduction via IRS1 (270,278).

Findings of increased basal, but decreased insulin-stimulated Akt activation (as seen in the present study) have been shown previously to result in insulin resistance. For example, it has been shown that overexpression of a constitutively active form of Akt increased basal glucose uptake, but blunted insulin-induced glucose uptake in cardiomyocytes (279). Similarly, cardiomyocytes that over-express FoxO1 showed elevated basal, but impaired insulin-stimulated Akt phosphorylation and downstream insulin signaling (280). *Hfe*$^{-/-}$ mice, a model of hemochromatosis, also show increased basal, but not insulin-stimulated glucose uptake in the skeletal muscle (246). Impaired activation of Akt in response to insulin treatment has also been shown in AML-2 mouse hepatocyte cell lines which were iron-loaded (281). The above reports, thus, support the findings of the present study.

6. Summary and conclusion

In conclusion, the results of this study show that increased levels of intracellular iron, in mouse primary hepatocytes, activated the Akt and AMPK pathways and resulted in decreased HGP. Insulin-induced activation of the Akt pathway was, however, impaired in cells with increased levels of intracellular iron, possibly due to decreased protein levels of IRS1/2. These findings are of relevance in disease conditions characterized by hepatic iron overload (such as hemochromatosis, thalassemia and non-alcoholic steatohepatitis), which are known to be associated with increased risk of type 2 diabetes.

STUDY 2

Interactions between insulin resistance and dysregulated iron homeostasis, produced by high-fat feeding in mice: a time-course study

1. Abstract

Increased body iron stores have been reported to be associated with type 2 diabetes mellitus (T2DM). However, the temporal association between onset of insulin resistance (IR) in T2DM and dysregulated iron homeostasis, and the cross-talk between the various events involved, are unclear. In an attempt to address these lacunae, a time-course study was carried out to determine the interplay between IR and systemic iron homeostasis, in mice fed a high-fat diet in order to induce IR.

Male C57Bl/6J mice were fed a high-fat (HFD) or control diet for various time periods (4, 8, 12, 16, 20 or 24 weeks). High-fat feeding induced obesity, hepato-steatosis and insulin resistance (IR) in mice. It also resulted in dysregulation of iron homeostasis in the liver as well as the adipose tissue. There was a progressive decline in hepatic iron stores with increasing durations of HFD-feeding. This was associated with an increase in iron content of the adipose tissue. Triglyceride levels in the liver correlated positively with IR and negatively with liver iron content; these associations remained significant after adjusting for potential confounders, using multiple linear regression analysis. The onset of IR (at 8 weeks), as determined by insulin tolerance test, preceded the onset of hepatic iron dysregulation (at 12 weeks). Hepatic expression of hepcidin, the chief iron regulatory hormone, was decreased after 24 weeks of HFD and was found to correlate positively with protein levels of transferrin receptor 2 in the liver. Other

factors known to regulate hepcidin, such as bone morphogenetic protein 6, matriptase–2, serum iron levels and inflammation, were not affected by HFD.

In summary, the results of this study showed that IR induced by HFD-feeding was associated with dysregulation of iron homeostasis in the liver and adipose tissue. The onset of IR in HFD-fed mice preceded that of hepatic iron dysregulation, suggesting that changes in iron homeostasis may not play a causative role in the pathogenesis of IR in this model.

2. Introduction

Insulin resistance (IR) is the hallmark of type 2 diabetes mellitus (T2DM). It is characterized by impaired sensitivity of tissues to the actions of insulin. Several studies have shown a strong association between increased levels of serum ferritin (generally considered to be a marker of body iron stores) and increased risk of T2DM (4,282,6,283,284). However, serum ferritin is an acute phase reactant; its levels are increased in inflammatory conditions (285,286). Since, T2DM is associated with chronic low-grade inflammation (287), it is possible that the raised serum ferritin levels seen in T2DM may be a consequence of inflammation. The results of the EPIC-InterAct study showed that other markers of iron status, such as transferrin saturation and serum iron, were not associated with increased risk of T2DM (194). In fact, increased transferrin saturation (>45%) was reported to be associated with a lower risk of T2DM among women (194). It, thus, appears that the association between body iron stores and T2DM is complex and is not completely understood.

Hepcidin, a peptide synthesized and secreted by the liver, is the chief regulator of systemic iron homeostasis (32). It regulates systemic iron fluxes and plasma iron levels by binding to

ferroportin, the cellular iron export protein, causing its internalization and degradation (24). Thus, hepcidin inhibits recycling of iron from macrophages and also decreases intestinal absorption of dietary iron.

A number of factors regulate hepatic hepcidin (*Hamp1*) expression; these include liver iron stores, serum iron levels, inflammation and the erythropoietic drive (31). Regulation of hepcidin in response to changes in liver and serum iron levels is mediated predominantly through signaling via the BMP-SMAD pathway (66). Although multiple bone morphogenetic proteins (BMPs) induce hepcidin, in mice it has been shown that BMP6 is probably the most important regulator of the *Hamp1* gene *in vivo* (72). BMP6, in turn, is regulated by hepatic iron stores (288). Matriptase-2, a membrane-associated serine protease (*Tmprss6*), regulates hepcidin expression by down-regulating signaling via the BMP-SMAD pathway (77,78). It has been shown that hepatic iron stores can regulate *Hamp1* expression by modulating *Tmprss6* expression (94). On the other hand, serum iron levels regulate *Hamp1* by activating BMP-SMAD signaling (independent of BMP6) through a multi-protein complex in which the hemochromatosis protein (HFE), hemojuvelin (HJV) and transferrin receptor 2 (TfR2) are essential components (86,289).

Obesity is known to be associated with dysregulation of iron homeostasis (290–292); however, it is not clear whether IR, which is frequently associated with obesity, is a cause or consequence of iron dysregulation. In addition, the temporal association between onset of IR and that of dysregulated iron homeostasis (including changes in hepcidin, liver iron stores and various factors that regulate hepcidin [as described above]), is not clear.

IR is associated with chronic low-grade inflammation (287). Systemic inflammation can induce *Hamp1* through the JAK-STAT3 pathway, activated by interleukin-6 (IL-6) (112). However, whether IR-associated inflammation has a significant effect on hepcidin is not clear.

Adipose tissue metabolism is known to have a major impact on energy homeostasis in the body (293). Inflammation in the adipose tissue is a key factor that is involved in initiating and driving whole-body insulin resistance in response to obesity (294). It has been shown, both in humans and in mice, that increased iron content in the adipose tissue is associated with elevated IR (17,226). In addition, adipocyte iron has been shown to regulate the expression of adipokines, such as adiponectin (225) and leptin (228), which play critical roles in energy homeostasis. However, very little is known about the effect of IR on adipose tissue iron homeostasis. In addition, it is not known whether elevated iron content in the adipose tissue is a cause or consequence of IR.

In summary, although increased body iron has been proposed to be associated with T2DM, the precise nature of the mechanistic link between iron and IR is not known. For example, the effects of IR on iron homeostasis in the liver and adipose tissue are not clear. It is also not known whether dysregulation of iron homeostasis is a cause or consequence of IR. The effect of IR on hepcidin and the various factors that regulate it (as described above) is not clear. In an attempt to answer these questions, a time-course study was carried out in high-fat diet-fed male C57Bl/6J mice, which is one of the most commonly used mouse models of T2DM (295).

3. Methodology

3.1. Experimental protocol:

Male C57Bl/6J mice were used for the study. All experiments were carried out with the approval of the Institutional Animal Ethics Committee at Christian Medical College, Vellore, India (IAEC No. 14/2013), in accordance with the regulations of the Committee for the Purpose of Control and Supervision of Experiments on Animals (CPCSEA), Government of India.

At 7 weeks of age, mice were shifted from a regular chow diet (cat no. #D131; Scientific Animal Food and Engineering [SAFE], France) to a control diet (CD) (cat no. #D12450J [10% of total calories derived from fat]; Research Diets, Inc., USA). Starting at 8 weeks of age, mice were either fed a high-fat diet (HFD) (cat no. #D12492 [60% of total calories derived from fat]; Research Diets, Inc., USA) or continued on CD for 4, 8, 12, 16, 20 or 24 weeks (Fig 6.2.1). The composition of the diets is provided in Appendix III and IV (page 330 and 331). The iron content of the regular chow diet (used after weaning and up to 7 weeks of age) was 250 mg/kg, and that of CD and HFD were 43 mg Fe/ kg and 58 mg Fe/kg respectively (290,296,297). All mice had access to food and water *ad libitum*. Food intake and weight gain in each mouse were monitored at weekly intervals.

Figure 6.2.1

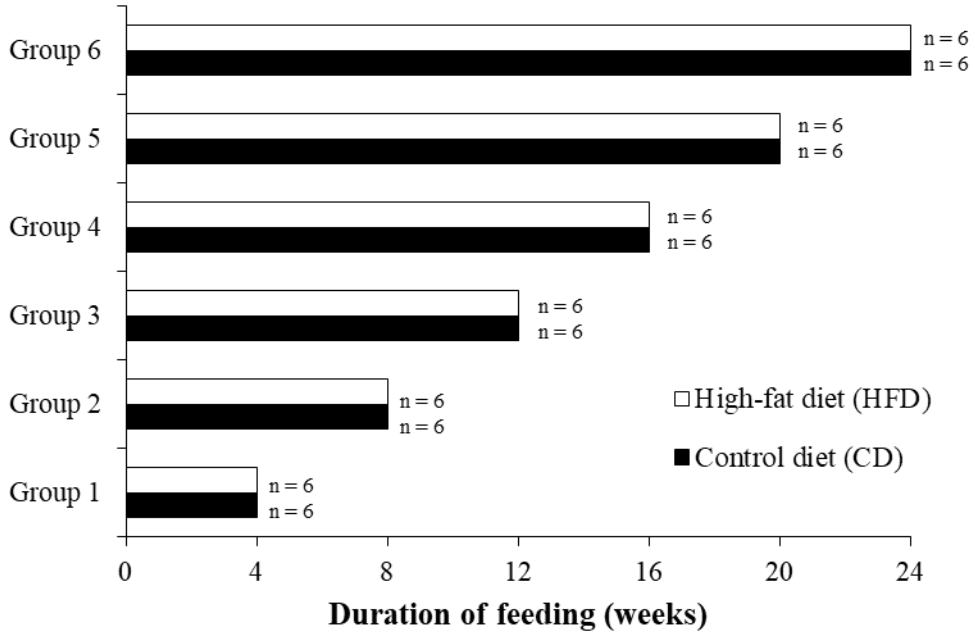

Figure 6.2.1: Pictorial representation of the study design

Male C57Bl/6J mice were fed a control diet (CD) or a high-fat diet (HFD) for various durations (as indicated).

3.2. Evaluation of insulin sensitivity in vivo

Glucose tolerance (GTT) and insulin tolerance tests (ITT) were carried out, as described below, in order to assess insulin sensitivity in the experimental mice.

3.2.1 Intraperitoneal glucose tolerance test (GTT) (298)

GTT was done 3 days prior to euthanasia in mice fed CD or HFD for various durations (as described above). To assess glucose tolerance, mice were placed in fresh cages and fasted for 6 hours with free access to water. They were then given an intra-peritoneal injection of glucose (2g/kg body weight). Blood samples were obtained from the tail vein immediately before the dose of glucose and 15, 30, 60 and 120 min after it. Glucose levels in these samples were estimated, using a glucometer (Bayer Contour, USA).

3.2.2. Insulin tolerance test (ITT) (299)

ITT was done 1 day prior to euthanasia in mice fed CD or HFD for various durations. To assess insulin tolerance, mice were placed in fresh cages and fasted for 4 hours with free access to water. They were then given an intra-peritoneal injection of insulin (Actrapid Human insulin, Novo Nordisk, Copenhagen, Denmark) (0.75 U/kg body weight). Glucose levels were estimated in blood samples obtained from the tail vein (using a glucometer), immediately before the insulin injection and 15, 30, 45 and 60 min later.

For both GTT and ITT, the glucose values obtained for each mouse was plotted against time and the area under curve (AUC) was estimated, using the linear trapezoid method.

3.3 Euthanasia of mice:

At the end of each of the time points studied (as shown in Fig. 6.2.1), 6 CD and 6 HFD-fed mice were euthanized by cervical dislocation under deep anesthesia (using inhalational isoflurane). Mice were not fasted prior to euthanasia. Following laparotomy, blood was collected from the inferior vena cava. The liver, epididymal white adipose tissue (eWAT) and spleen were isolated from each animal; each was weighed. These, along with the duodenum and a sample of skeletal muscle (the quadriceps), were immediately snap-frozen in liquid nitrogen and stored at -70°C, till further processing.

3.4 Western blot analysis:

Snap-frozen liver, adipose and duodenal tissue samples were homogenized (using a mechanical homogenizer) in ice-cold RIPA buffer (Tris-HCl 10mM, NaCl 140mM, EDTA 1·5mM, sodium deoxycholate 0·1%, Triton-X 1%, SDS 0·1%, pH 8·0), containing a cocktail of protease inhibitors (cat. no. P8340, Sigma, India). Homogenized samples were centrifuged at 14,000*g* for 10 min at 4°C. Fat that collected at the top was removed; the centrifugation step was repeated. Protein content in the supernatants obtained was estimated, using the Pierce BCA protein assay kit (cat. no. 23225, Thermo Fisher Scientific, USA).

SDS-PAGE and electroblotting were carried out, as described in detail in the methodology section for Study I. Briefly, samples were heated at 95°C for 5 minutes in Laemmli buffer, prior to loading (50µg protein) on 10% SDS-PAGE gels for electrophoretic separation. Separated proteins were transferred onto PVDF membrane (0.45µm, Immobilon-P, Millipore, Merck, Germany), blocked and probed with appropriate primary antibody (overnight at 4°C), followed

by incubation with secondary antibody (2 hours at room temperature). Sources and dilutions of primary and secondary antibodies and blocking agent used are given in Table 6.2.1. Bands were detected with a chemiluminescence substrate kit (SuperSignal West Dura, Thermo Fisher Scientific, USA), using a gel documentation system (Fluorochem SP, Alpha Innotech, USA). The intensities of the bands were quantified using ImageJ software (NIH, USA), and normalized to that of β-actin, which was used as a loading control in the case of liver and adipose tissue; for duodenal tissue, bands were normalized to total protein visualized by reversible Ponceau staining (300). In order to compare samples run on different membranes, inter-membrane normalization was done by normalizing the band intensities obtained for a calibrator sample, which was run on every gel.

3.5. Quantitative real-time polymerase chain reaction (qPCR)

Isolation of RNA, construction of cDNA and PCR reactions were carried out as described in detail in the methodology section for Study 1. Briefly, ~100 mg of tissue (liver, adipose tissue and duodenum) was homogenized in 1 mL of Tri-Reagent (Sigma, India) and RNA isolated according to manufacturer's instructions. For samples with increased fat content (adipose tissue and liver), homogenates were subjected to a preliminary centrifugation step (12,000*g* for 10 min at 4°C) in order to remove fat in the homogenate, prior to RNA isolation. Isolated RNA was quantitated using a NanoDrop 2000c Spectrophotometer (Thermo Fisher Scientific, USA). In all cases, integrity of the RNA was assessed by agarose gel electrophoresis. One microgram of isolated RNA was used to synthesize cDNA, using the Reverse Transcriptase Core Kit (Eurogentec, Belgium) (as described in Study 1). Quantitative PCR reactions were carried out in duplicate, using the Takyon qPCR SYBR master mix (Eurogentec, Belgium), using a BioRad

Chromo4 real-time PCR machine (as described in Study 1). The expression levels of genes of interest were normalized to *Rpl19*, which was used as the reference gene. Sequences of all primers used are listed in Table 6.2.2. The MIQE (Minimum Information for Publication of Quantitative Real-Time PCR Experiments) check-list and qPCR validation data are provided in Appendix no. I and II (page 323 and 327).

3.6. Estimation of content of non-heme iron in liver, spleen and skeletal muscle

Samples of the liver, spleen and skeletal muscle were processed for estimation of iron, as described earlier (301). Tissue samples were dried in a hot air oven at 48°C for 48 h; they were then weighed and digested in acid reagent (3M hydrochloric acid and 10% TCA) (10 mg of dried tissue/100 μL acid reagent) at 65°C for 24 hours. Following this, the digested samples were centrifuged at 12,000*g* for 5 min and the supernatants obtained were used for estimation of iron.

Non-heme iron was estimated using a colorimetric assay based on bathophenanthrolene dye-binding, as described earlier (259). Twenty microliters of the supernatant (diluted with 0.1N HCl as appropriate) was added to 180 μL of chromogen reagent (consisting of 0.01% bathophenanthrolene disulphonate sodium salt [cat. no. 11880, Sigma India] and 0.1% [v/v] thioglycollic acid [cat. no. 528056, Sigma, India] in 4M sodium acetate [cat. no. 22342, SRL chemicals, India]) in a microtiter plate, mixed and incubated at room temperature for 15 min. Absorbance was measured at 540 nm using a BioRad iMark microplate reader. The iron content in each sample was estimated based on a set of iron standards prepared by serial dilution of a 1000 μg/mL stock standard (cat. no. 02583, Sigma, India). The standards were run in parallel with the samples. Results were normalized to the dry weight of tissue samples.

Table 6.2.1: Primary and secondary antibodies

Protein	**Primary antibody (source and dilution)**	**Secondary antibody[#]**	**Blocking agent**
Ferritin (light chain)	Santa Cruz Biotechnology (sc-14420) 1:1000	Rabbit anti-goat IgG (H+L) HRP conjugate (#31402)	5% non-fat dry milk in TBS-T
Ferroportin	Alpha Diagnostics (#MTP11-A) 1:1000	Goat anti-rabbit IgG (H+L) HRP conjugate (#31460)	5% non-fat dry milk in TBS-T
TfR2	Alpha Diagnostics (#TFR21-A) 1:1000	Goat anti-rabbit IgG (H+L) HRP conjugate (#31460)	5% non-fat dry milk in TBS-T
Beta actin	Sigma-Aldrich (#A5316) 1: 5000	Goat anti-mouse IgG (H+L) HRP conjugate (#31430)	5% non-fat dry milk in TBS-T
p-Akt (Ser 473)	Cell signaling technology (#9271) 1:1000	Goat anti-rabbit IgG (H+L) HRP conjugate (#31460)	5% BSA in TBS-T
Total Akt	Cell signaling technology (#9272) 1:1000	Goat anti-rabbit IgG (H+L) HRP conjugate (#31460)	5% BSA in TBS-T

[#] Secondary antibodies were purchased from ThermoFisher Scientific, USA, and used at a dilution of 1:5000

Table 6.2.2: Primers used for qPCR

Sl. No.	Gene	Accession number	Primer sequence	Amplicon size (bp)
1	Hepcidin (*Hamp1*)	NM_032541.1	5'- ACATTGCGATACCAATGCAGAA-3' 3'- GCAACAGATACCACACTGGGA-5'	104
2	Transferrin receptor 1 (*Tfrc*)	NM_011638.4	5'-GAGGCGCTTCCTAGTACTCC-3' 3'-CTTGCCGAGCAAGGCTAAAC-5'	121
3	Ferroportin (*Slc40a1*)	NM_016917.2	5'-TAAAGTGGCCCAGACGTCAC-3' 3'-GCAGACAGTAAGGACCCATCC-5'	130
4	BMP6 (*Bmp6*)	NM_007556.2	5'-AACCTTTCTTATCAGCATTTACCA-3' 3'-GTGTCCAACAAAAATAGGTCAGAG-5'	75
5	Matriptase-2 (*Tmprss6*)	NM_027902.2	5'-TGGCCTGGATAAACAGAGGC-3' 3'-CTGGAAACATCTCGGCATCTTC-5'	84
6	TfR 2 (*Tfr2*)	NM_015799.3	5'-GGTCCTGATCACCCTGCTAA-3' 3'-GGAGGTCGCTCCAGTACAAC-5'	158
7	Rpl19 (*Rpl19*)	NM_009078.2	5'- ATGAGTATGCTCAGGCTACAGA-3' 5'- GCATTGGCGATTTCATTGGTC-3'	104
8	Glucokinase (*Gck1*)	NM_010292.4	5' – TTGCAACACTCAGCCAGACA - 3' 3' – TGCTCTACCAGAGTCAACGAC - 5'	147
9	PEPCK (*Pck1*)	NM_011044.2	5' – TGGTGGGAACTCACTACTCGG - 3' 3' – ATGCCCAGGATCAGCATATG - 5'	105
10	Glucose-6-phosphatase (*G6pc*)	NM_008061.3	5' – TCTGTCCCGGATCTACCTTG – 3' 3' – GTAGAATCCAAGCGCGAAAC – 5'	172
11	Acetyl CoA carboxylasae (*Acaca*)	NM_133360.2	5' – GCCTCTTCCTGACAAACGAG – 3' 3' – TGACTGCCGAAACATCTCTG – 5'	239

12	Fatty acid synthase (*Fasn*)	NM_007988.3	5’ – AAGGCTGGGCTCTATGGATT – 3’ 3’ – TGAGGCTGGGTTGATACCTC – 5’	177
13	PGC-1α (*Ppargc1a)*	NM_008904.2	5’ – CCGTAAATCTGCGGGATGATG – 3’ 3’ – CAGTTTCGTTCGACCTGCGTAA – 5’	114
14	PPARγ (*Pparg2*)	NM_011146.3	5’ – GGTGGGCCAGAATGGCATCT – 3’ 3’ – TCTGGGAGATTCTCCTGTTGA – 5’	112
15	Adiponectin (*Adipoq*)	NM_009605.4	5’ – GTTGCAAGCTCTCCTGTTCC – 3’ 3’ – CCAAGAAGACCTGCATCTCC – 5’	225
16	ATGL (*Pnpla2*)	NM_025802.3	5’ – TGTGGCCTCATTCCTCCTAC – 3’ 3’ – TCGTGGATGTTGGTGGAGCT – 5’	158
17	HSL (*Lipe*)	NM_010719.5	5’ – GCTGGGCTGTCAAGCACTGT – 3’ 3’ – GTAACTGGGTAGGCTGCCAT – 5’	160
18	Ferritin (L) (*Ftl*)	NM_010240.2	5’ – CGGACCCTCATCTCTGTGAC – 3’ 3’ – CGGAGGTTGGTCAGATGGTT – 5’	94
19	Ferritin (H) (*Fth*)	NM_010239.2	5’ – AGACCGTGATGACTGGGAGA – 3’ 3’ – TGAAGTCACATAAGTGGGGATCA– 5’	134

3.7 Estimation of content of non-heme iron in epididymal white adipose tissue (eWAT)

The epididymal white adipose tissue (eWAT) is considered a visceral fat depot in rodents. It is commonly used as a source of visceral fat in studies done in mice. Approximately 100 mg of adipose tissue was weighed and homogenized in 500µL RIPA buffer. The homogenate was centrifuged at 14,000*g* for 10 min; the fat in the homogenate that accumulated at the top at the end of this step was removed; the centrifugation step was repeated. The supernatant then obtained (100µL) was digested by adding acid reagent (3M hydrochloric acid and 10% TCA) (1:2 v/v) and incubated at room temperature for 30 min; it was then centrifuged at 12,000*g* for 10 min to remove the precipitated protein. The supernatant obtained was used for estimation of iron.

Iron estimation in the adipose tissue was carried out by atomic absorption spectrophotometry (AAS). This method is more sensitive than the colorimetric methods. This technique was used to accurately estimate the low levels of iron found in adipose tissue. AAS-based iron estimations were done using a Perkin-Elmer AA200 atomic absorption spectrometer. A Perkin-Elmer iron hollow cathode lamp was used as the light source and an atomization temperature of 2300°C was provided by an air-acetylene flame. Slit width of 0.2 nm and wavelength of 248.3 nm were used as spectrometer parameters. The iron content in each sample was calculated based on readings obtained from a set of standards prepared by serial dilution of a standard solution of iron (1000 µg/mL, cat. no. 02583, Sigma, India). Results were normalized to the wet weight of tissue processed.

3.8. Visualization of tissue iron by perfusion-Perls' staining

The iron content of tissue was visualized in the experimental mice, by in-situ perfusion-Perls' staining, as described earlier (292). Mice, under terminal anesthesia, were perfused (by cardiac puncture) with 30 mL PBS supplemented with heparin (5 U/mL) at a rate of 6 mL/min, using a peristaltic pump. Following this, perfusion was continued (at 6 mL/min) with 60 mL of Prussian blue staining solution (4% paraformaldehyde, 1% potassium ferrocyanide and 1% HCl). One hour post-perfusion, liver and adipose tissue were isolated for macroscopic examination; photographs were obtained of the tissue.

3.9. Estimation of serum non-heme iron

Serum levels of iron (non-heme) were measured, using a colorimetric assay based on bathophenanthrolene dye-binding, as described earlier (302). Twenty microliters of serum was mixed with acid-reagent (3M HCl in 10% trichloroacetic acid) and allowed to stand at room temperature for 30 min. The mixture was centrifuged at 12,000g for 10 min to pellet the precipitated proteins. Ten microliters of the supernatant was added to 90 μL of chromogen reagent (consisting of 0.01% bathophenanthrolene disulphonate sodium salt [cat. no. 11880, Sigma India] and 0.1% [v/v] thioglycollic acid [cat. no. 528056, Sigma, India] in 4M sodium acetate [cat. no. 22342, SRL chemicals, India]) in a microtiter plate, mixed and incubated at room temperature for 15 min. Absorbance was measured at 540 nm. Iron levels were estimated based on a set of iron standards run in parallel.

3.10. Estimation of triglyceride content in the liver

The triglyceride content in liver tissue was estimated, as previously described (303). Lipids from liver tissue were extracted by Folch's extraction procedure. Liver tissue (approximately 100 mg) was weighed, homogenized in 750 µL of PBS and the total volume made up to 1 mL (with PBS). Two hundred microliters of the homogenate was added to 1200 µL of chloroform: methanol mixture (2:1; v/v), and mixed using a vortex mixer, for 10 seconds. To this, 100 µL of PBS was added and mixed thoroughly so that the final mixture consisted of chloroform, methanol and water in the ratio 8:4:3 (v/v/v). After centrifugation at 2000*g* for 10 min at 4°C, 200 µL of the chloroform layer (bottom layer) was transferred into fresh tubes and evaporated to dryness. The dried lipids were re-dissolved in 200 µL of 1% Triton-X100 in absolute alcohol. The tubes were kept on a rotator for 4 h to ensure complete dissolution.

The triglyceride content in the extracted lipid was estimated using a commercially available kit, according to manufacturer's instructions (cat. no. TR212, Randox Laboratories, UK). Briefly, 5 µL of lipid extract was added to 200 µL of color reagent (R1) in a microplate well, mixed and incubated at room temperature for 10 min. Absorbance was measured at 500 nm. The triglyceride content was calculated based on a set of standards run in parallel with the samples. Results were represented as milligrams of triglyceride per gram liver tissue.

3.11. Estimation of serum triglyceride:

Serum triglyceride levels were estimated using a commercially available kit (#10010303, Cayman Chemicals, USA) according to manufacturer's instructions.

3.12. Enzyme-linked immunosorbent assays (ELISA) for various analytes of interest

Serum samples were used for estimation of the following analytes, using commercially available ELISA kits: insulin (#10-1247-01, Mercodia, Sweden), hepcidin (#S-1465.0001, Peninsula Laboratories, USA), ferritin (#Ab157713, Abcam, UK), adiponectin (#MRP300, R&D Systems, USA), C-reactive protein (#MCRP00, R&D Systems, USA) and interleukin-6 (#DY406-05, R&D Systems, USA). All assays were carried out according to manufacturer's instructions.

3.13. Histological examination of liver

Liver tissue was fixed in 10% buffered formalin, embedded in paraffin and sections made for histological examination. Tissue sections were stained with H&E for light microscopy. Additional sections were stained with Prussian blue for visualization of iron deposits in the liver. All slides were examined by a histopathologist. Grading of steatosis was done based on standard criteria (304). Steatosis was graded as mild (<33%), moderate (33-66%) or severe (> 66%) depending upon the proportion of hepatocytes that showed steatotic changes). Photographs were taken using an Olympus DP21 digital camera attached to an Olympus BX43 light microscope.

3.14 Statistical analysis

Statistical Package for Social Scientists (SPSS), version 16.0, was used for all statistical analyses. The Kolmogorov–Smirnov and Shapiro–Wilk tests were used to check distribution of data. These showed that the data were not normally distributed. Therefore, non-parametric tests were used for statistical analysis. The Kruskal-Wallis (KW) test was employed to look for significant differences between the various groups studied. For data where the KW test showed

significant differences across the various groups studied, pair-wise comparisons between groups were made by the Mann-Whitney test. Correlation analyses were done by Spearman's correlation test. Multivariate analysis was performed by stepwise linear regression. A p value of less than 0.05 was used to indicate statistical significance in all cases.

4. Results

4.1. HFD-feeding of the experimental mice induced obesity and hepatosteatosis

High-fat diet (HFD)-fed mice progressively gained weight through the period of the study; body weights were significantly higher in these mice than in control diet (CD)-fed mice, from 4 weeks onwards (Fig 6.2.2-A). The weight of epididymal white adipose tissue (eWAT) was significantly higher in the HFD-fed mice than in CD-fed mice, at all the time points studied. Maximum weights were seen at 16 weeks; eWAT weights tended to decline with longer durations of HFD-feeding (20 and 24 weeks) (Fig 6.2.2-B). Weights of the liver in HFD-fed mice were also significantly higher than those from CD-fed mice; this effect was seen from 16 weeks onwards (Fig 6.2.2-C). The content of triglycerides in the liver was significantly elevated in the HFD-fed mice, at all the time points studied (Fig 6.2.2-D. This was associated with the finding of moderate to severe hepato-steatosis at 16, 20 and 24 weeks, as assessed by H & E staining of liver sections (304) (Fig 6.2.3).

Figure 6.2.2

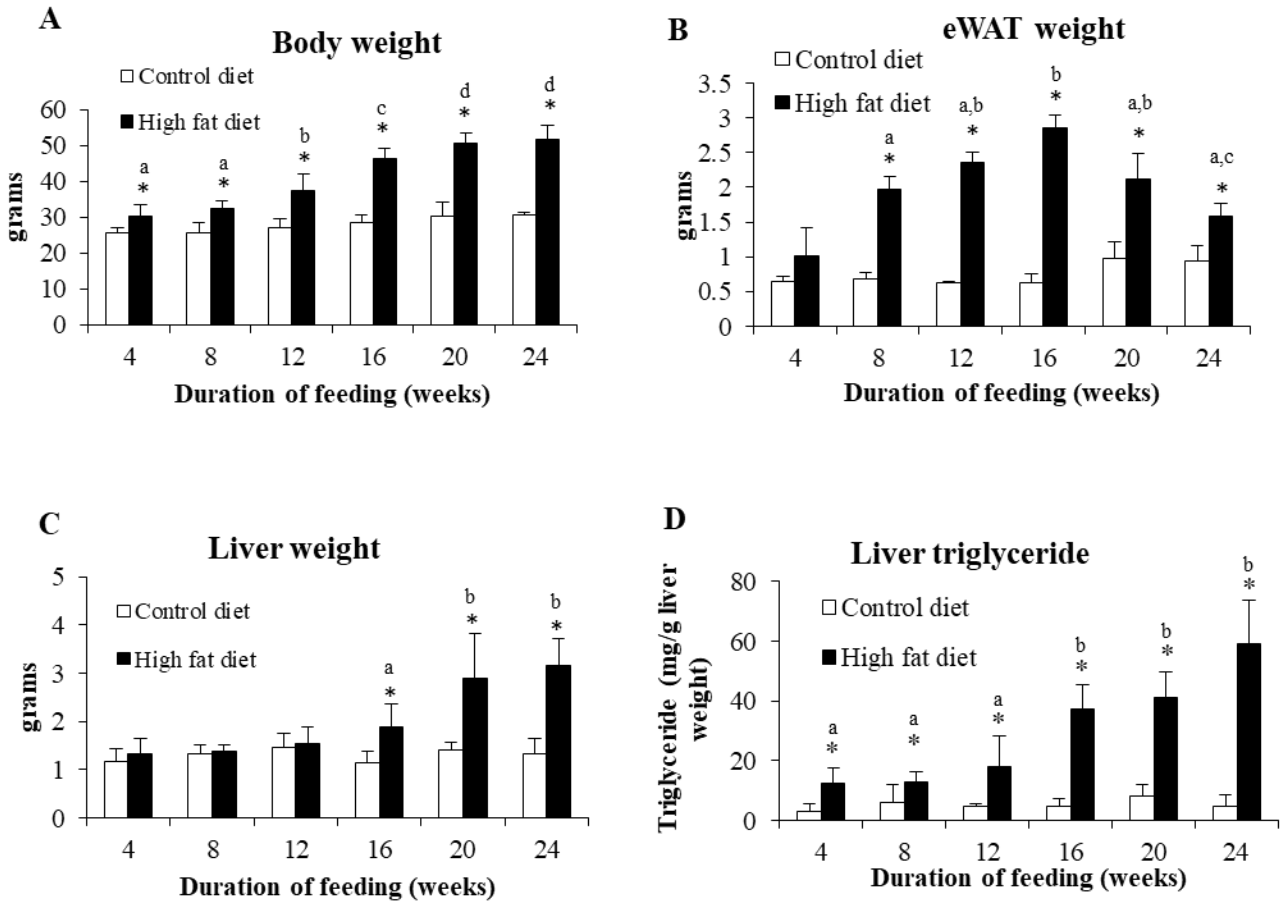

Figure 6.2.2.: Effect of HFD-feeding on body and tissue weights and liver triglyceride content.

Body (A), eWAT (B) and liver (C) weights in CD and HFD-fed mice at the end of each time point of feeding. Triglyceride content in the liver was estimated (D). Data are shown as means ± SD. In all cases, n = 6 (for both CD- and HFD-fed mice) at each time point. * indicates $p < 0.05$ when compared to the respective control group. Bars marked with dissimilar alphabets are significantly different from each other.

Figure 6.2.3

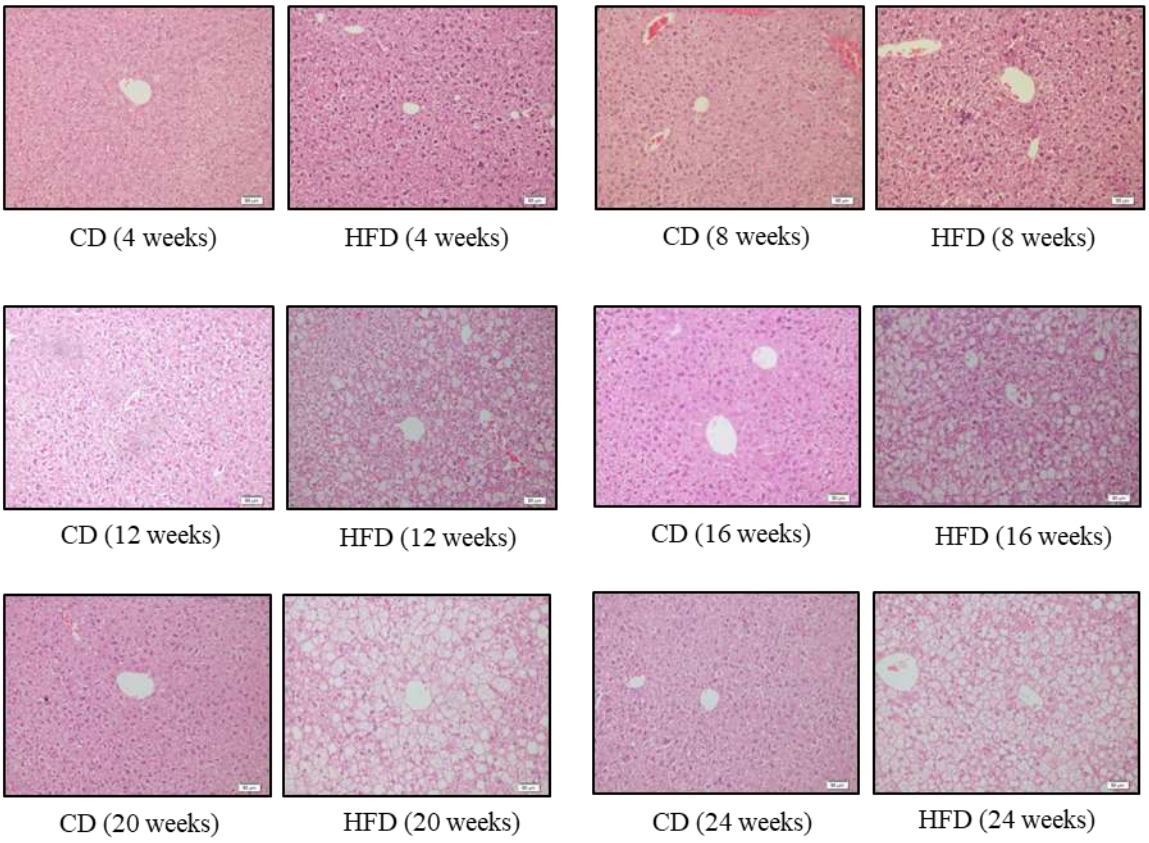

Figure 6.2.3: H & E staining of liver sections

Representative images of histological sections of the liver stained with hematoxylin and eosin (H & E) (20x), from mice fed CD or HFD for various time periods. Scale bars shown represent 50 µm.

4.2. HFD-feeding induced glucose intolerance, insulin resistance and hyperinsulinemia

HFD-feeding induced glucose intolerance in the mice (as assessed by GTT), as early as 4 weeks after initiation of feeding (Fig 6.2.4-A and B). However, there was no significant worsening of glucose tolerance with continuing HFD feeding for up to 24 weeks. Results of the ITT in these mice showed that HFD-feeding resulted in significantly increased IR from 8 weeks onwards (Fig 6.2.4-C and D). There was progressive worsening in IR with increasing durations of HFD feeding.

Serum insulin levels (non-fasting) were higher in HFD-fed mice, starting from 12 weeks onwards, with highest levels seen at 20 and 24 weeks (Fig 6.2.5-A). Serum adiponectin levels (Fig 6.2.5-B) increased initially in response to HFD (after 8, 12 and 16 weeks), but declined later at 20 and 24 weeks to levels similar to those in control mice. No significant changes were seen in serum triglyceride levels at any of the time points studied (Fig 6.2.5-C).

4.3. HFD-feeding induced hepatic insulin resistance

Phosphorylation-mediated activation of Akt is a key event in the intracellular signaling cascade triggered by binding of insulin to its cell surface receptor (20). As described above, mice fed HFD for 12, 16, 20 and 24 weeks showed increased serum insulin levels (Fig 6.2.5-A). Despite hyperinsulinemia, levels of phosphorylated Akt (p-Akt Ser473) were not significantly increased in the livers of HFD-fed mice except at 12 weeks (Fig 6.2.6-A). The ratio of liver p-Akt to plasma insulin (a marker of the degree of activation of intracellular signaling induced by insulin) (305) were generally lower than values in the CD-fed mice, with significant decreases seen after 20 and 24 weeks of HFD feeding (Fig 6.2.6-B).

Insulin is known to induce the expression of glucokinase (*Gck*), a glycolytic enzyme (306), and to suppress levels of phosphoenolpyruvate carboxykinase (PEPCK/ *Pck1*) and glucose-6-phosphatease (*G6pc*), both of which are key gluconeogenic enzymes in the liver (307). *Gck1* expression was generally higher in HFD-fed mice at all the time points studied, with the increase being significant at 12 weeks (Fig 6.2.7-A). There was no significant decrease in mRNA expression *Pck1* or *G6pc* in the liver at any of the time points studied, despite significant elevations in serum insulin levels in HFD-fed mice (at 12, 16, 20 and 24 weeks) (Fig 6.2.7-B-C). Peroxisome proliferator-activated receptor gamma co-activator-1 alpha (PGC-1α / *Ppargc1a*) is a transcriptional co-activator that plays a critical role in modulating hepatic gluconeogenesis and is strongly down-regulated by insulin (308). However, despite elevated insulin levels, expression of *Ppargc1a* was not significantly reduced in HFD-fed mice (Fig 6.2.7-D). Similarly, the genes for lipogenic enzymes, acetyl CoA carboxylase (*Acaca*) and fatty acid synthase (*Fasn*), are known to be induced by insulin; however, no significant increase in expression of these genes was seen in HFD-fed mice (Fig 6.2.7-E and F).

Overall, these results show that HFD-feeding in mice significantly dampened insulin-induced activation of the Akt pathway in the liver of these animals. Consistent with decreased hepatic insulin signaling, expression of lipogenic and gluconeogenic genes were not significantly altered in these mice, despite hyperinsulinemia. Taken together, these results appear indicative of hepatic insulin resistance induced by high-fat feeding in these mice.

Figure 6.2.4

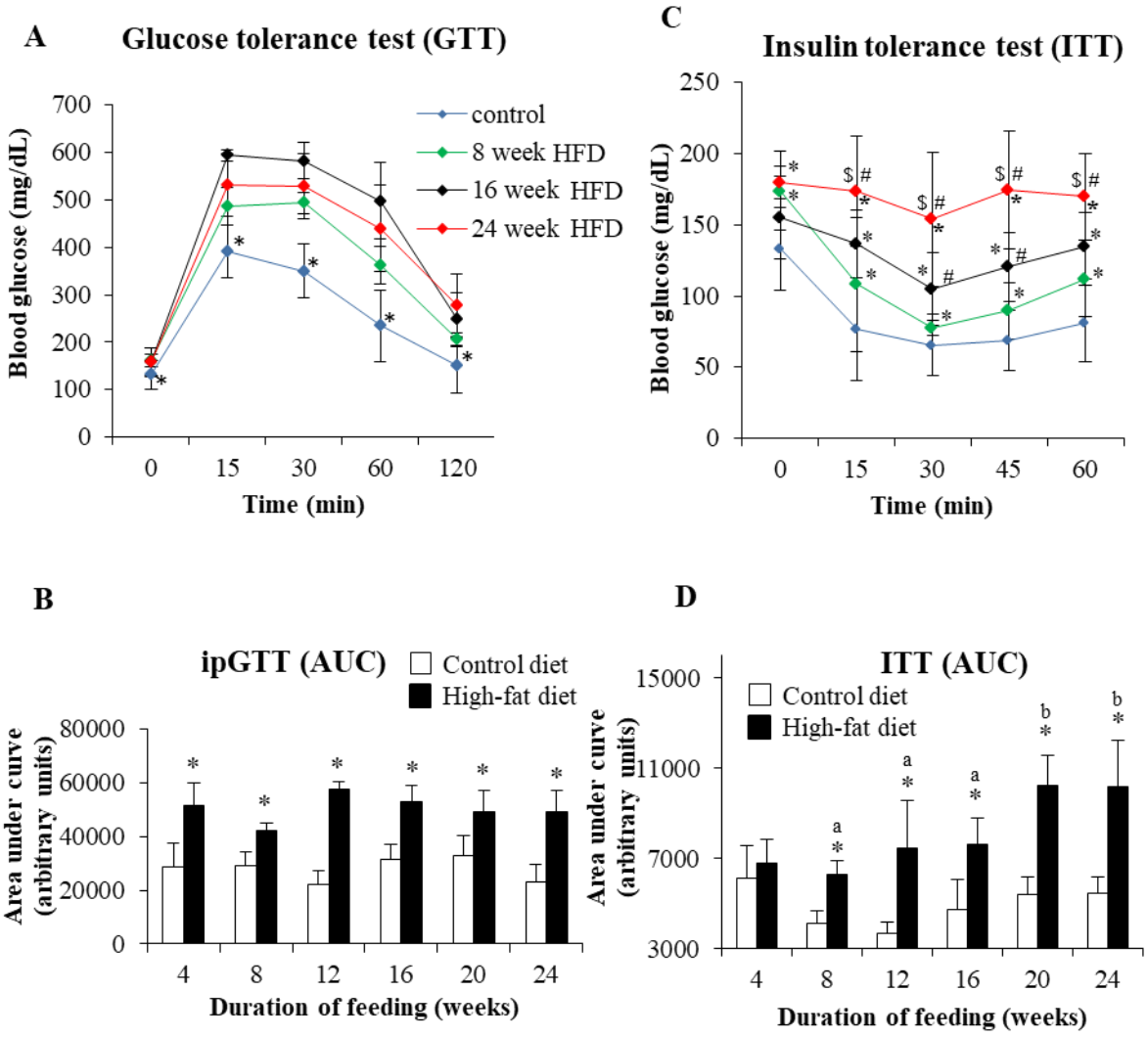

Fig 6.2.4.: Effect of HFD-feeding on glucose tolerance and insulin sensitivity in vivo

Intraperitoneal glucose tolerance (A, B) and insulin tolerance (C,D) tests were performed in mice fed CD or HFD for various durations. Data are shown as means ± SD. In A, * indicates comparison of control with 8, 16 and 24 weeks HFD. In C, * indicates comparison to control, # to 8 weeks HFD and $ to 16 weeks HFD. In B and D, * indicates $p < 0.05$ when compared to the respective control group. Bars marked with dissimilar alphabets are significantly different from each other. Area-under-curve (AUC) was calculated by the linear trapezoidal method. In all cases, n = 6 (for both CD- and HFD-fed mice) at each time point.

Figure 6.2.5

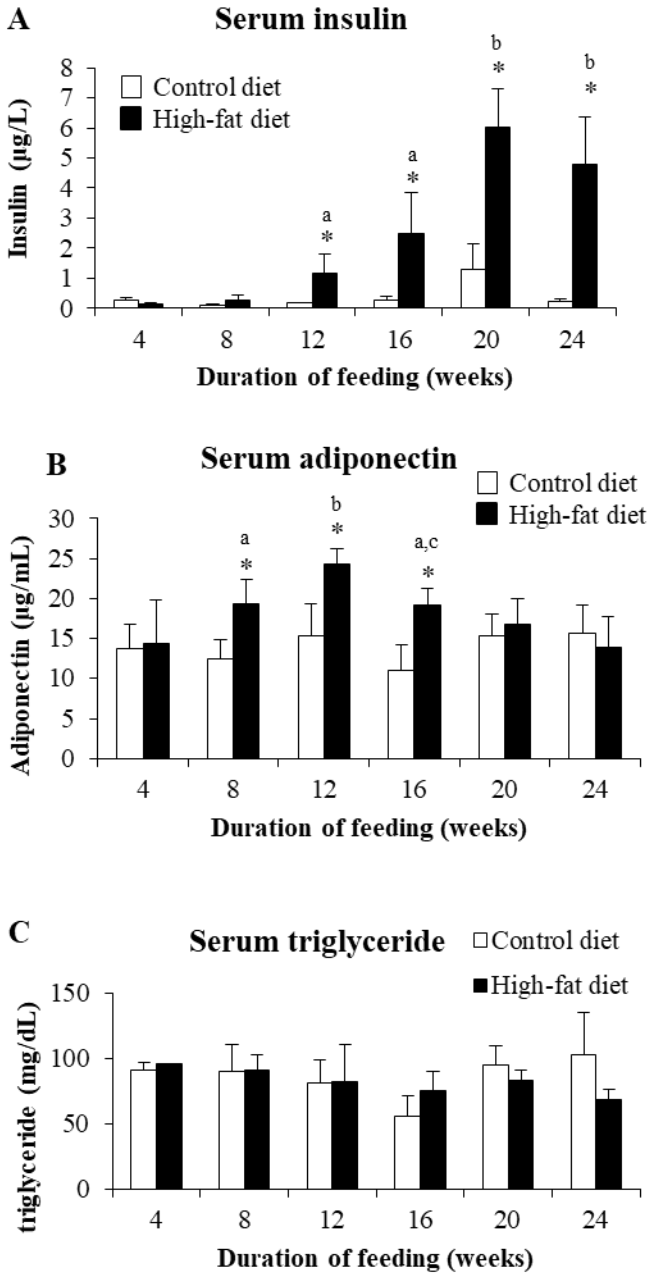

Figure 6.2.5: Effect of HFD-feeding on serum levels of insulin, adiponectin and triglycerides

Serum levels of insulin (non-fasting) (A), adiponectin (B) and triglycerides (C) in mice fed CD and HFD for various durations. Data are shown as means ± SD. In all cases, n = 6 (for both controls and HFD-fed mice) at each time point. * indicates $p < 0.05$ when compared to the respective control group. Bars marked with dissimilar alphabets are significantly different from each other.

Figure 6.2.6

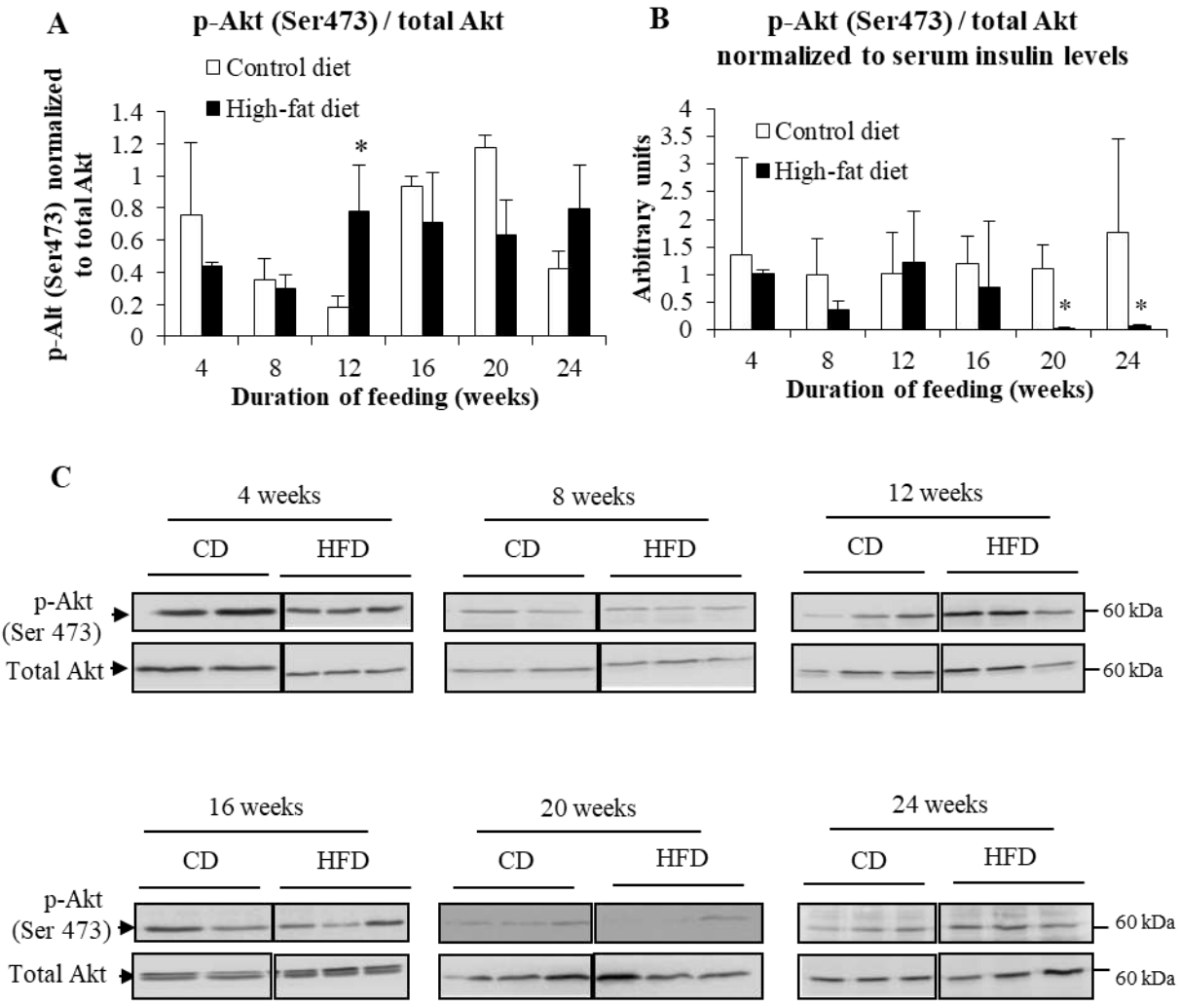

Figure 6.2.6: Effect of HFD-feeding on Akt phosphorylation (Ser 473) in the liver

A: Ratio of phosphorylated Akt to total Akt (p-Akt (Ser 473) / total Akt) in livers from CD and HFD-fed mice, as determined by western blotting. B: Liver p-Akt (Ser 473) / total Akt ratio normalized to serum insulin levels. C: Representative images of western blots for p-Akt (Ser 473) and total Akt in mice fed CD or HFD for various durations (as indicated). In A and B, data are shown as mean ± SE; n = 3 (for both controls and HFD-fed mice) at each time point. * indicates $p \leq 0.05$ when compared to the respective control group.

Figure 6.2.7

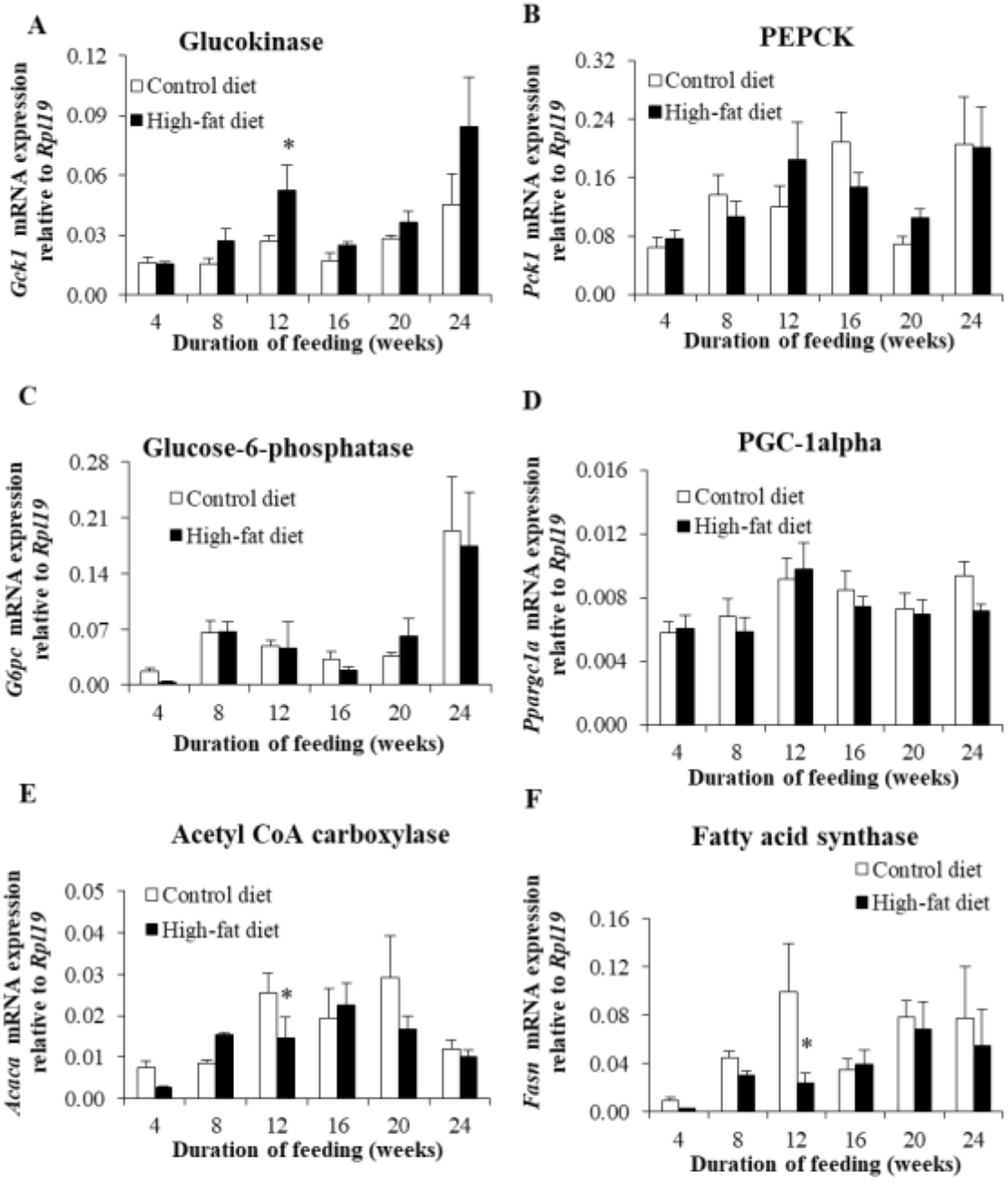

Figure 6.2.7: Effect of HFD-feeding on mRNA expression of genes known to be regulated by insulin in the liver

Gene expression of glucokinase (A), phosphoenolpyruvate carboxykinase (B), glucose-6-phosphatase (C), PGC-1α (D), acetyl CoA carboxylase (E) and fatty acid synthase (F), as determined by qPCR. A: Data are shown as mean ± SD; n = 6 (for both CD- and HFD-fed mice) at each time point. * indicates $p \leq 0.05$ when compared to the respective control group.

4.4. HFD-feeding decreased hepatic hepcidin expression and serum hepcidin levels

Gene expression of hepcidin (*Hamp1*) in the liver of HFD-fed mice was reduced at several of the time points studied, with significantly lower levels seen at 4 and 24 weeks (Fig 6.2.8-A). Serum hepcidin levels were also generally lower in HFD-fed mice at most of the time points studied, with significantly lower levels seen at 4, 20 and 24 weeks (Fig 6.2.8-B). Hepatic *Hamp1* mRNA expression was highly correlated with serum hepcidin levels (Fig 6.2.8-C).

4.5. Effect of HFD-feeding on liver iron content and iron-related proteins

HFD-feeding induced a progressive decrease in hepatic non-heme iron content from 12 weeks onwards (Fig 6.2.9-A). *In situ* perfusion of the liver with Perls' staining fluid, after 24 weeks of HFD, showed decreased staining of the liver (Fig 6.2.9-B), confirming reduced iron content. Gene expression of transferrin receptor 1 in the liver was increased in HFD-fed mice (Fig 6.2.9-C), an observation that is also indicative of decreased intracellular iron levels. This was associated with decreases in protein expression of ferritin (the iron storage protein) (Fig 6.2.10-C and D). However, mRNA levels of ferritin (L) (at 20 and 24 weeks) and ferritin (H) (at 16, 20 and 24 weeks) were significantly increased by HFD-feeding (Fig 6.2.10-A and B). Gene expression (Fig 6.2.11-A) and protein levels (Fig 6.2.11-B and C) of ferroportin, the only known cellular iron export protein, were not significantly affected by HFD feeding.

Figure 6.2.8

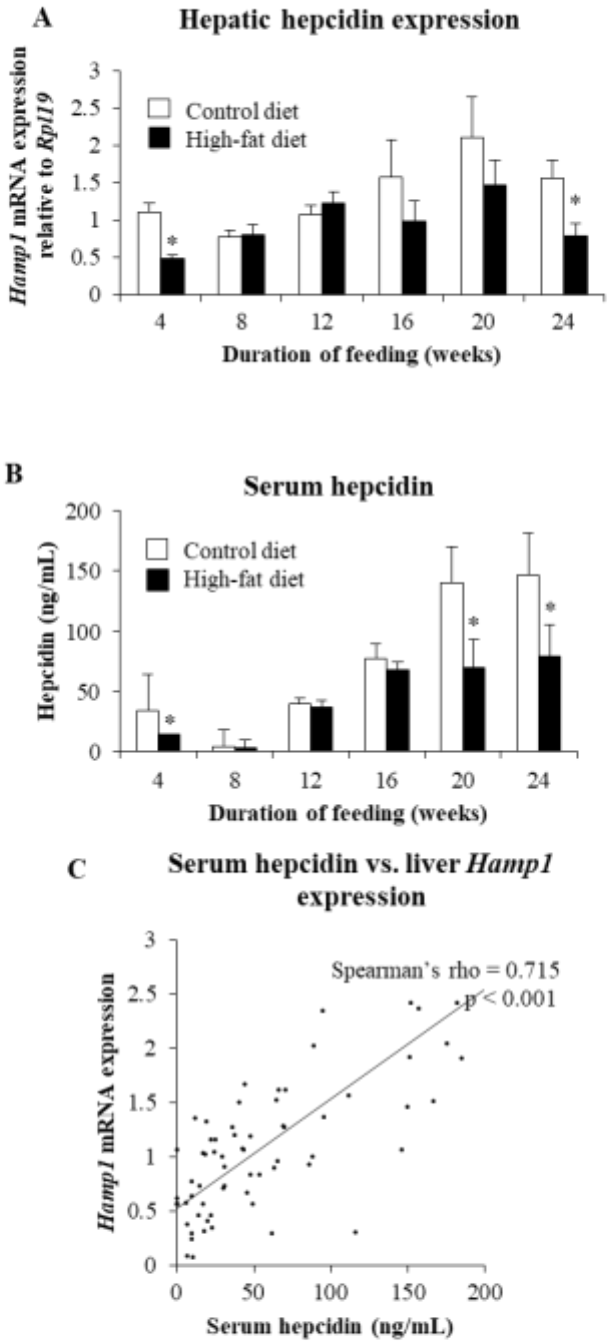

Figure 6.2.8: Effect of HFD-feeding on hepatic hepcidin expression and serum hepcidin levels

A: Hepatic *Hamp1* expression determined by qPCR. B: Serum hepcidin levels estimated by ELISA C: Correlation between serum hepcidin levels and hepatic *Hamp1* expression. In A and B, data show means ± SE; n = 6 (for both CD- and HFD-fed mice) at each time point. * indicates $p < 0.05$ when compared to the respective control group.

Fig 6.2.9

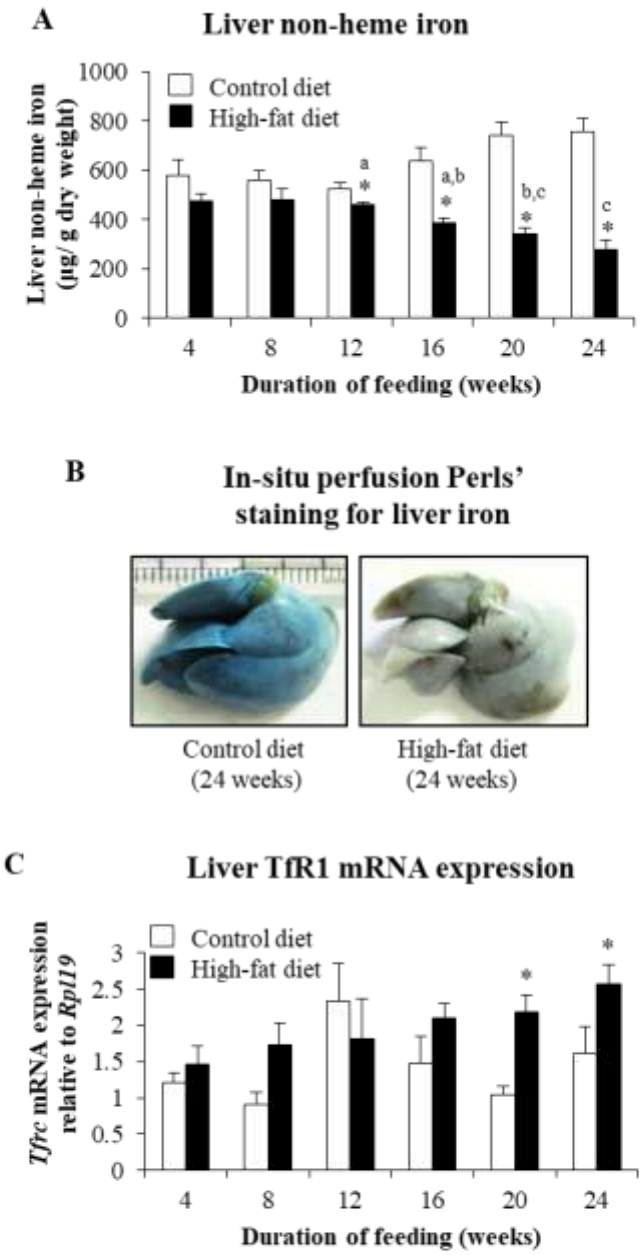

Figure 6.2.9: Effect of HFD-feeding on hepatic iron content and TfR1 mRNA expression

A: Liver non-heme iron estimated by a colorimetric assay based on bathophenanthrolene dye binding. B: Representative images of in-situ perfusion Perls' staining for iron in livers of mice fed CD or HFD for 24 weeks. C: Liver TfR1 *(Tfrc)* mRNA expression determined by qPCR Data are shown as mean ± SE; n = 6 (for both CD- and HFD-fed mice) at each time point. * indicates $p < 0.05$ when compared to the respective control group. Bars marked with dissimilar alphabets are significantly different from each other.

Figure 6.2.10

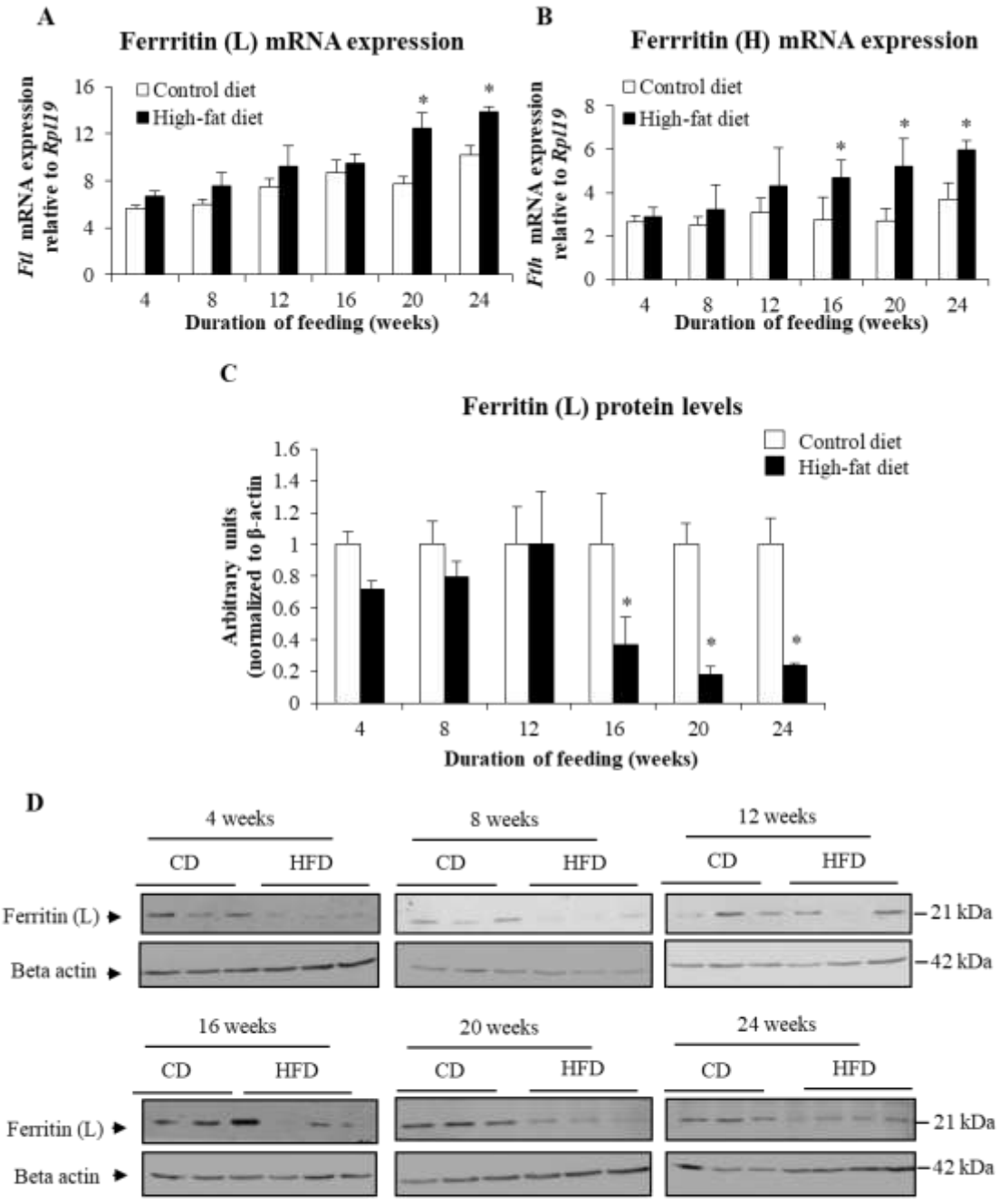

Figure 6.2.10: Effect of HFD-feeding on ferritin mRNA and protein expression in the liver

A-B: Liver ferritin (L) (*Ftl*) (A) and ferritin (H) (*Fth*) (B) mRNA expression determined by qPCR. C: Protein levels of ferritin (L) in the liver determined by western blotting. D: Representative images of western blots for ferritin (L) at all time points studied (as indicated). Data are shown as mean ± SE; n = 6 (for both CD- and HFD-fed mice) at each time point studied. * indicates $p < 0.05$ when compared to the respective control group.

Figure 6.2.11

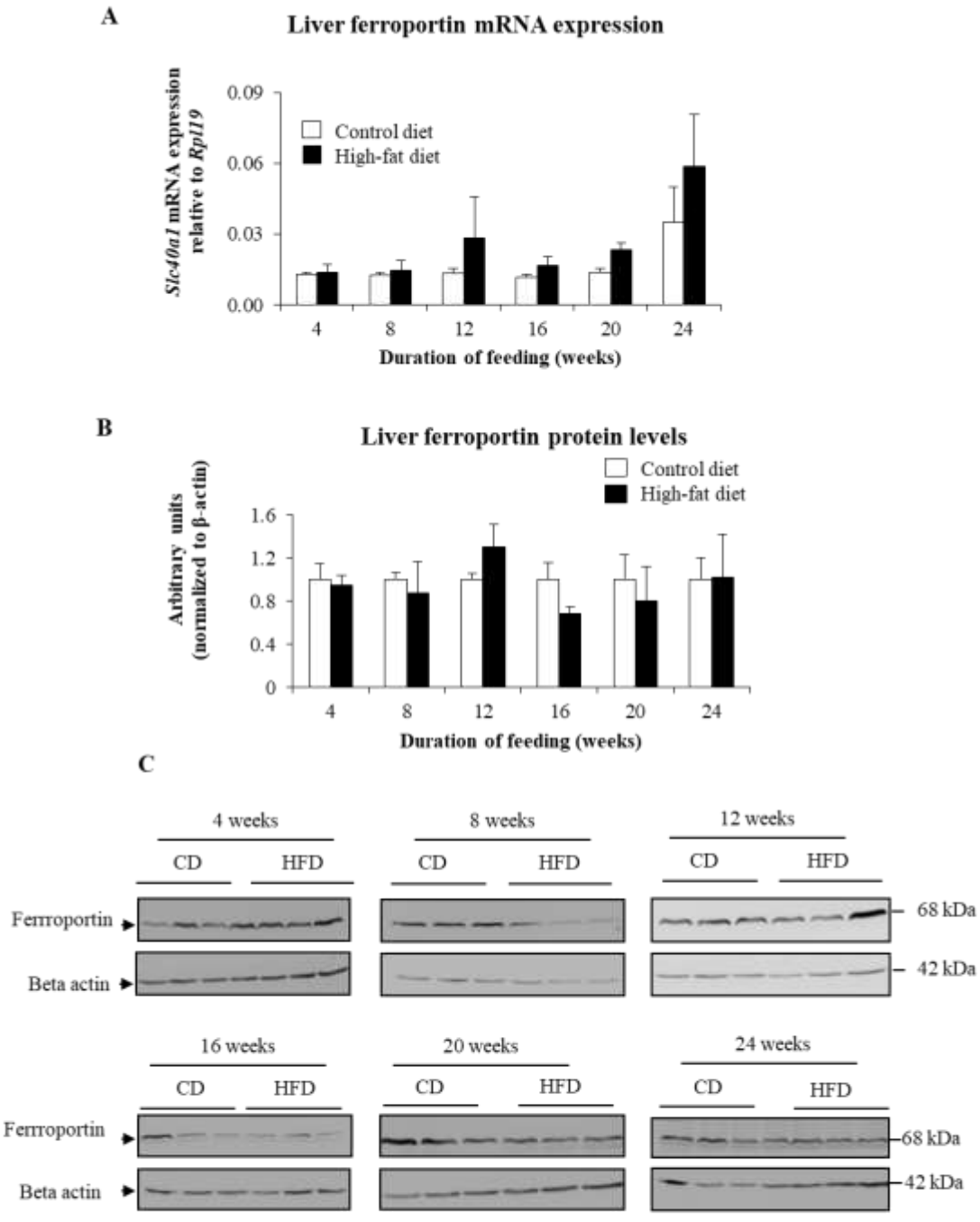

Figure 6.2.11: Effect of HFD-feeding on ferroportin mRNA and protein levels in the liver

A: Liver ferroportin (*Slc40a1*) mRNA levels determined by qPCR. B: Protein levels of ferroportin determined by western blotting. C: Representative images of western blots for ferroportin at all time points studied (as indicated). Data are shown as mean ± SE; n = 6 (for both CD- and HFD-fed mice) at each time point studied.

4.6 Effect of HFD-feeding on BMP6, matriptase-2 and TfR2 in the liver

BMP6 is a powerful inducer of hepcidin (72); it is secreted primarily by hepatic sinusoidal endothelial cells (92). Matriptase-2, on the other hand, is a membrane-bound serine protease that suppresses hepcidin expression by inhibiting signaling via the BMP-SMAD pathway (78). Both BMP6 (88,288) and matriptase-2 (94) are known to be regulated by hepatic iron stores. In the present study, *Bmp6* expression in the liver showed significant increases initially (at 4 and 8 weeks of HFD-feeding); however, its expression in HFD-fed mice was not different from CD-fed mice, with after longer periods of HFD-feeding (Fig 6.2.12-A). Matriptase-2 (*Tmprss6*) gene expression was higher in HFD-fed mice; the increases were statistically significant at 8 weeks and tended to be statistically significant at 4 weeks ($p=0.055$) and 24 weeks ($p=0.082$) (Fig 6.2.12-B). Transferrin receptor 2 (TfR2) plays an important role in regulating hepcidin expression in response to changes in serum iron levels / transferrin saturation (86). TfR2 (mRNA and protein levels) were not significantly affected by HFD-feeding at any of the time points studied (Fig 6.2.13).

4.7. HFD-feeding did not affect serum iron levels but increased serum ferritin

HFD-feeding did not affect serum levels of iron (Fig 6.2.14-A). However, serum ferritin, which is commonly considered to be a marker of body iron stores, was significantly increased by HFD-feeding at 12, 20 and 24 weeks (Fig 6.2.14-B).

Fig 6.2.12

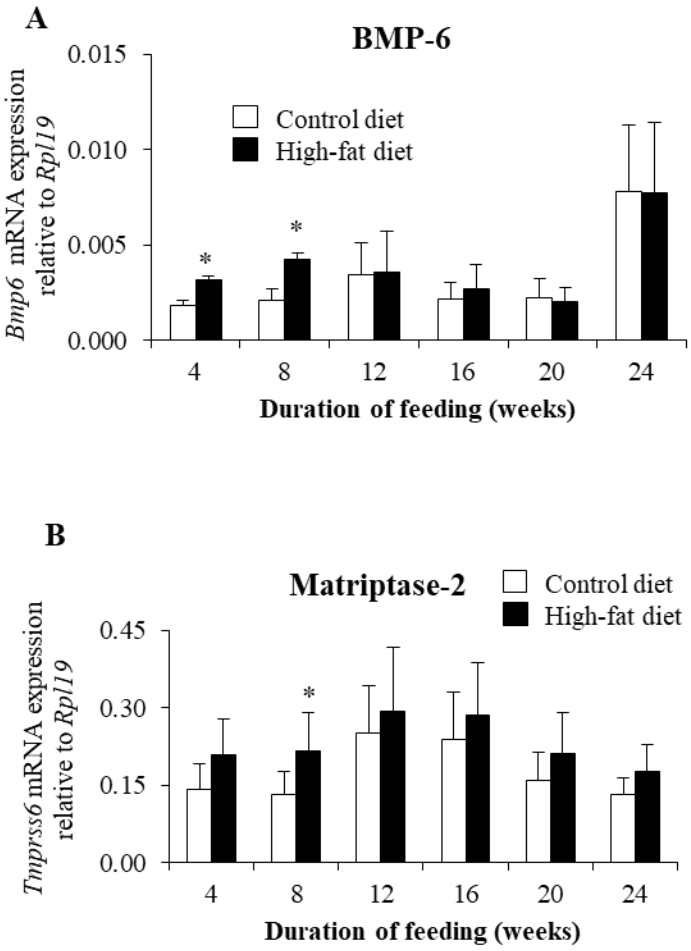

Figure 6.2.12: Effect of HFD-feeding on BMP6 and matriptase-2 mRNA expression

Gene (mRNA) expression of BMP6 (A) and matriptase-2 (B) in the liver determined by qPCR. Data are shown as mean ± SE; n = 6 (for both CD- and HFD-fed mice) at each time point. * indicates $p < 0.05$ when compared to the respective control group.

Figure 6.2.13

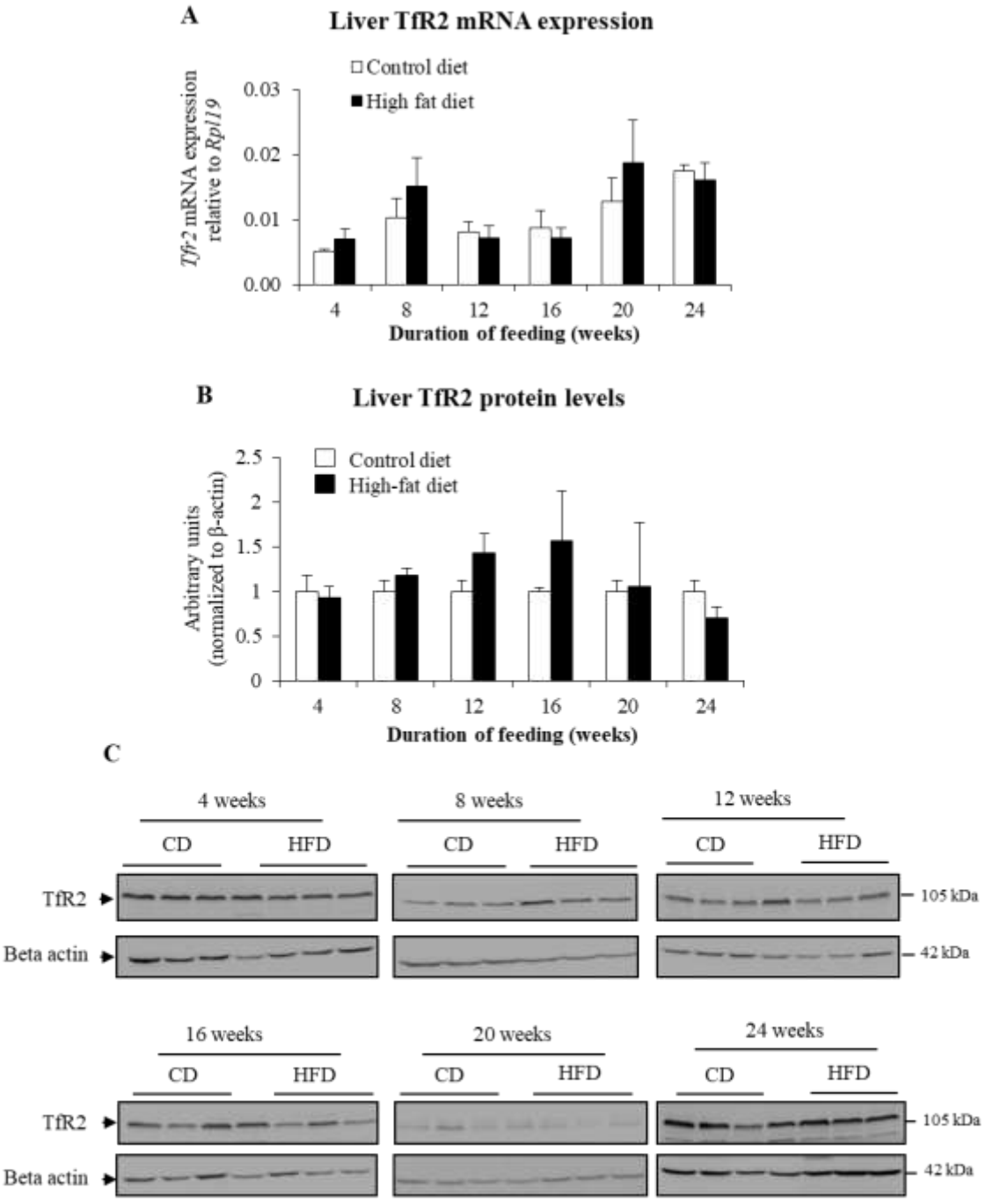

Figure 6.2.13: Effect of HFD-feeding on TfR2 protein levels in the liver

A: Liver TfR2 mRNA expression determined by qPCR. B: Protein levels of liver TfR2 as determined by western blotting. C: Representative images of western blots for TfR2 at all time points studied (as indicated). Data are shown as mean ± SE; n = 3 (for both CD- and HFD-fed mice) at each time point. * indicates $p < 0.05$ when compared to the respective control group.

Fig 6.2.14

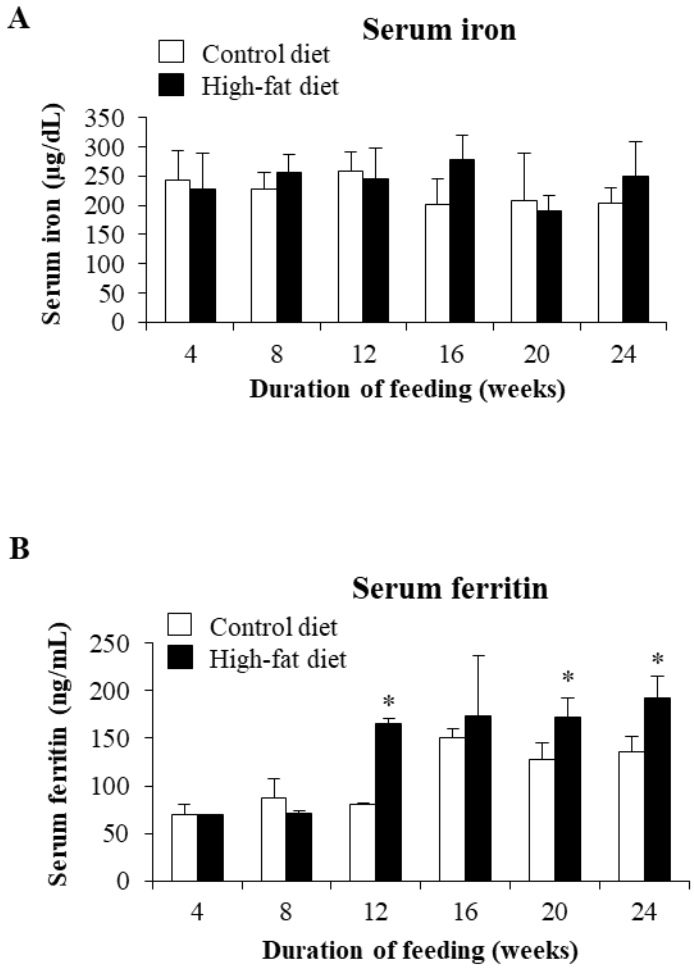

Figure 6.2.14: Effect of HFD-feeding on serum iron and ferritin levels

Serum levels of iron (A) and ferritin (B) in CD- and HFD-fed mice. Data are shown as mean ± SD; n = 6 for A and n=3 for B at each time point (for both CD- and HFD-fed mice). * indicates $p < 0.05$ when compared to the respective control group.

4.8 HFD-feeding did not affect markers of systemic or hepatic inflammation

Inflammation is known to affect systemic iron homeostasis and induce hepcidin expression in the liver, via interleukin-6 (IL-6) (112). HFD did not affect serum levels of C-reactive protein (CRP), a marker of systemic inflammation (Fig 6.2.15-A). In addition, in both CD- and HFD-fed mice, levels of IL-6 in the serum were low and below the detection limit (15.6 pg/mL) of the assay used for IL-6 estimation, at all the time points studied.

Hepatic mRNA expression levels of serum amyloid A (Saa1), an acute phase reactant, and IL-6 were also determined. HFD-feeding did not induce significant increases in *Saa1* mRNA at any of the time points studied (Fig 6.2.15-B). Gene expression of IL-6 in the liver was found to be very low and no significant increases were induced by HFD-feeding at any of the time points studied (Fig 6.2.15-C).

4.9 HFD-feeding resulted in metabolic dysfunction in the adipose tissue

The effects of HFD-feeding on expression of key genes involved in lipogenesis and lipolysis in the epididymal white adipose tissue (eWAT) were determined. Peroxisome proliferator activated receptor gamma (PPARγ), the master regulator of adipocyte differentiation and lipogenesis, was down-regulated in mice fed HFD for 16, 20 and 24 weeks (Fig 6.2.16-A). Fatty acid synthase and adiponectin are known targets of PPAR γ; mRNA levels of these were also down-regulated at the same time points (Fig 6.2.16-B and C). Gene expression of key enzymes involved in lipolysis, adipose tissue triglyceride lipase (ATGL) and hormone-sensitive lipase (HSL), were also found to be suppressed by HFD-feeding at these time points (Fig 6.2.16-D and E).

Figure 6.2.15

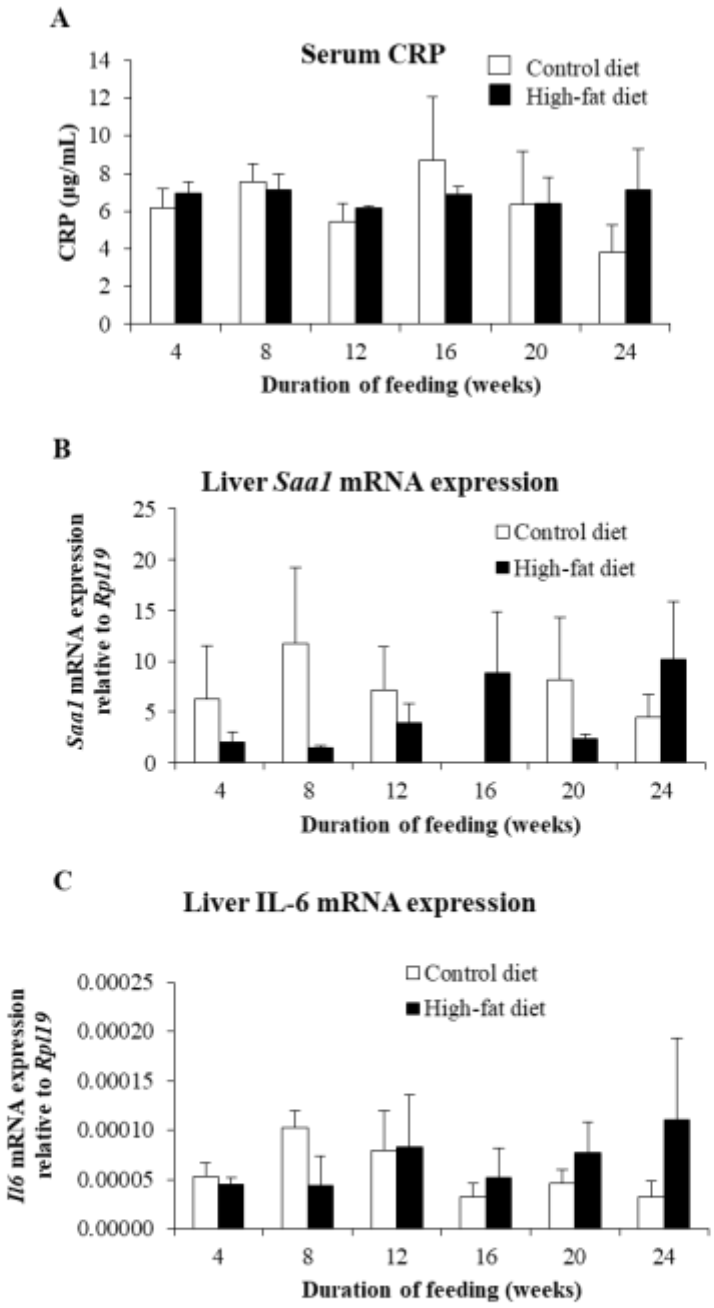

Figure 6.2.15: Effect of HFD-feeding on markers of hepatic and systemic inflammation

A: Serum levels of C-reactive protein (CRP) estimated by ELISA. B-C: Liver *Saa1* (B) and *Il6* mRNA expression determined by qPCR. Data are shown as mean ± SE; n = 3 for A and C and n = 6 for B (both CD- and HFD-fed mice) at each time point. * indicates $p < 0.05$ when compared to the respective control group.

Figure 6.2.16

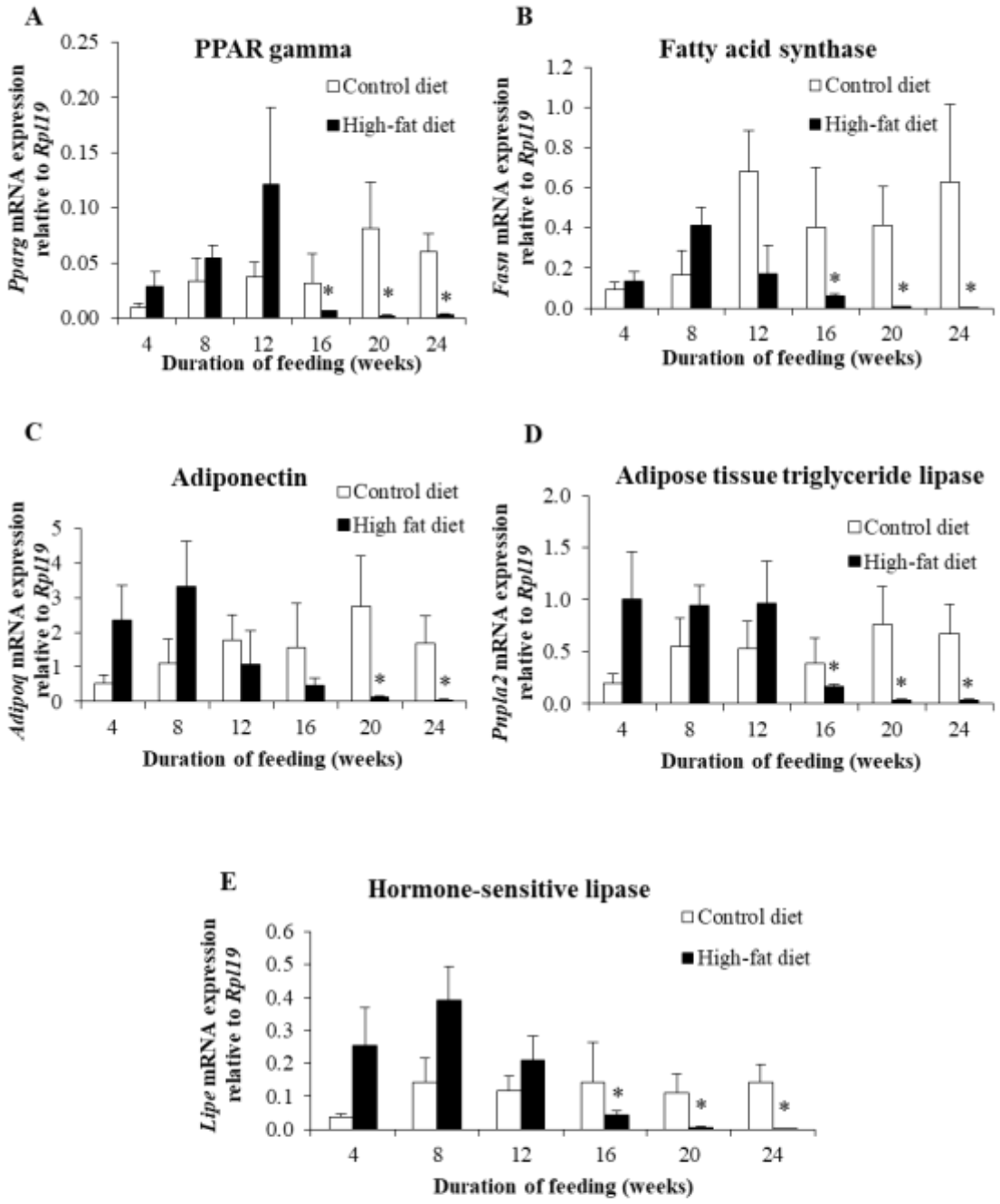

Figure 6.2.16: Effect of HFD-feeding on expression of key genes involved in lipogenesis and lipolysis in the adipose tissue

Gene (mRNA) expression of PPARγ (A), fatty acid synthase (B), adiponectin (C), ATGL (D) and HSL (E) in the adipose tissue, as determined by qPCR. Data are shown as mean ± SE; n = 3 (for both CD- and HFD-fed mice) at each time point. * indicates $p < 0.05$ when compared to the respective control group.

4.10 HFD-feeding resulted in alterations in parameters of iron metabolism in the adipose tissue

HFD-feeding tended to increase the iron content in eWAT at many of the time points studied. The increase was statistically significant at the 24 weeks time point (Fig 6.2.17-A). The weight of eWAT was found to be significantly higher in mice fed HFD than in those fed CD (Fig 6.2.2-B). The total iron content in the eWAT was calculated by multiplying the iron content per gram of adipose tissue by the total weight of the eWAT. This was found to be significantly higher in HFD-fed mice than CD-fed mice, from 8 weeks onwards (Fig 6.2.17-B). There was a significant negative correlation between levels of iron in the liver and total eWAT iron (Fig 6.2.17-C), showing that the decrease in liver iron content was associated with increased iron content in the adipose tissue.

Gene (mRNA) expression of ferritin (L) (at 12, 16, 20 and 24 weeks) and ferritin (H) (at 16, 20 and 24 weeks) was significantly up-regulated in the eWAT of HFD-fed mice (Fig 6.2.18-A and B). However, protein levels of ferritin (L) (Fig 6.2.18-C and D) were not correspondingly increased. *Tfrc* mRNA expression did not show significant changes, except for an increase in HFD-fed mice at 8 weeks (Fig 6.2.19-A). Protein levels of ferroportin were significantly lower in HFD-fed mice at 12 and 16 weeks, but unaffected at the other time points studied (Fig 6.2.19-B and C).

Fig 6.2.17

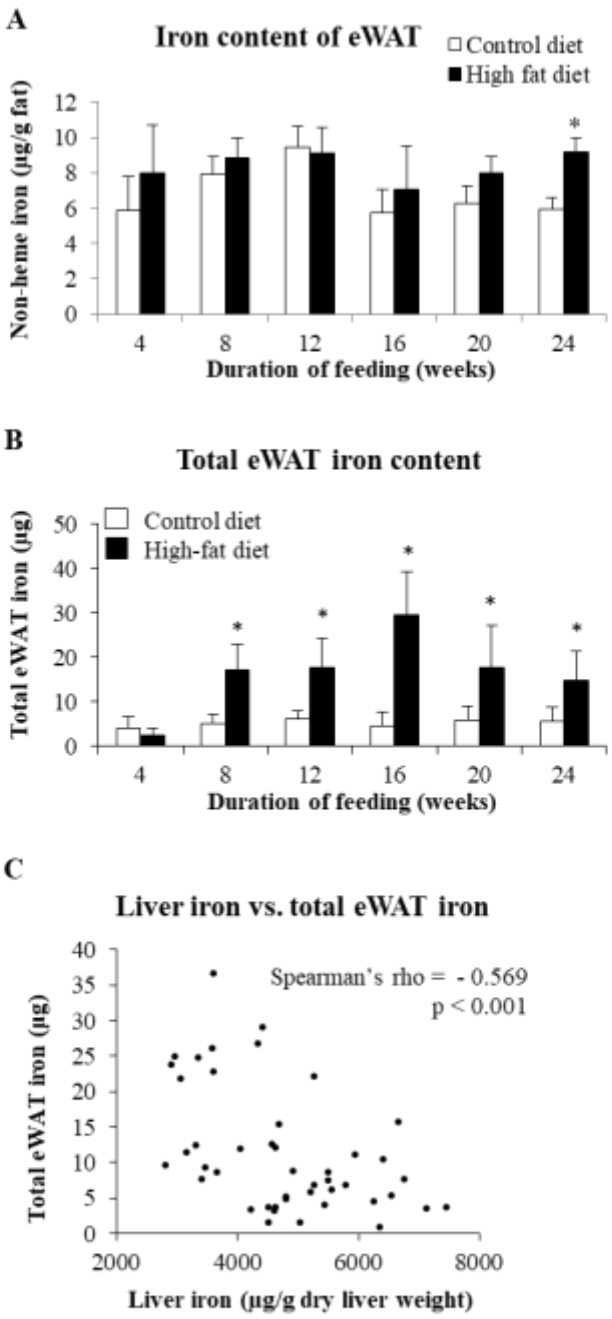

Figure 6.2.17: Effect of HFD-feeding on iron content in adipose tissue

A: Iron levels in epididymal white adipose tissue (eWAT) estimated by AAS. B: Total iron content in eWAT (iron content per gram adipose tissue multiplied by total eWAT weight in grams). C: Correlation between iron levels in the liver and total iron content in eWAT. Data are shown as mean ± SE; n = 6 (for both controls and HFD-fed mice) at each time point. * indicates $p < 0.05$ when compared to the respective control group.

Fig 6.2.18

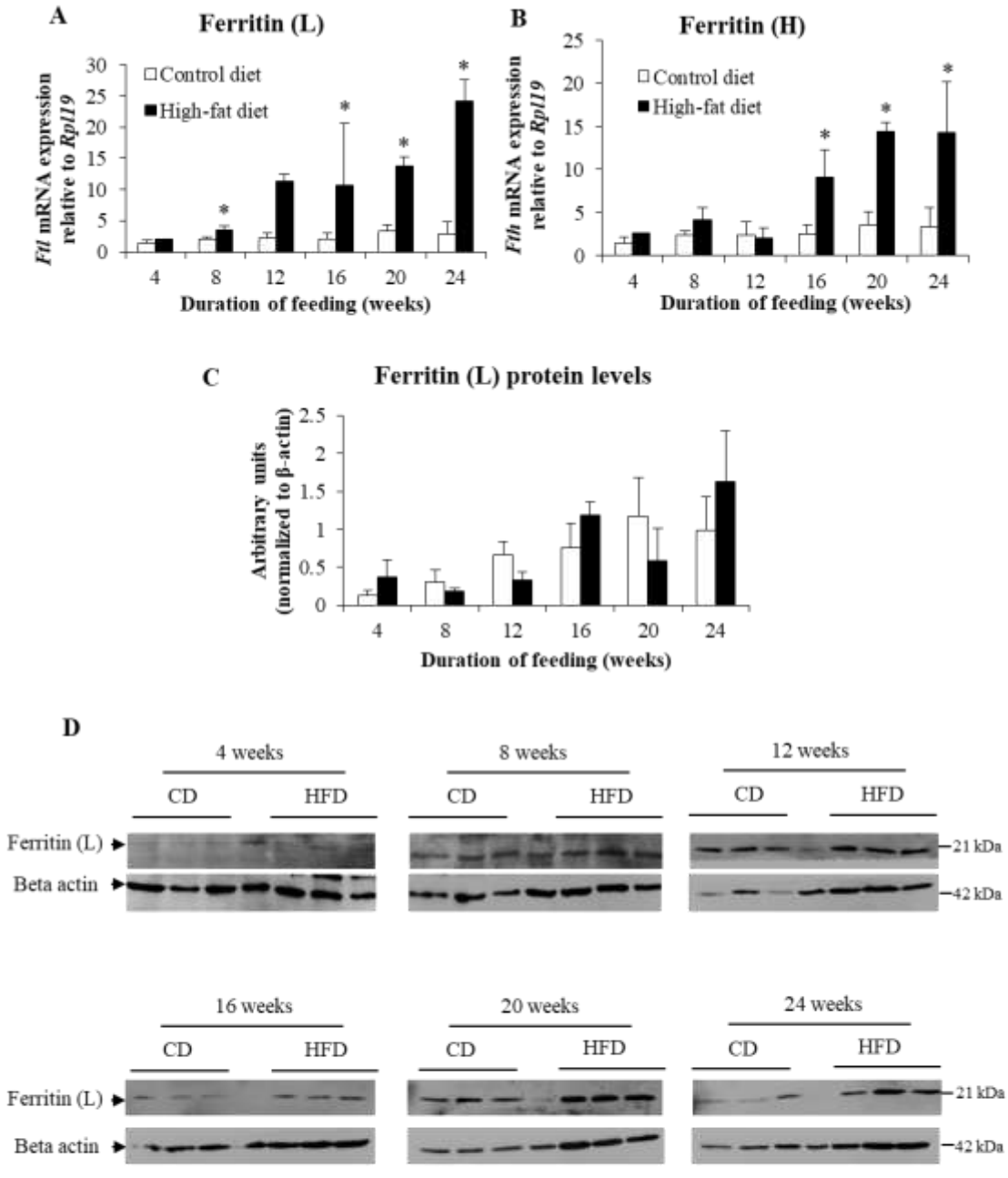

Fig 6.2.18: Effect of HFD-feeding on ferritin mRNA and protein levels in the adipose tissue

A-B: Ferritin (L) (*Ftl*) (A) and ferritin (H) (*Fth*) (B) mRNA expression in eWAT determined by qPCR. C: Protein levels of ferritin (L) determined by western blotting. D: Representative images of western blots for ferritin (L) at all time points studied (as indicated). Data are shown as mean ± SE; n = 3 (for both CD- and HFD-fed mice) at each time point studied. * indicates $p < 0.05$ when compared to the respective control group.

Figure 6.2.19

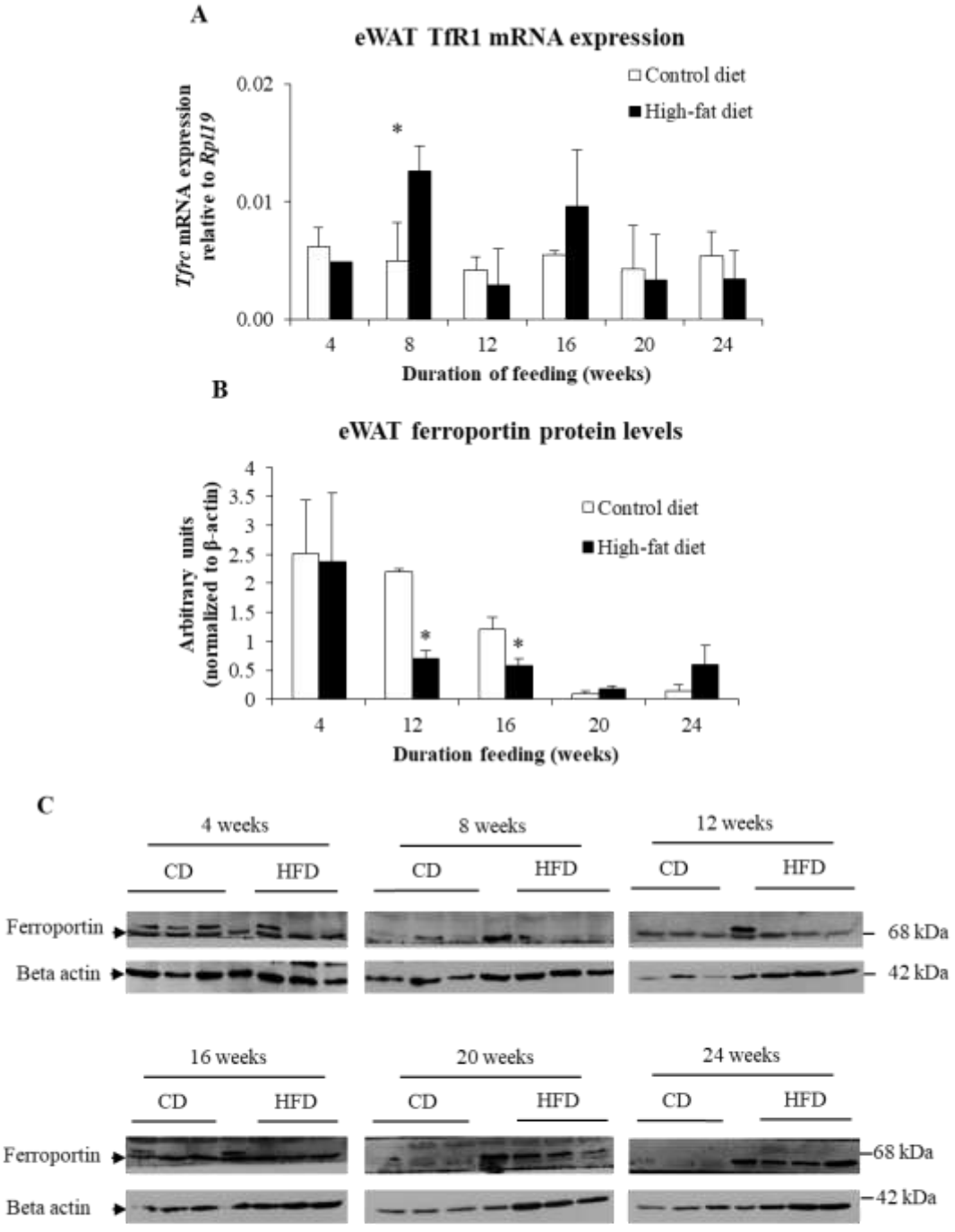

Figure 6.2.19: Effect of HFD-feeding on TfR1 mRNA and ferroportin protein levels in adipose tissue

A: eWAT TfR1 (*Tfrc*) mRNA levels determined by qPCR. B: Protein levels of ferroportin determined by western blotting. C: Representative images of western blots for ferroportin at all time points studied (as indicated). Data are shown as mean ± SE; n = 3 (for both CD- and HFD-fed mice) at each time point studied. * indicates $p \leq 0.05$ when compared to the respective control group.

4.11. Effect of HFD-feeding on iron content of spleen and skeletal muscle

The iron content in the spleen from mice fed HFD was significantly lower at 8 and 12 weeks than in that from CD-fed mice (Fig 6.2.20-A). The iron content of the skeletal muscle (quadriceps) was not affected by HFD-feeding (Fig 6.2.20-B).

4.12. Effect of HFD- feeding on expression of duodenal proteins involved in absorption of dietary non-heme iron

HFD feeding did not produce any significant effect on mRNA expression of duodenal proteins involved in iron absorption, viz. divalent metal transporter – 1 (DMT1), ferroportin and duodenal cytochrome b (Dcytb) (Fig 6.2.21-A-C) HFD did not have a consistent effect on protein expression of DMT-1, the apical iron transporter (Fig 6.2.22). Western blots for ferroportin using RIPA lysates of duodenal tissue did not show a specific band corresponding to the expected molecular weight (68 kDa). Under the circumstances, protein levels of duodenal ferroportin could not be reliably quantitated.

4.13. Results of univariate and multivariate analyses

4.13.1 Insulin resistance – associations with other variables

Insulin resistance (as assessed by the AUC in ITT) in HFD-fed mice was found to be significantly positively correlated with liver triglyceride levels, serum hepcidin (also seen in CD-fed mice) and serum ferritin and negatively correlated with liver iron (Table 6.2.3).

Fig 6.2.20

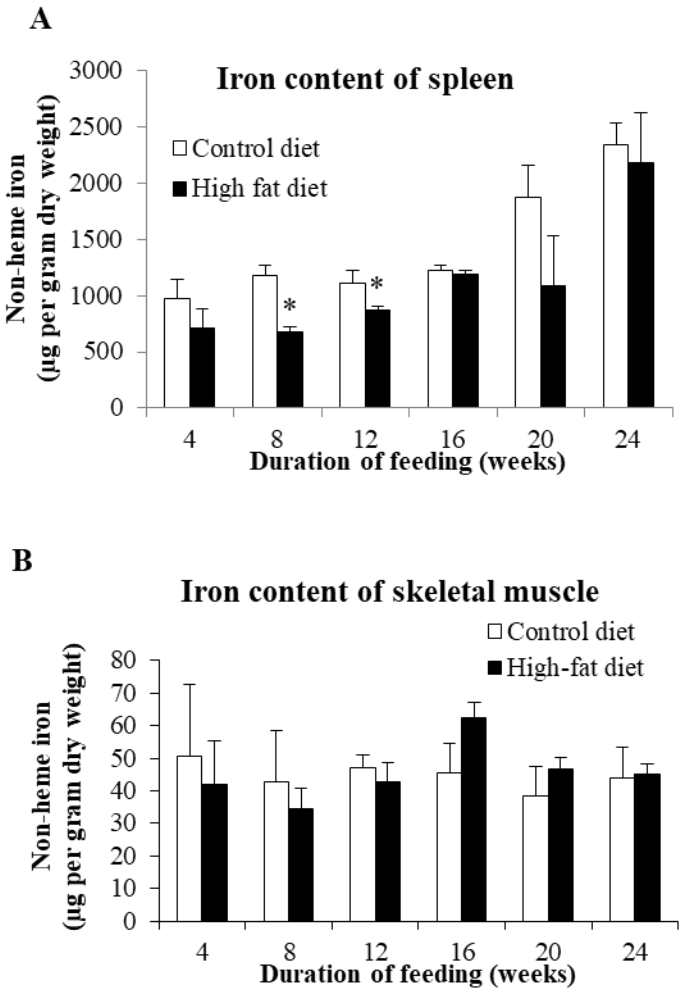

Figure 6.2.20: Effect of HFD-feeding on iron content in the spleen and skeletal muscle

Non-heme iron content of spleen (A) and skeletal muscle (B) estimated by a colorimetric assay based on bathophenanthrolene dye binding. Data are shown as mean ± SD; n = 3 (for both CD- and HFD-fed mice) at each time point. * indicates $p \leq 0.05$ when compared to the respective control group.

Fig 6.2.21

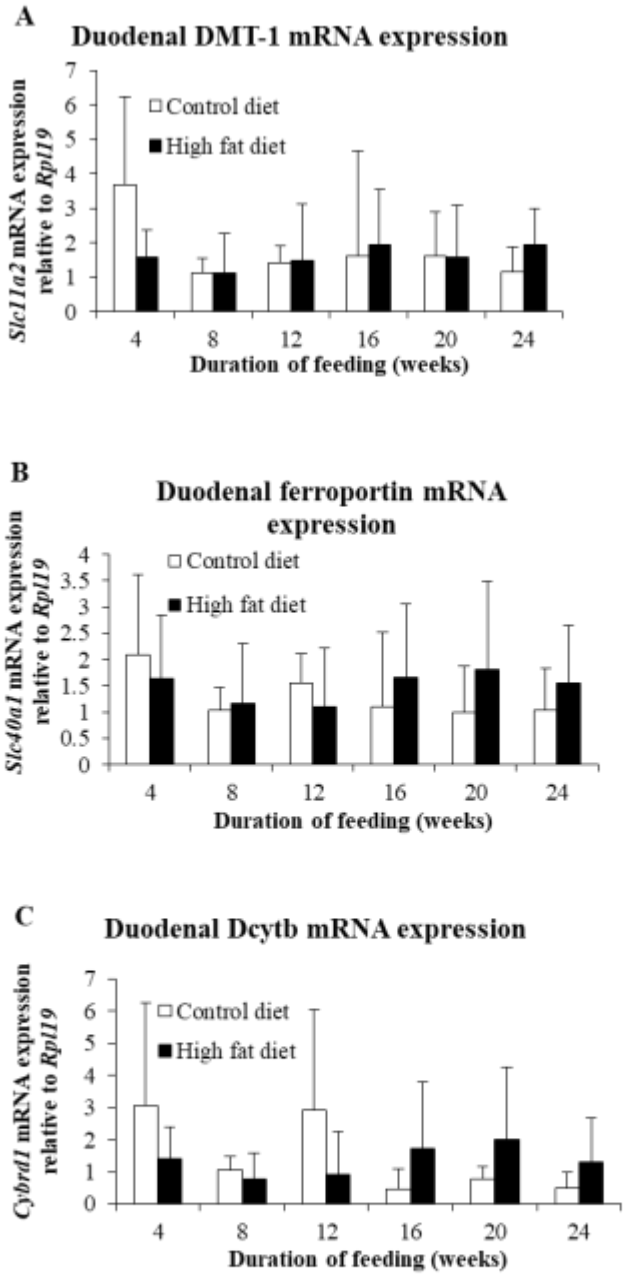

Fig 6.2.21: Effect of HFD-feeding on mRNA expression of duodenal proteins involved in non-heme iron absorption

Gene (mRNA) expression of DMT-1 (A), ferroportin (B) and duodenal cytochrome b (C) in duodenum determined by qPCR. Data are shown as mean ± SD; n = 6 (for both CD- and HFD-fed mice) at each time point studied.

Fig 6.2.22

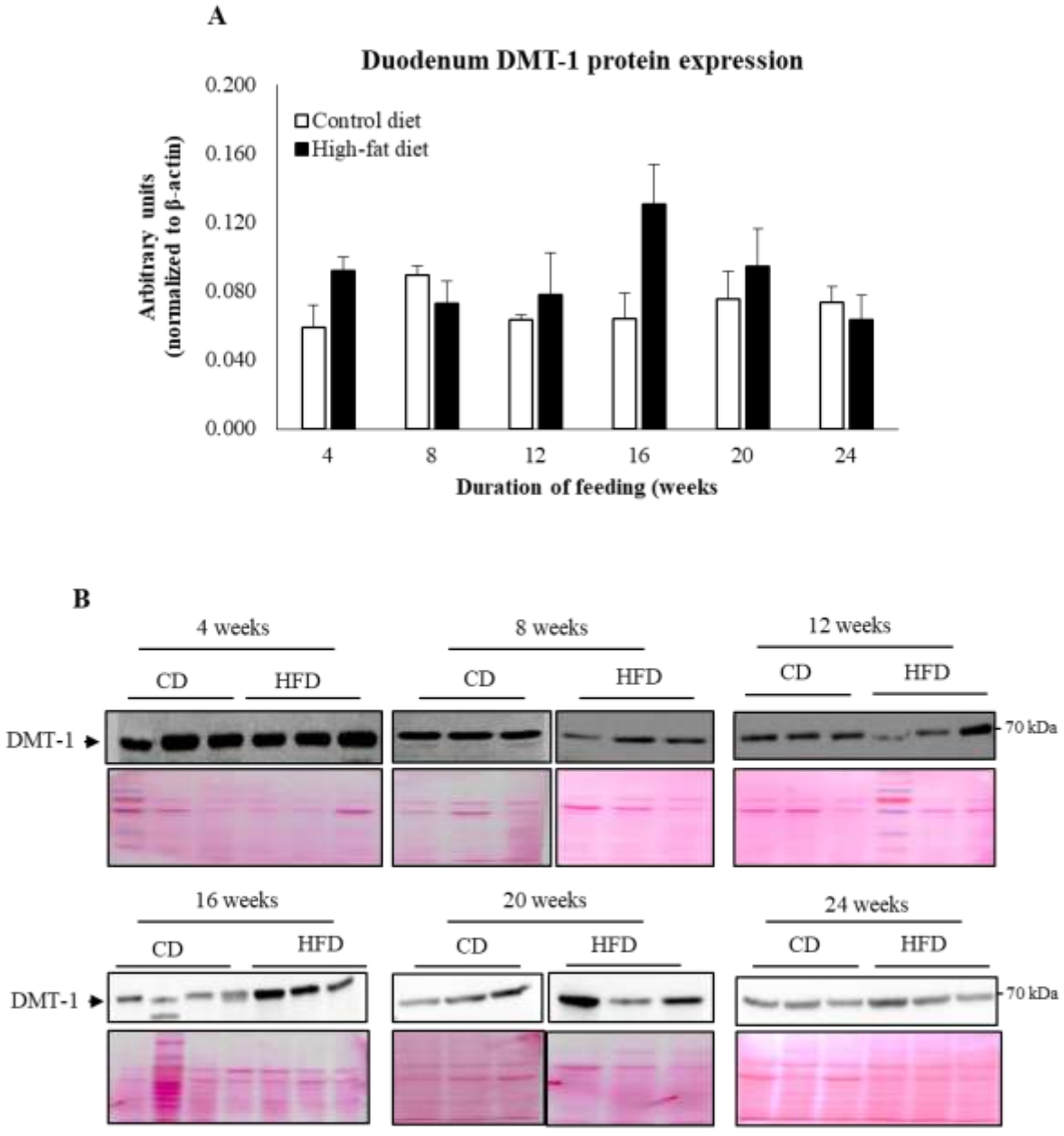

Fig 6.2.22: Effect of HFD-feeding on duodenal DMT-1 protein levels

A: Protein levels of duodenal DMT-1 determined by western blotting B: Representative images of western blots for DMT-1 at all time points studied (as indicated). Bands were normalized to total protein loaded visualized by reversible Ponsceau S staining Data are shown as mean ± SE; n = 3 (for both CD- and HFD-fed mice) at each time point.

On multivariate analyses using stepwise linear regression, the association of insulin resistance with liver triglyceride remained significant (B=82.70, SE=17.9, adjusted R^2=56%, p<0.001), but not those with serum hepcidin, serum ferritin and liver iron levels.

4.13.2 Liver iron – associations with other variables

In CD-fed mice, liver iron levels were significantly positively correlated with serum hepcidin and serum ferritin and negatively correlated with liver BMP6 mRNA expression. In mice fed HFD, liver iron was significantly negatively correlated with liver triglyceride, insulin resistance (AUC of ITT) and serum hepcidin (Table 6.2.4). On multivariate analyses using stepwise linear regression, the association of liver iron with serum ferritin in CD-fed mice (B= 1.29, SE= 0.46, adjusted R^2=29.6%, p<0.014) and with liver triglyceride in HFD-fed mice (B= -33.93, SE=13.01, adjusted R^2=36.7%, p<0.028) remained significant, while others did not.

4.13.3 Hepatic Hamp1 mRNA expression – associations with other variables

In CD-fed mice, hepatic *Hamp1* mRNA expression was positively correlated with liver iron, serum insulin and serum ferritin. On the other hand, in mice fed HFD, *Hamp1* expression was positively correlated with serum insulin, liver *Bmp6* mRNA expression and liver TfR2 protein levels (Table 6.2.5). On multivariate analyses using stepwise linear regression, the association of liver *Hamp1* mRNA with serum ferritin in CD-fed mice (B= 0.003, SE= 0.001, adjusted R^2=44.7%, p<0.002) and with liver TfR2 protein levels in HFD-fed mice (B= 1.687, SE=0.604, adjusted R^2=28.6%, p<0.013) remained significant, while the others did not.

Table 6.2.3: Correlational analyses of insulin resistance (as assessed by AUC in ITT) with other parameters of interest

Variable	Control diet		High-fat diet	
	r*	p	r*	p
Liver triglyceride	-0.059	0.750	**0.712**	**<0.001**
Liver iron	0.248	0.163	**-0.620**	**<0.001**
Serum adiponectin	-0.131	0.497	-0.183	0.307
Serum hepcidin	**0.454**	**0.009**	**0.387**	**0.022**
Serum CRP	0.050	0.860	0.212	0.414
Serum ferritin	0.055	0.829	**0.467**	**0.050**

* Spearman's correlational coefficients are reported.
A p value less than 0.05 was taken to indicate statistical significance. Statistically significant correlations are highlighted.

Table 6.2.4: Correlational analyses of liver iron with other parameters of interest

Variable	Control diet		High-fat diet	
	r	**p**	**r**	**p**
Liver triglyceride	-0.042	0.820	**-0.611**	**<0.001**
ITT (AUC)	0.248	0.163	**-0.617**	**<0.001**
Serum hepcidin	**0.551**	**0.001**	**-0.504**	**0.002**
Serum ferritin	**0.640**	**0.006**	-0.466	0.051
Serum CRP	-0.386	0.156	0.022	0.933
Serum iron	-0.343	0.051	0.118	0.494
Liver BMP6 mRNA	**-0.501**	**0.008**	-0.279	0.132
Liver matriptase-2 mRNA	-0.143	0.428	-0.299	0.090

* Spearman's correlational coefficients are reported.
A p value less than 0.05 was taken to indicate statistical significance. Statistically significant correlations are highlighted.

Table 6.2.5: Correlational analyses of liver hepcidin (*Hamp1*) mRNA expression with other parameters of interest

Variable	Control diet		High-fat diet	
	r	**p**	**r**	**p**
Liver triglyceride	0.121	0.509	0.205	0.230
Liver iron	**0.496**	**0.003**	-0.188	0.272
Serum insulin	**0.575**	**<0.001**	**0.366**	**0.028**
Serum ferritin	**0.535**	**0.022**	-0.154	0.542
Serum iron	-0.241	0.156	-0.029	0.866
Liver BMP6 mRNA	-0.256	0.172	**0.373**	**0.042**
Liver matriptase-2 mRNA	-0.133	0.438	0.245	0.151
Liver TfR2 protein	-0.020	0.938	**0.534**	**0.023**
Liver ferroportin protein	-0.289	0.087	0.075	0.663
eWAT ferroportin protein	-0.495	0.061	-0.271	0.328

* Spearman's correlational coefficients are reported.
A p value less than 0.05 was taken to indicate statistical significance. Statistically significant correlations are highlighted.

5. Discussion

Male C57Bl/6 mice fed a high-fat diet (HFD) develop many of the features of T2DM that are seen in humans, such as hyperglycemia, visceral adiposity and hyperinsulinemia (309–311). This model has been extensively used in studies that have investigated the pathogenesis of insulin resistance (IR) associated with diabetes mellitus and other related pathological conditions, such as non-alcoholic fatty liver disease (NAFLD) (295).

It has been shown that morphological, histological and metabolic changes induced by HFD are related both to the quantum and type of fat present in the diet as well as the duration of feeding (312–315). For example, it has been shown that induction of IR in different tissues occurs at different time points after initiation of HFD feeding. While increased hepatic glucose output, a marker of hepatic IR, is an early finding (developing 3 to 7 days after initiation of HFD-feeding) (314,316), development of IR in skeletal muscles occur at later time points (313,316). In addition, factors responsible for IR induced by short-term HFD-feeding are different from those involved in IR induced by long-term HFD-feeding. For example, adipose tissue inflammation is essential for development of whole-body IR in response to long-term HFD-feeding. However, the presence of inflammation is not required for short-term HFD-induced IR (312)

The present study was aimed at systematically documenting the interactions between HFD-induced IR and iron homeostasis in mice. Since, as described above, the effects of HFD are determined by the duration of feeding, a time-course study (from 4 weeks up to 24 weeks) was carried out to determine the temporal association between development of IR and changes in iron-related parameters in different tissues. Overall, the results of this study are consistent with

those reported earlier in this model (295,316,317). HFD-feeding resulted in progressive weight gain and development of glucose intolerance and IR. Whole-body IR, as assessed by insulin tolerance tests, was significantly higher in HFD-fed mice from 8 weeks onwards (Fig 6.2.4).

Onset of IR in the liver is one of the early effects of HFD-feeding. Hyperinsulinemic hyperglycemic clamp studies have shown that hepatic insulin resistance, as indicated by an increased hepatic glucose output, is seen as early as 1 week after onset of HFD feeding (316). Induction of hepatic IR is closely associated with alterations in lipid metabolism in the liver (182). In the present study, triglyceride levels were found to be significantly increased in the liver of mice fed HFD, from 4 weeks onwards (Fig. 6.2.2-D). Multivariate linear regression analyses showed that whole-body IR (as assessed by ITT) in mice fed HFD was independently associated with liver triglyceride levels, after adjusting for potential confounders (Table 6.2.3), suggesting that increased liver TG plays a role, not only in the development of hepatic IR, but also in the pathogenesis of whole-body IR. In this context, estimation of NEFA levels in serum would have provided useful information on net mobilization of fatty acids from the adipose tissue, by lipolysis. However, sufficient volume of serum samples was not available for this assay. Future work will address this lacuna.

It is known that accumulation of triglycerides in the liver is associated with increased levels of lipotoxic lipid intermediates such as diacylglycerol (DAG) and ceramide (180). Both DAG and ceramide have been shown to impair insulin signaling. DAG is known to activate atypical isoforms of protein kinase C resulting in impaired insulin-induced activation of the Akt pathway (318). Similarly, ceramide has been shown to activate the stress kinase, c-Jun amino terminal kinase (JNK), resulting in impaired activation of Akt by insulin (319,320).

In the present study, p-Akt levels in the liver of mice fed HFD were significantly increased at 12 weeks (Fig 6.2.6). Increased mRNA expression of glucokinase (*Gck*) (a known insulin-responsive gene in the liver) was also seen at 12 weeks (Fig 6.2.7-A). These effects corresponded with the onset of hyperinsulinemia at this time point (Fig 6.2.5-A). The lack of increase in p-Akt levels and *Gck* expression in the liver at the later time points, despite the sustained hyperinsulinemia suggests impairment in insulin signaling induced by prolonged HFD-feeding (Fig 6.2.6-B). These results suggest that hepatic IR is exacerbated after 16 weeks of HFD-feeding and this was co-incident with augmented TG deposition in the liver (Fig 6.2.2-D), hyperinsulinemia (Fig. 6.2.5-A) and whole body IR (6.2.4-D).

Previous studies that have reported the effect of HFD on hepatic expression of PEPCK and G-6-Pase have shown inconsistent results; some have shown increases (321–323), while others have shown decreases (324,325) or no change (311,326) in HFD-fed mice compared to those fed CD. The reasons for this are not clear. However, it is known that expression of these genes are induced under fasting conditions and suppressed by feeding (311). Information on whether the mice were in the fasted/fed condition at the time of euthanasia is not provided in the studies mentioned above. This makes comparison of results between studies difficult. In the present study, mice had ad lib access to food at the time of euthanasia. No significant differences were seen in PEPCK and G-6-Pase between CD and HFD-fed mice at any of the time-points studied (Fig. 6.2.7). Since insulin is known to decrease the expression of these genes (327), absence of suppression of PEPCK and G-6-Pase despite hyperinsulinemia in HFD-fed mice provides further evidence for hepatic IR induced under these conditions. Similarly, in the present study, lipogenic

genes, acetyl CoA carboxylase (ACC) and fatty acid synthase (FAS) (which are known to be induced by insulin (328)) were also not affected by HFD-feeding.

The liver is the major site for iron storage in the body. HFD-feeding resulted in a progressive decrease in liver iron content from 12 weeks onwards (Fig. 6.2.9). Chung et al (2011) have previously shown that HFD-feeding for 16 weeks decreased hepatic iron (290). In the present study, hepatic iron stores in HFD-fed mice were negatively correlated with liver triglyceride content (Spearman's rho= -0.611, $p<0.001$) (Table 6.2.4). Linear regression analyses showed that this association remained significant, after adjusting for potential confounders (section 4.13.2). This suggests that ectopic lipid accumulation in the liver may underlie the decrease seen in liver iron stores.

The liver plays a central role in the regulation of both iron and lipid metabolism. However, the molecular mechanisms that underlie the interaction between them are not clear. Several studies have shown that modulation of hepatic iron homeostasis can have profound effects on lipid metabolism. For example it has been shown that iron deficiency is associated with increased hepatic lipid uptake, synthesis and steatosis (329). On the other hand, iron overload has also been associated with hepatic steatosis and has been implicated in the pathogenesis of non-alcoholic steatohepatitis (NASH) (330).

The decrease in liver iron content induced by HFD in the present study was associated with a progressive decrease in ferritin, the intracellular iron storage protein (Fig 6.2.10). Work in recent years has shown that degradation of ferritin occurs primarily in the lysosomes, by a process called ferritinophagy. This is a specialized from of micro-autophagy, mediated by the cargo

receptor, nuclear receptor co-activator 4 (NCOA4) (50). It is triggered by conditions characterized by intracellular iron depletion but the mechanisms involved are not clear. Although hepatic steatosis is known to associated with increased autophagy (331), very little is known about its effect on ferritinophagy. Ferroptosis, a form of iron-dependent non-apoptotic cell death induced by oxidative stress-mediated lipid peroxidation, is strongly associated with ferritinophagy (332). Oxidative stress and lipid peroxidation are known to be associated with hepatosteatosis (333,334); whether activation of ferritinophagy plays a role in decreasing liver iron stores in this setting is not known.

Although ferritin protein levels were decreased by HFD-feeding, mRNA expression of both ferritin (L) as well as ferritin (H) in the liver were significantly increased by HFD-feeding at 16, 20 and 24 weeks (Fig 6.2.10). Gene expression of ferritin is known to be up-regulated by a number of factors, including inflammation and oxidative stress (335). HFD did not induce significant inflammation in the liver (Fig 6.2.15). However, as mentioned earlier, hepato-steatosis is known to be associated with increased oxidative stress in the liver (333,334). It is therefore possible that oxidative stress may underlie increased ferritin expression in this setting. Additional factors, including ferritinophagy (as described above), may be involved in decreasing ferritin protein levels despite increased gene expression in this setting.

The liver is the most important source of the iron-regulatory hormone, hepcidin (32). HFD feeding decreased hepatic *Hamp1* expression and serum hepcidin levels (Fig 6.2.8). It has been reported previously that mice fed HFD for 16 weeks had decreased hepatic *Hamp1* expression (290,291). Similar findings were reported in *db/db* mice, another mouse model of obesity-induced IR (336). The findings of the present study are in keeping with these reports.

A number of factors regulate hepcidin expression in the liver (Fig 3.6); hepatic iron stores is one such important factor (288). The results of the present study show that the decrease in liver iron stores (from 12 weeks onwards) preceded the decrease in *Hamp1* expression (from 16 weeks onwards) (Fig. 6.2.9). This suggested that diminished iron stores in the liver may underlie the reduction in *Hamp1* expression in this setting. A positive correlation between iron content and *Hamp1* expression was seen in the livers of CD-fed mice. However, in HFD-fed mice, *Hamp1* expression was found to correlate negatively with liver iron stores, rather than positively (Table 6.2.7). This suggests that in the setting of HFD-feeding, there may be other factors that may regulate hepcidin.

BMP6, which is primarily secreted by sinusoidal cells in the liver (92), is a powerful inducer of hepcidin (88). An increase in BMP6 expression has been consistently demonstrated in response to iron loading in the liver (88,91,288). In the present study, although liver iron and *Hamp1* expression were decreased by HFD-feeding, it has not been possible to document concomitant decreases in BMP6 (Fig. 6.2.12-A). As far as is ascertainable, there are no reported studies that have shown a decrease in BMP6 expression in response to depletion of hepatic iron. The present study is in keeping with this. Hence, it appears that BMP6 may not play an important role in the regulation of hepcidin in this setting. Correlational analysis showed that hepatic *Bmp6* expression showed a significant negative correlation with liver iron levels in CD-fed mice (Table 6.2.4). Considering that BMP6 is known to be induced by hepatic iron stores (88,91,288), this was an unexpected finding. On multivariate analysis, this negative correlation was not seen. This result suggests a ‘suppression effect’ by confounding factor(s) that correlate positively with liver iron, but negatively with *Bmp6* expression. Changes in such confounding factor(s) will have

opposite effects on liver iron and *Bmp6* expression. This may be a possible reason for the negative correlation between liver iron and *Bmp6* mRNA seen in this setting. Multivariate analysis will neutralize the effects of factors causing suppression. As seen in this case, the negative correlation was lost when the data was subjected to multivariate analysis.

Matriptase-2, a membrane-bound serine protease, decreases hepcidin expression by cleaving hemojuvelin (78,337). This results in decreased signaling via the BMP-SMAD pathway, leading to suppression of *Hamp1* expression. Matriptase-2 was found to be essential for down-regulation of hepcidin in response to an iron-deficient diet (338). In the present study, the diets used were iron-adequate (detailed in the methods section (page 126) and in appendix III and IV (page 330 and 331), where the diets have been described). HFD-feeding tended to increase matriptase-2 mRNA expression in the liver at many of the time points studied (Fig. 6.2.12-B). This suggests that matriptase-2 may play a role in mediating the down-regulation of hepcidin in the setting of the present study. However, there was no significant correlation between expression levels of hepcidin and matriptase-2 (Table 6.2.5). In addition, it has been shown that matriptase-2 activity is regulated pre-dominantly at the level of protein stability, and not by transcriptional mechanisms (339). At the time that this part of the study was carried out, an antibody specific to mouse matriptase-2 was not available commercially. Hence, it was not possible to determine matriptase-2 protein levels as part of this study.

TfR2 is a trans-membrane protein that is highly expressed in hepatocytes. TfR2 binds to holo-transferrin (*albeit* with much lower affinity than TfR1) and triggers an intracellular signaling pathway that results in increased *Hamp1* expression (289). Levels of TfR2 in hepatocytes have been shown to be regulated by changes in iron status of the body (340). The results of the present

study show that neither TfR2 mRNA nor its proteins levels were significantly affected by HFD-feeding at any of the time points studied (Fig. 6.2.13). However, TfR2 protein was significantly positively correlated with *Hamp1* mRNA expression in mice fed HFD (Table 6.2.7). This association remained statistically significant after adjusting for the effects of potential confounders (by multivariate linear regression analysis). These results suggest that TfR2 may be involved in regulation of hepcidin in the setting of HFD feeding. Additional work would be required to determine if this is so.

Systemic inflammation is known to induce hepcidin. This effect is mediated primarily by IL-6, which signals via the JAK-STAT3 pathway to increase *Hamp1* expression (112). HFD-feeding did not increase serum levels of CRP or IL-6 (Fig 6.2.15-C). Hence, there was no evidence of systemic inflammation in the experimental mice in the present study. In addition, mRNA expression of *Saa1* (an acute phase reactant widely used as a marker of hepatic inflammation) or *Il-6* in the liver were also not elevated by HFD (Fig 6.2.15). These results are consistent with those reported in an earlier study where mice were fed HFD for 24, 40 and 52 weeks (341). In this study, van der Heijden et al. show that hepatic inflammation developed only after 40 weeks of HFD and was not seen at 24 weeks (341). The lack of induction of hepcidin and absence of inflammation seen in the mice in the present study are consistent.

Serum iron levels are known to regulate hepcidin. Although the mechanisms involved are incompletely understood, a multi-protein iron-sensing complex on the hepatocyte membrane (that includes HFE, TfR2 and HJV as essential components) is involved in regulation of *Hamp1*, in response to changes in serum iron/transferrin saturation. Serum iron levels were not

significantly altered by HFD-feeding at any of the time points studied. Therefore, it does not seem that serum iron influences hepcidin levels in this setting.

Factors secreted by the bone marrow in response to an increased erythropoietic drive are known to powerfully repress hepatic *Hamp1* expression. The effects of HFD-feeding on erythroid maturation in the bone marrow and expression of the erythroid regulators of hepcidin in erythroid precursor cells (isolated from the bone marrow [TER119+ cells]) were studied in detail. These results are described in Study 3. HFD-feeding was not found to significantly affect the expression levels of the erythroid regulators of hepcidin, suggesting that they are not involved in *Hamp1* regulation in this setting.

Interestingly, hepatic *Hamp1* expression showed a positive correlation with serum insulin levels in CD and HFD-fed mice (Table 6.2.5). It has been reported earlier that insulin can induce *Hamp1* gene expression in HepG2 cells, a hepatoma cell line (342). However, in a separate set of experiments that were not part of the present study, it was found that treatment of mouse primary hepatocytes with insulin (under similar experimental conditions) did not induce hepcidin (data not shown). Hence, it does not appear that insulin directly affects *Hamp1* expression in mouse primary hepatocytes. Additional studies would be required to investigate this aspect further.

Overall, the results of this part of the study show that HFD-feeding decreased hepatic *Hamp1* expression; this was associated with decreased liver iron levels. Factors such as BMP6, matriptase-2, inflammation, serum iron level and erythroid regulators of hepcidin, all of which are known to regulate *Hamp1* expression, did not appear to do so in the setting of this study. TfR2 protein levels were found to be positively associated with *Hamp1* expression in HFD-fed

mice. Recently, it has been shown that hepcidin can be powerfully regulated by epigenetic modifications involving histone acetylation / deacetylation (343). Such epigenetic modifications were shown to be essential for down-regulation of hepcidin in response to iron deficiency and erythropoiesis. Whether such mechanisms are involved in regulation of hepcidin, in response to changes in liver iron stores is not known. Additional work would be required to look into this interesting possibility.

Inflammation in the adipose tissue plays a key role in the pathogenesis of whole-body IR. HFD-feeding is known to produce inflammation in adipose tissue, which is exacerbated by the infiltration of pro-inflammatory immune cells (especially macrophages) into the adipose tissue (165,166). Studies in mice have shown that gonadal WAT (in contrast to the subcutaneous and mesenteric WAT depots) has limited fat storage capacity. In response to long-term high-fat feeding (when body weight exceeds ~40g), expansion of the gonadal WAT was found to decline and was associated with marked exacerbation of IR (164,317,344). The observations of the present study are in agreement with these reports; eWAT weights (Fig 6.2.2) increased initially but tended to decline after 16 weeks of HFD (when the body weights were >40 g) and was associated with increased IR (Fig 6.2.4), hyperinsulinemia (Fig 6.2.5-A), a decline in serum adiponectin levels (which were elevated at earlier time points [Fig 6.2.5-B]) and exacerbation of hepatosteatosis (Fig 6.2.2-D and 6.2.3). These results support the view that the limited expandability of eWAT results in ectopic accumulation of fat in the liver and muscle, resulting in metabolic abnormalities (lipotoxicity) (164).

Inflammation induced in the adipose tissue by HFD has been shown to be associated with metabolic dysfunction in the adipose tissue (344). In the present study, mRNA expression of

PPARγ, a key transcription factor involved in adipocyte differentiation and maturation, was down-regulated after 16 weeks of HFD-feeding. PPARγ is known to be an insulin-responsive gene. In the present study, a decrease was seen in mRNA expression of this gene; this may be secondary to IR in adipose tissue. Levels of mRNA of known targets of PPARγ (fatty acid synthase and adiponectin) were also down-regulated, in parallel with PPARγ (Fig 6.2.16). Surprisingly, genes encoding the lipolytic enzymes, ATGL and HSL, were also found to be down-regulated at the same time points. A possible explanation for this finding is the fact that lipolysis is tightly coupled to both fatty acid synthesis and fatty acid oxidation by mechanisms that are not well characterized (345,346). Therefore, a decrease in lipogenesis (due to IR) may conceivably result in a concomitant decrease in expression of genes involved in lipolysis as well. The physiological significance of such coupling is not well understood. Overall, the results of the present study suggest that HFD-feeding in mice resulted in metabolic dysfunction in adipose tissue.

Iron is essential for adipocyte differentiation and mitochondrial biogenesis (212,221). Expansion of adipose tissue depots, in response to HFD feeding, has been shown to be associated with increased iron demands (347). In the present study, there was a significant increase in the iron content in the eWAT in response to HFD feeding (Fig. 6.2.17-A). This inversely correlated with liver iron content (Fig 6.2.17-C). These observations are in agreement with those reported in other studies (291,292). For example, Orr et al. have shown that HFD-feeding increased the iron content in adipocytes (292). Similarly, Park et al. have shown that HFD-induced decreases in hepatic iron stores were inversely proportional to body adiposity (291).

Elevated iron content in adipose tissue has previously been shown to be associated with increased IR in humans (226,348,349) and in mice (17,350). The mechanisms involved in these events are not clear. Increased levels of iron in adipose tissue can down-regulate the expression of adiponectin, an important insulin-sensitizing adipokine (225,226). Studies have also shown that increased levels of iron in the adipose tissue can increase the basal rate of lipolysis, thus increasing levels of free fatty acids in the blood and promoting ectopic lipid accumulation (219). HFD-feeding has also been shown to produce alterations in iron content of macrophages in adipose tissue, resulting in polarization of the macrophages towards a pro-inflammatory (M1) phenotype (292). It is, therefore, plausible that the increased iron content in adipose tissue seen in the present study may contribute to whole-body IR induced by HFD-feeding.

Absorption of iron in the duodenum is a highly regulated process. Gene (mRNA) expression of the proteins involved (DMT1, ferroportin and dcytb) was not significantly altered by HFD-feeding (Fig 6.2.21). Protein levels of DMT-1 were also not affected (Fig 6.2.22). Despite attempts to determine protein levels of duodenal ferroportin by western blotting, it was not possible to detect a specific band corresponding to ferroportin (~68 kDa) in the RIPA lysates prepared from duodenal mucosal samples. Other investigators have reported the use of a membrane preparation of duodenal mucosa in order to detect ferroportin by western blotting (210,351). However, it was not possible to do so in the present study due to logistical constraints. Hence, it is not possible to comment on this aspect and this is a limitation of the study.

It has been reported that HFD-feeding decreases duodenal iron absorption (218,291). In the study by Sonnweber et al (218), duodenal uptake of radio-labeled iron was measured in mice fasted for 24 hours, after 10 weeks of HFD-feeding. The authors showed that iron transport across the

apical membrane of duodenal enterocyte was decreased. However, the reason for decreased iron uptake is unclear, since mRNA and protein levels of DMT-1 were found to be (paradoxically) increased in their study. In another report, Park et al (291) show decreased expression of dcytb in mice on a HFD for 16 weeks, with no significant changes in DMT-1 and ferroportin. In the present study, mRNA expression of DMT-1, ferroportin and dcytb were found to be highly variable with no significant differences in expression levels in CD and HFD-fed mice (Fig. 6.2.21). The reasons for the differences in findings seen in the present study and those by Sonnweber et al and Park et al are not clear. It is possible that differences in experimental conditions may contribute. One such example, in the study by Park et al., is that the mice were fasted for 12 h prior to euthanasia. In the present study, mice were not fasted. Fasting is known to up-regulate hepcidin expression in the liver (120,352). It is plausible that induction of hepcidin may produce changes in the expression of duodenal proteins involved in iron absorption. In addition, it is not known whether the increased fat content in the HFD diet can have direct effects on iron bio-availability.

6. Summary and conclusion:

The current study presents data on the interactions of high-fat feeding-induced insulin resistance (IR) and iron metabolism. As far as is ascertainable, this is the first study that has reported a time-course analysis of changes in parameters involved in iron homeostasis, associated with development of IR. There was a significant increase in whole-body IR (after 8 weeks of high-fat feeding) that preceded the onset of dysregulated hepatic iron homeostasis (after 12 weeks). This suggests that it is unlikely that dysregulated iron homeostasis in the liver plays a causative role in the pathogenesis of IR in this model.

Hepatic steatosis was independently associated with IR and decreased hepatic iron stores, suggesting that ectopic lipid accumulation in the liver may play a role in the pathogenesis of IR, as well as in hepatic iron dysregulation. The decrease in hepatic iron stores was associated with concomitant increases in the iron content and metabolic dysfunction of the adipose tissue studied. Since increased iron in the adipose tissue has been reported to induce IR, it is possible that this may contribute to the increase in IR in response to high-fat feeding. The proposed sequence of events, showing possible cross talk between development of IR and dysregulated iron homeostasis, in response to HFD, is shown in Fig 6.2.23.

Figure 6.2.23

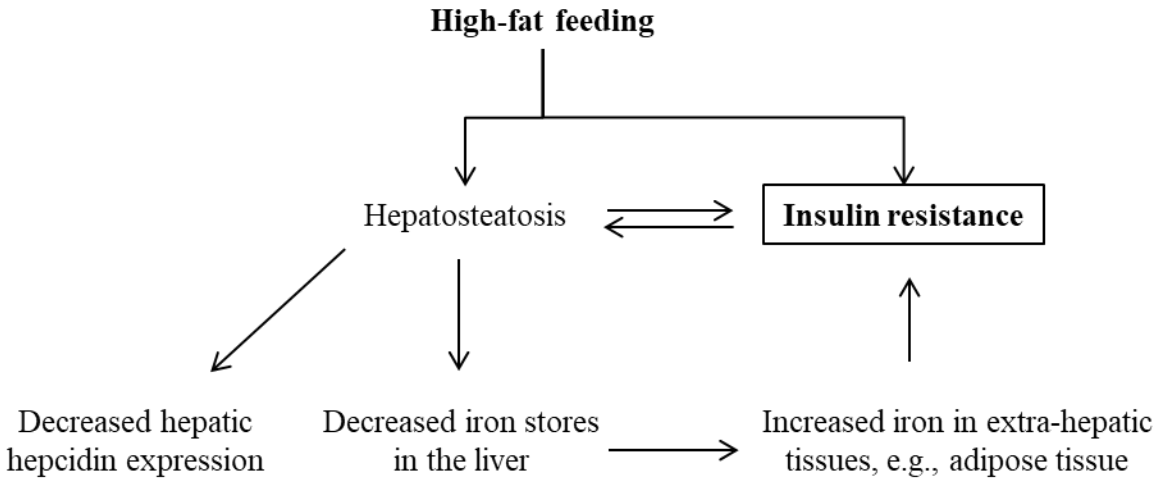

Figure 6.2.23: Proposed sequence of events induced by HFD feeding

High-fat feeding resulted in insulin resistance and hepatosteatosis. Accumulation of lipid in the liver resulted in decreased hepatic iron stores and decreased hepatic hepcidin expression. This was associated with accumulation of iron in the adipose tissue. Increased iron content in the adipose tissue may exacerbate insulin resistance, thus constituting a vicious cycle.

STUDY 3

Effect of high-fat diet-induced insulin resistance on erythroid maturation and erythroid regulators of hepcidin in the bone marrow in mice

1. Abstract

Insulin is known to augment erythropoiesis *in vitro* by stimulating the proliferation and differentiation of erythroid precursor cells. Insulin resistance (IR), the hallmark of type 2 diabetes mellitus (T2DM), is known to be associated with hyperinsulinemia. However, the effect of hyperinsulinemia on erythropoiesis *in vivo* is not known.

Erythroid precursors in the bone marrow are known to secrete factors that can powerfully down-regulate hepcidin expression in the liver. These are referred to as erythroid regulators of hepcidin. High-fat diet (HFD)-feeding in mice (a model of IR) was found to decrease hepatic hepcidin expression (Study 2). It was not known whether these erythroid regulators are involved in mediating hepcidin suppression in this setting. The hypothesis of the present study was that HFD-induced hyperinsulinemia may stimulate erythropoiesis in the bone marrow, which may, in turn, increase the expression of the erythroid regulators of hepcidin, resulting in hepcidin suppression.

In order to test this hypothesis, terminal erythroid differentiation (TED) was studied in the bone marrow and spleen from mice fed a control diet or HFD for various durations (as detailed in Study 2), using flow cytometry. In addition, erythroid (TER119-positive) cells were isolated from the bone marrow and used to determine gene expression of the putative erythroid regulators

of hepcidin (erythroferrone [ERFE], growth differentiation factor –15 [GDF-15] and twisted gastrulation factor –1 [TWSG-1]).

The results showed that HFD-feeding in mice did not stimulate erythropoiesis in the bone marrow or spleen. Terminal erythroid differentiation in the bone marrow was similar in the 2 groups of mice, fed either a control diet or a HFD. However, HFD-fed mice showed increased reticulocytes in the marrow, which suggests impaired reticulocyte maturation and release into the circulation. HFD did not affect the expression of ERFE, GDF-15 or TWSG-1 in erythroid cells isolated from the marrow. Hence, it appears unlikely that these factors play an important role in the down-regulation of hepatic hepcidin expression seen in response to HFD-feeding.

2. Introduction:

Erythropoiesis refers to the process of differentiation and maturation of hematopoietic stem cells into mature erythrocytes. It occurs in the bone marrow, which is the chief erythropoietic organ. The spleen can act as an accessory erythropoietic organ (especially in mice) under conditions of increased erythropoietic demand (stress erythropoiesis) (353).

The process of erythropoiesis consists of three phases: formation of early erythroid progenitors, terminal erythroid differentiation (TED) and reticulocyte maturation. In the first phase, hematological stem cells proliferate and differentiate to form early erythroid progenitor cells called burst forming units (BFU-E) and colony forming units (CFU-E) (354). The earliest morphologically recognizable erythroid precursor, the pro-erythroblast (pro-E), is derived from CFU-E. In the second phase (called terminal erythroid differentiation or TED), pro-E undergoes three cycles of mitosis, resulting in the sequential formation of basophilic, polychromatic and

orthochromatic erythroblasts respectively, at the end of each mitotic division. Accordingly, each pro-E produces 2 basophilic erythroblasts, which, in turn, produce 4 polychromatic erythroblasts and then 8 orthochromatic erythroblasts. Therefore, normal TED is characterized by the presence of pro-E, basophilic erythroblasts, polychromatic erythroblasts and orthochromatic erythroblasts in the ratio of 1:2:4:8. A deviation from this is suggestive of abnormal TED (355,356). In the third phase, orthochromatic erythroblasts extrude their nuclei (enucleation) to form reticulocytes. Nascent reticulocytes undergo a complex process of maturation where they transform into discoid erythrocytes and are released into circulation (357).

TED is characterized by a progressive decrease in cell size, condensation of chromatin and hemoglobinization. Synthesis of hemoglobin is initiated in pro- and basophilic erythroblasts and is nearly complete in the orthochromatic erythroblasts. This process is associated with rapid synthesis of heme and is characterized by increased demand for iron (358). Erythroblasts obtain iron required to support hemoglobinization, by taking up transferrin-bound iron from the blood via transferrin receptor 1 (TfR1)-mediated endocytosis. In fact, TfR1 (CD71) is highly expressed on the surface of erythroblasts; more than 80% of circulating transferrin-bound iron is utilized by differentiating erythroblasts for hemoglobin synthesis (359).

As described earlier, hepcidin, a small peptide synthesized and secreted by the liver, is the chief hormone that regulates iron homeostasis (32). It binds to and degrades the only known mammalian protein involved in iron export, ferroportin (24). In doing so, hepcidin decreases the recycling of iron from macrophages and also decreases absorption of dietary iron from the duodenum, thus limiting iron availability for hemoglobin synthesis. In conditions where erythropoiesis is stimulated, such as acute blood loss, anemia and hypoxia, hepcidin levels are

powerfully suppressed in order to meet the requirements of iron needed to support erythropoiesis (95). This phenomenon is also seen in hematological disorders characterized by ineffective erythropoiesis (such as thalassemia), where chronically suppressed hepcidin results in an iron overloaded state (202).

The mechanisms by which erythropoietic stimuli suppress hepcidin are not entirely clear. Several humoral factors secreted by erythroblasts during the process of TED have been shown to down-regulate hepcidin expression in the liver (100). These factors are collectively known as erythroid regulators of hepcidin. Erythroferrone (ERFE) (35), growth differentiation factor-15 (GDF-15) (33) and twisted gastrulation factor 1 (TWSG1) (34) have been proposed to be such candidate molecules (described in detail in the review of literature).

In study 2, high-fat feeding was shown to result in a decrease in hepatic hepcidin (*Hamp1*) expression (Fig 6.2.8). It was also seen that, although hepatic iron stores were decreased by HFD, *Hamp1* expression did not correlate with liver iron stores. In addition, other factors known to regulate *Hamp1* expression (such as liver BMP6 and matriptase-2 mRNA expression, serum iron and systemic inflammation) were not significantly correlated with *Hamp1* expression in HFD-fed mice. The effect of the erythroid regulators of hepcidin on *Hamp1* expression in this setting is not known.

Insulin resistance (IR) is a characteristic feature of type 2 diabetes mellitus (T2DM). Ever since Barbieri and colleagues (360) showed a significant association between IR and markers of enhanced erythropoiesis (such as increased RBC count, hematocrit and hemoglobin levels), multiple studies done in different parts of the world have confirmed this association (361–366).

IR is associated with hyperinsulinemia (due to compensatory increase in insulin secretion), especially early in the progression of T2DM (367). Insulin has been shown to stimulate proliferation and differentiation of early erythroid progenitors (BFU-E and CFU-E) *in vitro* (36,37,368,369). These cells express insulin receptors (368) and insulin-induced activation receptor tyrosine kinase activity is required for the stimulatory effects of insulin in these cells (370–372). In view of this, it has been postulated that hyperinsulinemia-induced increase in erythropoiesis may explain the increase in hemoglobin, RBC count and hematocrit (described above) that are associated with IR (360). In mice, HFD-induced IR has been shown to induce enhanced bone marrow hematopoiesis, with proportionate increases in both erythroid and myeloid lineages (373). However, very little is currently known about the effects of IR on the process of TED in the bone marrow.

Obesity-induced inflammation in the adipose tissue plays a key role in the pathogenesis of IR (165). It is now known that induction of obesity is associated with an increase in bone marrow adipose tissue (MAT) (374,375). MAT is metabolically active and can have local, as well as systemic, effects which can impact energy metabolism, bone turnover and hematopoiesis (376). Although the precise role of MAT as a modulator of hematopoiesis is not clear, it is thought to have an inhibitory effect on the hematological niche in the marrow (377). In addition, pro-inflammatory cytokines secreted by MAT can potentially have a direct inhibitory effect on erythropoiesis (378,379). HFD-feeding in mice has been shown to result in an increase in MAT (374). Therefore, mice fed HFD have co-existent hyperinsulinemia (which may stimulate erythropoiesis) and increased MAT (which may inhibit erythropoiesis). In such a setting, the net effects of these factors on TED have not been studied.

This study was designed to investigate the effect of HFD on TED in the bone marrow. The hypothesis tested was that HFD-induced changes in TED may result in increased expression of the erythroid regulators of hepcidin, which may mediate hepatic *Hamp1* suppression in this setting. In order to test this hypothesis, TED in the bone marrow and spleen (isolated from mice fed HFD for various durations - from 4 weeks to 24 weeks as described in study 2) was studied, using flow cytometry. In addition, erythroid cells (TER119-positive cells) were isolated from the bone marrow to study the expression of the putative erythroid regulators of hepcidin.

3. Methods

3.1. Animals

All animal experiments in this study were done in the mouse model of HFD-induced obesity and IR, which was described in detail in Study 2 (page 126). Briefly, 8 weeks old male C57Bl/6J mice were fed either a control diet (CD) (Research Diets, Inc., USA, #D12450J, with 10% of total calories derived from fat) or a high-fat diet (HFD) (Research Diets, Inc., USA, #D12492, with 60% of total calories derived from fat) for 4, 8, 12, 16, 20 or 24 weeks. Six CD-fed and 6 HFD-fed mice were sacrificed at each time point studied. At the time of sacrifice, blood was collected from the inferior vena cava. The tibia and femur from both hind-limbs were removed and used for bone marrow isolation (as described below).

3.2. Preparation of single-cell suspensions of bone marrow

Single-cells suspensions of bone marrow were prepared as described by Koulnis et al (380). The ends of the femur and tibia were snipped off using a pair of scissors and bone marrow was

flushed out with 3–4 mL of ice-cold staining buffer (PBS with 0.2% BSA and 5mM glucose), using a syringe fitted with a 26G needle inserted into the marrow cavity. The marrow cells were dissociated by repeatedly pipetting the suspension up and down and passing it through a pre-wetted 40 μm strainer to remove cell clumps. The cells in the suspension were washed twice with staining buffer and finally re-suspended in 1 mL of ice-cold staining buffer.

3.3. Preparation of single-cell suspensions of splenocytes

The freshly isolated spleen was placed on a pre-wetted 40 μm strainer, kept on top of a 50 mL conical tube. The spleen was mechanically disrupted by gently shearing it using a syringe plunger. The dissociated cells were washed through the strainer using 3-4 mL of ice-cold staining buffer. The splenocytes were washed again with staining buffer, and finally re-suspended in 1 mL of ice-cold staining buffer.

3.4. Cell counts

The isolated bone marrow cells and splenocytes were counted, using a Neubauer hemocytometer. Briefly, 50 μL of the cell suspension was mixed gently with 50 μL of 0.4% trypan blue solution (cat. no. T8154, Sigma, India). One minute later, 10 μL of the stained cell suspension was applied to the hemocytometer chamber. Cells in 4 corner squares were counted; the average number of cells in each square was used to calculate the total number of cells using the formula given below:

Total number of cells per mL = average number of cells per square x 10^4 x 2 (dilution factor)

3.5. Flow cytometric analyses

Flow cytometry was used for immune-phenotyping the bone marrow cells and splenocytes isolated, in order to distinguish the successive developmental stages of TED. Flow cytometric analysis was carried out in accordance with published protocols (356,381).

3.5.1. Staining of cells

For staining, 1 x 10^6 cells of each sample were re-suspended in 200 µL of ice-cold staining buffer, containing rat anti-mouse CD16/CD32 blocking antibody (cat. no. 553142, BD Biosciences, USA) at a concentration of 25 µg/mL. An adequate volume of an antibody pre-mix, consisting of fluorochrome-conjugated antibodies, was prepared as shown in Table 6.3.1.

Two hundred microliters of the antibody pre-mix (containing all the three antibodies) was added to each of the sample tubes, and mixed by gently inverting the tubes.

Table 6.3.1: Antibodies used for flow cytometric analyses

Antibody (fluorochrome)	**Clone**	**Reactivity**	**Supplier (cat.no.)**	**Conc. (mg/mL)**	**Dilution**
CD71 (FITC)	C2	Mouse	BD Pharmingen, USA (#553266)	0.5 mg/ml	1:200
TER-119 (PE)	TER-119	Mouse	BD Pharmingen, USA (#553673)	0.2 mg/ml	1:200
C44 (APC)	IM7	Mouse	BD Pharmingen, USA (#559250)	0.2 mg/ml	1:200

FITC – Fluorescein isothiocyanate; PE – Phycoerythrin; APC - Allophycocyanin

3.5.2. Preparation of control samples

A mixture of cells prepared from all the samples, available for analysis on a particular day, was used for preparation of controls. The following control samples were prepared:

- Unstained controls: 1 x 10^6 cells were re-suspended in 400 µL of staining buffer.
- 'Single-stained' controls: 1 x 10^6 cells were re-suspended in 200 µL of staining buffer and 200 µL of each antibody (diluted as shown in Table 6.3.1) was added. Thus, there was one 'single-stained' control for each of the 3 antibodies used.
- 'Fluorescence minus one' or FMO controls: 1 x 10^6 cells were re-suspended in 200 µL of staining buffer and 200 µL of an antibody pre-mix containing all the antibodies, except one, was added. Thus, FMO for CD71-FITC consisted of an antibody pre-mix containing anti-TER119 (PE) and anti-CD44 (APC), but not CD71 (FITC). Similarly, FMO for anti-TER119 (PE) contained anti-CD44 (APC) and anti-CD71 (FITC), but not anti-TER119 (PE) and FMO for anti-CD44 (APC) contained anti-CD71 (FITC) and anti-TER119 (PE), but not anti-CD44 (APC).

3.5.3. Incubations

All the samples and controls were incubated for 1 hour in the dark at 4°C. At the end of the incubations, 3 mL of staining buffer was added to each of the tubes, mixed and centrifuged at 400*g* for 5 min at 4°C. This step was repeated; cells were finally re-suspended in 500 µL of staining buffer and used for flow cytometric analyses.

3.5.4 Data acquisition

The samples were analyzed using a BD FACS Aria III instrument with 5 lasers (561-nm [Y/G], 488-nm [Blue], 633-nm [Red], 405-nm [Violet], and 375-nm [UV]) and 11 colors, at the Core Facility, Center for Stem Cell Research, CMC, Vellore, India. BD FACS Diva software was used for operating the instrument.

3.5.5 Data analysis

Data analysis was done using FlowJo, version 10.4. Compensation was done based on the 'single-stained' controls and the compensation matrix generated by the software was applied to all the samples within each group. The unstained and single-stained controls showed a high degree of specificity for all the three antibodies used (Fig 6.3.1). The FMO controls showed that there was no significant spectral overlap between the fluorophores used (FITC, PE and APC) (Fig 6.3.2).The gating strategy was based on published protocols (356,380,381) and is described in detail in the results section.

Figure 6.3.1

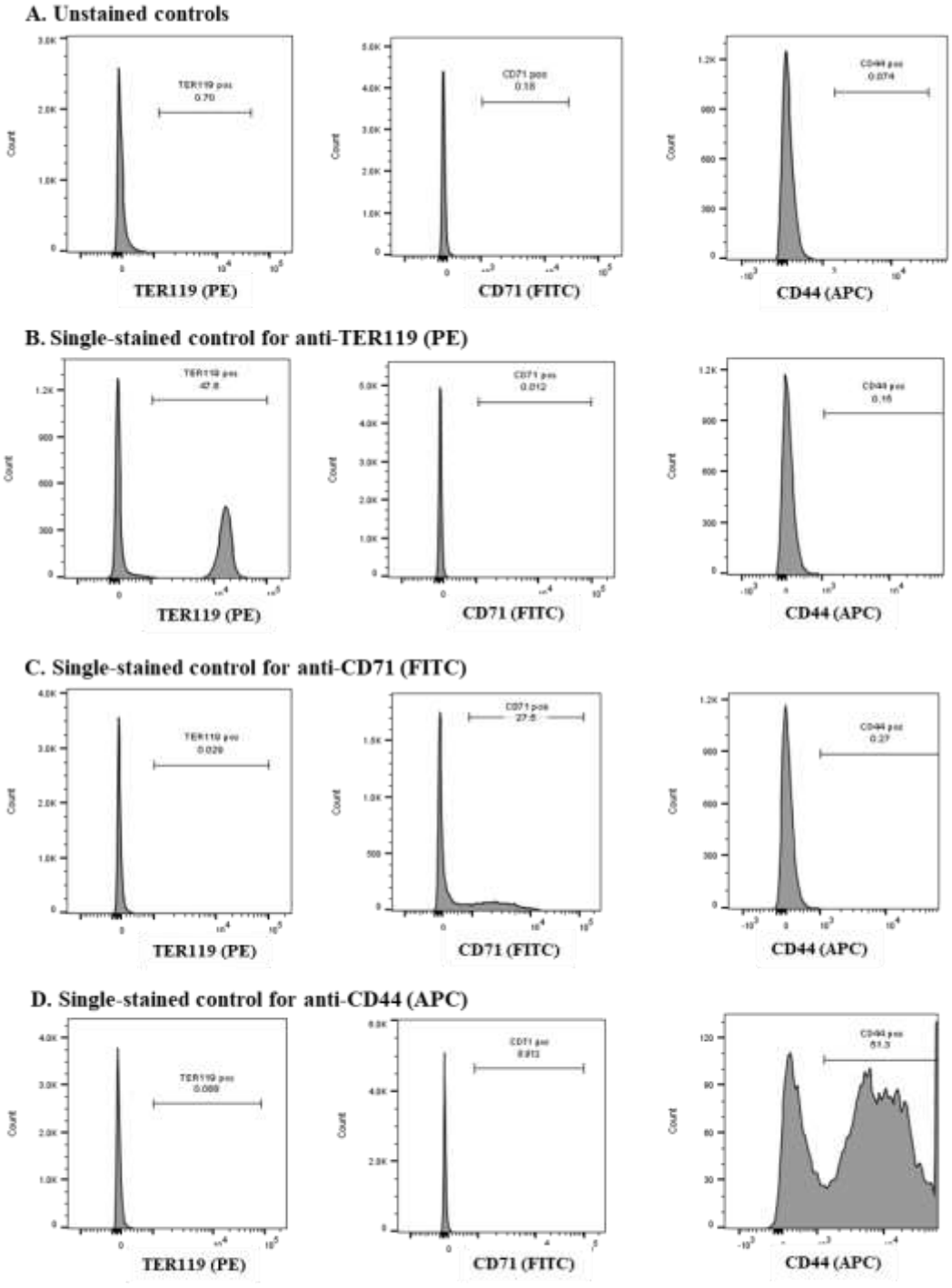

Figure 6.3.1: Unstained and single-stained controls

Unstained controls (A) and single-stained controls for anti-TER119 (PE) (A), anti-CD71 (FITC) (B) and anti-CD44 (APC) (C), showing specificity of each antibody used.

Figure 6.3.2

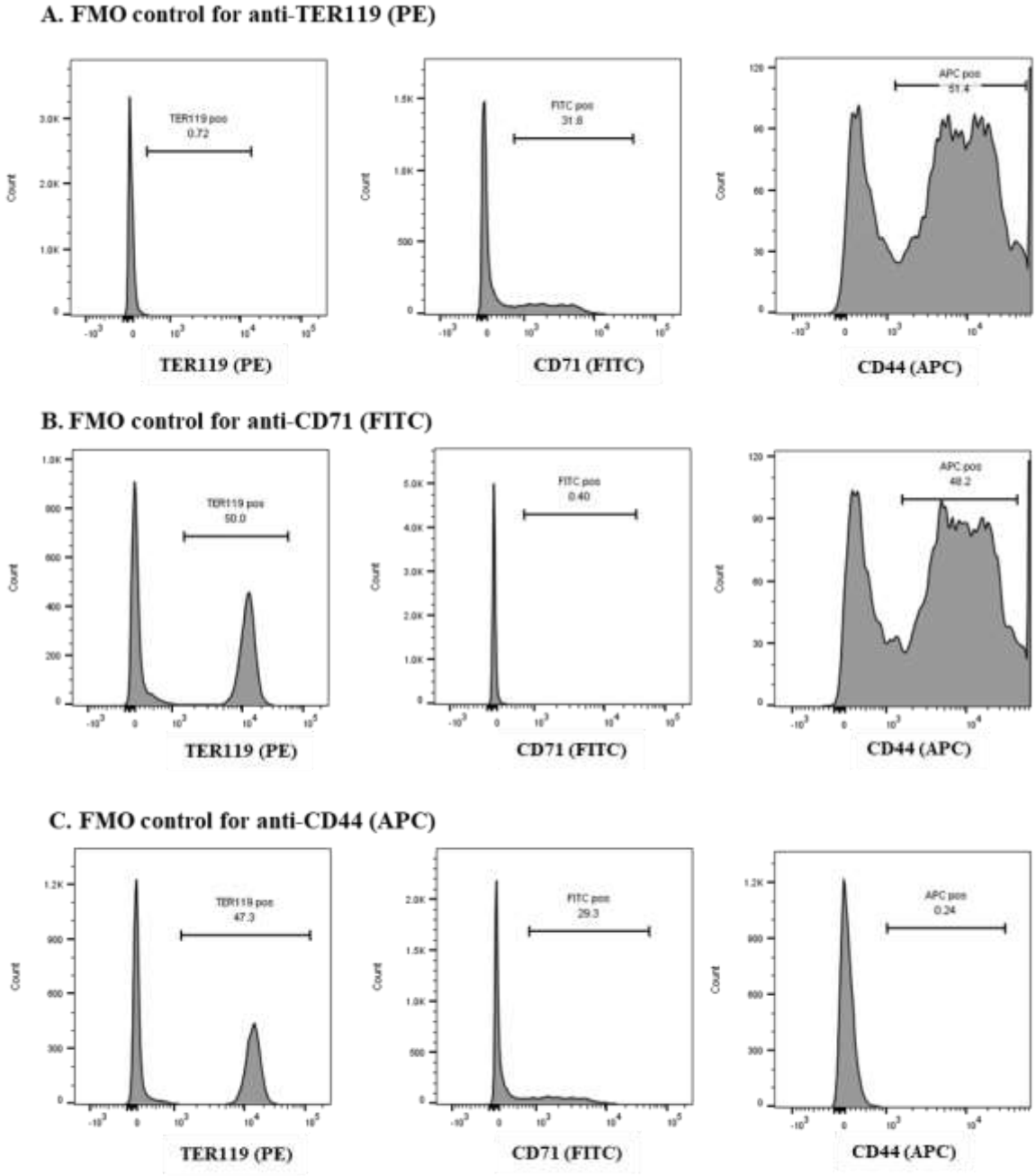

Figure 6.3.2: FMO controls

FMO controls for anti-TER119 (PE) (A), anti-CD71 (FITC) (B) and anti-CD44 (APC) (C) showing no spectral overlap between any of the fluorophores used.

3.6. Isolation of erythroid cells (TER119-positive cells) from the bone marrow

TER119 is widely used as a marker for cells of the erythroid lineage (382). It binds to an antigen, which is associated with the erythrocyte membrane protein, glycophorin A (GPA). TER119 is not expressed by myeloid, lymphoid, BFU-E or CFU-E cells; pro-erythroblasts show moderate levels of expression, while basophilic, polychromatic and orthochromatic erythroblasts, as well as reticulocytes and erythrocytes, show high expression. TER119 is, therefore, used as a specific marker of the erythroid lineage (382,383).

To isolate TER119-positive cells from the bone marrow, an immuno-magnetic procedure using anti-TER119 MicroBeads was employed (cat. no. 130-049-901, Miltenyi Biotec, Germany). In this procedure, cells expressing TER119 were labeled with anti-TER119 antibodies, which were attached to magnetically active micro-beads. Cells tagged with the beads were then applied to a column placed under the influence of a magnetic field. The labeled cells were retained in the column, while the unlabeled cells were allowed to flow through. After this, the column was removed from the magnetic field and the retained (TER119-positive) cells were eluted.

3.6.1 Sample preparation

Single-cell suspension of bone marrow (prepared as described for flow cytometric analysis [Section 3.2]) was used for isolation of TER119-positive cells. The samples were passed through a 40 μm strainer, in order to remove cell clumps. For each sample, 1 x 10^7 cells were aliquoted to fresh tubes and re-suspended in 90 μL of separation buffer (PBS containing 0.5% BSA and 2 mM EDTA).

3.6.2 Magnetic labeling

The vial containing the anti-TER119 micro-beads was gently inverted several times to re-suspend the beads. Ten microliters of the beads were added to 90 μL of the cell suspension, prepared as described above; mixing was done by flicking the tubes with fingers. They were then incubated at 4°C for 15 min. Following incubation, 2 mL of separation buffer was added to each sample; the tubes were centrifuged at 300*g* for 10 min at 4°C. The supernatant was discarded and the pellet was re-suspended in 500 μL of the separation buffer.

3.6.3. Magnetic separation

MACS separation columns (MS column; cat. no. 130-042-201, Miltenyi Biotec, Germany) were placed on an OctoMACS separator (Miltenyi Biotec, Germany), which can run 8 samples simultaneously (Fig 6.3.3)

The column was pre-wetted by adding 0.5 mL of the separation buffer. Following this, the cell-suspension (prepared as described above) was applied to the column and allowed to run through; the effluent was discarded. The column was washed thrice by adding 0.5 mL of the separation buffer. After washing, the column was removed from the OctoMACS separator and placed in a fresh collection tube. One milliliter of separation buffer was added and the column was flushed out, using the plunger. The elute that was collected in the collection tube contained the TER119-positive cells that were labeled by the magnetic beads.

Figure 6.3.3

Figure 6.3.3. OctoMACS magnetic separator with MACS LS columns

Source of image: http://www.miltenyibiotec.com

3.7. Quantitative real-time PCR

The suspension containing the TER119-positive cells (isolated as described above) was centrifuged at 300*g* for 5 min at 4°C. The supernatant was discarded and the pellet (containing TER119-positive cells) was homogenized in 1 mL of Tri-Reagent (Sigma, India), by repeated up and down pipetting. RNA was isolated according to the manufacturer's instructions (as described in detail in Study 1). One microgram of isolated RNA was used to synthesize cDNA, using the Reverse Transcriptase Core Kit (Eurogentec, Belgium) (as described in detail in Study 1). Quantitative PCR reactions were carried out in duplicate, using the Takyon qPCR SYBR master mix (Eurogentec, Belgium), on a BioRad Chromo4 real-time PCR machine. The reaction conditions were identical to those described in study 1. The expression levels of genes of interest were normalized to *Rpl19*, which was used as the reference gene. Sequences of all primers used are listed in Table 6.3.2. The MIQE check-list and qPCR validation data are provided in Appendix I and II (page 323 and 327).

3.8. Estimation of hemoglobin

Estimation of hemoglobin was done by the Drabkin's method (384,385). Five microliters of whole blood (collected in K_2-EDTA tubes) was added to 995 µL of Drabkin's solution (cat. no. D5941, Sigma, India). After centrifugation at 12000*g* for 5 min, the absorbance of the solution was measured at 540 nm, using a spectrophotometer (UV-1800, Shimadzu, Japan). Hemoglobin levels (in g/dL) was obtained by multiplying the optical density (OD) at 540nm by a factor of 29.32, which was calculated based on the extinction coefficient of cyanmethemoglobin (44,000) (386).

Table 6.3.2: Primers used for qPCR

Sl. No.	Gene	Accession number	Primer sequence	Amplicon size (bp)
1	TfR1 (*Tfrc*)	NM_011638.4	5'-GAGGCGCTTCCTAGTACTCC-3' 3'-CTTGCCGAGCAAGGCTAAAC-5'	121
2	TfR 2 (*Tfr2*)	NM_015799.3	5'-GGTCCTGATCACCCTGCTAA-3' 3'-GGAGGTCGCTCCAGTACAAC-5'	158
3	ERFE (*Erfe*)	NM_173395.2	5'-ATGGGGCTGGAGAACAGC-3' 3'-TGGCATTGTCCAAGAAGACA-5'	100
4	GDF-15 (*Gdf15*)	NM_011819.3	5'-GAGCTACGGGGTCGCTTC-3' 3'-GGGACCCCAATCTCACCT-5'	130
5	TWSG1 (*Twsg1*)	NM_023053.3	5'-TGAGCAAATGCCTCATTCAG-3' 3'-CAGGGGCAGTTCCCTTCT-5'	61
6	Rpl19 (*Rpl19*)	NM_009078.2	5'- ATGAGTATGCTCAGGCTACAGA-3' 5'- GCATTGGCGATTTCATTGGTC-3'	104

3.9 Estimation of serum growth differentiation factor–15 (GDF-15) levels

Estimation of GDF-15 in serum samples was done using a commercially available ELISA kit (cat. no. DY6385; Mouse GDF-15 Duo Set ELISA Development System R&D Systems, USA), according to the manufacturer's instructions.

3.9.1 Plate preparation:

The capture antibody (sheep anti-mouse GDF-15) was reconstituted with 1 mL of PBS and further diluted to a working concentration of 0.8 μg/mL. It was then coated on a Nunc 96-well microplate (100 μL per well). The plate was sealed and left overnight at room temperature. The next day, the excess antibody was aspirated and the plate was washed thrice with wash buffer (PBS with 0.05% Tween-20). The coated plate was blocked with reagent diluent (PBS with 1% BSA) for 1h and washed again before addition of the sample.

3.9.2 Preparation of standards and samples

The vial containing mouse GDF-15 standard was reconstituted with 0.5 mL of reagent diluent, to obtain a final concentration of 500 pg/mL. Serial dilutions were made to obtain standards of the following concentrations: 500, 250, 125, 62.5, 31.8, 15.6 and 7.8 pg/mL. Serum samples were diluted 1: 5, using the reagent diluent.

3.9.3 Assay procedure

One hundred microliters of the diluted serum samples and the prepared standards were added to appropriate wells and incubated at room temperature for 2h. All reactions were carried out in

duplicate. After incubation, the wells were washed thrice with wash buffer. One hundred microliters of detection antibody (biotinylated sheep anti-mouse GDF-15 diluted to a final concentration of 100 ng/mL in reagent diluent) was added to all the wells and incubated at room temperature for 2 h. Following this, the plate was washed again and 100 µL of reconstituted streptavidin-HRP conjugate was added to all the wells and incubated for 20 min at room temperature. After washing, 100 µL of substrate solution (1:1 mixture of Color Reagent A (H_2O_2) and Color Reagent B (Tetramethylbenzidine); R&D Systems, Catalog # DY999) was added and incubated at room temperature for 20 min. The reaction was stopped by adding the stop solution (2N H_2SO_4). The color was measured immediately using iMark microplate reader (BioRad, USA), set to a wavelength of 450 nm with wavelength correction at 540 nm. OD readings obtained for the standards were used to plot a standard curve using a 4-parameter logistic (4-PL) curve fit. The average OD reading for each sample was used to estimate levels of GDF-15. A factor of 5 was used to correct for the 1:5 dilution of serum samples.

3.10 Estimation of serum erythropoietin (EPO) levels

Serum levels of EPO was estimated using a commercially available ELISA kit (cat. no. MEP00B, mouse erythropoietin Quantikine ELISA kit, R&D Systems, USA), according to the manufacturer's instructions.

3.10.1 Standard and sample preparation

Serial dilutions of the mouse EPO standard were made to obtain standards of the following concentrations: 3000, 1500, 750, 375, 188, 94 and 47 pg/mL. Serum samples were diluted 1: 2, using the calibrator diluent provided with the kit.

3.10.2 Assay procedure

Fifty microliters of assay diluent were added to each well. Following this, 50 μL of the diluted serum samples and the prepared standards were added to appropriate wells and incubated at room temperature for 2h. All reactions were carried out in duplicate. After incubation, the wells were washed five times with wash buffer. One hundred microliters of the detection antibody (mouse Epo conjugate) was added to all the wells and incubated at room temperature for 2 h. Following this, the plate was washed again; 100 μL of substrate solution was added and incubated at room temperature for 20 min. The reaction was stopped by adding the stop solution. The color was measured immediately using iMark microplate reader (BioRad, USA), set to a wavelength of 450 nm with wavelength correction at 540 nm. OD readings obtained for the standards were used to plot a standard curve using a 4-parameter logistic (4-PL) curve fit. The average OD reading for each sample was used to estimate levels of EPO. A factor of 2 was used to correct for the 1:2 dilution of samples.

3.11 Statistical analysis

SPSS version 16.0, was used for all statistical analyses. Since the data were found to be skewed, non-parametric tests were used for statistical analysis. The Kruskal-Wallis (KW) test was employed to look for significant differences between the various groups studied. Pair-wise comparisons between groups were made by the Mann-Whitney test. Correlation analyses were done by Spearman's correlation test. A p value of less than 0.05 was used to indicate statistical significance in all cases.

4. Results

4.1 Resolution of distinct stages in TED, based on surface expression of CD71, by flow cytometry

CD71 (or transferrin receptor 1 [TfR1]) is highly expressed on the surface of erythroblasts. Its expression peaks in pro-erythroblasts and basophilic erythroblasts and then declines to lower levels in reticulocytes; it is not detectable in mature erythrocytes (387). It was shown that TED could be resolved into four distinct stages (called ProE, EryA, EryB and EryC) by flow cytometry, based on changes in surface expression of CD71 (388) and in cell size (381).

Bone marrow cells and splenocytes were processed as described in section 3.2 and 3.3. Representative images for the gating strategy employed for bone marrow cells are shown in Fig 6.3.4; an identical procedure was used for gating splenocytes as well. In Fig 6.3.4-A, the parent population (P1) was chosen by excluding cellular debris, nuclei and other small events. The P1 population was further analyzed, with TER119 expression (PE) taken on the x-axis and CD71 expression on the y-axis (Fig 6.3.4-B). Here, a clear and distinct population of TER119-positive cells was gated, based on the FMO control for TER119-PE (shown in Fig 6.3.2). In addition, a gate defining a population of $CD71^{high}$ $TER119^{intermediate}$ cells (pro-E) was added. The TER119-positive population was further analyzed with forward scatter (a parameter that reflects cell size) taken along the x-axis and CD71 expression on the y-axis (Fig 6.3.4-C). Here, the cells were divided in three distinct populations - EryA ($CD71^{high}TER119^{high}FSC^{high}$), EryB ($CD71^{high}TER119^{high}FSC^{low}$) and EryC ($CD71^{low}TER119^{high}FSC^{low}$). EryA represents the early erythroblasts (basophilic and polychromatic erythroblasts), EryB represents orthochromatic erythroblasts and reticulocytes, and EryC represents erythrocytes.

Figure 6.3.4

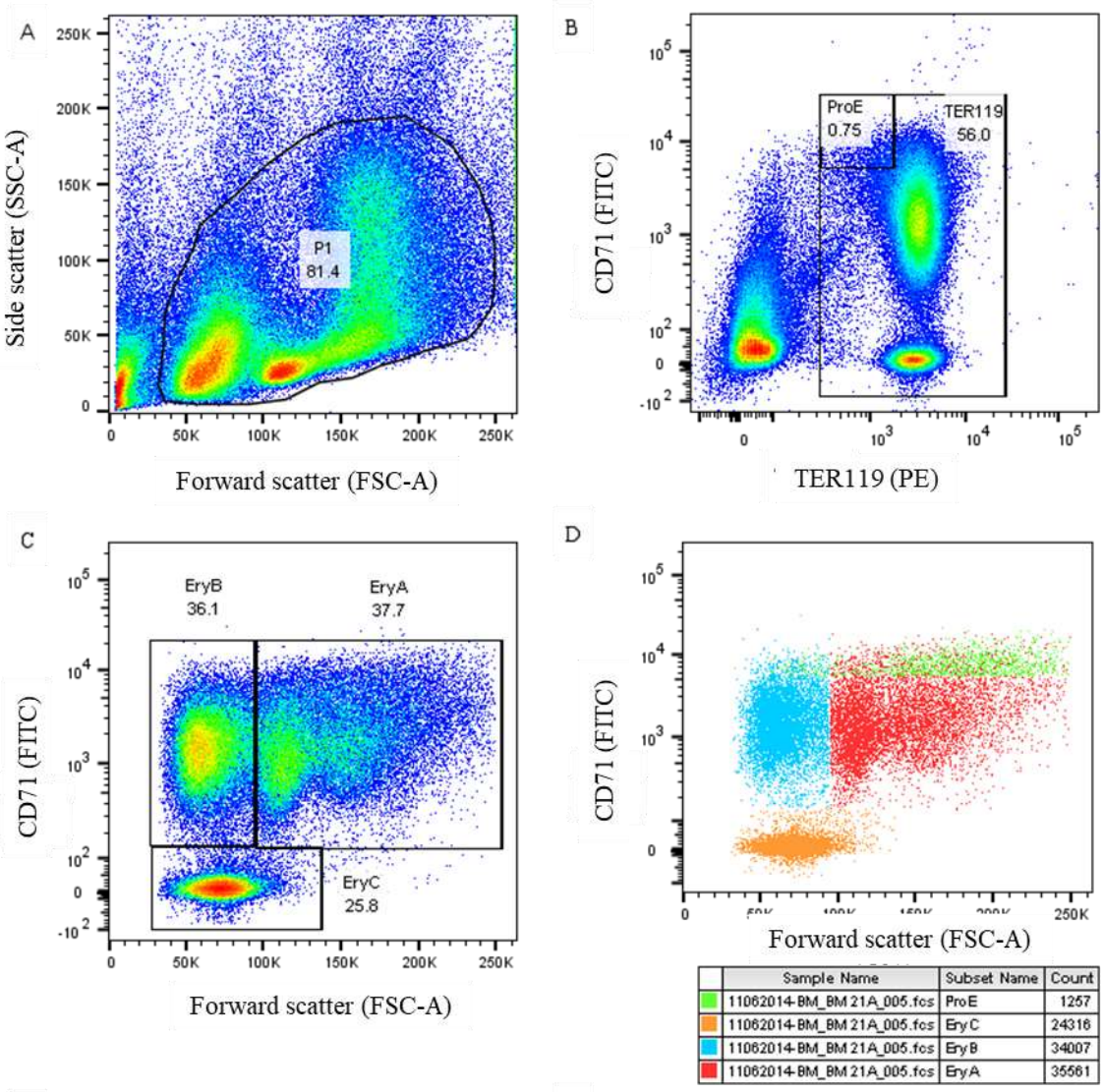

Figure 6.3.4: Gating strategy for resolution of stages in TED, based on CD71 expression and cell size

Bone marrow cells were labeled with anti-CD71 (FITC), anti-TER119 (PE) and anti-CD44 (APC) antibodies. A: The parent population (P1) was chosen by excluding cellular debris, nuclei and other small events. B: The P1 population was further analyzed with TER119 expression (PE) on the x-axis and CD71 expression on the y-axis. The pro-E population was defined as a population of $CD71^{high}$ $TER119^{intermediate}$ cells. C: The TER119+ population was further analyzed with forward scatter (FSC-A) taken along the x-axis and CD71 (FITC). D: A dot plot (generated as an overlay) showing pro-E, EryA, EryB and EryC cells in different colors.

4.2. Resolution of distinct stages in TED, based on surface expression of CD44, by flow cytometry

CD44 is a ubiquitously expressed type-1 transmembrane glycoprotein, which acts as a cell adhesion molecule involved in various cell-cell and cell-matrix interactions (389). CD44 is highly expressed on early erythroblasts; its expression decreases in erythroblasts that are more mature. Chen et al (355) showed that successive developmental stages during TED could be discriminated based on CD44 expression. This method was further refined by Liu et al (356), allowing them to resolve the various populations of erythroblasts to a greater extent than that achieved previously using CD71 expression. Using this method, six distinct populations were defined as shown in Fig 6.3.5.

Bone marrow cells and splenocytes were processed as described in sections 3.2 and 3.3. Representative images for the gating strategy employed for bone marrow cells are shown in Fig 6.3.5. In Fig 6.3.5-A, the parent population (P1) was chosen by excluding cellular debris, nuclei and other small events. TER119-positive cells in the P1 population were gated (based on FMO control for TER119-PE) (Fig 6.3.5-B). The TER119-positive cells were further analyzed with CD44 (APC) taken on the y-axis (Fig 6.3.5-C) and a gate defining a population of $CD44^{high}$ $TER119^{intermediate}$ cells (population I) was added. The TER119-positive population was further analyzed with forward scatter taken along the x-axis and C44 expression on the y-axis (Fig 6.3.5-D). Here, the cells were divided in five populations (II to VI) as shown in Fig 6.3.5-E and F. Population I represents pro-erythroblast (pro-E); II, basophilic erythroblasts; III, polychromatic erythroblasts; IV, orthochromatic erythroblasts; V, reticulocytes and VI, erythrocytes.

Figure 6.3.5

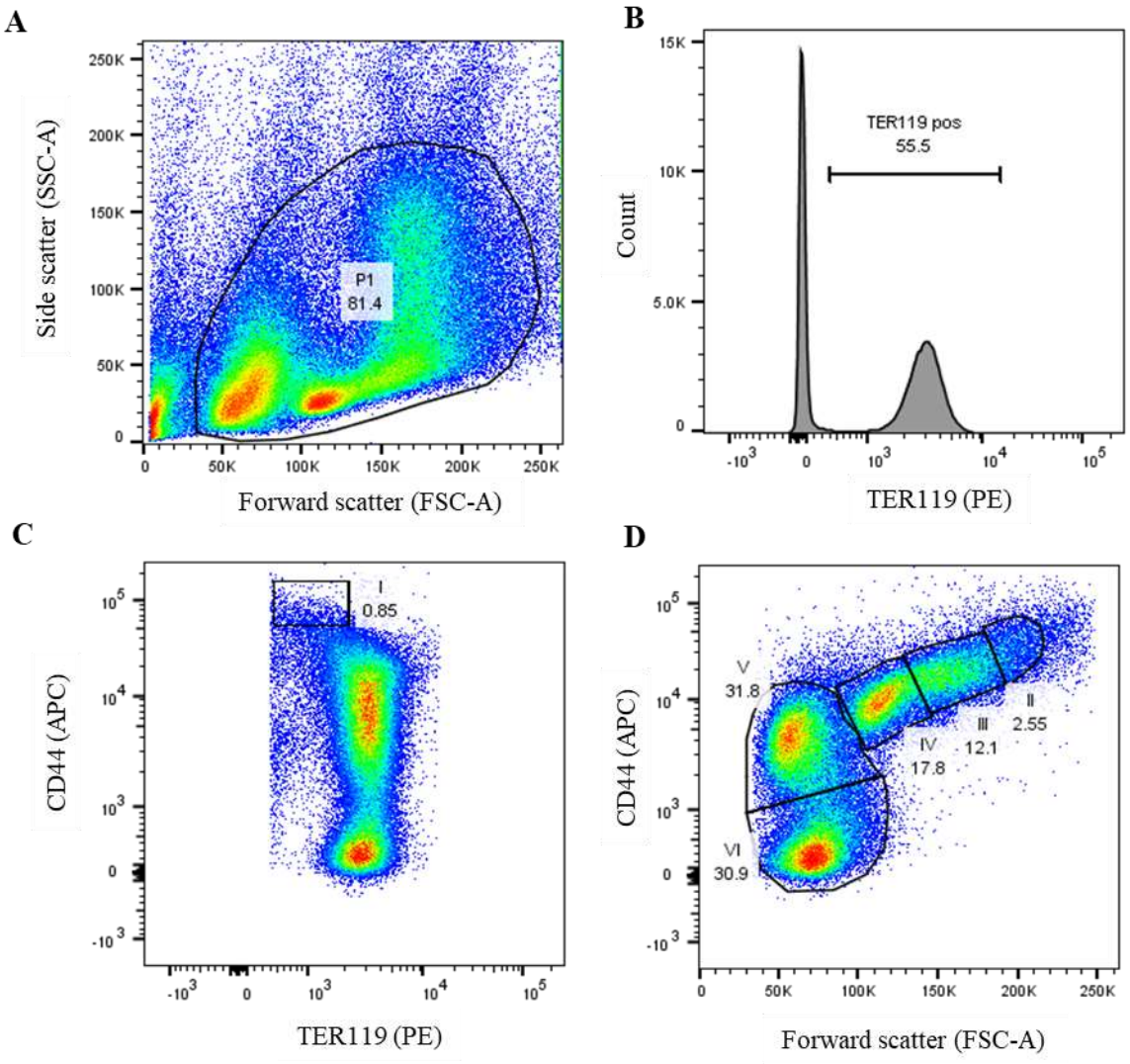

Continued on the next page

Figure 6.3.5 (continued from previous page)

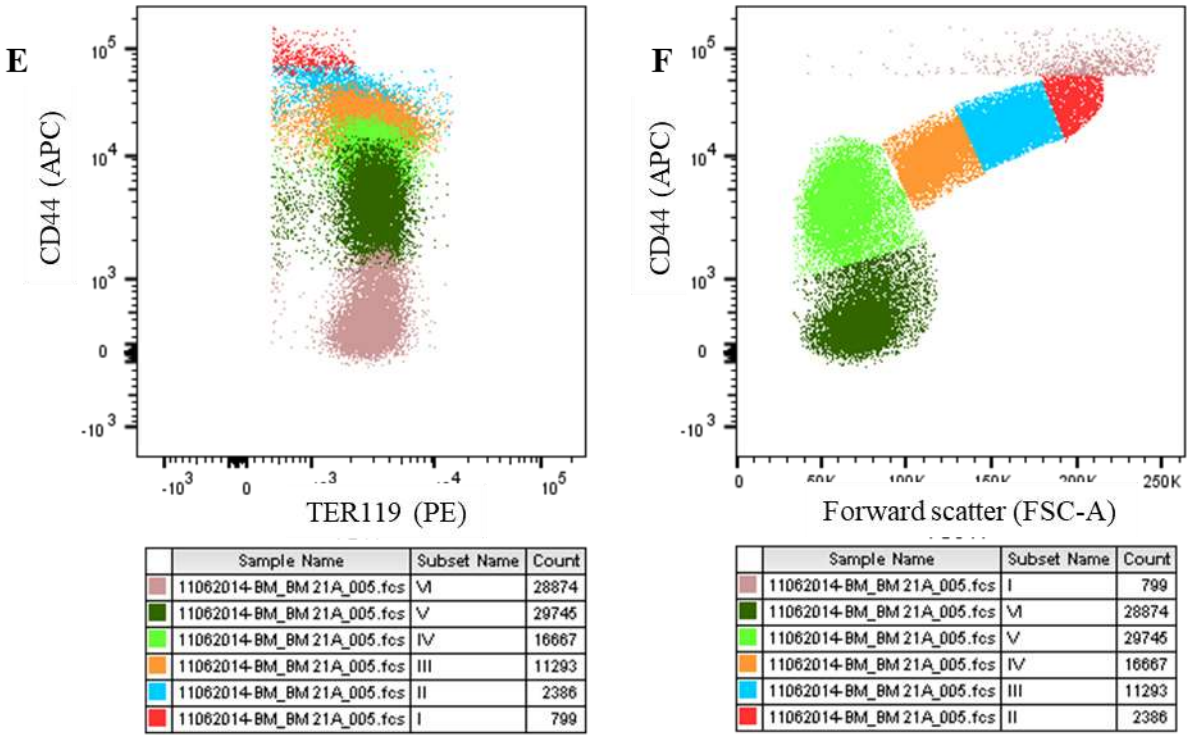

	Sample Name	Subset Name	Count
	11062014-BM_BM 21A_005.fcs	VI	28874
	11062014-BM_BM 21A_005.fcs	V	29745
	11062014-BM_BM 21A_005.fcs	IV	16667
	11062014-BM_BM 21A_005.fcs	III	11293
	11062014-BM_BM 21A_005.fcs	II	2386
	11062014-BM_BM 21A_005.fcs	I	799

	Sample Name	Subset Name	Count
	11062014-BM_BM 21A_005.fcs	I	799
	11062014-BM_BM 21A_005.fcs	VI	28874
	11062014-BM_BM 21A_005.fcs	V	29745
	11062014-BM_BM 21A_005.fcs	IV	16667
	11062014-BM_BM 21A_005.fcs	III	11293
	11062014-BM_BM 21A_005.fcs	II	2386

Figure 6.3.5*: Gating strategy for resolution of stages in TED, based on CD44 expression and cell size*

Bone marrow cells were labeled with anti-CD71 (FITC), anti-TER119 (PE) and anti-CD44 (APC) antibodies. A: The parent population (P1) was chosen by excluding cellular debris, nuclei and other small events. B: TER119 positive cells in the P1 population were gated. C: Dot plot of TER119 - PE (x-axis) versus CD44 – APC (y-axis). Population I was gated as a population of $CD44^{high}$ $TER119^{intermediate}$ cells. D: Dot plot of forward scatter (FSC-A) taken (x-axis) versus CD44-APC (y-axis) E and F: Dot plots (generated as overlay) of TER119 vs. CD44 (E) and FSC vs. CD44 (F) showing populations I to VI in different colors.

4.3. Effect of HFD on erythroid maturation in bone marrow

The proportions of erythroid cells (TER119-positive) in the bone marrow was not significantly affected by HFD at any of the time points studied (Fig 6.3.6–A).

4.3.1. Analysis of erythroid maturation in the bone marrow, based on CD71 expression

Flow cytometric analysis of TED, based on CD71 expression and cell size, showed that the pro-E (pro-erythroblast) (Fig 6.3.6–B) and EryA (basophilic and polychromatic erythroblasts) (Fig 6.3.7–A) populations were not affected by HFD at any of the time points studied. EryB (orthochromatic erythroblasts and reticulocytes) was increased in HFD-fed mice, with the increases being statistically significant at 8 weeks and 20 weeks (Fig 6.3.7–B). EryC (erythrocytes) tended to be lower in HFD-fed mice but these changes were not statistically significant at any of the time points studied (Fig 6.3.7–C). Fig 6.3.8 shows representative images of flow cytometric contour plots from CD and HFD-fed mice at all the time points studied.

Figure 6.3.6

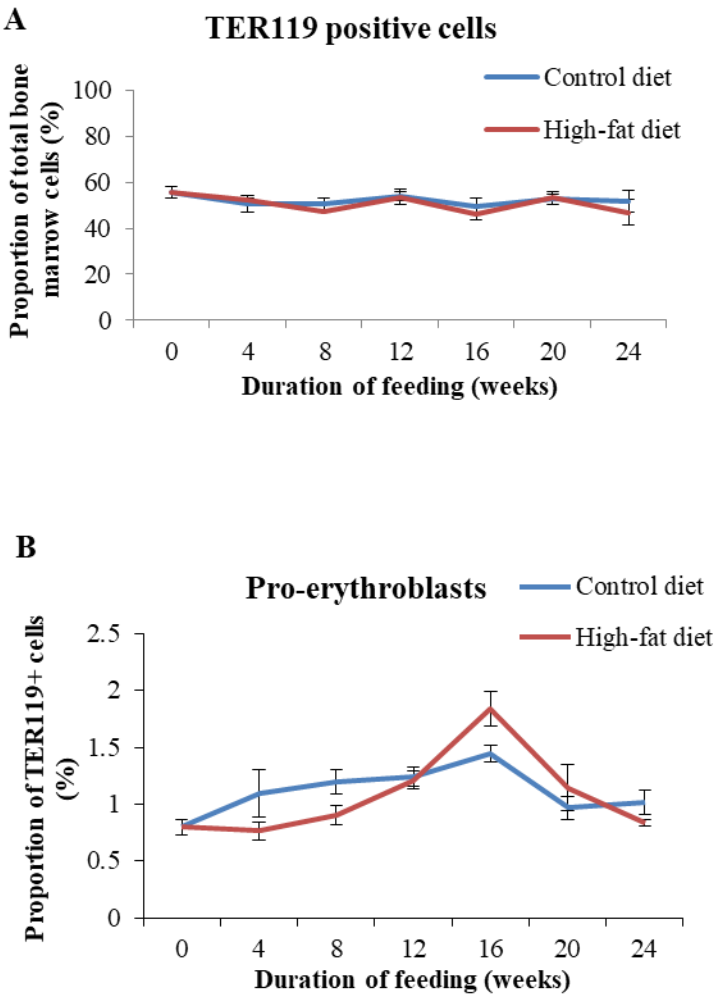

Figure 6.3.6: Effect of HFD-feeding on TER119-positive cells and pro-erythroblasts in the bone marrow

Total TER119-positive cells (A) pro-erythroblasts ($TER119^{intermediate}CD71^{high}$) (B) in the bone marrow of mice fed CD and HFD for various durations (as indicated). Data are shown as mean ± SE; n = 6 (for both CD- and HFD-fed mice) at each time point.

Figure 6.3.7

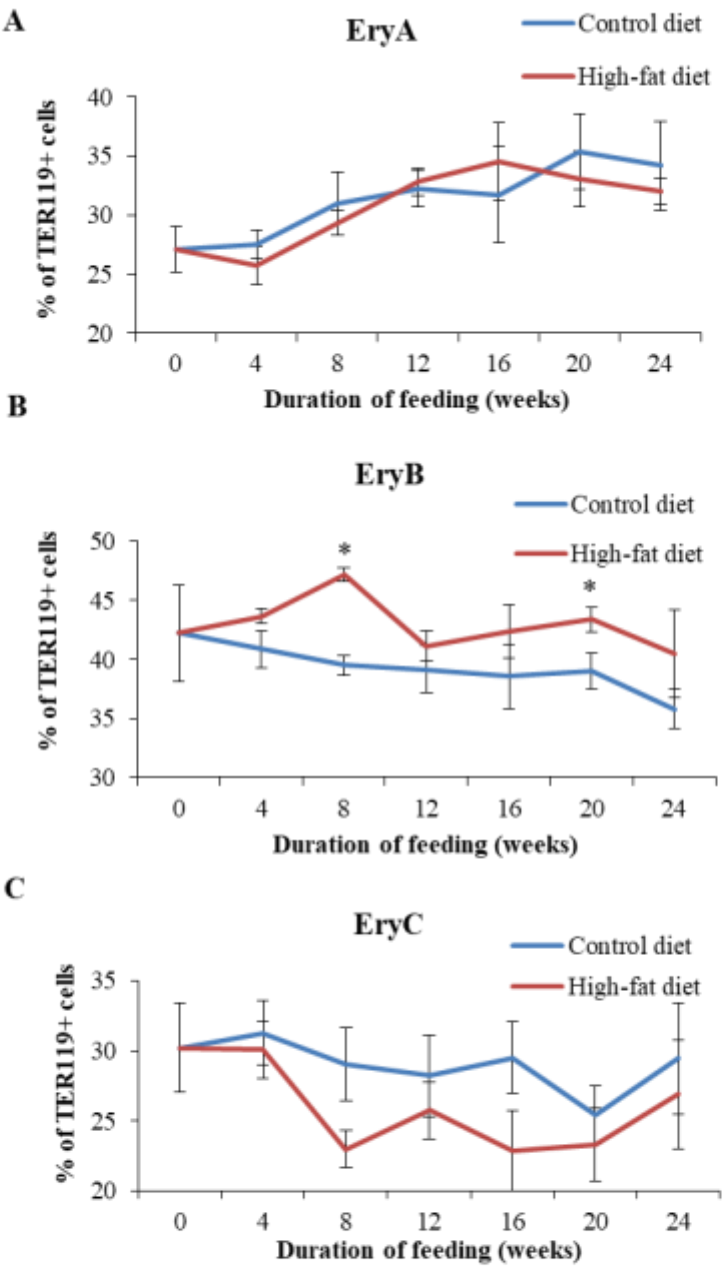

Figure 6.3.7: Effect of HFD-feeding on TED in the bone marrow

TER119 positive cells in the bone marrow were resolved into 3 populations, EryA (A), EryB (B) and EryC (C) based on CD71 expression and cell size in mice fed CD or HFD for various durations (as indicated) Data are shown as mean ± SE; n = 6 (for both CD- and HFD-fed mice) at each time point. * indicates $p < 0.05$ when compared to the respective control group.

Figure 6.3.8

A. 4 weeks

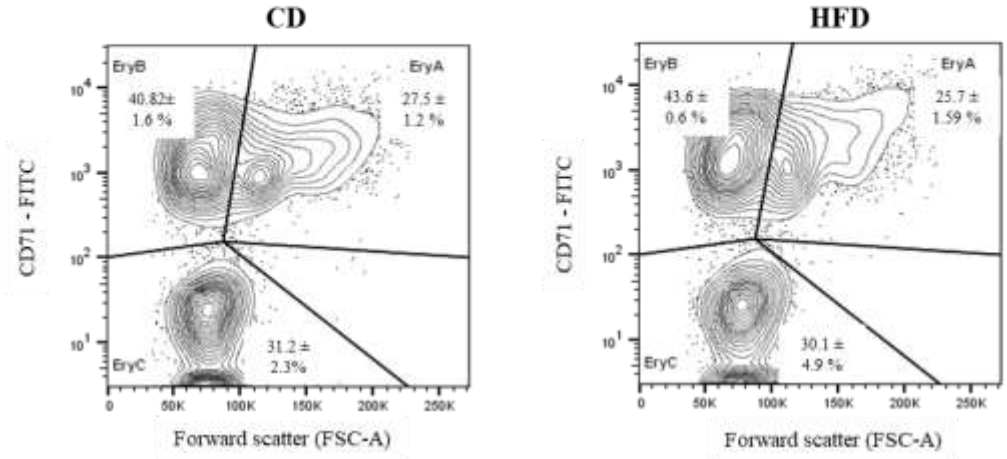

B. 8 weeks

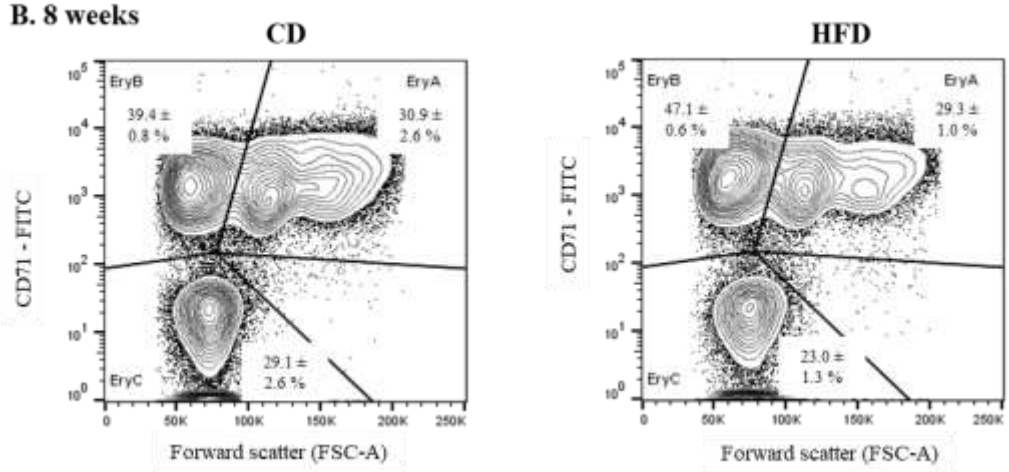

C. 12 weeks

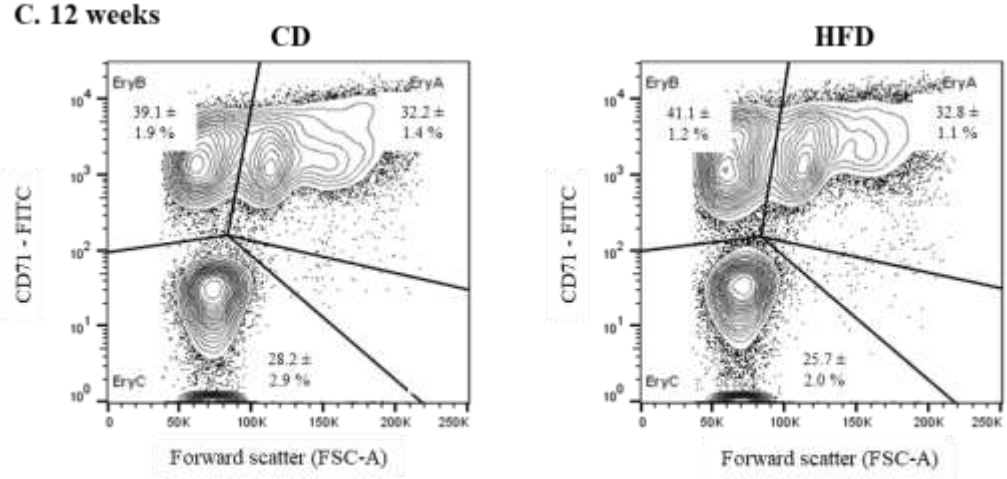

Continued on the next page

Figure 6.3.8 continued from previous page

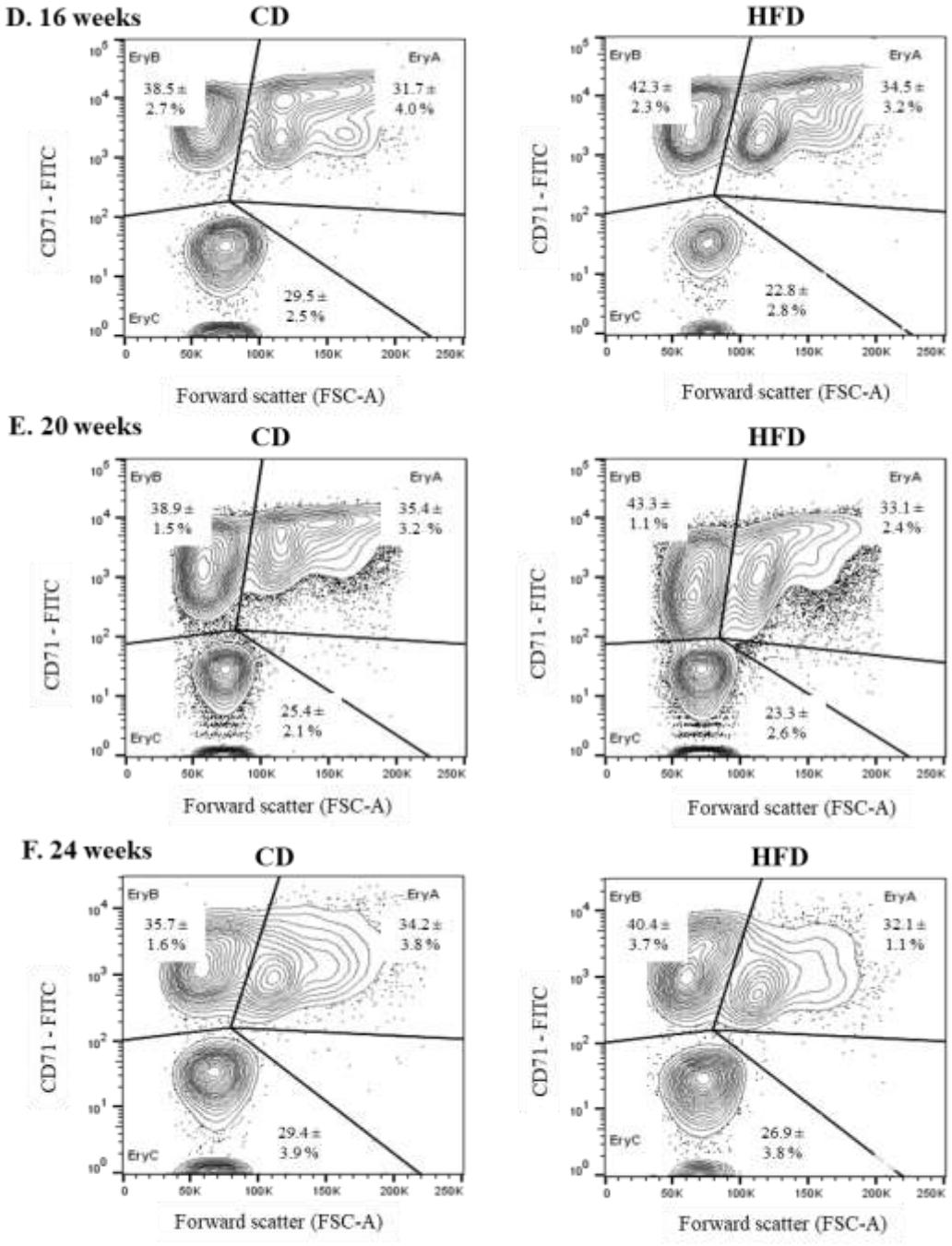

Figure 6.3.8: Effect of HFD-feeding on TED in the bone marrow

Representative images of contour plots showing bone marrow TER119-positive cells resolved into 3 populations (EryA, EryB and EryC), based on CD71 expression (y-axis) and forward scatter (x-axis) in mice fed CD or HFD for 4 (A), 8 (B), 12 (C), 16 (D), 20 (E) or 24 (F) weeks. Proportion of total TER119 cells present within each gate is shown (mean ± SE).

4.3.2 Analysis of erythroid maturation in the bone marrow, based on CD44 expression

Analysis of TED, based on CD44 expression and cell size, showed that the early erythroblasts (pro-erythroblasts, basophilic and polychromatic erythroblasts) tended to be decreased in HFD-fed mice at 4 and 8 weeks; these changes were, however, statistically significant only for polychromatic erythroblasts at 4 weeks (Fig 6.3.9). Longer durations of HFD-feeding (12, 16, 20 and 24 weeks) did not have a significant effect upon the early erythroblasts. On the other hand, reticulocytes were found to be consistently increased in HFD-fed mice, with the increase being statistically significant at 8 weeks (Fig 6.3.9–E). The ratio of pro-, basophilic, polychromatic and orthochromatic erythroblasts (I:II:III:IV) was found to conform to the expected ratio of 1:2:4:8 in CD and HFD-fed mice. Fig 6.3.10 shows representative images of flow cytometric contour plots from CD and HFD-fed mice at all the time points studied.

4.4. Effect of HFD on erythroid maturation in the spleen

TER119-positive cells and early erythroblasts (EryA) in the spleen were not affected by HFD-feeding (Fig 6.3.11–A and B). The EryB population (orthochromatic erythroblasts and reticulocytes) was significantly lower in mice fed HFD for 24 weeks (Fig 6.3.1–C). This was accompanied by a corresponding increase in EryC cells at the same time point (Fig 6.3.11–D). Fig 6.3.12 shows representative images of flow cytometric dot plots from CD and HFD-fed mice at all the time points studied.

Figure 6.3.9

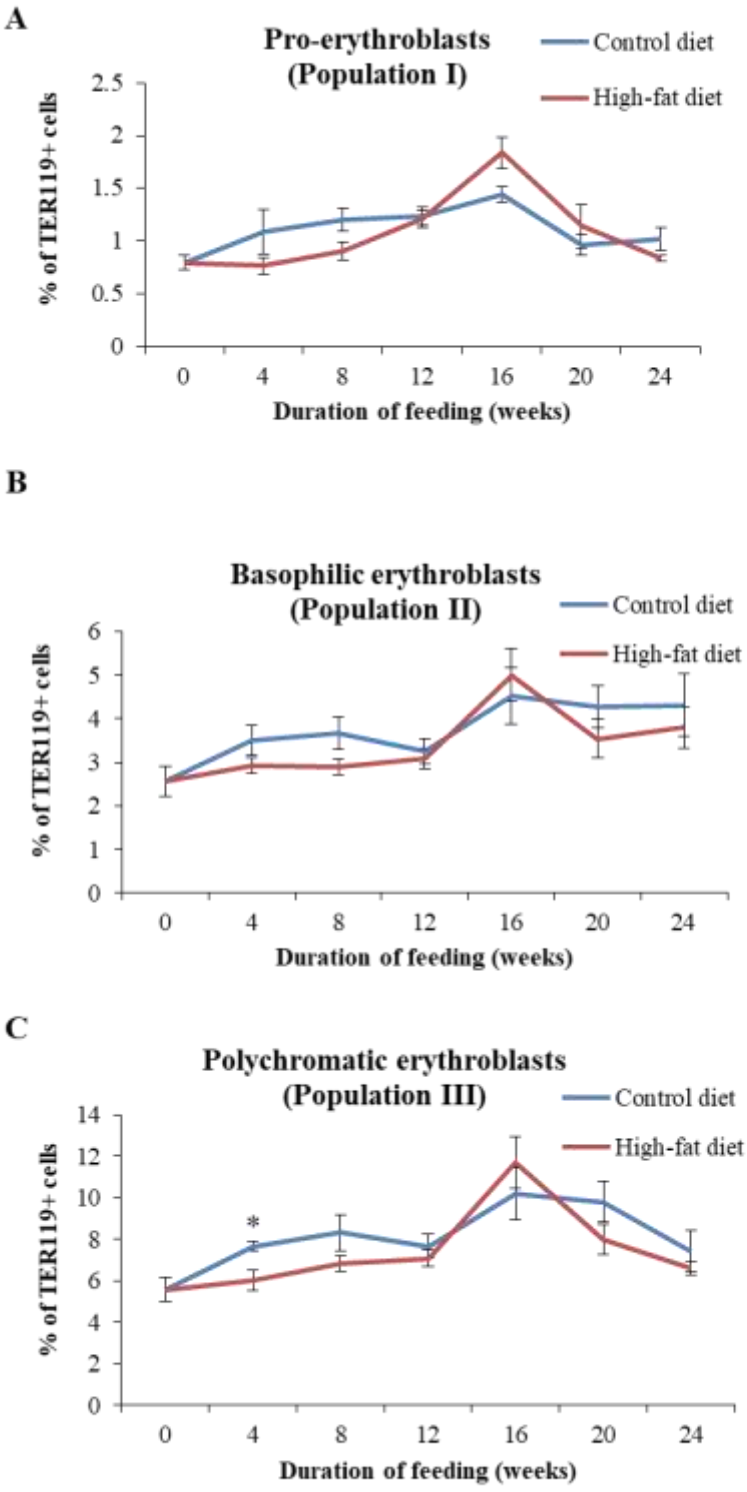

Continued on the next page

Figure 6.3.9 continued from the previous page

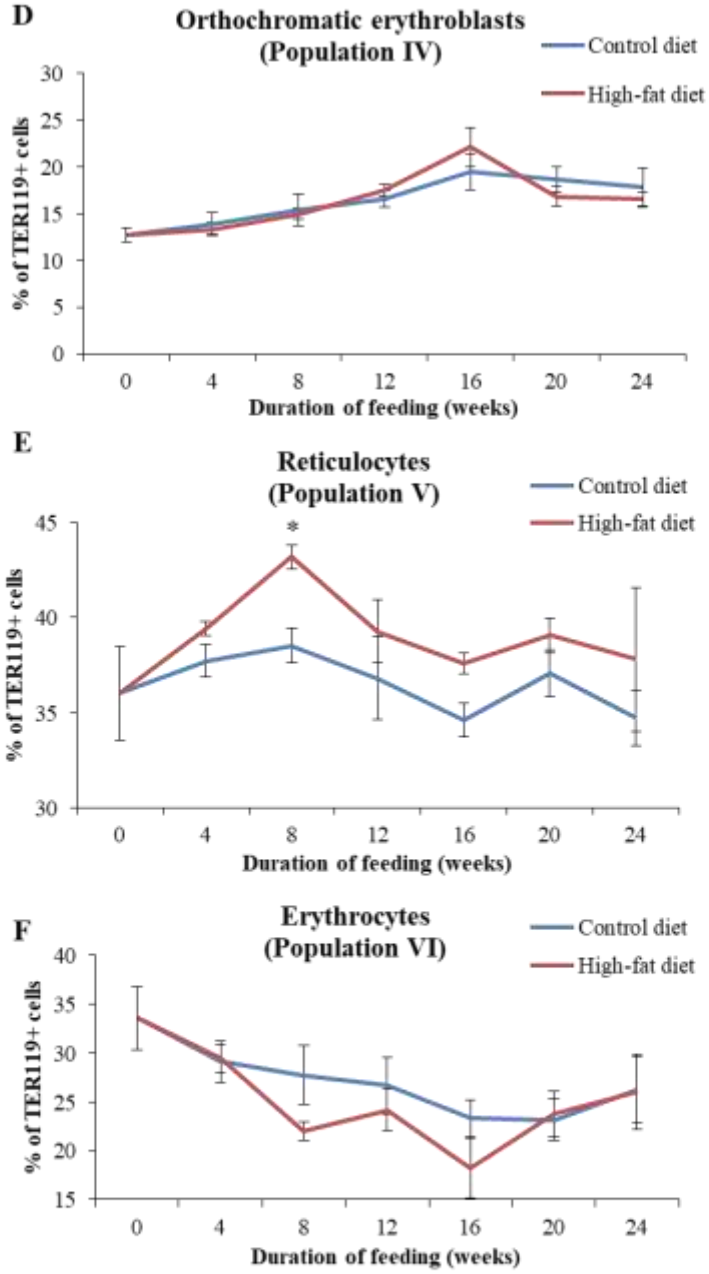

Figure 6.3.9: Effect of HFD-feeding on TED in the bone marrow

TER119 positive cells in the bone marrow were resolved into 6 distinct populations of erythroblasts, pro-erythroblast (A), basophilic (B), polychromatic (C) and orthochromatic (D) erythroblasts, reticulocytes (E) and mature erythrocytes (F) and based on CD44 expression and cell size in mice fed CD or HFD for various durations (as indicated) Data are shown as mean ± SE; n = 6 (for both CD- and HFD-fed mice) at each time point. * indicates $p < 0.05$ when compared to the respective control group.

Figure 6.3.10

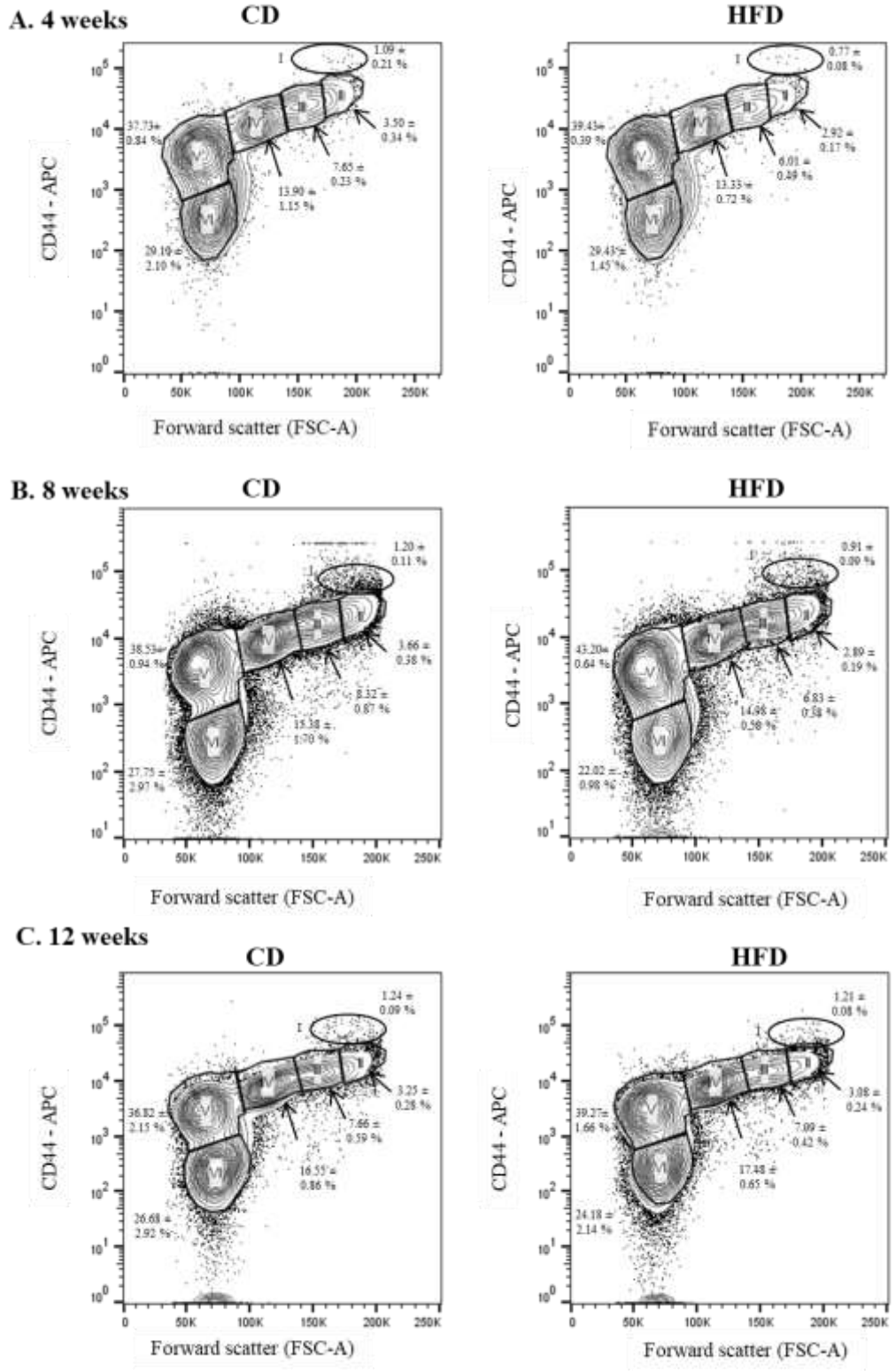

Continued on the next page

Figure 6.3.10 continued from previous page

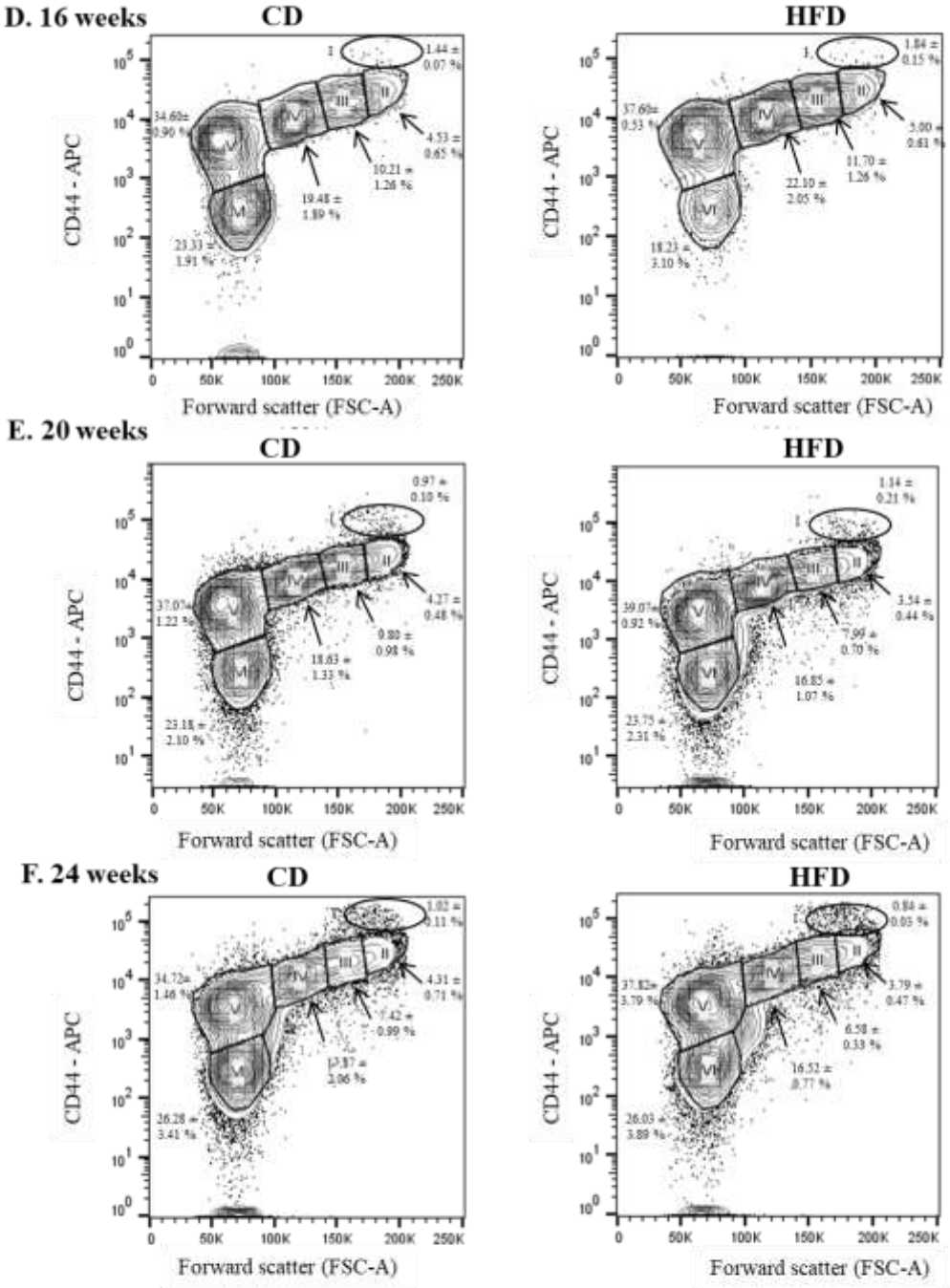

Figure 6.3.10: Effect of HFD-feeding on TED in the bone marrow

Representative images of contour plots showing bone marrow TER119-positive cells resolved into 6 populations (I, II, III, IV, V, and VI), based on CD44 expression (y-axis) and forward scatter (x-axis), in mice fed CD or HFD for 4 (A), 8 (B), 12 (C), 16 (D), 20 (E) or 24 (F) weeks. Proportion of total TER119 cells present within each gate is shown (mean ± SE).

Figure 6.3.11

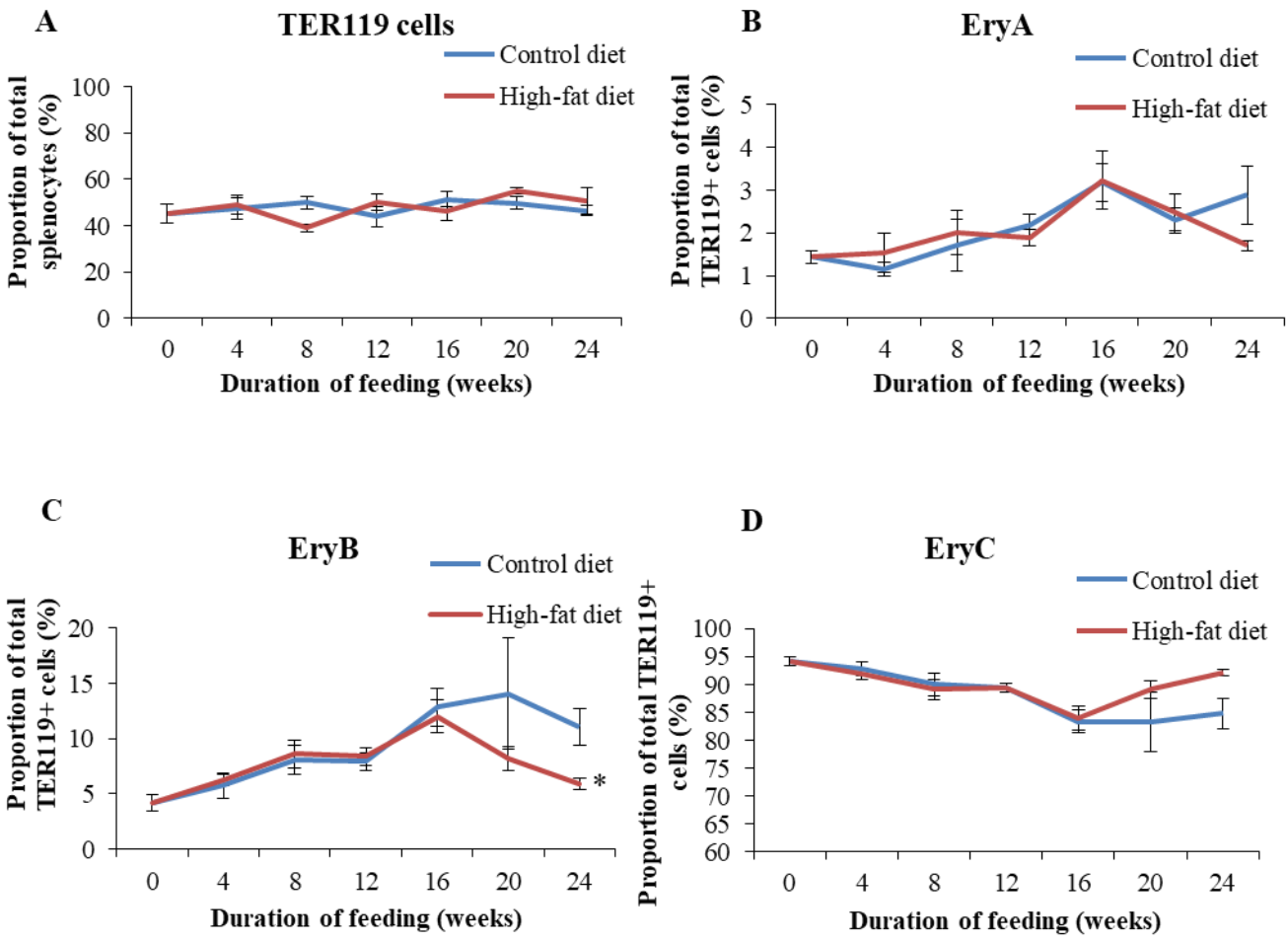

Figure 6.3.11: Effect of HFD-feeding on TED in the spleen

A: Proportion of TER119-positive cells in the spleen. B-D: Splenic TER119-positive cells were resolved into 3 populations, EryA (B), EryB (C) and EryC (D), based on CD71 expression and cell size, in mice fed CD or HFD for various durations (as indicated) Data are shown as mean ± SE; n = 3-6 (for both CD- and HFD-fed mice) at each time point. * indicates $p < 0.05$ when compared to the respective control group.

Figure 6.3.12

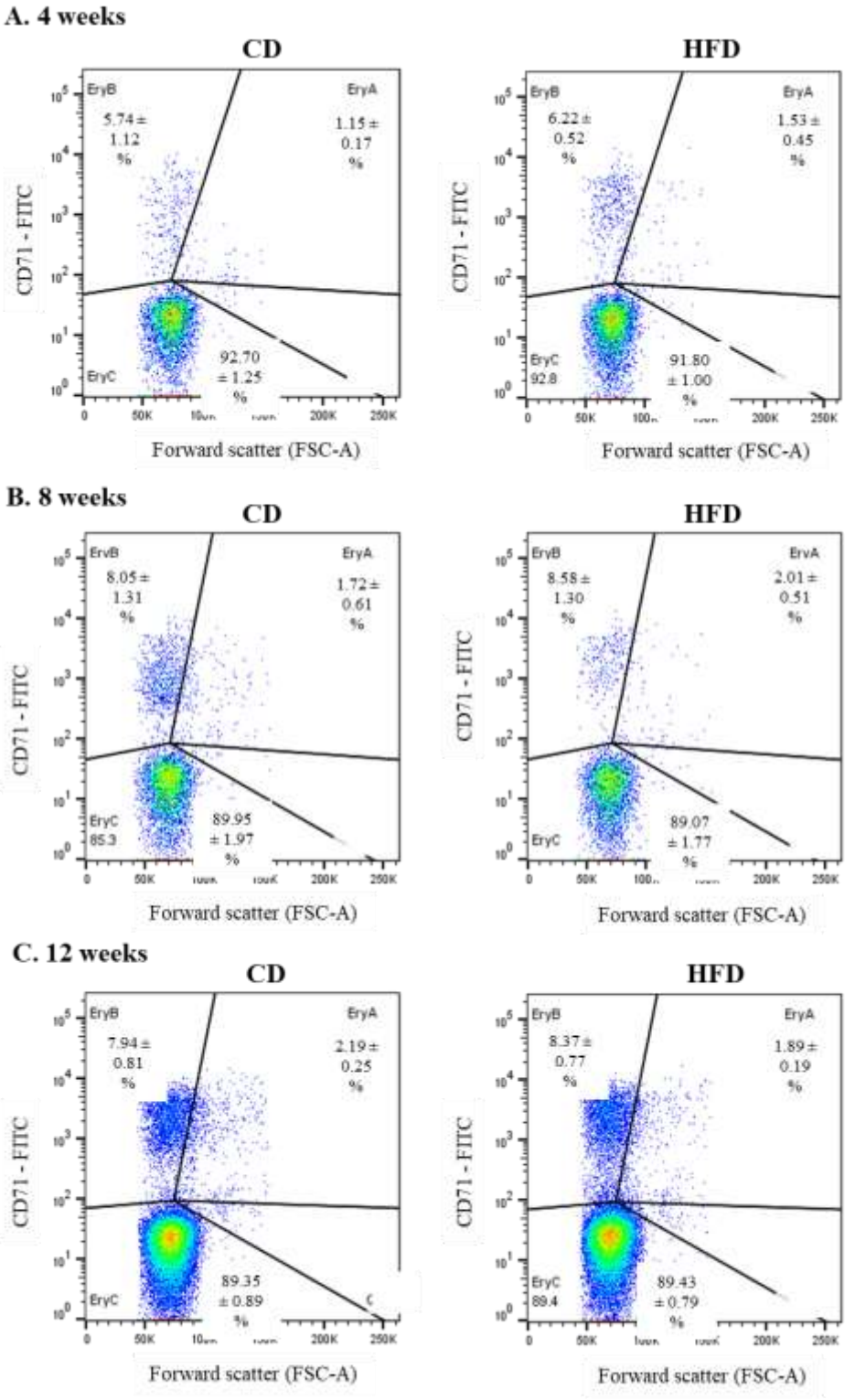

Continued on the next page

Figure 6.3.12 continued from previous page

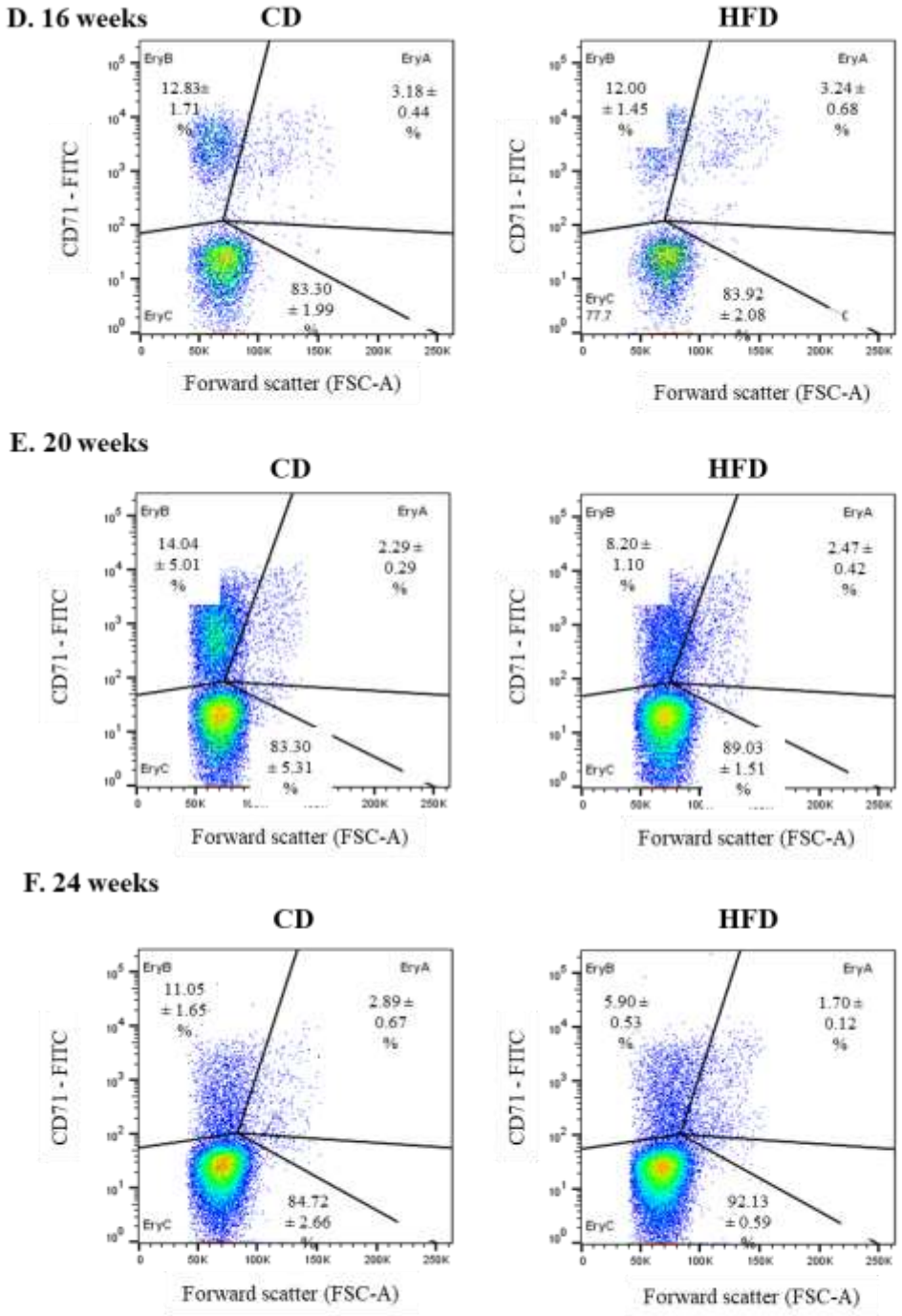

Figure 6.3.12: Effect of HFD-feeding on TED in the spleen

Representative images of dot plots showing splenic TER119-positive cells resolved into 3 populations (EryA, EryB and EryC), based on CD71 expression (y-axis) and forward scatter (x-axis), in mice fed CD or HFD for 4 (A), 8 (B), 12 (C), 16 (D), 20 (E) or 24 (F) weeks. Proportion of total TER119 cells present within each gate is shown (mean ± SE).

4.5 Effect of HFD-feeding on hemoglobin

Hemoglobin levels in blood were not significantly different between CD and HFD-fed mice, except at 16 weeks, where HFD-fed mice had significantly higher levels (Fig 6.3.13).

4.6 Effect of HFD-feeding on gene (mRNA) expression of erythroid regulators of hepcidin in TER119-positive cells

Erythroferrone, GDF-15, and TWSG-1 are putative erythroid regulators of hepcidin expression; they are synthesized and secreted by erythroid precursor cells in the bone marrow (100). TER119-positive cells were isolated by positive selection (using the MACS immuno-magnetic micro-bead system, Miltenyi Biotec, Germany), as described in section 3.6. Gene expression of erythroferrone (Fig 6.3.14–A) and TWSG-1 (6.3.14–C) were not significantly different in CD and HFD-fed mice at any of the time points studied. GDF-15 expression, on the other hand, was found to be significantly decreased after 24 weeks of HFD (Fig 6.3.14–B).

4.7 Effect of HFD-feeding on gene (mRNA) expression of transferrin receptors 1 and 2 in TER119-positive cells

Expression of TfR1 (390) and TfR2 (391) in bone marrow erythroid cells have been shown to be associated with the regulation of hepcidin expression in the liver. In the present study, HFD-feeding did not have a significant effect on the expression of these genes (Fig 6.3.15).

Figure 6.3.13

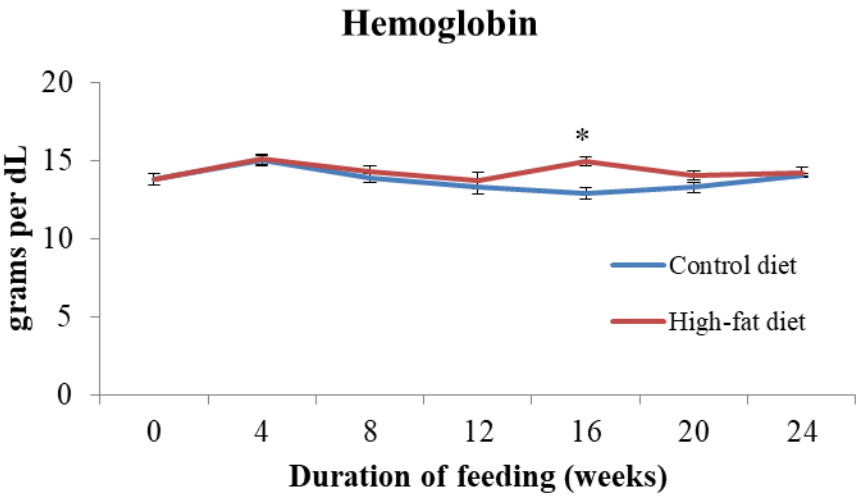

Figure 6.3.13: Effect of HFD-feeding on hemoglobin levels

Hemoglobin levels, measured by Drabkins's method, in mice fed CD or HFD for various durations (as indicated). Data are shown as mean ± SE; n = 3-6 (for both CD- and HFD-fed mice) at each time point. * indicates $p < 0.05$ when compared to the respective control group.

Figure 6.3.14

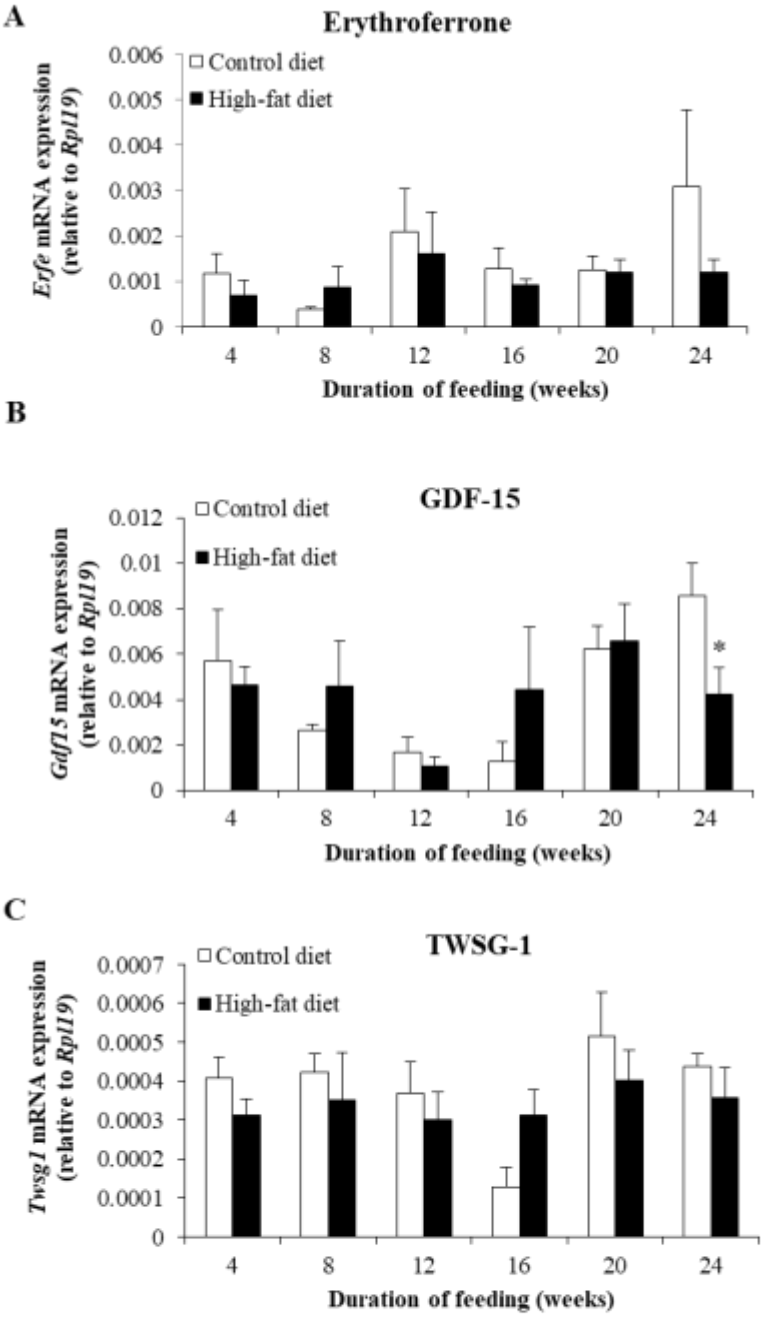

Figure 6.3.14: Effect of HFD-feeding on expression of erythroid regulators of hepcidin

Gene (mRNA) expression of erythroferrone (A), GDF-15 (B) and TWSG-1 (C) in TER119-positive cells isolated from the bone marrow. Data are shown as mean ± SE; n = 6 (for both CD- and HFD-fed mice) at each time point. * indicates $p < 0.05$ when compared to the respective control group.

Figure 6.3.15

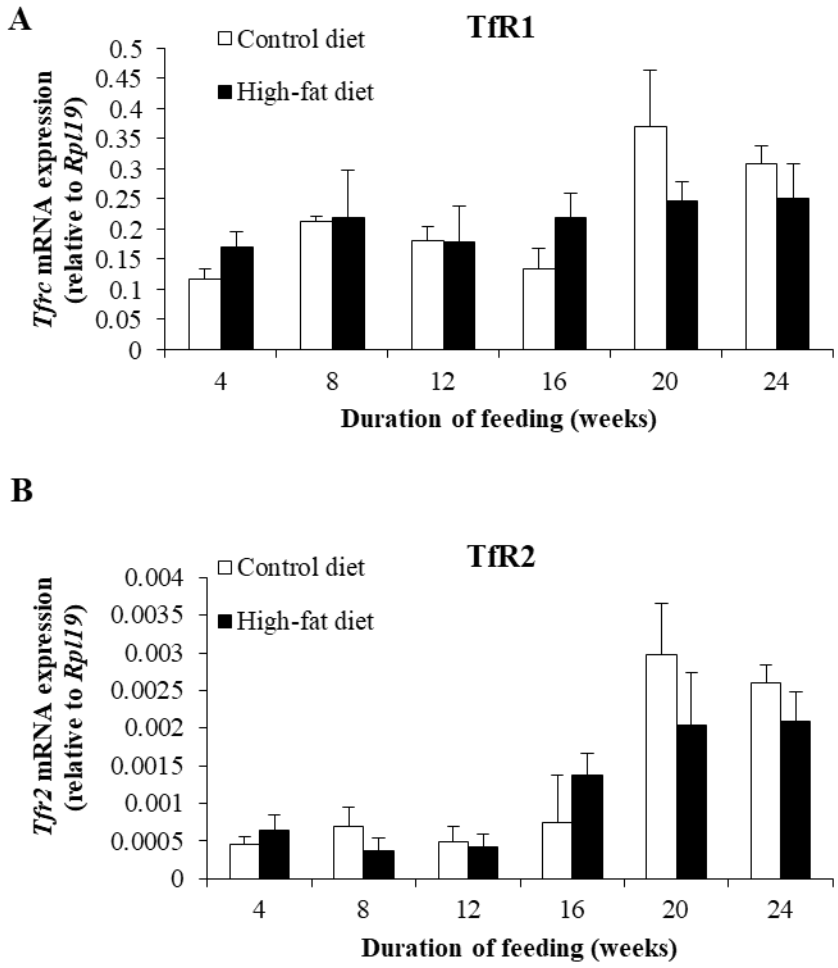

Figure 6.3.15: Effect of HFD-feeding on expression of TfR1 and TfR2 in TER119-positive cells

Gene (mRNA) expression of TfR1 (A) and TfR2 (B) in TER119-positive cells isolated from the bone marrow. Data are shown as mean ± SE; n = 6 (for both CD- and HFD-fed mice) at each time point.

4.8 Effect of HFD-feeding on serum levels of EPO and GDF-15

There were no differences in serum EPO levels between CD and HFD-fed mice at any of the time points studied. Serum GDF-15 levels were significantly elevated after 16, 20 and 24 weeks of HFD-feeding (Fig 6.3.16).

4.9 Effect of HFD-feeding on erythroferrone expression in the skeletal muscle

ERFE is has been reported to be expressed in the skeletal muscle (392). In view of this, the effect of HFD on muscle *Erfe* mRNA expression was also studied. There was a statistically significant increase in mRNA levels of ERFE in the skeletal muscle at 24 weeks of HFD-feeding, but not at the other time points studied (Fig 6.3.17).

4.10 Correlation analyses

Correlation analyses showed that gene expression of erythroid regulators of hepcidin (ERFE, GDF-15 and TWSG-1) in TER119-positive cells correlated among themselves and with those of TfR1 and TfR2 (Table 6.3.3). They did not show any correlation with hepatic hepcidin expression, either in CD-fed mice or in those fed HFD (Table 6.3.4). GDF-15 and TfR2 mRNA correlated positively with hepatic hepcidin in CD-fed mice but not in those fed HFD. In mice fed HFD, hemoglobin correlated negatively with hepcidin expression (Table 6.3.4).

Figure 6.3.16

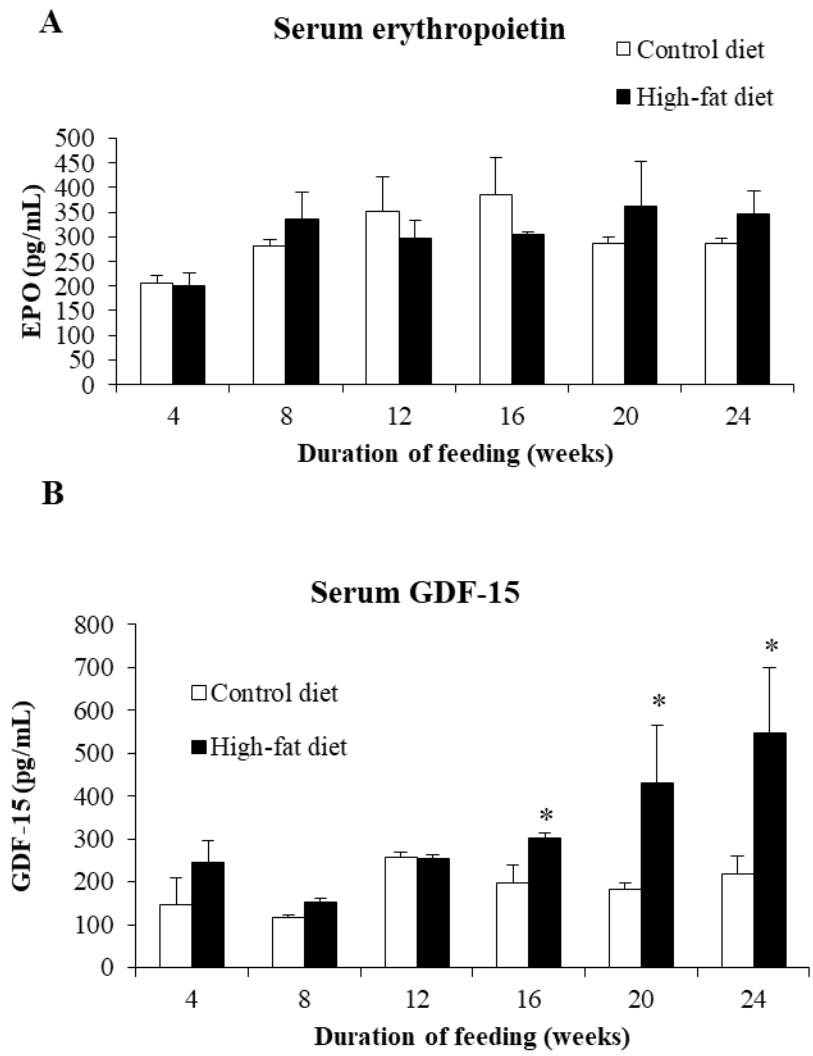

Figure 6.3.16: Effect of HFD-feeding on serum levels of erythropoietin and GDF-15

Serum levels of erythropoietin (A) and GDF-15 (B) in mice fed CD or HFD for various durations (as indicated). Data are shown as mean ± SE; n = 3 (for both CD- and HFD-fed mice) at each time point. * indicates $p < 0.05$ when compared to the respective control group.

Figure 6.3.17

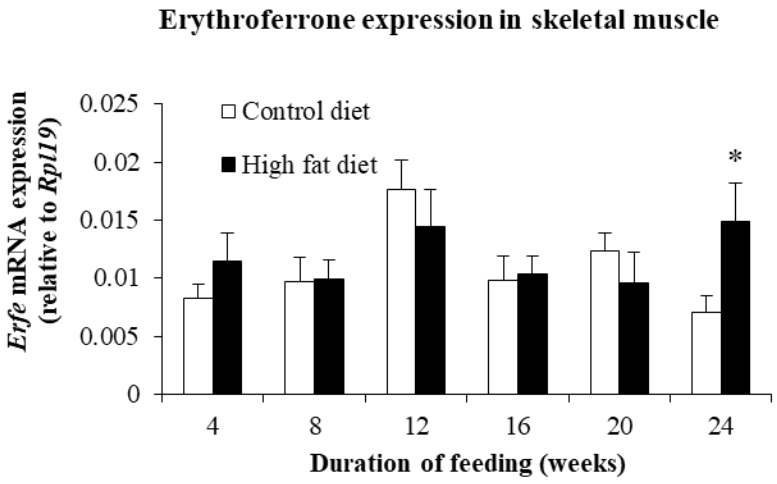

Figure 6.3.17: Effect of HFD-feeding on erythroferrone mRNA expression in skeletal muscle

Gene (mRNA) expression of erythroferrone in the skeletal muscle in mice fed CD or HFD for various durations (as indicated). Data are shown as mean ± SE; n = 6 (for both CD and HFD-fed mice) at each time point. * indicates $p < 0.05$ when compared to the respective control group.

Table 6.3.3: Correlation among the erythroid regulators of hepcidin, TfR1 and TfR2 (gene expression in TER119-positive cells)

Spearman's rho	ERFE	GDF-15	TWSG-1	TfR1	TfR2
ERFE	-	**0.32***	**0.12**	**0.38****	**0.36****
GDF-15		-	**0.47****	**0.51****	**0.55****
TWSG-1			-	**0.54****	**0.41****
TfR1				-	**0.62****
TfR2					-

Spearman's correlational coefficients are shown
* $p < 0.05$, ** $p < 0.01$

Table 6.3.4: Correlational analyses of liver hepcidin (*Hamp1*) expression with other parameters of interest

Variables	**All mice**	**CD-fed mice**	**HFD-fed mice**
ERFE mRNA expression in TER119-positive cells	0.16	0.05	0.30
GDF-15 mRNA expression in TER119-positive cells	**0.34****	**0.36***	0.24
TWSG-1 mRNA expression in TER119-positive cells	0.03	-0.05	-0.01
TfR1 mRNA expression in TER119-positive cells	0.19	0.18	0.23
TfR2 mRNA expression in TER119-positive cells	**0.25***	**0.53****	0.03
Serum erythropoietin	0.02	0.16	0.17
Serum GDF-15	0.16	0.29	0.23
Hemoglobin	-0.19	0.13	**-0.44***

Spearman's correlational coefficients are shown
* $p < 0.05$, ** $p < 0.01$

5. Discussion:

HFD-feeding in mice (a model of IR) was shown to decrease hepatic hepcidin expression (Study 2). Erythroid precursors in the bone marrow are known to secrete factors (erythroid regulators of hepcidin) that can powerfully down-regulate hepcidin expression in the liver (100). However, it was not known whether these factors had a role in mediating hepcidin suppression in the setting of HFD feeding. Since insulin is known to stimulate erythropoiesis *in vitro* (37,368,369), it was hypothesized that HFD-induced hyperinsulinemia may stimulate erythropoiesis *in vivo* as well, which may, in turn, increase the expression of the erythroid regulators of hepcidin, resulting in hepcidin suppression. In order to test this hypothesis, maturation of erythroid precursors in the bone marrow was studied in HFD-fed mice. The expression of the erythroid regulators of hepcidin in bone marrow erythroid precursors (TER119-positive cells) was also determined, to attempt to elucidate their role in HFD-induced suppression of hepcidin.

Two strategies were used to study terminal erythroid differentiation (TED) by flow cytometry. The first was based on CD71 expression (381), while the second was based on CD44 expression (356). The latter has the advantage of resolving each stage in TED with greater precision than that which could be achieved by the first strategy based on CD71 expression (355).

The results obtained showed that the proportion of TER119-positive cells in the bone marrow was similar in CD and HFD-fed mice. The ratio of pro-, basophilic, polychromatic and orthochromatic erythroblasts was similar (in keeping with normal ratios of ~1:2:4:8) in both groups of mice, and was not affected by their diet (CD or HFD). The number of early erythroblasts (pro-, basophilic and polychromatic erythroblasts) tended to be lower in HFD-fed

mice at 4 and 8 weeks and higher at 16 weeks, compared to CD-fed mice. These changes, however, were not statistically significant. Overall, the results suggested that the process of TED, *per se*, was not significantly affected by HFD feeding.

The last stage in TED is the formation of orthochromatic erythroblasts, which then enucleate to form immature reticulocytes. The reticulocyte population in the bone marrow (EryB [identified based on CD71 expression] and population V [identified based on CD44]) was consistently higher in HFD-fed mice than in CD-fed mice (Fig 6.3.7 and 6.3.9). It does not seem likely that increased erythropoiesis contributed to this increase, as the proportion of TER119-positive cells and early erythroblasts in the bone marrow was not significantly increased by HFD-feeding. It is possible that this may be due to delayed release of reticulocytes from the marrow.

Newly formed (nascent) reticulocytes undergo a complex process of maturation during which they transform morphologically into discoid erythrocytes. This process occurs in two stages (over approximately 48 hours) and is not well-understood. The first stage (initial 24 hours) occurs in the bone marrow. During this time, nascent reticulocytes get rid of their intracellular membrane-bound organelles by a process that involves autophagy and exocytosis. They are then released into the circulation, where they undergo a further 24 hours of maturation, before they become erythrocytes (357,393). For release of reticulocytes from the marrow into the circulation, it is essential for them to pass through an endothelial barrier, which separates the marrow hematopoietic cords from the blood vessels (sinuses). This process requires a high degree of reticulocyte membrane deformability (394–396). The process of reticulocyte maturation, which occurs in the marrow, involves distinct changes in membrane fluidity as well as protein

composition, which are essential to increase their deformability (395). Impairment in this maturation process can hinder their release into circulation.

It has been shown that diabetes mellitus is associated with decreased erythrocyte deformability (397–399). This has also been shown in mice fed HFD (400). Although the reasons for this are not well-understood, hyperglycemia-induced glycation of cytoskeletal components and changes in membrane composition may play important roles (401,402). It is possible that decreased reticulocyte deformability in mice fed HFD may impair the release of reticulocytes from the marrow into the circulation; this may account for the increase in reticulocytes in the bone marrow seen in the present study. Additional studies would be required to test this hypothesis.

Insulin has been shown to have a stimulatory effect on erythropoiesis *in vitro* (as has been described earlier (37,368,369)). The stimulatory effects of insulin on proliferation of CFU-E in these studies were seen at concentrations in the range of 50 to 500 µg/L (37,368). In addition, these effects were seen in the presence of high concentrations of EPO (>33 ng/mL or 5 U/mL) (368). The results of the present study show that HFD-fed mice had insulin levels in the range of 4-8 µg/L (Fig 6.2.5-A) and EPO in the range of 200-400 pg/mL (Fig 6.3.16-A). These concentrations are much lower than those used in the *in vitro* studies discussed above. It is therefore possible that, at the concentrations of insulin and EPO seen *in vivo*, the stimulatory effects of insulin on erythropoiesis may not be substantial.

Interestingly, hemoglobin levels (Fig 6.3.13), as well as the proportion of early erythroblasts in the bone marrow (Fig 6.3.9), increased in HFD-fed mice, at 16 weeks. This corresponded with the onset of hyperinsulinemia in this model (described in Study 2 [Fig 6.2.5] and also reported by

other investigators (164,344)). However, this effect did not persist with HFD feeding continuing for 20 and 24 weeks, although hyperinsulinemia peaked at these time points (Fig 6.2.4). The reasons for this are not clear.

In mice, the spleen is an important accessory organ for erythropoiesis. It contributes significantly to 'stress erythropoiesis', which occurs in conditions where erythropoiesis is stimulated, such as in response to acute blood loss, hemolysis and iron deficiency (353). In the present study, no significant change was found in the proportion of TER119-positive cells and early erythroblasts (EryA) in the spleen in response to HFD-feeding (Fig 6.3.11). This showed that erythropoiesis in the spleen was not stimulated in this setting.

In the present study, gene expression of ERFE, GDF-15 and TWSG-1 in TER119-positive cells was not significantly affected by HFD-feeding (except for a significant decrease in GDF-15 expression in mice fed HFD for 24 weeks). The expression of ERFE and TWSG-1 also did not correlate with that of hepatic *Hamp1* expression or serum hepcidin levels. On the other hand, GDF-15 expression had a significant positive correlation with hepatic hepcidin expression (instead of the expected negative correlation). The explanation for this observation is not clear. Overall, these results indicate that ERFE, GDF-15 and TWSG-1 do not appear to contribute significantly to hepcidin suppression in this setting. However, it is possible that other hitherto unidentified erythroid regulators of hepcidin may be operational, as has been suggested by Pasricha et al (100).

Among the 3 putative candidates that have been identified as erythroid regulators of hepcidin, ERFE is considered to be the most relevant, physiologically (100,101). The expression of ERFE,

but not that of GDF-15 and TWSG-1, was positively correlated with serum EPO levels and negatively correlated with hemoglobin. These findings support the view that ERFE expression in the bone marrow is regulated by physiological stimuli that affect erythropoiesis.

ERFE is also highly expressed in skeletal muscles. It was initially discovered and identified as a myokine ('myonectin') that regulates systemic lipid homeostasis by increasing fatty acid uptake in the liver and adipose tissue (392). However, the role of skeletal muscle-derived ERFE in the regulation of hepatic hepcidin expression has not been studied. In the present study, HFD was found to increase ERFE mRNA in the skeletal muscle at 24 weeks (Fig 6.3.17). Although this corresponded with a significant decrease in hepatic hepcidin expression at the same time point, there was no correlation found between skeletal muscle ERFE expression and liver hepcidin expression. Additional work would be required to determine whether ERFE in the skeletal muscle has any role in regulation of hepcidin.

Serum levels of GDF-15 were elevated in mice fed HFD for 16, 20 or 24 weeks (Fig 6.3.16). Recently, it has been shown that GDF-15 is an important myomitokine (a humoral factor released by skeletal muscles in response to mitochondrial dysfunction) that increases insulin sensitivity and plays a key role in systemic energy homeostasis (403). It is possible that the source for the elevated serum levels of GDF-15 (seen in this study in response to HFD-feeding) is the skeletal muscle. However, expression of GDF-15 in skeletal muscle was not determined in the present study. Hence, it is not possible to definitively localize the source(s) of the increased blood levels of GDF-15. In addition, it is also not clear whether elevated serum GDF-15 plays a role in mediating hepcidin suppression in this setting; this aspect requires further investigation.

Gene expression of ERFE, GDF-15 and TWSG-1 in TER119-positive cells showed strong positive correlations among themselves, suggesting that these factors were coordinately regulated (Table 6.3.3). It has been reported that TfR1 expression in erythroid cells is associated with decreased hepatic hepcidin expression (390). In the present study, expression of TfR1 was highly correlated with that of the ERFE, GDF-15 and TWSG-1, but not with that of hepatic hepcidin expression (Table 6.3.4). This suggests that TfR1 may be involved in the regulation of the erythroid regulators of hepcidin; however, in the current setting, these factors did not affect hepatic hepcidin expression. On the other hand, TfR2 expression in TER119-positive cells was positively correlated with the erythroid regulators of hepcidin and with hepatic *TfR2* and *Hamp1* expression levels. TfR2 in the liver regulates hepcidin expression (404); in erythroid cells, it acts as a modulator of EPO signaling (405). It is therefore possible that TfR2 may play a role in hepcidin regulation in the liver and EPO-induced expression of erythroid regulators of hepcidin in the bone marrow.

6. Summary and conclusions:

In summary, the results presented in this study show that high-fat feeding in mice, with associated hyperinsulinemia, did not stimulate erythropoiesis in the bone marrow or spleen. Terminal erythroid differentiation in the bone marrow was similar in both groups of mice, irrespective of the diet they were fed. On the other hand, HFD-fed mice showed increased numbers of reticulocytes in the marrow, which possibly suggests impairments in maturation of reticulocytes and their release into the circulation.

HFD did not affect the expression of the putative erythroid regulators of hepcidin, viz., ERFE, GDF-15 and TWSG-1, in erythroid cells isolated from the marrow. Hence, it appears unlikely that these factors play an important role in the down-regulation of hepatic hepcidin expression seen in response to high-fat feeding.

STUDY 4

Dysregulated iron homeostasis in patients newly diagnosed with diabetes mellitus or pre-diabetes

1. Abstract

Type 2 diabetes mellitus (T2DM) has been reported to be associated with increased body iron stores. However, studies that have estimated serum levels of hepcidin, the chief hormone involved in regulation of iron homeostasis, in patients with T2DM have shown variable results. Possible reasons for this may include differences in many patient-related factors in these studies, such as duration since diagnosis of diabetes, extent of glycemic control, therapeutic interventions and presence of chronic complications of diabetes. In an attempt to minimize the effects of such confounding factors, the present investigation aimed to study hepcidin and other iron-related parameters in patients newly diagnosed with diabetes mellitus or pre-diabetes.

Adult males who were newly diagnosed to have diabetes mellitus (n=40) or pre-diabetes (n=40), based on fasting plasma glucose (FPG) levels (as per the criteria of the American Diabetic Association [ADA]) were the subjects of the study. Men, who were found to be normoglycemic, using the criteria of the ADA, were recruited as control subjects. Anthropometric measurements were made on all subjects. Blood samples were obtained for measurement of hematological parameters, markers of iron status (ferritin, hepcidin, iron, total iron-binding capacity and transferrin saturation), C-reactive protein (CRP) (marker of inflammation) and insulin. Homeostatic model assessment–insulin resistance (HOMA-IR) and HOMA-β (indices of insulin resistance and pancreatic insulin secretory capacity respectively), were calculated. In addition, reticulocytes were isolated from peripheral venous blood obtained from a sub-set of control and

diabetic patients to determine gene expression of erythroferrone, a factor known to regulate hepcidin levels.

The results of this study showed that diabetics (but not pre-diabetics) had significantly elevated HOMA-IR values, while both pre-diabetics and diabetics showed significantly lower HOMA-β values. Serum levels of ferritin and hepcidin were higher in patients with diabetes mellitus than in control subjects. In the pre-diabetics, levels of these parameters were similar to levels in control subjects. CRP levels also tended to be higher in the diabetic group compared to controls; levels in the pre-diabetic group and controls were similar. Classification of patients into sub-groups, based on CRP levels (using a cut-off of 3.0 mg/L), did not reveal an association of ferritin or hepcidin with this marker in either the pre-diabetic or diabetic groups. Serum markers of iron status (such as serum iron, TIBC and transferrin saturation), were not significantly different in the three groups. Expression of erythroferrone in reticulocytes isolated from peripheral blood was similar in the controls and diabetics.

In conclusion, the results of this study show that, patients, who were newly diagnosed with either diabetes mellitus or pre-diabetes, showed evidence of early-onset beta cell failure. Serum levels of ferritin and hepcidin were higher in the diabetic group. Additional studies are required to elucidate the etiopathological factors that underlie these findings.

2. Introduction

A number of epidemiological studies have shown that increased ferritin levels are strongly associated with risk of developing type 2 diabetes mellitus (T2DM) (4,6,192,406). Ferritin levels in the blood are indicative of body iron stores, thereby linking iron homeostasis with diabetes mellitus. However, as described in the review of literature, the mechanisms that underlie the association between the two are not clear.

Hepcidin is the chief regulator of iron homeostasis in the body. There are very few human studies on hepcidin levels in patients with diabetes mellitus. Available literature shows that the results of these studies are inconsistent, with some showing increased hepcidin levels in diabetics (25,26), while others have shown either decreased levels (27–29,407) or levels similar to those in control subjects (30). There is no Indian data in this area, as far as is ascertainable.

Several factors may contribute to the variable reports on hepcidin and iron-related parameters in patients with diabetes mellitus. The duration from the time of diagnosis of diabetes mellitus, extent of glycemic control, various therapeutic interventions used (such as use of anti-diabetic drugs / insulin), presence of chronic complications of diabetes and inflammation are some factors that need to be considered in this context (187). In addition, among women, parity, phase of the menstrual cycle (in pre-menopausal women) and menopausal changes can also significantly affect iron homeostasis (408,409). In order to avoid these confounding factors, this study aimed to look at hepcidin and other iron-related parameters in males who were newly diagnosed to have either pre-diabetes or diabetes mellitus. The data obtained was compared with age-matched control men, who had normal glycemic status.

Among the factors that regulate hepatic hepcidin expression, the most potent regulators are those that are known to be secreted by erythroid precursors in the bone marrow (called the erythroid regulators of hepcidin). As described in detail in Study 3, putative erythroid regulators of hepcidin that have been identified include erythroferrone [ERFE/Fam132b] (35), growth differentiation factor-15 [GDF-15] (33) and twisted gastrulation factor-1 [TWSG-1] (34). Recent studies done in various mouse models have shown that, among these, ERFE appears to be the most promising candidate (100). Whether these factors (ERFE, GDF-15 and/or TWSG-1) play a role in regulation of hepcidin in patients with pre-diabetes/diabetes has not been studied.

Reticulocytes found in the peripheral circulation represent the final stage of erythroid development before mature RBCs are formed. It has been shown that RNA in reticulocytes represents gene expression during the final stages of erythropoiesis (410). Hence, it is plausible that mRNA expression of erythroid regulators of hepcidin in reticulocytes in peripheral blood may provide useful information on events in the bone marrow.

3. Methods

3.1 Setting

The subjects of this cross-sectional observational study were recruited from the out-patient clinic of the Community Health and Development Hospital, at Christian Medical College, Vellore, Tamil Nadu, India.

3.2 Subjects

Male patients, who were referred for medically-indicated estimations of fasting plasma glucose, were recruited into the study, using the inclusion and exclusion criteria detailed below.

3.2.1 Inclusion criteria:

- Male patients
- Between the ages of 30 to 70 years
- Not been diagnosed to have diabetes or pre-diabetes anytime in the past

3.2.2 Exclusion criteria

- BMI more than 35 kg/m^2
- Hemoglobin less than 13 g/dL
- Serum CRP levels more than 12 mg/L
- Appeared to have complications of diabetes, as assessed by history, clinical findings or results of laboratory tests

Informed consent was obtained from all patients who were recruited. An information sheet for patients was provided in English or Tamil, depending on each patient's preference. Consent

forms were also made available in the 2 languages. The information sheet and consent form (in both languages) are included in Appendix V to VIII.

Basic demographic details were collected, using the proforma in Appendix IX. Anthropometric measurements (height, weight, waist circumference and hip circumference) were made on each subject.

Patients who were found to be eligible for the study were classified as controls, pre-diabetics or diabetics, based on fasting plasma glucose levels, as per the criteria of the American Diabetes Association (ADA) (2015) (411).

Table 6.4.1: Classification of subjects recruited into the study based on fasting plasma glucose levels as per ADA criteria (2015)

Classification	**Fasting plasma glucose level (mg/dL)**
Control (n = 40)	≤ 99
Pre-diabetes (n = 40)	100 - 125
Diabetes mellitus (n = 40)	≥ 126

The sample size for the study was calculated based on data from the study by Jiang et al (26), who estimated serum hepcidin levels in patients with diabetes mellitus and age-matched controls. Based on this study, in order to achieve an effect size of 0.65, power of 80% and 5% level of significance (2-tailed), the number of subjects to be studied was calculated to be 38. Hence, 40 subjects were recruited in each group (control, diabetic and pre-diabetic).

3.3 Collection of blood

Blood samples were obtained after an overnight fast (defined as no calorie intake for at least 8 hours prior to collection). A total of 15 mL of blood was collected; 2 mL for glucose estimation (in BD Vacutainer Fluoride tubes), 5 mL for serum separation (in BD Vacutainer Serum tubes) and 8 mL for hematological parameters and reticulocyte isolation (in BD Vacutainer Heparin tubes). Blood collected in serum tubes was allowed to clot; it was then centrifuged at 2000*g* for 10 min at room temperature. Serum obtained was aliquoted into 4-5 micro-centrifuge tubes and stored at – 70°C until further use.

3.4. *Estimation of hematological parameters*

Hemoglobin, total RBC count, mean corpuscular volume (MCV), mean corpuscular hemoglobin (MCH), mean corpuscular hemoglobin concentration (MCHC), reticulocyte hemoglobin content (CHr) and absolute reticulocyte count were estimated using the Sysmex XN 9000 automated hematology analyzer (Department of Transfusion Medicine and Immunohematology, CMC, Vellore).

3.4 Estimation of parameters in serum

3.4.1. Hepcidin

Hepcidin was measured using a commercially available kit (cat. no. S-1337, Hepcidin–25 [human] EIA kit, Peninsula Laboratories, USA). This is a competitive immunoassay where hepcidin in the sample competes with a biotinylated tracer to bind to anti-hepcidin antibodies. The amount of biotinylated tracer that is bound is inversely proportional to hepcidin levels in the sample.

The assay was carried out according to manufacturer's instructions. Briefly, anti-hepcidin antibodies were added to wells in a micro-plate to coat its walls. Standards or serum samples (diluted 1:10 using the diluent provided) were then added, along with the biotinylated tracer, and the plate was incubated at 4°C overnight. Following this, the plate was washed and incubated with streptavidin-HRP conjugate for 1 hour. For color development, TMB (tetramethylbenzidine) substrate was added. The reaction was stopped by addition of 2N HCl 1 h later. OD readings were taken at 450 nm using an iMark plate reader (BioRad, USA). All standards and samples were analyzed in duplicates; the average of the OD readings was used for calculations. OD values obtained for the standards were used to plot a standard curve by 4-parameter logistic regression. Serum hepcidin levels were calculated using equation of the standard curve, after adjusting for sample dilution (dilution factor of 10).

3.4.2. C-reactive protein (CRP)

CRP was estimated using a high sensitivity assay (hsCRP). This was a two-site chemiluminescent enzyme immunometric assay done using IMMULITE 2000 XPi system (Siemens GmBH, Germany), in the Department of Clinical Biochemistry, CMC, Vellore.

3.4.3. Ferritin

Ferritin was estimated by a sandwich immunoassay with chemiluminescence detection, using the ADVIA Centaur XP immunoassay system (Siemens GmBH, Germany) in the Department of Clinical Biochemistry, CMC, Vellore.

3.4.4. Iron

Iron was estimated by a colorimetric method based on ferrozine dye-binding, using the Roche Cobas c702 auto-analyzer (Roche Diagnostics, Switzerland) in the Department of Clinical Biochemistry, CMC, Vellore.

3.4.5. Total iron-binding capacity (TIBC) and transferrin saturation

Serum samples were incubated with a known concentration of iron. The iron that remained unbound after incubation was estimated using a ferrozine-based assay, as described above. Based on this, the amount of added iron that was bound (mainly by transferrin in serum) was calculated as the unbound iron-binding capacity (UIBC). TIBC was the calculated as the sum of serum iron and UIBC.

Transferrin saturation was calculated using the formula:

Transferrin saturation (%) = (Serum iron x 100) / TIBC

3.4.6. Insulin

Insulin was estimated by a solid-phase enzyme-labeled chemiluminescent immunoassay, using the IMMULITE 2000 XPi system (Siemens GmBH, Germany), in the Department of Clinical Biochemistry, CMC, Vellore.

3.5 Calculation of HOMA-IR and HOMA-β indices

Homeostatic model assessment (insulin resistance) or HOMA-IR is an index of insulin resistance (412). It is calculated using the formula given below:

HOMA-IR = (Fasting plasma glucose [mg/dL] x Fasting insulin [μIU/mL]) / 405

HOMA – β is an index of insulin secretion by the pancreas (412). It is calculated using the formula given below:

HOMA – β (%) = (360 x fasting insulin [μIU/mL]) / (fasting plasma glucose [mg/dL] – 63)

3.6 Isolation of reticulocytes from blood

Reticulocytes were isolated from 8 mL of heparinized blood, following a procedure based on leukodepletion (described by Bresnick) (413). Leukocytes were concentrated by centrifugation of heparinized blood at 2000*g* for 30 min at 4 °C. This resulted in the formation of a white disc (buffy coat) at the plasma-red cell interface. Plasma was collected and stored for future use; the buffy coat was discarded. The red cells were washed three times with 5 mL of ice-cold PBS. After the third wash, reticulocytes, which have a lower density compared to mature erythrocytes, were concentrated by centrifugation at 2000*g* for 30 min at 4°C. The supernatant was removed; 400 μL of packed cells (reticulocyte-rich fraction) at the top of the tube was removed and added to 5 ml of ice-cold PBS. This red cell suspension was then layered on top of a column (prepared in a 10 mL syringe) consisting of 5 mL of a mixture containing 2 parts cellulose (C-8002; Sigma, India) and 1 part Sigmacell cellulose type 50 (50 μm) (S-5504; Sigma, India). The red cells were eluted by gentle centrifugation of the column at 150*g* at 4 °C for 1 min. The leukodepleted elute was washed three times using 5 mL of ice-cold PBS. After the third wash, the reticulocyte-enriched, leukocyte-depleted pellet was vigorously mixed in 1 mL TRIzol LS (cat. no. 10296028, Thermo Fisher Scientific, USA), using a vortex mixer. Samples were stored at -70°C till used further for RNA extraction.

3.7 Quantitative real-time PCR

Reticulocyte-enriched samples homogenized in TRIzol LS were used for isolation of RNA. This was done according to the manufacturer's instructions (as described in Study 1). One microgram of isolated RNA was used to synthesize cDNA, using the Reverse Transcriptase Core Kit (Eurogentec, Belgium) (as described in Study 1). Quantitative PCR reactions were carried out in duplicate, using the Takyon qPCR SYBR master mix (Eurogentec, Belgium) on a BioRad Chromo4 real-time PCR machine. The genes studied and the sequences of the primers used are listed in Table 6.4.2. The reaction conditions were identical to those described in study 1. The expression levels of these genes of interest were normalized to *GAPDH,* which was used as the reference gene (414). The MIQE check-list and qPCR validation data are provided in Appendix I and II (page 323 and 327).

3.8 Statistical analysis

Statistical analyses was done using SPSS version 16.0. The Shapiro-Wilk test was used to test for normality of distribution of data. For normally distributed data, one-way ANOVA followed by pair-wise comparisons using Bonferroni test was done. For skewed data, the Krushkal – Wallis test followed by pair-wise comparisons using Mann Whitney test was done. For correlational analysis, Pearson's correlation was used for normally distributed data and Spearman's correlation for skewed data. Multivariate analysis was done using linear regression. A p-value less than 0.05 was taken to indicate statistical significance in all cases.

Table 6.4.2: Primers used for qPCR

Sl. No.	Gene	Accession number	Primer sequence	Amplicon size (bp)
1	ERFE	NM_001291832.1	CAGCAGTGAGCTCTTCACCA CAAGAACACGGAGGTCCACT	76
2	GDF-15	NM_004864.2	CTGCAGTCCGGATACTCACG GAACAGAGCCCGGTGAAGG	125
3	TWSG-1	NM_020648.5	GAATGTGTCTGTCCCCAGCA GGATGCTCCCATGGACTCAC	136
4	TFR1	NM_003234.2	AGCAGGGAAAATCACCTTTGC GTCCCCAGATGAGCATGTCC	141
5	TFR2	NM_003227.3	GTGGACCGACACGCACTAC TGTAGGGGCAGTAGACGTCAG	134
6	GAPDH	NM_002046.5	GAAGGTGAAGGTCGGAGTC GAAGATGGTGATGGGATTTC	226

4. Results:

4.1 Characteristics of participants in the study:

One hundred and twenty subjects were recruited, based on the inclusion and exclusion criteria listed in section 3.2. They were classified as control subjects, pre-diabetics or diabetics, based on fasting plasma glucose levels (as per criteria of the American Diabetic Association) (ADA) (2015) (411), given in Table 6.4.1. There were 40 subjects in each group. Subjects in all three groups were similar in age and had similar anthropometric measurements (BMI, waist and hip circumferences and the waist-hip ratio) (Table 6.4.3).

4.2 Metabolic parameters

As expected, fasting plasma glucose (FPG) showed significant differences among the groups. Pre-diabetics had significantly higher plasma glucose levels than control subjects. The diabetics had significantly higher levels of plasma glucose than the control subjects and pre-diabetics (Fig 6.4.1-A). Surprisingly, fasting insulin levels were similar in all three groups (Fig 6.4.1-B). HOMA-IR, an index of insulin resistance, was significantly higher among the diabetics than in control subjects and pre-diabetics; there was no significant difference between values in the control and pre-diabetic groups (Fig 6.4.2-A). HOMA-β, an index of pancreatic insulin secretory function, was significantly lower in the diabetic and pre-diabetic groups compared to the control group. Diabetics had significantly lower values compared to pre-diabetics (Fig 6.4.2-B).

Table 6.4.3: Age and anthropometric measurements of the study subjects

Parameter	**Control subjects (mean ± SD)**	**Pre-diabetics (mean ± SD)**	**Diabetics (mean ± SD)**	**p value***
Age (years)	45.8 ± 9	48.7 ± 9.8	45.9 ± 7.1	0.26
Height (m)	1.7 ± 0.1	1.6 ± 0.1	1.6 ± 0.1	0.004
Weight (kg)	72.7 ± 11.2	68.6 ± 9.8	70.6 ± 10.8	0.25
BMI (kg/m^2)	25.7 ± 3.7	25.8 ± 3.2	26 ± 3.6	0.9
Waist circumference (cm)	92.4 ± 9.3	91.2 ± 9.3	91.8 ± 9.7	0.84
Hip circumference (cm)	95 ± 7.5	92.1 ± 8.6	92.5 ± 9.6	0.27
Waist-to-hip ratio	1 ± 0.05	1 ± 0.1	1 ± 0.04	0.11

* Statistical analyses were done using ANOVA.

Figure 6.4.1

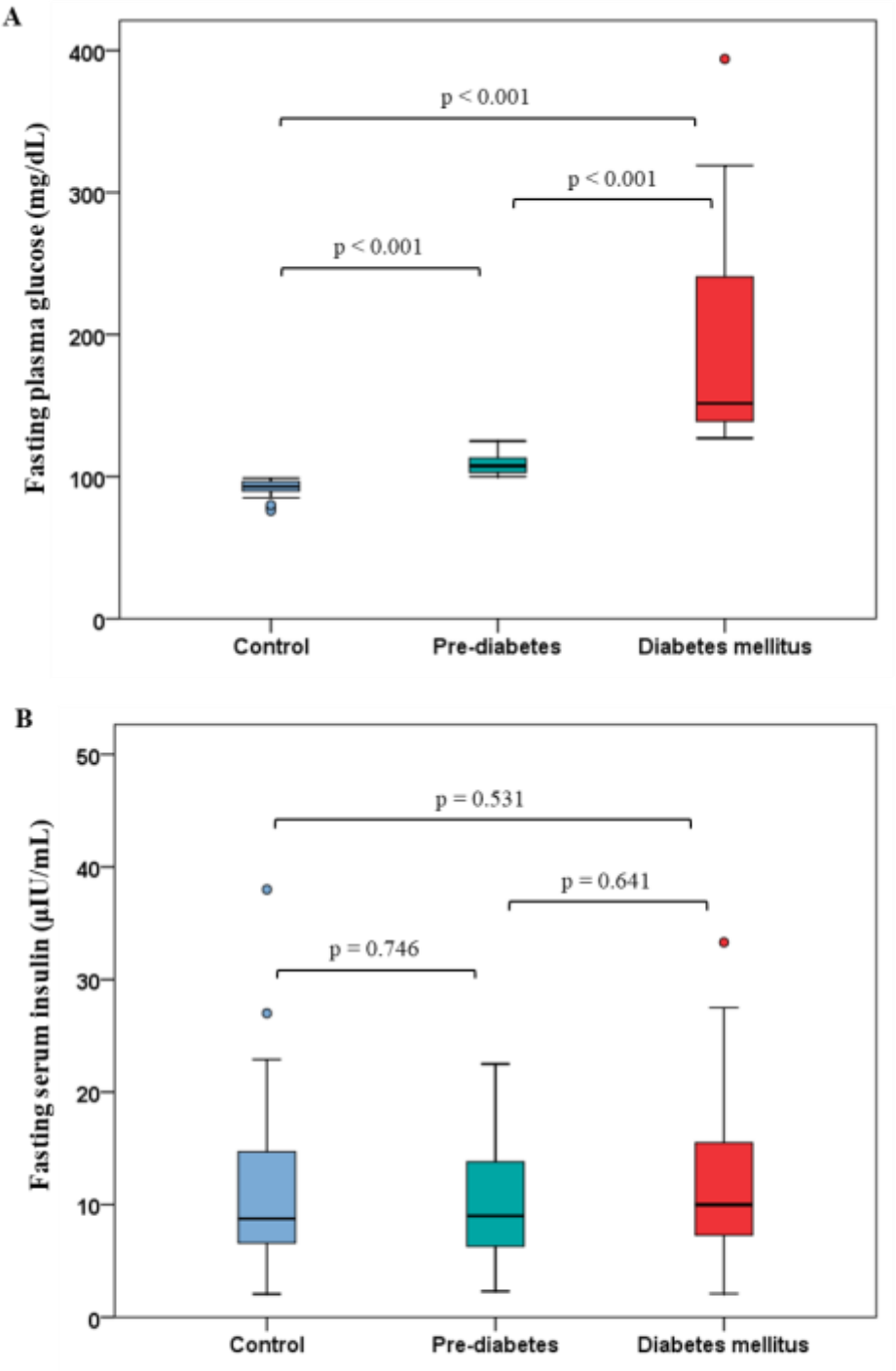

Figure 6.4.1: Fasting plasma glucose and insulin

Fasting plasma glucose (A) and insulin (B) levels in control, pre-diabetic and diabetic subjects. Box plots indicate median and interquartile range. ° indicate distribution outliers.

Figure 6.4.2

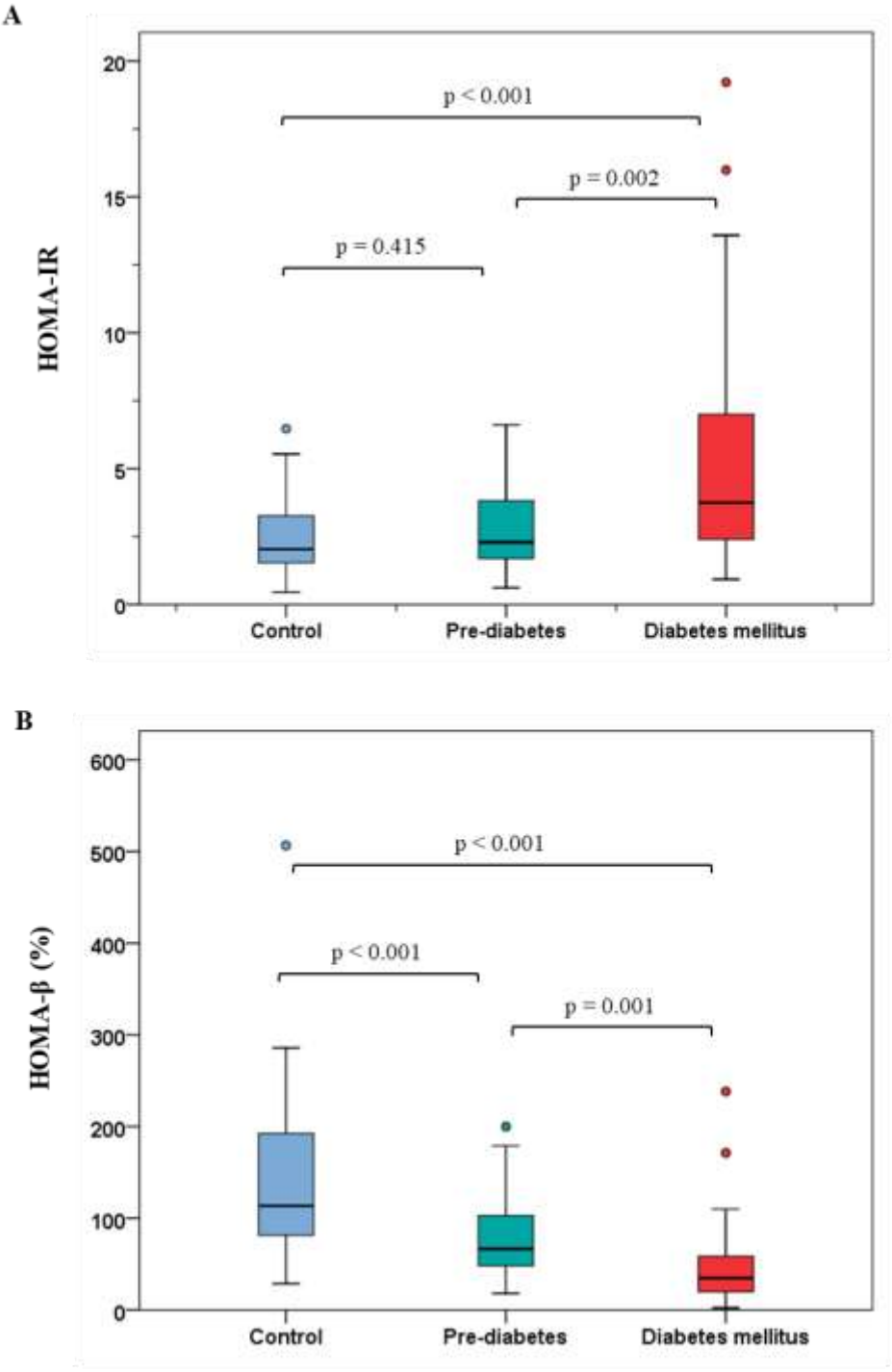

Figure 6.4.2: HOMA-IR and HOMA-β

HOMA-IR (A) and HOMA-β (B) values in control, pre-diabetic and diabetic subjects. Box plots indicate median and interquartile range. ° indicate distribution outliers.

4.3 Hematological parameters

Among the hematological parameters, values for mean corpuscular hemoglobin (MCH) and reticulocyte hemoglobin (CHr) were significantly lower in the pre-diabetic group than in control subjects. All the other hematological parameters (hemoglobin, RBC count, mean corpuscular volume [MCV] and reticulocyte count) were similar in the 3 groups (Table 6.4.4)

4.4 Iron-related parameters

Serum iron, TIBC and transferrin saturation were similar in the 3 groups (Table 6.4.5). Serum ferritin levels were significantly higher in the diabetic group than in the control and pre-diabetic groups; levels in the control and pre-diabetic groups were similar (Fig 6.4.3–A). Serum hepcidin levels were also higher in the diabetic group than in the control group. Levels in the diabetic group also tended to be higher than that in the pre-diabetic group (p=0.063). Hepcidin levels were similar in the control and pre-diabetic groups (Fig 6.4.3–B).

4.5 Serum levels of CRP

Serum levels of CRP, a marker of inflammation, tended to be higher in the diabetic group compared to the control subjects (p = 0.065); levels in the pre-diabetic group were higher than in control subjects, but not significantly so. Levels in the diabetic group were higher than in the pre-diabetics, but once again, not significantly so (Fig 6.4.4).

In order to ascertain whether the higher levels of serum ferritin and hepcidin seen in the diabetics were associated with inflammation, patients were categorized into sub-groups with low and high CRP levels. A cut-off value of 3.0 mg/L of CRP was used for this purpose (415). The results showed that, in the control group, both ferritin (p = 0.063) and hepcidin (p = 0.049) tended to be

higher in the high-CRP sub-group compared to the low-CRP sub-group. Among the diabetics, ferritin and hepcidin levels were slightly higher in the high-CRP sub-group, compared to the low-CRP sub-group (Fig 6.4.5), but not significantly so. Levels in the pre-diabetics were similar in the 2 sub-groups.

Sub-categorization was also done using a cut-off value for CRP of 6 mg/L, which is the upper limit of the reference range for CRP (416). Both ferritin ($p = 0.073$) and hepcidin ($p = 0.068$) tended to be higher in the high-CRP sub-group compared to the low-CRP sub-group among the controls. No significant difference was seen between high and low CRP sub-groups in the pre-diabetic and diabetic groups (Fig. 6.4.6).

4.5 Expression of erythroid regulators of hepcidin in reticulocytes isolated from peripheral blood

Reticulocytes were isolated from peripheral blood in a sub-set of control (n=20) and diabetic (n = 21) subjects, and used to determine gene expression of erythroid regulators of hepcidin, viz., ERFE, GDF-15 and TWSG-1. ERFE mRNA was found to be expressed at low-to-moderate levels in reticulocytes and could be reliably quantitated by qPCR. However, there was no significant difference in its expression levels in control and diabetic patients (Fig 6.4.7-A). Expression levels of GDF-15 and TWSG1, the other putative erythroid regulators, were found to be extremely low in all the samples; hence, these could not be reliably quantitated. On the other hand, TfR1 and TfR2 were found to be highly expressed in reticulocytes; there were, however, no significant differences in their gene expression in control and diabetic patients (Fig 6.4.7–B, C)

Table 6.4.4: Hematological parameters

	Control subjects	**Pre-diabetics**	**Diabetics**	**P value (Kruskal Wallis test)**
Hb (g/dL)	15.5 [14.6 - 16.4]	15.2 [14.5 -16.1]	15.9 [15.3 - 16.3]	0.113
RBC count ($x10^6$ cells/µL)	5.21 [4.9 - 5.5]	5.41 [5.1 - 5.8]	5.48 [5.1 - 5.8]	0.074
MCV (fL)	85.9 [82.9 - 89.7]	83.3 [81.2 - 87]	83 [80.6 - 88.8]	0.105
MCH (pg)	29.9 [28.2 - 30.9]	28.8 [27.6 - 29.6]*	28.6 [28 - 30.7]	**0.015**
Reticulocyte hemoglobin (pg)	33.1 [31.5 - 34.3]	32.2 [30.5 - 33.1]*	32.3 [31.3 - 33.5]	**0.022**
Reticulocyte count (x 10^4 cells/µL)	6.37 [5.24 - 7.09]	6.1 [5.16 - 7.02]	6.91 [5.43 - 8.46]	0.145

Data are expressed as median [interquartile range]. Statistically significant values are shown in bold. * indicates $p < 0.05$ when compared to control group.

Table 6.4.5: Iron-related parameters

	Control subjects	Pre-diabetics	Diabetics	P value (Kruskal Wallis test)
Serum iron (µg/dL)	98 [79 - 129.3]	95 [71.8 - 114.5]	97 [80.3 - 116.3]	0.628
UIBC (µg/dL)	239.5 [200.3 - 278.5]	256.5 [232.3 -308]	242.5 [213 - 278.8]	0.105
TIBC (µg/dL)	352 [307.3 - 372.5]	365.5 [318 - 402]	350 [324 - 366.8]	0.225
Transferrin saturation (%)	30.2 [22.8 - 38.4]	27.1 [19.3 -33.3]	29.8 [23 - 33.9]	0.242
Hepcidin-ferritin ratio	0.33 [0.22 - 0.52]	0.47 [0.21 - 0.78]	0.31 [0.17 -0.51]	0.437

Data are expressed as median [interquartile range].

UIBC, unbound iron binding capacity; TIBC, total iron binding capacity

Figure 6.4.3

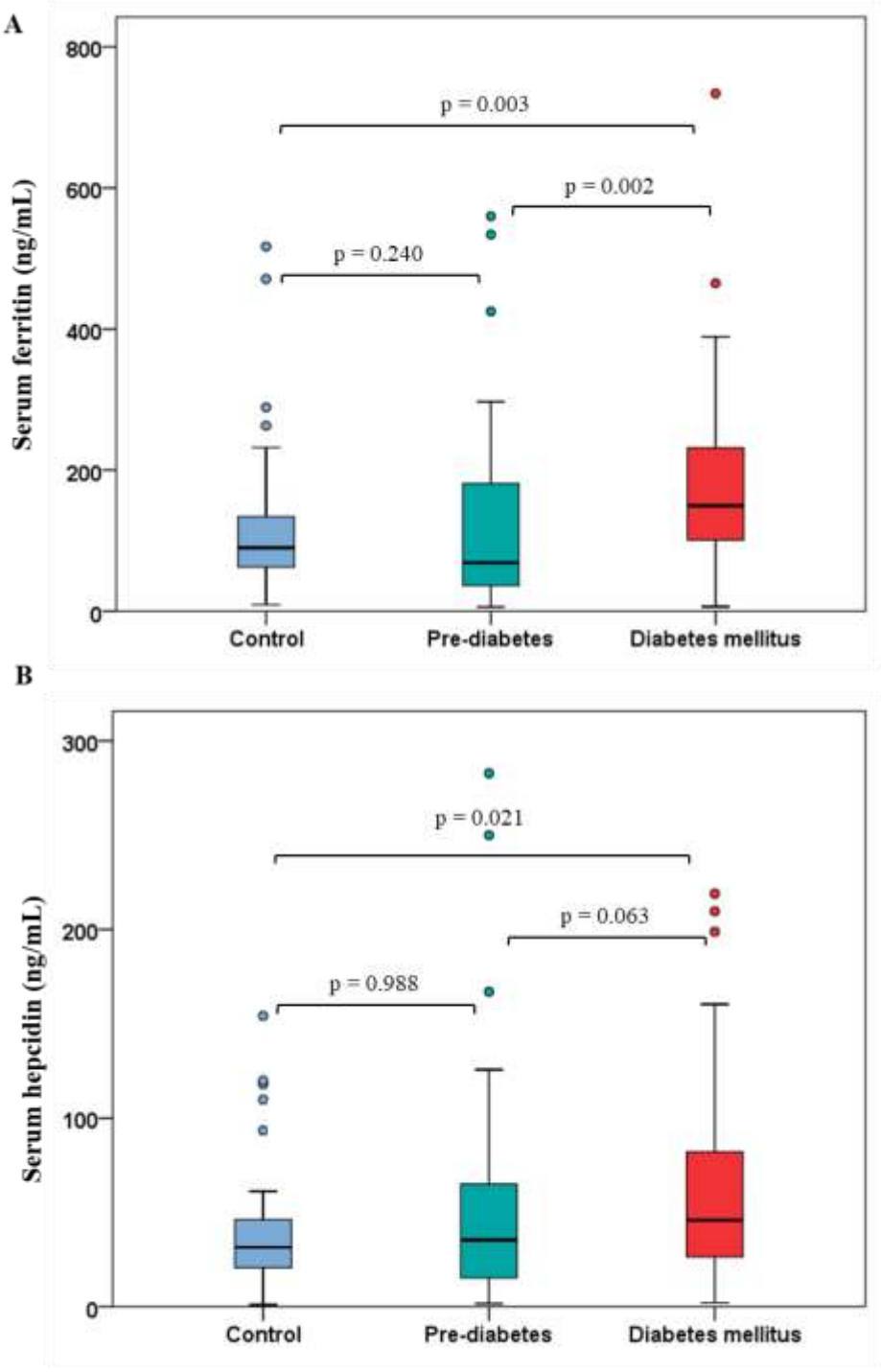

Figure 6.4.3: Serum ferritin and hepcidin levels

Serum levels of ferritin (A) and hepcidin (B) in control, pre-diabetic and diabetic subjects. Box plots indicate median and interquartile range. ° indicate distribution outliers.

Figure 6.4.4

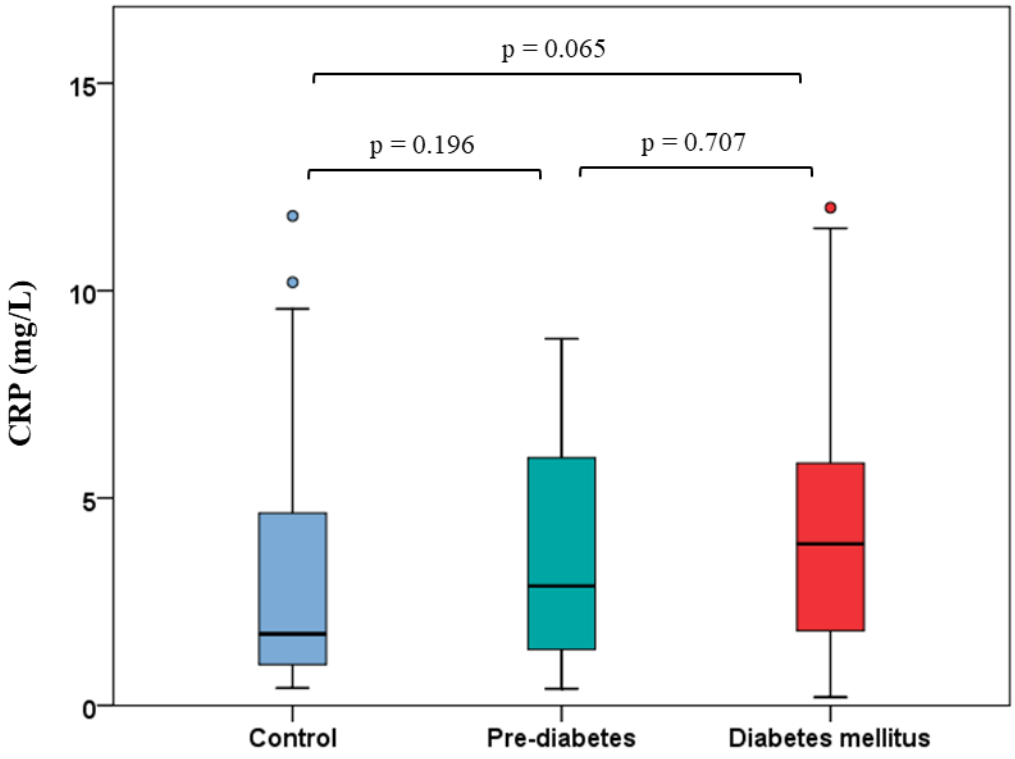

Figure 6.4.4: Serum levels of CRP

Serum CRP levels, estimated using a high-sensitivity assay (hsCRP), in control, pre-diabetic and diabetic subjects. Box plots indicate median and interquartile range. ° indicate distribution outliers.

Figure 6.4.5

A

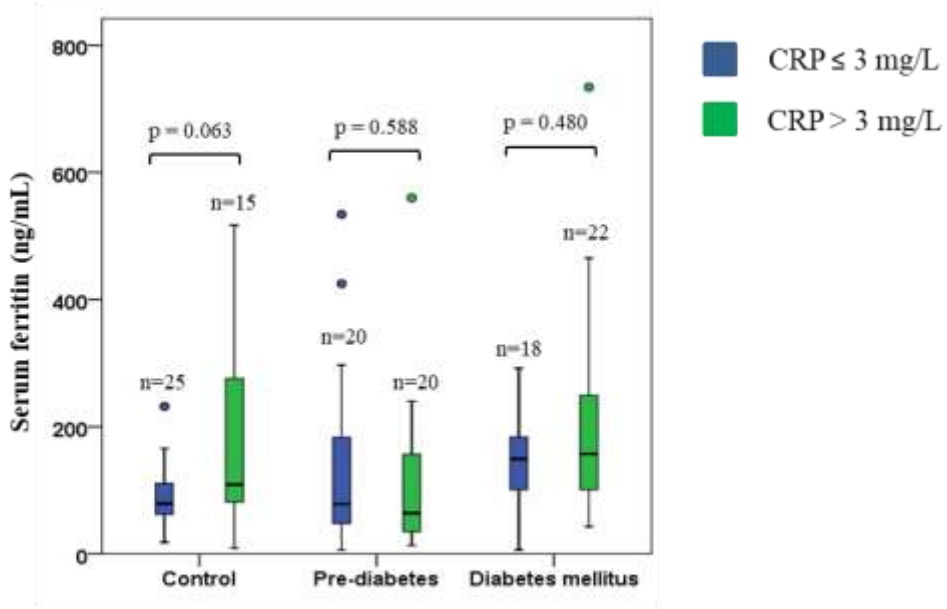

B

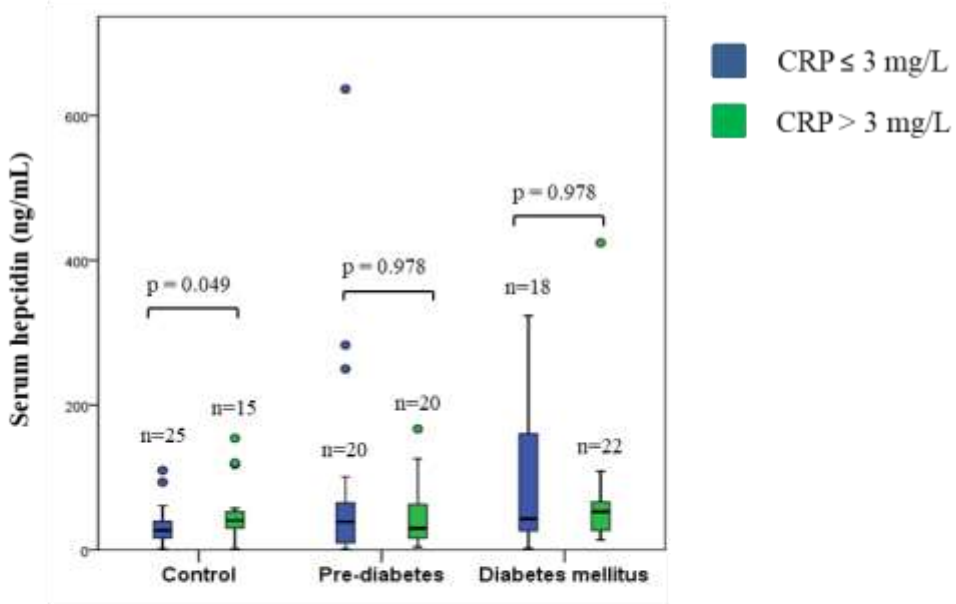

Figure 6.4.5: Serum ferritin and hepcidin levels in patients, classified based on CRP levels

Serum levels of ferritin (A) and hepcidin (B) in control, pre-diabetic and diabetic subjects. Within each group, patients were classified based on their CRP levels into those with CRP ≤ 3 mg/L (blue boxes) and those with CRP > 3 mg/L (green boxes). ° indicate distribution outliers. Box plots indicate median and interquartile range.

Figure 6.4.6

A

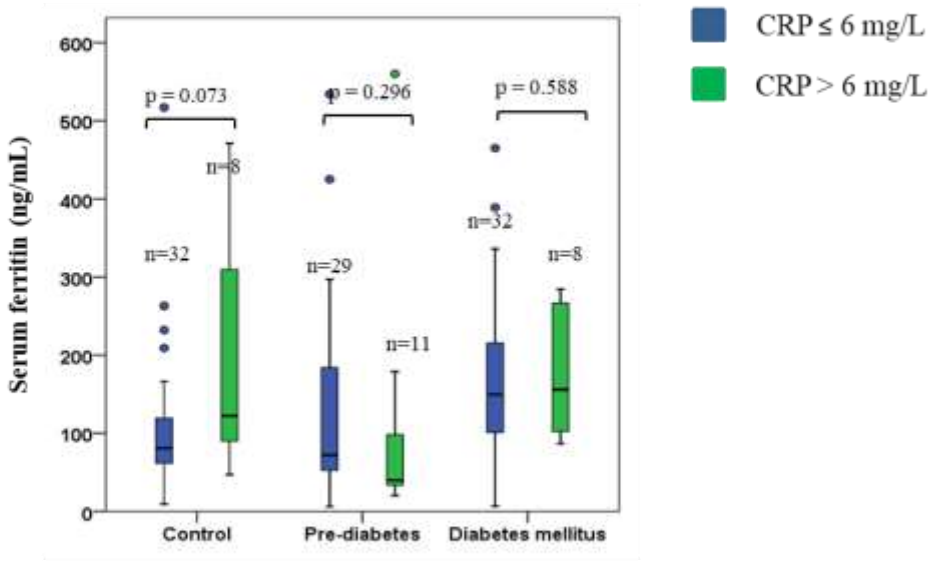

B

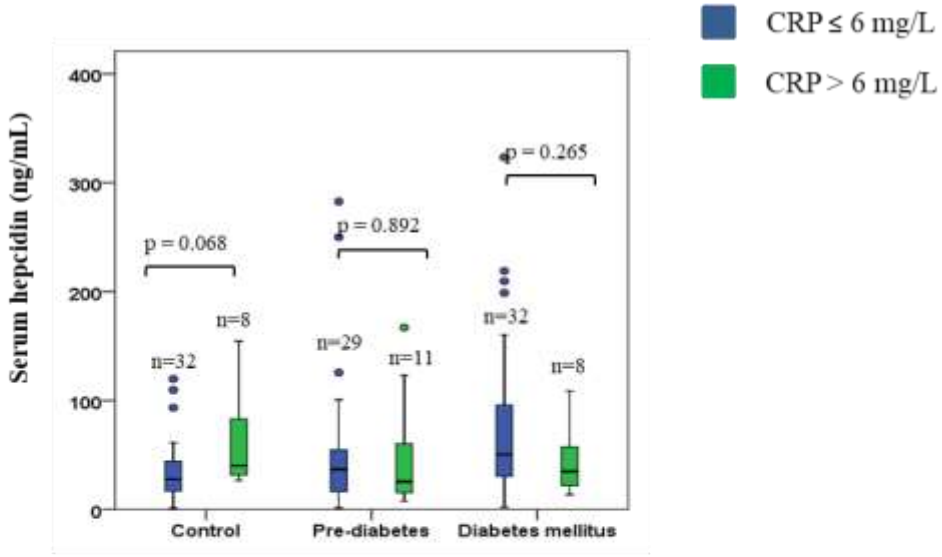

Figure 6.4.6: Serum ferritin and hepcidin levels in patients, classified based on CRP levels

Serum levels of ferritin (A) and hepcidin (B) in control, pre-diabetic and diabetic subjects. Within each group, patients were classified based on their CRP levels into those with CRP ≤ 6 mg/L (blue boxes) and those with CRP > 6 mg/L (green boxes). ° indicate distribution outliers. Box plots indicate median and interquartile range.

Figure 6.4.7

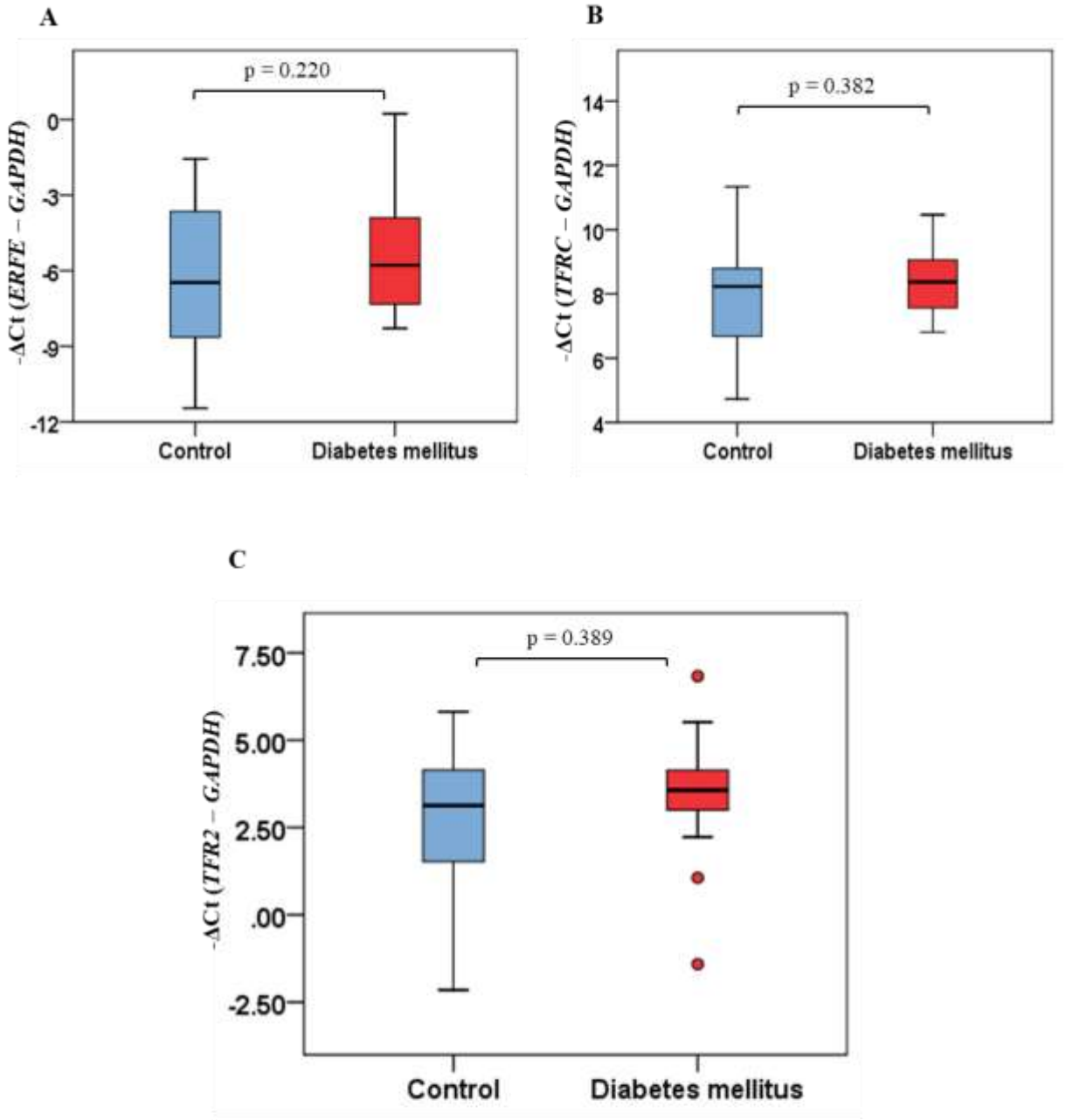

Figure 6.4.7: Gene expression in reticulocytes

Gene (mRNA) expression of erythroferrone (ERFE) (A), TfR1 (TFRC) (B) and TfR2 (TFR2) (C), determined by qPCR, in reticulocytes isolated from control (n = 20) and diabetic (n = 21) patients. Box plots indicate median and interquartile range of data represented as $-\Delta C_t$ values. ° indicate distribution outliers.

4.6 Correlation analyses

4.6.1 Serum ferritin

Serum ferritin was positively correlated with serum hepcidin in all the three groups studied. A positive correlation with markers of iron status (serum iron and transferrin saturation) was seen in the control and pre-diabetic groups, but not in the diabetic group (in which ferritin levels were found to be significantly increased [Fig 6.4.3-A]). A positive correlation with CRP was seen only in the control group (Table 6.4.6).

Stepwise multiple linear regression analysis showed an independent association of serum ferritin with MCH (B = 16.6, SE = 4.1, $p < 0.001$), HOMA-IR (B = 11.4, SE = 3.3, $p = 0.001$) and serum hepcidin (B = 0.36, SE = 0.15, $p = 0.021$). The model explained 24.8% of variation in serum ferritin ($p < 0.001$).

4.6.2. Serum hepcidin

Similar to serum ferritin, serum hepcidin was positively correlated with markers of iron status (serum iron and transferrin saturation) in the control and pre-diabetic groups but not in the diabetic group. It did not correlate with CRP in any of the groups (Table 6.4.7).

Stepwise multiple linear regression analysis showed that serum hepcidin was independently associated only with serum ferritin (B = 0.13, SE = 0.05, $p = 0.013$). However, serum ferritin explained only 4.7% of variation in serum hepcidin ($p = 0.013$). This indicates that other factors appear to influence hepcidin, apart from serum ferritin.

4.5.3. Fasting plasma glucose

Fasting plasma glucose (FPG) levels showed significant positive correlations with serum iron and transferrin saturation in the control group, but not in the pre-diabetic or diabetic group. It correlated positively with serum levels of hepcidin and ferritin, when data on all patients were considered. However, when data on the diabetic group alone was considered, glucose levels correlated negatively with hepcidin and insulin (Table 6.4.8).

Stepwise multiple linear regression analysis showed that FPG was independently associated only with CRP (B = 4.47, SE = 1.63, p = 0.007). However, the association with CRP explained only 5.6% of variation in FPG (p = 0.007).

4.5.4 Fasting serum insulin

Fasting serum insulin showed a significant positive correlation with CRP in the control group and in the pre-diabetic group; no association was not seen in the diabetic group. Serum insulin did not correlate with any of the other metabolic, hematological or iron-related parameters (Table 6.4.9).

Stepwise multiple linear regression analysis showed that fasting insulin was independently associated with BMI (B = 0.71, SE = 0.2, p = 0.001) and CRP (B = 0.51, SE = 0.22, p = 0.021). The model explained 14.8% of variation in HOMA-IR (p <0.001).

Table 6.4.6: Correlation of serum ferritin with various parameters of interest (univariate analyses)

		Control subjects	Pre-diabetics	Diabetics	All subjects
		Spearman's correlation coefficients			
Metabolic parameters	Fasting plasma glucose	0.26	0.08	0.06	**0.27****
	Serum insulin	0.07	0.14	0.09	0.14
	HOMA-IR	0.08	0.14	0.11	**0.22***
	HOMA-β	0.003	0.09	0.082	-0.09
Hematological parameters	Hemoglobin	-0.06	0.26	**0.32***	**0.24****
	RBC count	-0.28	-0.11	0.16	-0.04
	MCV	0.26	**0.31***	0.12	**0.21***
	MCH	0.28	**0.43****	0.18	**0.30****
	Reticulocyte hemoglobin	0.19	**0.50****	0.17	**0.31****
	Reticulocyte count	0.01	0.21	0.05	0.14
Iron-related parameters	Serum hepcidin	**0.55****	**0.69****	**0.42****	**0.59****
	Serum iron	**0.51****	**0.49****	0.07	**0.40****
	Transferrin saturation (%)	**0.59****	**0.50****	0.06	**0.44****
Inflammation	hsCRP	**0.326***	-0.071	0.123	0.164

Spearman's correlation coefficients are shown. Significant correlations are in bold font and highlighted. *$p < 0.05$, ** $p < 0.01$

Table 6.4.7: Correlation of serum hepcidin with various parameters of interest (univariate analyses)

		Control subjects	Pre-diabetics	Diabetics	All subjects
		Spearman's correlation coefficients			
Metabolic parameters	Fasting plasma glucose	0.19	0.07	**-0.32***	**0.18***
	Serum insulin	-0.08	0.11	0.04	0.05
	HOMA-IR	-0.07	0.13	0.02	0.12
	HOMA-β	-0.19	0.08	0.14	0.06
Hematological parameters	Hemoglobin	0.22	0.15	0.21	**0.23***
	RBC count	0.08	-0.07	0.13	0.06
	MCV	0.26	**0.38***	0.27	**0.27****
	MCH	0.14	0.27	0.11	0.17
	Reticulocyte hemoglobin	0.09	0.10	-0.19	0.03
	Reticulocyte count	-0.02	0.01	-0.23	-0.05
Iron-related parameters	Serum ferritin	**0.55****	**0.69****	**0.42****	**0.59****
	Serum iron	**0.46****	**0.35***	0.16	**0.33****
	Transferrin saturation (%)	**0.48****	**0.38***	0.17	0.34
Inflammation	hsCRP	0.302	0.046	-0.074	0.123

Spearman's correlation coefficients are shown. Significant correlations are in bold font and highlighted. *$p < 0.05$, ** $p < 0.01$

Table 6.4.8: Correlation of fasting plasma glucose with various parameters of interest (univariate analyses)

		Control subjects	**Pre-diabetics**	**Diabetics**	**All subjects**
		Spearman's correlation coefficients			
Metabolic parameters	Serum insulin	0.08	0.16	**-0.32***	0.03
Hematological parameters	Hemoglobin	-0.07	-0.17	0.15	0.10
	RBC count	-0.19	-0.02	0.08	0.17
	MCV	0.07	-0.18	-0.05	-0.16
	MCH	0.16	-0.13	0.08	-0.13
	Reticulocyte hemoglobin	0.08	-0.03	0.25	-0.08
	Reticulocyte count	0.15	-0.02	0.04	0.14
Iron-related parameters	Serum ferritin	0.26	0.08	0.06	**0.27****
	Serum hepcidin	0.19	0.06	**-0.32***	**0.18***
	Serum iron	**0.46****	0.01	-0.26	0.01
	Transferrin saturation (%)	**0.51****	-0.08	-0.15	0.02
Inflammation	CRP	0.006	0.036	0.179	0.179

Spearman's correlation coefficients are shown. Significant correlations are in bold font and highlighted. *p < 0.05, ** p < 0.01

Table 6.4.9: Correlation of fasting serum insulin with various parameters of interest (univariate analyses)

		Control subjects	**Pre-diabetics**	**Diabetics**	**All subjects**
		Spearman's correlation coefficients			
Metabolic parameters	Fasting plasma glucose	0.080	0.161	-0.318	0.027
Hematological parameters	Hemoglobin	-0.121	0.037	-0.006	-0.013
	RBC count	-0.161	-0.191	0.092	-0.066
	MCV	-0.107	0.170	-0.154	-0.025
	MCH	0.039	0.302	-0.145	0.056
	Reticulocyte hemoglobin	0.142	0.239	0.031	0.120
	Reticulocyte count	-0.101	0.114	0.239	0.101
Iron-related parameters	Serum ferritin	0.075	0.138	0.087	0.136
	Serum hepcidin	-0.087	0.108	0.042	0.057
	Serum iron	-0.165	0.119	0.142	0.044
	TIBC	-0.194	0.034	0.207	-0.004
	Transferrin saturation (%)	-0.062	0.139	-0.045	0.026
Inflammation	hsCRP	**0.375***	**0.547****	0.178	**0.349****

Spearman's correlation coefficients are shown. Significant correlations are in bold font and highlighted. *p < 0.05, ** p < 0.01

Table 6.4.10: Correlation among ERFE, TfR1 and TfR2 mRNA expression in reticulocytes, hemoglobin and serum hepcidin.

	Spearman's correlation coefficients are shown				
	ERFE	TfR1	TfR2	Hemoglobin	Serum hepcidin
ERFE	-	0.365	0.296	-0.02	-0.214
TfR1	**0.692****	-	**0.831****	-0.055	0.086
TfR2	**0.723****	**0.932****	-	-0.106	0.200
Hemoglobin	**-0.427***	-0.039	-0.097	-	0.207
Serum hepcidin	0.084	-0.026	-0.084	0.220	-

Control group, Diabetes group

Spearman's correlation coefficients are shown. Significant correlations are in bold font.
* $p < 0.05$, ** $p < 0.01$

4.5.5 mRNA expression of ERFE, TfR1 and TfR2 in reticulocytes

ERFE mRNA expression in reticulocytes correlated positively with TfR1 and TfR2 mRNA (in reticulocytes) and negatively with hemoglobin in the control group, but not in the diabetic group. TfR1 and TfR2 mRNA levels were highly positively correlated with each other in both groups studied. However, ERFE, TfR1 and TfR2 mRNA did not correlate with serum hepcidin levels (Table 6.4.10).

5. Discussion

There are many reports of dysregulated iron homeostasis in patients with diabetes mellitus (4,6–9). However, in these studies, many factors that could influence the parameters of interest have not been adequately controlled for. For example, factors such as duration of the disease, extent of glycemic control in the past or currently, therapeutic interventions used and presence or absence of chronic complications of diabetes can all have a significant bearing upon the outcomes studied (187). In an attempt to minimize the effects of these potential confounding factors, in the present study, only patients who were newly diagnosed to have diabetes mellitus were recruited. Those diagnosed to be pre-diabetic, a state in which patients are at increased risk of developing diabetes, were also recruited. As far as is ascertainable, there are no published studies on hepcidin and other iron-related parameters in such categories of patients.

Only males were investigated in this study. This was because many factors are known to affect iron homeostasis in women. These include parity, phase of the menstrual cycle (in pre-menopausal women) and menopausal changes (408,409).

Inflammation (417), anemia (418) and severe obesity (419–421) are other factors that are known to affect iron homeostasis. Hence, patients with CRP > 12 mg/dL, hemoglobin < 13 g/dL (422) and BMI > 35 kg/m^2 (423) were excluded from the study. Subjects in all three groups (control, pre-diabetic and diabetic) were matched for age and BMI, as much as was possible (Table 6.4.3).

Insulin resistance (IR) is a characteristic feature of T2DM, which is the most common type of diabetes mellitus. The natural history of T2DM is characterized by an early stage where IR is compensated by increased insulin secretion. However, this compensatory hyperinsulinemia tends to decline with progressively increasing IR and beta-cell fatigue (or failure) (424). In the present study, there was no evidence of hyperinsulinemia, either in the pre-diabetics or the diabetics (Fig 6.4.1-B). HOMA-IR, a marker of insulin resistance, was not different in control subjects and in the pre-diabetics, but was ~ 2-fold higher in the diabetics (Fig 6.4.2-A). On the other hand, HOMA-β, a marker of the pancreatic insulin secretory capacity, was lower by 40% in the pre-diabetics and by 76% in the diabetics (Fig 6.4.2-B), suggesting onset of beta cell failure. These results are consistent with previous reports that have shown early onset of beta cell failure among South Asians with varying degrees of dysglycemia (425–429). It has been shown that, compared to Caucasians and other ethnic groups, South Asians have decreased beta cell reserve (426), early onset of beta cell failure (426,429) and rapid deterioration of beta cell function in the presence of IR (427). Iron has been implicated in the pathogenesis of beta cell damage, especially in type 1 diabetes (232,430). However, very little is known about the role of iron in beta cell function and insulin secretion.

It is generally held that serum levels of ferritin are indicative of iron stores in the body (53,431). However, the source of ferritin in the blood is not well-characterized. Circulating ferritin has

been shown to be made up of ferritin light chains that are iron-poor (432). In mice, it has been shown to be actively secreted by the macrophages, and is not a product of cell turnover, as was previously thought (52). However, the factors regulating the secretion of ferritin are not well-characterized and how body iron stores influence serum ferritin levels is not known.

The results of the present study show that, except for a significant increase in serum levels of ferritin and hepcidin in patients with diabetes (but not in pre-diabetes), parameters of iron status (such as serum iron, TIBC and transferrin saturation) (Table 6.4.4), were not different in the three groups studied. These results are in keeping with results of the EPIC-INTERACT study (194), which showed that diabetes mellitus was associated only with elevated ferritin levels and not with serum iron or transferrin saturation. In fact, among women, transferrin saturation >45% was associated with significantly decreased risk of diabetes (194). In the present study, multivariate analyses showed that serum ferritin was independently associated HOMA-IR and hepcidin, but not with serum iron or transferrin saturation. These results suggest that the etiopathogenesis of elevated serum ferritin levels associated with T2DM is more complex than previously thought and does not simply reflect an iron-overloaded state.

Ferritin is an acute phase protein and its levels in blood increase in inflammatory conditions (285,286). Hepcidin is also induced by inflammation (417). Hence, serum levels of CRP, a marker of inflammation, were measured to ascertain whether inflammation was responsible for the elevations seen in serum levels of hepcidin and ferritin. Serum CRP levels tended to be higher in the diabetic group compared to those in control subjects (p=0.065) (Fig. 6.4.4). On classification of subjects based on the ‘high-risk’ cut-off for CRP (proposed by the American Heart Association) viz., >3.0 mg/dL (415), it was found that control subjects with higher CRP

levels had significantly higher hepcidin levels and a tendency to higher serum ferritin levels ($p = 0.063$). However, these parameters were similar in the same sub-categories in the pre-diabetics and diabetics (Fig 6.4.5-A and B). These results suggest that the presence of inflammation may influence serum hepcidin and ferritin values, but this influence does not seem to be very distinct in the pre-diabetic and diabetic groups.

Correlation analyses showed that ferritin and hepcidin were positively correlated with each other in all the three groups studied. However, they were not correlated with CRP or markers of iron status (serum iron and transferrin saturation). This is surprising, given that both ferritin and hepcidin are well-known to be linked to inflammation and iron status. The reasons for these observations are unclear.

While multiple studies (described above) have consistently shown increased serum ferritin in patients with diabetes, studies that have looked at serum hepcidin levels have reported variable results. For example, Andrews et al (25) and Jiang et al (26) have reported increased serum hepcidin levels in patients with T2DM compared to control subjects. On the other hand, Suarez-Ortegon et al (29), Pechlaner et al (407), Sam et al (28) and Aso et al (27) showed lower levels in diabetics. Guo et al (30) showed no significant differences in hepcidin levels in diabetics and non-diabetics. In all of the studies mentioned above, the subjects recruited were patients who were already known to be diabetic. Hence, many factors such as duration of condition, extent of glycemic control, etc. may contribute to variations seen. These have not been controlled for in these published studies.

In the present study, serum hepcidin was found to be increased in the diabetic group, but not in the pre-diabetic group. As discussed above, the contribution of inflammation to this increase is

not clear (Fig 6.4.5-B). Adipose tissue has been shown to secrete hepcidin and contribute significantly to serum hepcidin levels in obese patients (433). Hence, it is possible that the adipose tissue may be the source of increased serum hepcidin in the diabetic group. However, patients in all the 3 groups studied had similar mean values for BMI; none of them were obese. Little is known about the effects of factors, such as iron content in the adipose tissue and inflammation, on expression of hepcidin in adipose tissue. It has been suggested that increased iron content in adipose tissue iron may play a role in the pathogenesis of IR (17,225,349). A few studies, using magnetic resonance (MRI) imaging for quantification of tissue iron, have shown increased iron content in the liver, skeletal muscle and adipose tissue in patients with diabetes mellitus (348,419,434). Overall, the role of tissue iron overload, especially in the adipose tissue, in the pathogenesis of diabetes mellitus is poorly understood and is an under-investigated area.

Hepcidin is known to be regulated by factors secreted by the erythroid precursors. In the present study, patients with pre-diabetes and diabetes tended to have higher RBC counts and lower MCH and reticulocyte hemoglobin (Table 6.4.4). ERFE mRNA was found to be expressed at low-to-moderate levels in reticulocytes and could be reliably quantitated by qPCR. Therefore, reticulocyte ERFE expression may be considered a surrogate marker of ERFE expression in late erythroid precursors in subjects in whom it is not ethically possible to obtain bone marrow samples. The present results showed that ERFE expression was similar in control and diabetic patients; expression levels of GDF-15 and TWSG-1 (the other putative erythroid regulators of hepcidin) in reticulocytes were too low to be reliably determined.

Expression of TfR1 in the bone marrow has been shown to mediate hepatic hepcidin expression, probably by regulating the expression of the erythroid regulators of hepcidin (390). Expression

of TfR2, a component of the EpoR complex, which mediates EPO-induced expression of ERFE (391), has also been shown to affect hepcidin expression (405). A significant positive correlation was seen between ERFE, TfR1 and TfR2 mRNA expression in reticulocytes among the control patients; this was not observed in the diabetics. In addition, ERFE was negatively correlated with hemoglobin in the control subjects, but not in the diabetics (Table 6.4.10). These results possibly indicate alterations in iron-related proteins in the erythroid cells obtained from patients with diabetes. Expression levels of TfR1 and TfR2 were highly correlated, both in the controls and the diabetics. This finding suggests that the expression of TfR1 and TfR2 are coordinately regulated. Further investigations would be required to elucidate the physiological importance of these findings.

A limitation of the present study is the fact that, although only newly diagnosed diabetic/ pre-diabetic patients were recruited, it was not possible to know how long these patients had been diabetic/ pre-diabetic prior to diagnosis at the time of recruitment.

6. Summary and conclusions:

As far as is ascertainable, this is the first study that has determined hepcidin and other iron-related parameters in patients newly diagnosed with diabetes or pre-diabetes. The results of this study show that serum levels of ferritin and hepcidin were elevated in patients with diabetes mellitus (but not in those with pre-diabetes), compared to control subjects.

Serum levels of CRP tended to be higher in the diabetics and may have some bearing upon the elevations seen in serum levels of hepcidin and ferritin. Markers of iron status, apart from ferritin (serum iron, TIBC and transferrin saturation) were not significantly different in the 3 groups studied. Expression of erythroferrone, the erythroid regulator of hepcidin, in reticulocytes was similar in control and diabetic patients. Surprisingly, although the patients recruited in this study were diagnosed to have pre-diabetes/diabetes for the first time, they showed evidence of beta cell dysfunction. These results add to the growing body of evidence that South Asians are prone to early onset of beta cell failure. How iron is linked to this is currently unclear.

7. SUMMARY OF RESULTS

A summary of the major findings of this study is given below:

Study 1: Iron induces basal activation of Akt but decreases its activation in response to insulin in mouse primary hepatocytes

- Mouse primary hepatocytes loaded with iron *in vitro* showed phosphorylation-mediated activation of the Akt pathway and AMP-activated protein kinase (AMPK). These effects tended to be attenuated by treatment with an iron chelator, desferrioxamine.
- Hepatocyte glucose production was significantly decreased in iron-loaded hepatocytes. Iron also attenuated forskolin (a glucagon agonist)-induced activation of the key gluconeogenic enzyme, glucose-6-phosphatase.
- On the other hand, iron decreased protein levels of insulin receptor substrates 1 and 2 (which are upstream of Akt in the insulin signaling pathway), resulting in decreased insulin-stimulated Akt activation.

In conclusion, the results show that high intracellular iron had a dual effect on the insulin signalling pathway in hepatocytes. It increased Akt activation in a ligand-independent manner (in the absence of insulin), but decreased insulin-induced Akt activation resulting in insulin resistance.

Study 2: Interactions between insulin resistance and dysregulated iron homeostasis, produced by high-fat feeding in mice: a time-course study

- In a mouse model of type 2 diabetes mellitus, induced by feeding male C57Bl/6 mice a high-fat diet, progressive worsening of insulin resistance (with increasing duration of HFD-feeding) was associated with dysregulation of systemic iron homeostasis and hyperinsulinemia.
- Onset of insulin resistance appeared to precede the onset of iron dysregulation. This suggests that it is unlikely that dysregulated iron homeostasis in the liver plays a causative role in the pathogenesis of IR in this model.
- Hepatic steatosis was independently associated with IR and decreased hepatic iron stores, suggesting that ectopic lipid accumulation in the liver may play a role in the pathogenesis of IR, as well as in hepatic iron dysregulation.
- The decrease in hepatic iron stores was associated with concomitant increases in the iron content and metabolic dysfunction in the adipose tissue. Since increased iron in the adipose tissue has been reported to induce IR, it is possible that this may contribute to the increase in IR in response to high-fat feeding.
- Levels of hepcidin, the chief iron regulatory hormone, were decreased in high-fat diet-fed mice. Factors that regulate hepcidin, such as inflammation, serum iron levels and hepatic BMP6 were not significantly affected by HFD-feeding. Protein levels of TfR2 (known to induce hepcidin expression) were independently associated with hepatic hepcidin expression in HFD-fed mice. Further studies would be required to further elucidate its role in hepcidin regulation in this setting.

In conclusion, the results showed that IR induced by HFD-feeding was associated with dysregulation of iron homeostasis in the liver and adipose tissue. Ectopic lipid accumulation in the liver may play a role in the pathogenesis of IR, as well as in hepatic iron dysregulation. Increased iron in the adipose tissue induced by HFD-feeding may play a role in the pathogenesis of IR in response to high-fat feeding.

Study 3: Effect of high-fat diet-induced insulin resistance on erythroid maturation and erythroid regulators of hepcidin in the bone marrow in mice

- Flow cytometric analyses of maturation and differentiation of erythroid progenitors in the bone marrow showed no significant effects of HFD-feeding on terminal erythroid differentiation.
- An increase in reticulocytes in the marrow of HFD-fed mice suggested impaired reticulocyte maturation and release into the circulation.
- Gene expression of the putative erythroid regulators of hepcidin, such as erythroferrone, growth differentiation factor 15, twisted gastrulation factor 1 was not affected by HFD-feeding.

In conclusion, HFD-feeding induced IR did not affect erythroid maturation in the bone marrow or gene expression of the putative erythroid regulators of hepcidin. Hence, it appears unlikely that these factors play a role in the down-regulation of hepcidin seen in response to high-fat feeding.

Study 4: Dysregulated iron homeostasis in patients newly diagnosed with diabetes mellitus or pre-diabetes

- Male patients newly diagnosed to have diabetes mellitus and pre-diabetes showed evidence of beta cell failure.
- Diabetics (but not pre-diabetics) had significantly elevated levels of serum ferritin and hepcidin compared to controls. However, other markers of iron status (serum levels of iron, total iron-binding capacity and transferrin saturation) were similar in the 3 groups studied (controls, pre-diabetics and diabetics).
- Serum levels of CRP tended to be higher in the diabetics. Inflammation may therefore have some bearing upon the elevations seen in serum levels of hepcidin and ferritin.
- Expression of erythroferrone, the putative erythroid regulator of hepcidin, in reticulocytes, was not significantly different between control and diabetic patients.

In conclusion, patients newly diagnosed with diabetes mellitus and pre-diabetes showed evidence of beta cell failure. Dysregulation of iron homeostasis was seen in the diabetics but not in the pre-diabetics. Erythroferrone, an erythroid regulator of hepcidin, did not appear to play a role in regulation of hepcidin in the diabetics.

8. CONCLUSIONS

Currently, management of diabetes is primarily based on attempts to achieve adequate glycemic control in an effort to delay/prevent chronic complications of diabetes (such as nephropathy, neuropathy, and retinopathy). There are very few effective strategies aimed at primary prevention in genetically pre-disposed persons, other than measures to reduce body weight and increase physical activity. Iron stores in the body can be easily manipulated by dietary means, phlebotomy or by using iron chelators. A better understanding of the role of iron in the pathogenesis of diabetes will possibly provide newer therapeutic options, based on manipulation of body iron stores, in the management of diabetes.

Overall, this study attempted to address the question "Why does iron overload associated with insulin resistance occur?" using multiple approaches - *in vitro* (using hepatocytes in culture), *in vivo* (using a mouse model of diabetes) and in patients newly diagnosed with diabetes mellitus/pre-diabetes.

The results show that increased intracellular iron impaired insulin signalling, resulting in insulin resistance (study 1). In the mouse model of insulin resistance, onset of insulin resistance preceded that of iron dysregulation (study 2). In addition, in the human study, dysregulation of iron homeostasis was seen in the diabetics but not in the pre-diabetics (study 4). These results suggest that dysregulation of iron homeostasis is unlikely to play a causative role in the pathogenesis of diabetes mellitus. In the mouse model of insulin resistance, hepatic steatosis decreased iron levels in the liver, while increasing iron levels in the adipose tissue. Iron overload in the adipose tissue may play an important role in the progression of insulin resistance (study 2).

Although the erythroid regulators of hepcidin are known to regulate hepcidin expression, there was no evidence for a role for these regulators (erythroferrone, growth differentiation factor – 15 and twisted gastrulation factor 1) in regulation of hepcidin in the mouse model of insulin resistance (study 3) or in humans newly diagnosed with diabetes mellitus/pre-diabetes (study 4).

9. RECOMMENDATIONS AND FUTURE DIRECTIONS

The present study has attempted to address several questions related to the interactions between iron homeostasis and insulin resistance in the pathogenesis of diabetes mellitus. The results have also raised several new ones.

The results of study 1 show that increased levels of intracellular iron impaired insulin signaling in hepatocytes. Based on these results, we speculate that similar mechanisms may be operational in other tissues as well, such as skeletal muscle and adipose tissue. This would be a new and interesting avenue for further research in this area. As far as we have been able to ascertain, such avenues have not been explored. Studies of this nature would contribute significantly to the field.

At the time that the current study was designed, it was generally accepted that increased body iron stores were associated with diabetes. However, these conclusions were based on estimations of serum ferritin, which was used a surrogate marker of body iron stores. More recent studies have shown that iron overload is not invariably associated with diabetes and that iron dysregulation in diabetes mellitus is a complex phenomenon. The results of study 2 have shown the interactions between insulin resistance and systemic iron homeostasis in a mouse model of insulin resistance. One of the key findings was that insulin resistance was associated with increased iron stores in the adipose tissue. A few studies have shown that iron in the adipose tissue in humans can contribute to insulin resistance (1,2); however, the molecular mechanisms involved have not been studied in detail. This is an important area for future research.

Results from study 2 showed that hepatic steatosis induced by high-fat feeding in mice resulted in a decrease in iron stores in the liver. Ferritinophagy is a specialized form of autophagy that

specifically targets ferritin, the iron storage protein, for lysosomal degradation. It is not known whether activation of ferritinophagy plays a role in steatosis-induced decrease in liver iron. This is an interesting possibility that would require further experimental work for confirmation.

Hepatic iron stores are important regulators of hepcidin expression. However, the molecular mechanisms by which iron stores in the liver signal to regulate hepcidin are not clear. Interestingly, results of study 2 showed that protein levels of transferrin receptor 2 (TfR2) in the liver were independently associated with hepatic hepcidin expression. In addition, the role of matriptase-2 (a negative regulator of hepcidin) and iron-induced epigenetic changes in hepcidin regulation are not clear. Further work would be required to clarify the role of these molecules in regulation of hepcidin, in response to changes in liver iron stores.

Results of study 4 show increased serum levels of ferritin and hepcidin in patients with diabetes, but not in those with pre-diabetes. However, the reason(s) for these findings are not clear. Future work aimed at elucidating the dysregulation of iron metabolism in adipose tissue of patients with diabetes/pre-diabetes may throw light on this aspect.

10. BIBLIOGRAPHY

1. Anjana RM, Pradeepa R, Deepa M, Datta M, Sudha V, Unnikrishnan R, et al. Prevalence of diabetes and prediabetes (impaired fasting glucose and/or impaired glucose tolerance) in urban and rural India: Phase I results of the Indian Council of Medical Research-INdia DIABetes (ICMR-INDIAB) study. Diabetologia. 2011 Dec;54(12):3022–7.

2. DeFronzo RA. Pathogenesis of type 2 (non-insulin dependent) diabetes mellitus: a balanced overview. Diabetologia. 1992 Apr;35(4):389–97.

3. Andrews NC, Schmidt PJ. Iron homeostasis. Annu Rev Physiol. 2007;69:69–85.

4. Ford ES, Cogswell ME. Diabetes and serum ferritin concentration among U.S. adults. Diabetes Care. 1999 Dec;22(12):1978–83.

5. Afkhami-Ardekani M, Rashidi M. Iron status in women with and without gestational diabetes mellitus. J Diabetes Complications. 2009 Jun;23(3):194–8.

6. Jiang R, Manson JE, Meigs JB, Ma J, Rifai N, Hu FB. Body iron stores in relation to risk of type 2 diabetes in apparently healthy women. JAMA J Am Med Assoc. 2004 Feb 11;291(6):711–7.

7. Sharifi F, Nasab NM, Zadeh HJ. Elevated serum ferritin concentrations in prediabetic subjects. Diabetes Vasc Dis Res Off J Int Soc Diabetes Vasc Dis. 2008 Mar;5(1):15–8.

8. Tuomainen TP, Nyyssönen K, Salonen R, Tervahauta A, Korpela H, Lakka T, et al. Body iron stores are associated with serum insulin and blood glucose concentrations. Population study in 1,013 eastern Finnish men. Diabetes Care. 1997 Mar;20(3):426–8.

9. Wilson JG, Lindquist JH, Grambow SC, Crook ED, Maher JF. Potential role of increased iron stores in diabetes. Am J Med Sci. 2003 Jun;325(6):332–9.

10. Simcox JA, McClain DA. Iron and Diabetes Risk. Cell Metab. 2013 Mar 5;17(3):329–41.

11. McClain DA, Abraham D, Rogers J, Brady R, Gault P, Ajioka R, et al. High prevalence of abnormal glucose homeostasis secondary to decreased insulin secretion in individuals with hereditary haemochromatosis. Diabetologia. 2006 Jul;49(7):1661–9.

12. Dmochowski K, Finegood DT, Francombe W, Tyler B, Zinman B. Factors determining glucose tolerance in patients with thalassemia major. J Clin Endocrinol Metab. 1993 Aug;77(2):478–83.

13. Merkel PA, Simonson DC, Amiel SA, Plewe G, Sherwin RS, Pearson HA, et al. Insulin resistance and hyperinsulinemia in patients with thalassemia major treated by hypertransfusion. N Engl J Med. 1988 Mar 31;318(13):809–14.

14. Gamberini MR, De Sanctis V, Gilli G. Hypogonadism, diabetes mellitus, hypothyroidism, hypoparathyroidism: incidence and prevalence related to iron overload and chelation therapy in patients with thalassaemia major followed from 1980 to 2007 in the Ferrara Centre. Pediatr Endocrinol Rev PER. 2008 Oct;6 Suppl 1:158–69.

15. Fernández-Real JM, Peñarroja G, Castro A, García-Bragado F, Hernández-Aguado I, Ricart W. Blood letting in high-ferritin type 2 diabetes: effects on insulin sensitivity and beta-cell function. Diabetes. 2002 Apr;51(4):1000–4.

16. Facchini FS. Effect of phlebotomy on plasma glucose and insulin concentrations. Diabetes Care. 1998 Dec;21(12):2190.

17. Dongiovanni P, Ruscica M, Rametta R, Recalcati S, Steffani L, Gatti S, et al. Dietary iron overload induces visceral adipose tissue insulin resistance. Am J Pathol. 2013 Jun;182(6):2254–63.

18. Minamiyama Y, Takemura S, Kodai S, Shinkawa H, Tsukioka T, Ichikawa H, et al. Iron restriction improves type 2 diabetes mellitus in Otsuka Long-Evans Tokushima fatty rats. Am J Physiol - Endocrinol Metab. 2010 Jun 1;298(6):E1140–9.

19. Cooksey RC, Jones D, Gabrielsen S, Huang J, Simcox JA, Luo B, et al. Dietary iron restriction or iron chelation protects from diabetes and loss of beta-cell function in the obese (ob/ob lep-/-) mouse. Am J Physiol Endocrinol Metab. 2010 Jun;298(6):E1236–43.

20. Alessi DR, Andjelkovic M, Caudwell B, Cron P, Morrice N, Cohen P, et al. Mechanism of activation of protein kinase B by insulin and IGF-1. EMBO J. 1996 Dec 2;15(23):6541–51.

21. Manning BD, Cantley LC. AKT/PKB signaling: navigating downstream. Cell. 2007 Jun 29;129(7):1261–74.

22. Fernández-Real JM, Equitani F, Moreno JM, Manco M, Ortega F, Ricart W. Study of circulating prohepcidin in association with insulin sensitivity and changing iron stores. J Clin Endocrinol Metab. 2009 Mar;94(3):982–8.

23. Nicolas G, Bennoun M, Devaux I, Beaumont C, Grandchamp B, Kahn A, et al. Lack of hepcidin gene expression and severe tissue iron overload in upstream stimulatory factor 2 (USF2) knockout mice. Proc Natl Acad Sci U S A. 2001 Jul 17;98(15):8780–5.

24. Nemeth E, Tuttle MS, Powelson J, Vaughn MB, Donovan A, Ward DM, et al. Hepcidin regulates cellular iron efflux by binding to ferroportin and inducing its internalization. Science. 2004 Dec 17;306(5704):2090–3.

25. Andrews M, Soto N, Arredondo-Olguín M. Association between ferritin and hepcidin levels and inflammatory status in patients with type 2 diabetes mellitus and obesity. Nutr Burbank Los Angel Cty Calif. 2015 Jan;31(1):51–7.

26. Jiang F, Sun Z-Z, Tang Y-T, Xu C, Jiao X-Y. Hepcidin expression and iron parameters change in Type 2 diabetic patients. Diabetes Res Clin Pract [Internet]. 2011 Apr 20 [cited 2011 May 26]; Available from: http://www.ncbi.nlm.nih.gov/pubmed/21513996

27. Aso Y, Takebayashi K, Wakabayashi S, Momobayashi A, Sugawara N, Terasawa T, et al. Relation between serum high molecular weight adiponectin and serum ferritin or prohepcidin in patients with type 2 diabetes. Diabetes Res Clin Pract [Internet]. 2010 Sep 30 [cited 2010 Oct 13]; Available from: http://www.ncbi.nlm.nih.gov/pubmed/20888657

28. Sam AH, Busbridge M, Amin A, Webber L, White D, Franks S, et al. Hepcidin levels in diabetes mellitus and polycystic ovary syndrome. Diabet Med J Br Diabet Assoc. 2013 Dec;30(12):1495–9.

29. Suárez-Ortegón MF, Moreno M, Arbeláez A, Xifra G, Mosquera M, Moreno-Navarrete JM, et al. Circulating hepcidin in type 2 diabetes: A multivariate analysis and double blind evaluation of metformin effects. Mol Nutr Food Res. 2015 Dec;59(12):2460–70.

30. Guo X, Zhou D, An P, Wu Q, Wang H, Wu A, et al. Associations between serum hepcidin, ferritin and Hb concentrations and type 2 diabetes risks in a Han Chinese population. Br J Nutr. 2013 Dec;110(12):2180–5.

31. Andrews NC. Forging a field: the golden age of iron biology. Blood. 2008 Jul 15;112(2):219–30.

32. Ganz T. Hepcidin and iron regulation, 10 years later. Blood. 2011 Apr 28;117(17):4425–33.

33. Tanno T, Bhanu NV, Oneal PA, Goh S-H, Staker P, Lee YT, et al. High levels of GDF15 in thalassemia suppress expression of the iron regulatory protein hepcidin. Nat Med. 2007 Sep;13(9):1096–101.

34. Tanno T, Porayette P, Sripichai O, Noh S-J, Byrnes C, Bhupatiraju A, et al. Identification of TWSG1 as a second novel erythroid regulator of hepcidin expression in murine and human cells. Blood. 2009 Jul 2;114(1):181–6.

35. Kautz L, Jung G, Valore EV, Rivella S, Nemeth E, Ganz T. Identification of erythroferrone as an erythroid regulator of iron metabolism. Nat Genet. 2014 Jul;46(7):678–84.

36. Bersch N, Groopman JE, Golde DW. Natural and biosynthetic insulin stimulates the growth of human erythroid progenitors in vitro. J Clin Endocrinol Metab. 1982 Dec;55(6):1209–11.

37. Kurtz A, Jelkmann W, Bauer C. Insulin stimulates erythroid colony formation independently of erythropoietin. Br J Haematol. 1983 Feb;53(2):311–6.

38. Stonestreet BS, Goldstein M, Oh W, Widness JA. Effects of prolonged hyperinsulinemia on erythropoiesis in fetal sheep. Am J Physiol. 1989 Nov;257(5 Pt 2):R1199–204.

39. Murray R, Jacob M, Varghese J. Plasma Proteins & Immunoglobulins. In: Harpers Illustrated Biochemistry. 30th edition. McGraw Hill; 2012. p. 629–49.

40. Hubert N, Hentze MW. Previously uncharacterized isoforms of divalent metal transporter (DMT)-1: implications for regulation and cellular function. Proc Natl Acad Sci U S A. 2002 Sep 17;99(19):12345–50.

41. McKie AT, Barrow D, Latunde-Dada GO, Rolfs A, Sager G, Mudaly E, et al. An Iron-Regulated Ferric Reductase Associated with the Absorption of Dietary Iron. Science. 2001 Mar 2;291(5509):1755–9.

42. Andrews NC. When is a heme transporter not a heme transporter? When it's a folate transporter. Cell Metab. 2007 Jan;5(1):5–6.

43. West AR, Oates PS. Mechanisms of heme iron absorption: Current questions and controversies. World J Gastroenterol WJG. 2008 Jul 14;14(26):4101–10.

44. McKie AT, Marciani P, Rolfs A, Brennan K, Wehr K, Barrow D, et al. A Novel Duodenal Iron-Regulated Transporter, IREG1, Implicated in the Basolateral Transfer of Iron to the Circulation. Mol Cell. 2000 Feb;5(2):299–309.

45. Donovan A, Brownlie A, Zhou Y, Shepard J, Pratt SJ, Moynihan J, et al. Positional cloning of zebrafish ferroportin1 identifies a conserved vertebrate iron exporter. Nature. 2000 Feb 17;403(6771):776–81.

46. Vulpe CD, Kuo YM, Murphy TL, Cowley L, Askwith C, Libina N, et al. Hephaestin, a ceruloplasmin homologue implicated in intestinal iron transport, is defective in the sla mouse. Nat Genet. 1999 Feb;21(2):195–9.

47. Brissot P, Ropert M, Le Lan C, Loréal O. Non-transferrin bound iron: a key role in iron overload and iron toxicity. Biochim Biophys Acta. 2012 Mar;1820(3):403–10.

48. White C, Yuan X, Schmidt PJ, Bresciani E, Samuel TK, Campagna D, et al. HRG1 is essential for heme transport from the phagolysosome of macrophages during erythrophagocytosis. Cell Metab. 2013 Feb 5;17(2):261–70.

49. Shi H, Bencze KZ, Stemmler TL, Philpott CC. A cytosolic iron chaperone that delivers iron to ferritin. Science. 2008 May 30;320(5880):1207–10.

50. Mancias JD, Wang X, Gygi SP, Harper JW, Kimmelman AC. Quantitative proteomics identifies NCOA4 as the cargo receptor mediating ferritinophagy. Nature. 2014 May 1;509(7498):105–9.

51. Mancias JD, Pontano Vaites L, Nissim S, Biancur DE, Kim AJ, Wang X, et al. Ferritinophagy via NCOA4 is required for erythropoiesis and is regulated by iron dependent HERC2-mediated proteolysis. eLife. 2015 Oct 5;4.

52. Cohen LA, Gutierrez L, Weiss A, Leichtmann-Bardoogo Y, Zhang D, Crooks DR, et al. Serum ferritin is derived primarily from macrophages through a nonclassical secretory pathway. Blood. 2010 Sep 2;116(9):1574–84.

53. Ferraro S, Mozzi R, Panteghini M. Revaluating serum ferritin as a marker of body iron stores in the traceability era. Clin Chem Lab Med. 2012 Nov;50(11):1911–6.

54. Lou D-Q, Nicolas G, Lesbordes J-C, Viatte L, Grimber G, Szajnert M-F, et al. Functional differences between hepcidin 1 and 2 in transgenic mice. Blood. 2004 Apr 1;103(7):2816–21.

55. Valore EV, Ganz T. Posttranslational processing of hepcidin in human hepatocytes is mediated by the prohormone convertase furin. Blood Cells Mol Dis. 2008 Feb;40(1):132–8.

56. Itkonen O, Stenman U-H, Parkkinen J, Soliymani R, Baumann M, Hämäläinen E. Binding of hepcidin to plasma proteins. Clin Chem. 2012 Jul;58(7):1158–60.

57. Peslova G, Petrak J, Kuzelova K, Hrdy I, Halada P, Kuchel PW, et al. Hepcidin, the hormone of iron metabolism, is bound specifically to alpha-2-macroglobulin in blood. Blood. 2009 Jun 11;113(24):6225–36.

58. Nemeth E, Preza GC, Jung C-L, Kaplan J, Waring AJ, Ganz T. The N-terminus of hepcidin is essential for its interaction with ferroportin: structure-function study. Blood. 2006 Jan 1;107(1):328–33.

59. Jordan JB, Poppe L, Haniu M, Arvedson T, Syed R, Li V, et al. Hepcidin revisited, disulfide connectivity, dynamics, and structure. J Biol Chem. 2009 Sep 4;284(36):24155–67.

60. Sham RL, Phatak PD, Nemeth E, Ganz T. Hereditary hemochromatosis due to resistance to hepcidin: high hepcidin concentrations in a family with C326S ferroportin mutation. Blood. 2009 Jul 9;114(2):493–4.

61. Rice AE, Mendez MJ, Hokanson CA, Rees DC, Björkman PJ. Investigation of the biophysical and cell biological properties of ferroportin, a multipass integral membrane protein iron exporter. J Mol Biol. 2009 Feb 27;386(3):717–32.

62. Liu X-B, Yang F, Haile DJ. Functional consequences of ferroportin 1 mutations. Blood Cells Mol Dis. 2005 Aug;35(1):33–46.

63. Qiao B, Sugianto P, Fung E, Del-Castillo-Rueda A, Moran-Jimenez M-J, Ganz T, et al. Hepcidin-induced endocytosis of ferroportin is dependent on ferroportin ubiquitination. Cell Metab. 2012 Jun 6;15(6):918–24.

64. Ross SL, Tran L, Winters A, Lee K-J, Plewa C, Foltz I, et al. Molecular mechanism of hepcidin-mediated ferroportin internalization requires ferroportin lysines, not tyrosines or JAK-STAT. Cell Metab. 2012 Jun 6;15(6):905–17.

65. Bergamaschi G, Di Sabatino A, Pasini A, Ubezio C, Costanzo F, Grataroli D, et al. Intestinal expression of genes implicated in iron absorption and their regulation by hepcidin. Clin Nutr Edinb Scotl. 2016 Sep 30;

66. Babitt JL, Huang FW, Xia Y, Sidis Y, Andrews NC, Lin HY. Modulation of bone morphogenetic protein signaling in vivo regulates systemic iron balance. J Clin Invest. 2007 Jul;117(7):1933–9.

67. Xia Y, Babitt JL, Sidis Y, Chung RT, Lin HY. Hemojuvelin regulates hepcidin expression via a selective subset of BMP ligands and receptors independently of neogenin. Blood. 2008 May 15;111(10):5195–204.

68. Steinbicker AU, Bartnikas TB, Lohmeyer LK, Leyton P, Mayeur C, Kao SM, et al. Perturbation of hepcidin expression by BMP type I receptor deletion induces iron overload in mice. Blood. 2011 Oct 13;118(15):4224–30.

69. Truksa J, Lee P, Beutler E. Two BMP responsive elements, STAT, and bZIP/HNF4/COUP motifs of the hepcidin promoter are critical for BMP, SMAD1, and HJV responsiveness. Blood. 2009 Jan 15;113(3):688–95.

70. Casanovas G, Spasic MV, Casu C, Rivella S, Strelau J, Unsicker K, et al. The murine growth differentiation factor 15 is not essential for systemic iron homeostasis in phlebotomized mice. Haematologica. 2013 Mar;98(3):444–7.

71. Wang R-H, Li C, Xu X, Zheng Y, Xiao C, Zerfas P, et al. A role of SMAD4 in iron metabolism through the positive regulation of hepcidin expression. Cell Metab. 2005 Dec;2(6):399–409.

72. Andriopoulos B, Corradini E, Xia Y, Faasse SA, Chen S, Grgurevic L, et al. BMP6 is a key endogenous regulator of hepcidin expression and iron metabolism. Nat Genet. 2009 Apr;41(4):482–7.

73. Koch P-S, Olsavszky V, Ulbrich F, Sticht C, Demory A, Leibing T, et al. Angiocrine Bmp2 signaling in murine liver controls normal iron homeostasis. Blood. 2017 Jan 26;129(4):415–9.

74. Niederkofler V, Salie R, Arber S. Hemojuvelin is essential for dietary iron sensing, and its mutation leads to severe iron overload. J Clin Invest. 2005 Aug;115(8):2180–6.

75. Papanikolaou G, Samuels ME, Ludwig EH, MacDonald MLE, Franchini PL, Dubé M-P, et al. Mutations in HFE2 cause iron overload in chromosome 1q-linked juvenile hemochromatosis. Nat Genet. 2004 Jan;36(1):77–82.

76. Huang FW, Pinkus JL, Pinkus GS, Fleming MD, Andrews NC. A mouse model of juvenile hemochromatosis. J Clin Invest. 2005 Aug;115(8):2187–91.

77. Finberg KE, Whittlesey RL, Fleming MD, Andrews NC. Down-regulation of Bmp/Smad signaling by Tmprss6 is required for maintenance of systemic iron homeostasis. Blood. 2010 May 6;115(18):3817–26.

78. Folgueras AR, de Lara FM, Pendás AM, Garabaya C, Rodríguez F, Astudillo A, et al. Membrane-bound serine protease matriptase-2 (Tmprss6) is an essential regulator of iron homeostasis. Blood. 2008 Sep 15;112(6):2539–45.

79. Silvestri L, Pagani A, Nai A, De Domenico I, Kaplan J, Camaschella C. The serine protease matriptase-2 (TMPRSS6) inhibits hepcidin activation by cleaving membrane hemojuvelin. Cell Metab. 2008 Dec;8(6):502–11.

80. Lee D-H, Lee D-H, Zhou L-J, Zhou L-J, Zhou Z, Xie J-X, et al. Neogenin inhibits HJV secretion and regulates BMP-induced hepcidin expression and iron homeostasis. Blood. 2010 Apr 15;115(15):3136–45.

81. Zhang A-S, West AP, Wyman AE, Bjorkman PJ, Enns CA. Interaction of hemojuvelin with neogenin results in iron accumulation in human embryonic kidney 293 cells. J Biol Chem. 2005 Oct 7;280(40):33885–94.

82. Enns CA, Ahmed R, Zhang A-S. Neogenin interacts with matriptase-2 to facilitate hemojuvelin cleavage. J Biol Chem. 2012 Oct 12;287(42):35104–17.

83. Goswami T, Andrews NC. Hereditary hemochromatosis protein, HFE, interaction with transferrin receptor 2 suggests a molecular mechanism for mammalian iron sensing. J Biol Chem. 2006 Sep 29;281(39):28494–8.

84. Ramos E, Kautz L, Rodriguez R, Hansen M, Gabayan V, Ginzburg Y, et al. Evidence for distinct pathways of hepcidin regulation by acute and chronic iron loading in mice. Hepatol Baltim Md. 2011 Apr;53(4):1333–41.

85. Lebrón JA, West AP, Bjorkman PJ. The hemochromatosis protein HFE competes with transferrin for binding to the transferrin receptor. J Mol Biol. 1999 Nov 19;294(1):239–45.

86. D'Alessio F, Hentze MW, Muckenthaler MU. The hemochromatosis proteins HFE, TfR2, and HJV form a membrane-associated protein complex for hepcidin regulation. J Hepatol. 2012 Nov;57(5):1052–60.

87. Meynard D, Babitt JL, Lin HY. The liver: conductor of systemic iron balance. Blood. 2014 Jan 9;123(2):168–76.

88. Kautz L, Meynard D, Monnier A, Darnaud V, Bouvet R, Wang R-H, et al. Iron regulates phosphorylation of Smad1/5/8 and gene expression of Bmp6, Smad7, Id1, and Atoh8 in the mouse liver. Blood. 2008 Aug 15;112(4):1503–9.

89. Corradini E, Meynard D, Wu Q, Chen S, Ventura P, Pietrangelo A, et al. Serum and liver iron differently regulate the bone morphogenetic protein 6 (BMP6)-SMAD signaling pathway in mice. Hepatol Baltim Md. 2011 Jul;54(1):273–84.

90. Meynard D, Kautz L, Darnaud V, Canonne-Hergaux F, Coppin H, Roth M-P. Lack of the bone morphogenetic protein BMP6 induces massive iron overload. Nat Genet. 2009 Apr;41(4):478–81.

91. Enns CA, Ahmed R, Wang J, Ueno A, Worthen C, Tsukamoto H, et al. Increased iron loading induces Bmp6 expression in the non-parenchymal cells of the liver independent of the BMP-signaling pathway. PloS One. 2013;8(4):e60534.

92. Canali S, Zumbrennen-Bullough KB, Core AB, Wang C-Y, Nairz M, Bouley R, et al. Endothelial cells produce bone morphogenetic protein 6 required for iron homeostasis in mice. Blood. 2017 Jan 26;129(4):405–14.

93. Feng Q, Migas MC, Waheed A, Britton RS, Fleming RE. Ferritin upregulates hepatic expression of bone morphogenetic protein 6 and hepcidin in mice. Am J Physiol Gastrointest Liver Physiol. 2012 Jun 15;302(12):G1397–404.

94. Meynard D, Vaja V, Sun CC, Corradini E, Chen S, López-Otín C, et al. Regulation of TMPRSS6 by BMP6 and iron in human cells and mice. Blood. 2011 Jul 21;118(3):747–56.

95. Pak M, Lopez MA, Gabayan V, Ganz T, Rivera S. Suppression of hepcidin during anemia requires erythropoietic activity. Blood. 2006 Dec 1;108(12):3730–5.

96. Vokurka M, Krijt J, Sulc K, Necas E. Hepcidin mRNA levels in mouse liver respond to inhibition of erythropoiesis. Physiol Res. 2006;55(6):667–74.

97. Sasaki Y, Noguchi-Sasaki M, Yasuno H, Yorozu K, Shimonaka Y. Erythropoietin stimulation decreases hepcidin expression through hematopoietic activity on bone marrow cells in mice. Int J Hematol. 2012 Dec;96(6):692–700.

98. Cazzola M, Finch CA. Iron balance in thalassemia. Prog Clin Biol Res. 1989;309:93–100.

99. Pippard MJ, Callender ST, Warner GT, Weatherall DJ. Iron absorption and loading in beta-thalassaemia intermedia. Lancet Lond Engl. 1979 Oct 20;2(8147):819–21.

100. Pasricha S-R, McHugh K, Drakesmith H. Regulation of Hepcidin by Erythropoiesis: The Story So Far. Annu Rev Nutr. 2016 Jul 17;36:417–34.

101. Mirciov CSG, Wilkins SJ, Dunn LA, Anderson GJ, Frazer DM. Characterization of Putative Erythroid Regulators of Hepcidin in Mouse Models of Anemia. PloS One. 2017;12(1):e0171054.

102. Kautz L, Jung G, Nemeth E, Ganz T. Erythroferrone contributes to recovery from anemia of inflammation. Blood. 2014 Oct 16;124(16):2569–74.

103. Kautz L, Jung G, Du X, Gabayan V, Chapman J, Nasoff M, et al. Erythroferrone contributes to hepcidin suppression and iron overload in a mouse model of β-thalassemia. Blood. 2015 Oct 22;126(17):2031–7.

104. Merryweather-Clarke AT, Atzberger A, Soneji S, Gray N, Clark K, Waugh C, et al. Global gene expression analysis of human erythroid progenitors. Blood. 2011 Mar 31;117(13):e96–108.

105. Casanovas G, Swinkels DW, Altamura S, Schwarz K, Laarakkers CM, Gross H-J, et al. Growth differentiation factor 15 in patients with congenital dyserythropoietic anaemia (CDA) type II. J Mol Med Berl Ger. 2011 Aug;89(8):811–6.

106. Jones E, Pasricha S-R, Allen A, Evans P, Fisher CA, Wray K, et al. Hepcidin is suppressed by erythropoiesis in hemoglobin E β-thalassemia and β-thalassemia trait. Blood. 2015 Jan 29;125(5):873–80.

107. Peyssonnaux C, Zinkernagel AS, Schuepbach RA, Rankin E, Vaulont S, Haase VH, et al. Regulation of iron homeostasis by the hypoxia-inducible transcription factors (HIFs). J Clin Invest. 2007 Jul;117(7):1926–32.

108. Mastrogiannaki M, Matak P, Mathieu JRR, Delga S, Mayeux P, Vaulont S, et al. Hepatic hypoxia-inducible factor-2 down-regulates hepcidin expression in mice through an erythropoietin-mediated increase in erythropoiesis. Haematologica. 2012 Jun;97(6):827–34.

109. Volke M, Gale DP, Maegdefrau U, Schley G, Klanke B, Bosserhoff A-K, et al. Evidence for a lack of a direct transcriptional suppression of the iron regulatory peptide hepcidin by hypoxia-inducible factors. PloS One. 2009 Nov 18;4(11):e7875.

110. Sonnweber T, Nachbaur D, Schroll A, Nairz M, Seifert M, Demetz E, et al. Hypoxia induced downregulation of hepcidin is mediated by platelet derived growth factor BB. Gut. 2014 Dec;63(12):1951–9.

111. Michels K, Nemeth E, Ganz T, Mehrad B. Hepcidin and Host Defense against Infectious Diseases. PLoS Pathog. 2015 Aug;11(8):e1004998.

112. Nemeth E, Rivera S, Gabayan V, Keller C, Taudorf S, Pedersen BK, et al. IL-6 mediates hypoferremia of inflammation by inducing the synthesis of the iron regulatory hormone hepcidin. J Clin Invest. 2004 May;113(9):1271–6.

113. Wrighting DM, Andrews NC. Interleukin-6 induces hepcidin expression through STAT3. Blood. 2006 Nov 1;108(9):3204–9.

114. Verga Falzacappa MV, Vujic Spasic M, Kessler R, Stolte J, Hentze MW, Muckenthaler MU. STAT3 mediates hepatic hepcidin expression and its inflammatory stimulation. Blood. 2007 Jan 1;109(1):353–8.

115. Theurl I, Schroll A, Nairz M, Seifert M, Theurl M, Sonnweber T, et al. Pathways for the regulation of hepcidin expression in anemia of chronic disease and iron deficiency anemia in vivo. Haematologica. 2011 Dec;96(12):1761–9.

116. Besson-Fournier C, Latour C, Kautz L, Bertrand J, Ganz T, Roth M-P, et al. Induction of activin B by inflammatory stimuli up-regulates expression of the iron-regulatory peptide hepcidin through Smad1/5/8 signaling. Blood. 2012 Jul 12;120(2):431–9.

117. Canali S, Core AB, Zumbrennen-Bullough KB, Merkulova M, Wang C-Y, Schneyer AL, et al. Activin B Induces Noncanonical SMAD1/5/8 Signaling via BMP Type I Receptors in Hepatocytes: Evidence for a Role in Hepcidin Induction by Inflammation in Male Mice. Endocrinology. 2016 Mar;157(3):1146–62.

118. Vecchi C, Montosi G, Zhang K, Lamberti I, Duncan SA, Kaufman RJ, et al. ER stress controls iron metabolism through induction of hepcidin. Science. 2009 Aug 14;325(5942):877–80.

119. Canali S, Vecchi C, Garuti C, Montosi G, Babitt JL, Pietrangelo A. The SMAD Pathway Is Required for Hepcidin Response During Endoplasmic Reticulum Stress. Endocrinology. 2016 Oct;157(10):3935–45.

120. Vecchi C, Montosi G, Garuti C, Corradini E, Sabelli M, Canali S, et al. Gluconeogenic signals regulate iron homeostasis via hepcidin in mice. Gastroenterology. 2014 Apr;146(4):1060–9.

121. Saltiel AR, Pessin JE. Mechanisms of Insulin Action. Springer Science & Business Media; 2007. 223 p.

122. Taniguchi CM, Emanuelli B, Kahn CR. Critical nodes in signalling pathways: insights into insulin action. Nat Rev Mol Cell Biol. 2006 Feb;7(2):85.

123. Pessin JE, Saltiel AR. Signaling pathways in insulin action: molecular targets of insulin resistance. J Clin Invest. 2000 Jul;106(2):165–9.

124. Chiang SH, Baumann CA, Kanzaki M, Thurmond DC, Watson RT, Neudauer CL, et al. Insulin-stimulated GLUT4 translocation requires the CAP-dependent activation of TC10. Nature. 2001 Apr 19;410(6831):944–8.

125. Baumann CA, Ribon V, Kanzaki M, Thurmond DC, Mora S, Shigematsu S, et al. CAP defines a second signalling pathway required for insulin-stimulated glucose transport. Nature. 2000 Sep 14;407(6801):202–7.

126. Foretz M, Guichard C, Ferré P, Foufelle F. Sterol regulatory element binding protein-1c is a major mediator of insulin action on the hepatic expression of glucokinase and lipogenesis-related genes. Proc Natl Acad Sci U S A. 1999 Oct 26;96(22):12737–42.

127. Titchenell PM, Lazar MA, Birnbaum MJ. Unraveling the Regulation of Hepatic Metabolism by Insulin. Trends Endocrinol Metab. 2017 Jul 1;28(7):497–505.

128. Saltiel AR, Kahn CR. Insulin signalling and the regulation of glucose and lipid metabolism. Nature. 2001 Dec 13;414(6865):799–806.

129. Rizza RA. Pathogenesis of fasting and postprandial hyperglycemia in type 2 diabetes: implications for therapy. Diabetes. 2010 Nov;59(11):2697–707.

130. Jiang G, Zhang BB. Glucagon and regulation of glucose metabolism. Am J Physiol Endocrinol Metab. 2003 Apr;284(4):E671–8.

131. Lin HV, Accili D. Hormonal regulation of hepatic glucose production in health and disease. Cell Metab. 2011 Jul 6;14(1):9–19.

132. Edgerton DS, Kraft G, Smith M, Farmer B, Williams PE, Coate KC, et al. Insulin's direct hepatic effect explains the inhibition of glucose production caused by insulin secretion. JCI Insight [Internet]. 2017 Mar 23 [cited 2017 Dec 29];2(6). Available from: https://insight.jci.org/articles/view/91863

133. Titchenell PM, Chu Q, Monks BR, Birnbaum MJ. Hepatic insulin signalling is dispensable for suppression of glucose output by insulin in vivo. Nat Commun. 2015 May 12;6:7078.

134. Titchenell PM, Quinn WJ, Lu M, Chu Q, Lu W, Li C, et al. Direct Hepatocyte Insulin Signaling Is Required for Lipogenesis but Is Dispensable for the Suppression of Glucose Production. Cell Metab. 2016 Jun 14;23(6):1154–66.

135. Lu M, Wan M, Leavens KF, Chu Q, Monks BR, Fernandez S, et al. Insulin regulates liver metabolism in vivo in the absence of hepatic Akt and Foxo1. Nat Med. 2012 Mar;18(3):388–95.

136. Perry RJ, Camporez J-PG, Kursawe R, Titchenell PM, Zhang D, Perry CJ, et al. Hepatic acetyl CoA links adipose tissue inflammation to hepatic insulin resistance and type 2 diabetes. Cell. 2015 Feb 12;160(4):745–58.

137. Obici S, Zhang BB, Karkanias G, Rossetti L. Hypothalamic insulin signaling is required for inhibition of glucose production. Nat Med. 2002 Dec;8(12):1376.

138. Pocai A, Obici S, Schwartz GJ, Rossetti L. A brain-liver circuit regulates glucose homeostasis. Cell Metab. 2005 Jan 1;1(1):53–61.

139. Könner AC, Janoschek R, Plum L, Jordan SD, Rother E, Ma X, et al. Insulin Action in AgRP-Expressing Neurons Is Required for Suppression of Hepatic Glucose Production. Cell Metab. 2007 Jun 6;5(6):438–49.

140. Inoue H, Ogawa W, Asakawa A, Okamoto Y, Nishizawa A, Matsumoto M, et al. Role of hepatic STAT3 in brain-insulin action on hepatic glucose production. Cell Metab. 2006 Apr 1;3(4):267–75.

141. Hardie DG, Ross FA, Hawley SA. AMPK: a nutrient and energy sensor that maintains energy homeostasis. Nat Rev Mol Cell Biol. 2012 Apr;13(4):251–62.

142. Yamauchi T, Kamon J, Minokoshi Y, Ito Y, Waki H, Uchida S, et al. Adiponectin stimulates glucose utilization and fatty-acid oxidation by activating AMP-activated protein kinase. Nat Med. 2002 Nov;8(11):1288.

143. Zhou G, Myers R, Li Y, Chen Y, Shen X, Fenyk-Melody J, et al. Role of AMP-activated protein kinase in mechanism of metformin action. J Clin Invest. 2001 Oct 15;108(8):1167–74.

144. Shaw RJ, Kosmatka M, Bardeesy N, Hurley RL, Witters LA, DePinho RA, et al. The tumor suppressor LKB1 kinase directly activates AMP-activated kinase and regulates apoptosis in response to energy stress. Proc Natl Acad Sci U S A. 2004 Mar 9;101(10):3329–35.

145. Lee J-M, Seo W-Y, Song K-H, Chanda D, Kim YD, Kim D-K, et al. AMPK-dependent repression of hepatic gluconeogenesis via disruption of CREB.CRTC2 complex by orphan nuclear receptor small heterodimer partner. J Biol Chem. 2010 Oct 15;285(42):32182–91.

146. Johanns M, Lai Y-C, Hsu M-F, Jacobs R, Vertommen D, Van Sande J, et al. AMPK antagonizes hepatic glucagon-stimulated cyclic AMP signalling via phosphorylation-induced activation of cyclic nucleotide phosphodiesterase 4B. Nat Commun. 2016 Mar 8;7:10856.

147. Kasper DL, Jameson JL, Hauser S, Loscalzo J, Fauci AS, Longo D. Harrison's Principles of Internal Medicine 19/E (Vol.1 & Vol.2). McGraw-Hill Education; 2015. 3000 p.

148. WHO | Diabetes [Internet]. WHO. [cited 2017 Dec 22]. Available from: http://www.who.int/mediacentre/factsheets/fs312/en/

149. IDF diabetes atlas - Home [Internet]. [cited 2017 Dec 22]. Available from: http://www.diabetesatlas.org/

150. Hwang CK, Han PV, Zabetian A, Ali MK, Narayan KMV. Rural diabetes prevalence quintuples over twenty-five years in low- and middle-income countries: a systematic review and meta-analysis. Diabetes Res Clin Pract. 2012 Jun;96(3):271–85.

151. Anjana RM, Deepa M, Pradeepa R, Mahanta J, Narain K, Das HK, et al. Prevalence of diabetes and prediabetes in 15 states of India: results from the ICMR-INDIAB population-based cross-sectional study. Lancet Diabetes Endocrinol. 2017 Aug;5(8):585–96.

152. Bellamy L, Casas J-P, Hingorani AD, Williams D. Type 2 diabetes mellitus after gestational diabetes: a systematic review and meta-analysis. The Lancet. 2009 May 23;373(9677):1773–9.

153. American Diabetes Association. 2. Classification and Diagnosis of Diabetes. Diabetes Care. 2017 Jan;40(Suppl 1):S11–24.

154. Cnop M, Welsh N, Jonas J-C, Jörns A, Lenzen S, Eizirik DL. Mechanisms of Pancreatic β-Cell Death in Type 1 and Type 2 Diabetes: Many Differences, Few Similarities. Diabetes. 2005 Dec 1;54(suppl 2):S97–107.

155. Eizirik DL, Colli ML, Ortis F. The role of inflammation in insulitis and β-cell loss in type 1 diabetes. Nat Rev Endocrinol. 2009 Apr;5(4):219.

156. Taplin CE, Barker JM. Autoantibodies in type 1 diabetes. Autoimmunity. 2008 Jan 1;41(1):11–8.

157. Kahn SE. The relative contributions of insulin resistance and beta-cell dysfunction to the pathophysiology of Type 2 diabetes. Diabetologia. 2003 Jan 1;46(1):3–19.

158. Kahn SE, Hull RL, Utzschneider KM. Mechanisms linking obesity to insulin resistance and type 2 diabetes. Nature. 2006 Dec 14;444(7121):840–6.

159. WHO | Obesity and overweight [Internet]. WHO. [cited 2017 Dec 21]. Available from: http://www.who.int/mediacentre/factsheets/fs311/en/

160. Fontana L, Eagon JC, Trujillo ME, Scherer PE, Klein S. Visceral Fat Adipokine Secretion Is Associated With Systemic Inflammation in Obese Humans. Diabetes. 2007 Apr 1;56(4):1010–3.

161. Wellen KE, Hotamisligil GS. Inflammation, stress, and diabetes. J Clin Invest. 2005 May;115(5):1111–9.

162. Scherer PE. Adipose tissue: from lipid storage compartment to endocrine organ. Diabetes. 2006 Jun;55(6):1537–45.

163. Shoelson SE, Lee J, Goldfine AB. Inflammation and insulin resistance. J Clin Invest. 2006 Jul;116(7):1793–801.

164. Strissel KJ, Stancheva Z, Miyoshi H, Perfield JW, DeFuria J, Jick Z, et al. Adipocyte death, adipose tissue remodeling, and obesity complications. Diabetes. 2007 Dec;56(12):2910–8.

165. Weisberg SP, McCann D, Desai M, Rosenbaum M, Leibel RL, Ferrante AW. Obesity is associated with macrophage accumulation in adipose tissue. J Clin Invest. 2003 Dec;112(12):1796–808.

166. Xu H, Barnes GT, Yang Q, Tan G, Yang D, Chou CJ, et al. Chronic inflammation in fat plays a crucial role in the development of obesity-related insulin resistance. J Clin Invest. 2003 Dec;112(12):1821–30.

167. Hill AA, Reid Bolus W, Hasty AH. A decade of progress in adipose tissue macrophage biology. Immunol Rev. 2014 Nov;262(1):134–52.

168. Boden G. Role of fatty acids in the pathogenesis of insulin resistance and NIDDM. Diabetes. 1997 Jan;46(1):3–10.

169. Carey DG, Jenkins AB, Campbell LV, Freund J, Chisholm DJ. Abdominal fat and insulin resistance in normal and overweight women: Direct measurements reveal a strong relationship in subjects at both low and high risk of NIDDM. Diabetes. 1996 May;45(5):633–8.

170. Cnop M, Landchild MJ, Vidal J, Havel PJ, Knowles NG, Carr DR, et al. The concurrent accumulation of intra-abdominal and subcutaneous fat explains the association between insulin resistance and plasma leptin concentrations : distinct metabolic effects of two fat compartments. Diabetes. 2002 Apr;51(4):1005–15.

171. Maeda K, Okubo K, Shimomura I, Mizuno K, Matsuzawa Y, Matsubara K. Analysis of an expression profile of genes in the human adipose tissue. Gene. 1997 May 6;190(2):227–35.

172. Montague CT, O'Rahilly S. The perils of portliness: causes and consequences of visceral adiposity. Diabetes. 2000 Jun;49(6):883–8.

173. Kim SP, Ellmerer M, Van Citters GW, Bergman RN. Primacy of hepatic insulin resistance in the development of the metabolic syndrome induced by an isocaloric moderate-fat diet in the dog. Diabetes. 2003 Oct;52(10):2453–60.

174. Chusyd DE, Wang D, Huffman DM, Nagy TR. Relationships between Rodent White Adipose Fat Pads and Human White Adipose Fat Depots. Front Nutr [Internet]. 2016 Apr 19;3. Available from: https://www.ncbi.nlm.nih.gov/pmc/articles/PMC4835715/

175. Casteilla L, Pénicaud L, Cousin B, Calise D. Choosing an adipose tissue depot for sampling: factors in selection and depot specificity. Methods Mol Biol Clifton NJ. 2008;456:23–38.

176. Krssak M, Petersen KF, Dresner A, DiPietro L, Vogel SM, Rothman DL, et al. Intramyocellular lipid concentrations are correlated with insulin sensitivity in humans: a 1H NMR spectroscopy study. Diabetologia. 1999 Jan 1;42(1):113–6.

177. Jacob S, Machann J, Rett K, Brechtel K, Volk A, Renn W, et al. Association of increased intramyocellular lipid content with insulin resistance in lean nondiabetic offspring of type 2 diabetic subjects. Diabetes. 1999 May 1;48(5):1113–9.

178. Virkamäki A, Korsheninnikova E, Seppälä-Lindroos A, Vehkavaara S, Goto T, Halavaara J, et al. Intramyocellular Lipid Is Associated With Resistance to In Vivo Insulin Actions on Glucose Uptake, Antilipolysis, and Early Insulin Signaling Pathways in Human Skeletal Muscle. Diabetes. 2001 Oct 1;50(10):2337–43.

179. Utzschneider KM, Kahn SE. The Role of Insulin Resistance in Nonalcoholic Fatty Liver Disease. J Clin Endocrinol Metab. 2006 Dec 1;91(12):4753–61.

180. Samuel VT, Shulman GI. Mechanisms for insulin resistance: common threads and missing links. Cell. 2012 Mar 2;148(5):852–71.

181. DeFronzo RA. Insulin resistance, lipotoxicity, type 2 diabetes and atherosclerosis: the missing links. The Claude Bernard Lecture 2009. Diabetologia. 2010 Jul 1;53(7):1270–87.

182. Perry RJ, Samuel VT, Petersen KF, Shulman GI. The role of hepatic lipids in hepatic insulin resistance and type 2 diabetes. Nature. 2014 Jun;510(7503):84.

183. Chavez JA, Summers SA. A ceramide-centric view of insulin resistance. Cell Metab. 2012 May 2;15(5):585–94.

184. Prentki M, Nolan CJ. Islet β cell failure in type 2 diabetes. J Clin Invest. 2006 Jul 3;116(7):1802–12.

185. Halban PA, Polonsky KS, Bowden DW, Hawkins MA, Ling C, Mather KJ, et al. β-Cell Failure in Type 2 Diabetes: Postulated Mechanisms and Prospects for Prevention and Treatment. Diabetes Care. 2014 Jun 1;37(6):1751–8.

186. Weyer C, Bogardus C, Mott DM, Pratley RE. The natural history of insulin secretory dysfunction and insulin resistance in the pathogenesis of type 2 diabetes mellitus. J Clin Invest. 1999 Sep 15;104(6):787–94.

187. Fernández-Real JM, McClain D, Manco M. Mechanisms Linking Glucose Homeostasis and Iron Metabolism Toward the Onset and Progression of Type 2 Diabetes. Diabetes Care. 2015 Nov;38(11):2169–76.

188. ROOT HF. Insulin Resistance and Bronze Diabetes. N Engl J Med. 1929 Aug 1;201(5):201–6.

189. Walters GO, Miller FM, Worwood M. Serum ferritin concentration and iron stores in normal subjects. J Clin Pathol. 1973 Oct;26(10):770–2.

190. Beutler E, Felitti V, Ho NJ, Gelbart T. Relationship of body iron stores to levels of serum ferritin, serum iron, unsaturated iron binding capacity and transferrin saturation in patients with iron storage disease. Acta Haematol. 2002;107(3):145–9.

191. Jacobs A, Miller F, Worwood M, Beamish MR, Wardrop CA. Ferritin in the serum of normal subjects and patients with iron deficiency and iron overload. Br Med J. 1972 Oct 28;4(5834):206–8.

192. Kunutsor SK, Apekey TA, Walley J, Kain K. Ferritin levels and risk of type 2 diabetes mellitus: an updated systematic review and meta-analysis of prospective evidence. Diabetes Metab Res Rev. 2013 May;29(4):308–18.

193. Orban E, Schwab S, Thorand B, Huth C. Association of iron indices and type 2 diabetes: a meta-analysis of observational studies. Diabetes Metab Res Rev. 2014 Jul;30(5):372–94.

194. Podmore C, Meidtner K, Schulze MB, Scott RA, Ramond A, Butterworth AS, et al. Association of Multiple Biomarkers of Iron Metabolism and Type 2 Diabetes: The EPIC-InterAct Study. Diabetes Care. 2016 Apr;39(4):572–81.

195. Pietrangelo A. Hereditary Hemochromatosis: Pathogenesis, Diagnosis, and Treatment. Gastroenterology [Internet]. 2010 Jun 11 [cited 2010 Jul 17]; Available from: http://www.ncbi.nlm.nih.gov/pubmed/20542038

196. Buysschaert M, Paris I, Selvais P, Hermans MP. Clinical aspects of diabetes secondary to idiopathic haemochromatosis in French-speaking Belgium. Diabetes Metab. 1997 Sep;23(4):308–13.

197. Moirand R, Adams PC, Bicheler V, Brissot P, Deugnier Y. Clinical features of genetic hemochromatosis in women compared with men. Ann Intern Med. 1997 Jul 15;127(2):105–10.

198. Hatunic M, Finucane FM, Norris S, Pacini G, Nolan JJ. Glucose metabolism after normalization of markers of iron overload by venesection in subjects with hereditary hemochromatosis. Metabolism [Internet]. 2010 Jul 30 [cited 2010 Sep 28]; Available from: http://www.ncbi.nlm.nih.gov/pubmed/20673928

199. Hramiak IM, Finegood DT, Adams PC. Factors affecting glucose tolerance in hereditary hemochromatosis. Clin Investig Med Med Clin Exp. 1997 Apr;20(2):110–8.

200. Mendler MH, Turlin B, Moirand R, Jouanolle AM, Sapey T, Guyader D, et al. Insulin resistance-associated hepatic iron overload. Gastroenterology. 1999 Nov;117(5):1155–63.

201. Abraham D, Rogers J, Gault P, Kushner JP, McClain DA. Increased insulin secretory capacity but decreased insulin sensitivity after correction of iron overload by phlebotomy in hereditary haemochromatosis. Diabetologia. 2006 Nov;49(11):2546–51.

202. Gardenghi S, Marongiu MF, Ramos P, Guy E, Breda L, Chadburn A, et al. Ineffective erythropoiesis in beta-thalassemia is characterized by increased iron absorption mediated by down-regulation of hepcidin and up-regulation of ferroportin. Blood. 2007 Jun 1;109(11):5027–35.

203. Borgna-Pignatti C, Rugolotto S, De Stefano P, Piga A, Di Gregorio F, Gamberini MR, et al. Survival and disease complications in thalassemia major. Ann N Y Acad Sci. 1998 Jun 30;850:227–31.

204. Vogiatzi MG, Macklin EA, Trachtenberg FL, Fung EB, Cheung AM, Vichinsky E, et al. Differences in the prevalence of growth, endocrine and vitamin D abnormalities among the various thalassaemia syndromes in North America. Br J Haematol. 2009 Sep;146(5):546–56.

205. Merkel PA, Simonson DC, Amiel SA, Plewe G, Sherwin RS, Pearson HA, et al. Insulin resistance and hyperinsulinemia in patients with thalassemia major treated by hypertransfusion. N Engl J Med. 1988 Mar 31;318(13):809–14.

206. Cavallo-Perin P, Pacini G, Cerutti F, Bessone A, Condo C, Sacchetti L, et al. Insulin resistance and hyperinsulinemia in homozygous beta-thalassemia. Metabolism. 1995 Mar;44(3):281–6.

207. Cario H, Holl RW, Debatin K-MM, Kohne E. Insulin sensitivity and beta-cell secretion in thalassaemia major with secondary haemochromatosis: assessment by oral glucose tolerance test. Eur J Pediatr. 2003 Mar;162(3):139–46.

208. Borgna-Pignatti C, Rugolotto S, De Stefano P, Zhao H, Cappellini MD, Del Vecchio GC, et al. Survival and complications in patients with thalassemia major treated with transfusion and deferoxamine. Haematologica. 2004 Oct;89(10):1187–93.

209. Lesbordes-Brion J-C, Viatte L, Bennoun M, Lou D-Q, Ramey G, Houbron C, et al. Targeted disruption of the hepcidin 1 gene results in severe hemochromatosis. Blood. 2006 Aug 15;108(4):1402–5.

210. Viatte L, Lesbordes-Brion J-C, Lou D-Q, Bennoun M, Nicolas G, Kahn A, et al. Deregulation of proteins involved in iron metabolism in hepcidin-deficient mice. Blood. 2005 Jun 15;105(12):4861–4.

211. Jenkitkasemwong S, Wang C-Y, Coffey R, Zhang W, Chan A, Biel T, et al. SLC39A14 Is Required for the Development of Hepatocellular Iron Overload in Murine Models of Hereditary Hemochromatosis. Cell Metab. 2015 Jul 7;22(1):138–50.

212. Festa M, Ricciardelli G, Mele G, Pietropaolo C, Ruffo A, Colonna A. Overexpression of H ferritin and up-regulation of iron regulatory protein genes during differentiation of 3T3-L1 pre-adipocytes. J Biol Chem. 2000 Nov 24;275(47):36708–12.

213. Pinhas-Hamiel O, Newfield RS, Koren I, Agmon A, Lilos P, Phillip M. Greater prevalence of iron deficiency in overweight and obese children and adolescents. Int J Obes Relat Metab Disord J Int Assoc Study Obes. 2003 Mar;27(3):416–8.

214. Cepeda-Lopez AC, Osendarp SJ, Melse-Boonstra A, Aeberli I, Gonzalez-Salazar F, Feskens E, et al. Sharply higher rates of iron deficiency in obese Mexican women and

children are predicted by obesity-related inflammation rather than by differences in dietary iron intake. Am J Clin Nutr. 2011 May;93(5):975–83.

215. Yanoff LB, Menzie CM, Denkinger B, Sebring NG, McHugh T, Remaley AT, et al. Inflammation and iron deficiency in the hypoferremia of obesity. Int J Obes 2005. 2007 Sep;31(9):1412–9.

216. Chung J, Kim MS, Han SN. Diet-induced obesity leads to decreased hepatic iron storage in mice. Nutr Res N Y N. 2011 Dec;31(12):915–21.

217. Orr JS, Kennedy A, Anderson-Baucum EK, Webb CD, Fordahl SC, Erikson KM, et al. Obesity alters adipose tissue macrophage iron content and tissue iron distribution. Diabetes. 2014 Feb;63(2):421–32.

218. Sonnweber T, Ress C, Nairz M, Theurl I, Schroll A, Murphy AT, et al. High-fat diet causes iron deficiency via hepcidin-independent reduction of duodenal iron absorption. J Nutr Biochem. 2012 Dec;23(12):1600–8.

219. Rumberger JM, Peters T Jr, Burrington C, Green A. Transferrin and iron contribute to the lipolytic effect of serum in isolated adipocytes. Diabetes. 2004 Oct;53(10):2535–41.

220. Levi S, Rovida E. The role of iron in mitochondrial function. Biochim Biophys Acta. 2009 Jul;1790(7):629–36.

221. Moreno-Navarrete JM, Ortega F, Moreno M, Ricart W, Fernández-Real JM. Fine-tuned iron availability is essential to achieve optimal adipocyte differentiation and mitochondrial biogenesis. Diabetologia. 2014 Sep;57(9):1957–67.

222. Antuna-Puente B, Feve B, Fellahi S, Bastard J-P. Adipokines: the missing link between insulin resistance and obesity. Diabetes Metab. 2008 Feb;34(1):2–11.

223. Rabe K, Lehrke M, Parhofer KG, Broedl UC. Adipokines and insulin resistance. Mol Med Camb Mass. 2008 Dec;14(11-12):741–51.

224. Ohashi K, Yuasa D, Shibata R, Murohara T, Ouchi N. Adiponectin as a Target in Obesity-related Inflammatory State. Endocr Metab Immune Disord Drug Targets. 2015;15(2):145–50.

225. Gabrielsen JS, Gao Y, Simcox JA, Huang J, Thorup D, Jones D, et al. Adipocyte iron regulates adiponectin and insulin sensitivity. J Clin Invest. 2012 Oct 1;122(10):3529–40.

226. Wlazlo N, van Greevenbroek MMJ, Ferreira I, Jansen EHJM, Feskens EJM, van der Kallen CJH, et al. Iron metabolism is associated with adipocyte insulin resistance and plasma adiponectin: the Cohort on Diabetes and Atherosclerosis Maastricht (CODAM) study. Diabetes Care. 2013 Feb;36(2):309–15.

227. Ku B-J, Kim S-Y, Lee T-Y, Park K-S. Serum ferritin is inversely correlated with serum adiponectin level: population-based cross-sectional study. Dis Markers. 2009;27(6):303–10.

228. Gao Y, Li Z, Gabrielsen JS, Simcox JA, Lee S, Jones D, et al. Adipocyte iron regulates leptin and food intake. J Clin Invest. 2015 Sep;125(9):3681–91.

229. Fernández-Real JM, Moreno JM, Chico B, López-Bermejo A, Ricart W. Circulating visfatin is associated with parameters of iron metabolism in subjects with altered glucose tolerance. Diabetes Care. 2007 Mar;30(3):616–21.

230. Fernández-Real JM, Moreno JM, Ricart W. Circulating Retinol-Binding Protein-4 Concentration Might Reflect Insulin Resistance–Associated Iron Overload. Diabetes. 2008 Jul;57(7):1918–25.

231. Hubler MJ, Peterson KR, Hasty AH. Iron homeostasis: a new job for macrophages in adipose tissue? Trends Endocrinol Metab TEM. 2015 Jan 16;

232. Hansen JB, Tonnesen MF, Madsen AN, Hagedorn PH, Friberg J, Grunnet LG, et al. Divalent metal transporter 1 regulates iron-mediated ROS and pancreatic β cell fate in response to cytokines. Cell Metab. 2012 Oct 3;16(4):449–61.

233. Gorasia DG, Dudek NL, Veith PD, Shankar R, Safavi-Hemami H, Williamson NA, et al. Pancreatic beta cells are highly susceptible to oxidative and ER stresses during the development of diabetes. J Proteome Res. 2015 Feb 6;14(2):688–99.

234. Walter PB, Knutson MD, Paler-Martinez A, Lee S, Xu Y, Viteri FE, et al. Iron deficiency and iron excess damage mitochondria and mitochondrial DNA in rats. Proc Natl Acad Sci U S A. 2002 Feb 19;99(4):2264–9.

235. Ceriello A, Motz E. Is Oxidative Stress the Pathogenic Mechanism Underlying Insulin Resistance, Diabetes, and Cardiovascular Disease? The Common Soil Hypothesis Revisited. Arterioscler Thromb Vasc Biol. 2004 May 1;24(5):816–23.

236. Ponugoti B, Dong G, Graves DT. Role of forkhead transcription factors in diabetes-induced oxidative stress. Exp Diabetes Res. 2012;2012:939751.

237. Montes-Cortes DH, Hicks JJ, Ceballos-Reyes GM, Garcia-Sanchez JR, Medina-Navarro R, Olivares-Corichi IM. Chemical and functional changes of human insulin by in vitro incubation with blood from diabetic patients in oxidative stress. Metabolism. 2010 Jul;59(7):935–42.

238. Tiedge M, Lortz S, Drinkgern J, Lenzen S. Relation between antioxidant enzyme gene expression and antioxidative defense status of insulin-producing cells. Diabetes. 1997 Nov;46(11):1733–42.

239. Sakai K, Matsumoto K, Nishikawa T, Suefuji M, Nakamaru K, Hirashima Y, et al. Mitochondrial reactive oxygen species reduce insulin secretion by pancreatic beta-cells. Biochem Biophys Res Commun. 2003 Jan 3;300(1):216–22.

240. Drews G, Krippeit-Drews P, Düfer M. Oxidative stress and beta-cell dysfunction. Pflugers Arch. 2010 Sep;460(4):703–18.

241. Semenza GL. Hypoxia-inducible factors in physiology and medicine. Cell. 2012 Feb 3;148(3):399–408.

242. Cheng K, Ho K, Stokes R, Scott C, Lau SM, Hawthorne WJ, et al. Hypoxia-inducible factor-1alpha regulates beta cell function in mouse and human islets. J Clin Invest. 2010 Jun 1;120(6):2171–83.

243. Aragonés J, Fraisl P, Baes M, Carmeliet P. Oxygen sensors at the crossroad of metabolism. Cell Metab. 2009 Jan 7;9(1):11–22.

244. Dongiovanni P, Valenti L, Ludovica Fracanzani A, Gatti S, Cairo G, Fargion S. Iron depletion by deferoxamine up-regulates glucose uptake and insulin signaling in hepatoma cells and in rat liver. Am J Pathol. 2008 Mar;172(3):738–47.

245. Huang J, Simcox J, Mitchell TC, Jones D, Cox J, Luo B, et al. Iron regulates glucose homeostasis in liver and muscle via AMP-activated protein kinase in mice. FASEB J Off Publ Fed Am Soc Exp Biol. 2013 Jul;27(7):2845–54.

246. Huang J, Gabrielsen JS, Cooksey RC, Luo B, Boros LG, Jones DL, et al. Increased glucose disposal and AMP-dependent kinase signaling in a mouse model of hemochromatosis. J Biol Chem. 2007 Dec 28;282(52):37501–7.

247. Henderson SA, Dallman PR, Brooks GA. Glucose turnover and oxidation are increased in the iron-deficient anemic rat. Am J Physiol. 1986 Apr;250(4 Pt 1):E414–21.

248. Borel MJ, Beard JL, Farrell PA. Hepatic glucose production and insulin sensitivity and responsiveness in iron-deficient anemic rats. Am J Physiol. 1993 Mar;264(3 Pt 1):E380–90.

249. Pietrangelo A. Hereditary hemochromatosis--a new look at an old disease. N Engl J Med. 2004 Jun 3;350(23):2383–97.

250. Berry MN, Friend DS. High-yield preparation of isolated rat liver parenchymal cells: a biochemical and fine structural study. J Cell Biol. 1969 Dec;43(3):506–20.

251. Zhang W, Sargis RM, Volden PA, Carmean CM, Sun XJ, Brady MJ. PCB 126 and other dioxin-like PCBs specifically suppress hepatic PEPCK expression via the aryl hydrocarbon receptor. PloS One. 2012;7(5):e37103.

252. Zhang W. Primary Mouse Hepatocytes [Internet]. [cited 2017 Dec 17]. Available from: http://www.mouselivercells.com/

253. Silva-Gomes S, Santos AG, Caldas C, Silva CM, Neves JV, Lopes J, et al. Transcription factor NRF2 protects mice against dietary iron-induced liver injury by preventing hepatocytic cell death. J Hepatol. 2014 Feb;60(2):354–61.

254. Mosmann T. Rapid colorimetric assay for cellular growth and survival: application to proliferation and cytotoxicity assays. J Immunol Methods. 1983 Dec 16;65(1-2):55–63.

255. Galluzzi L, Aaronson S, Abrams J, Alnemri E, Andrews D, Baehrecke E, et al. Guidelines for the use and interpretation of assays for monitoring cell death in higher eukaryotes. Cell Death Differ. 2009 Aug;16(8):1093–107.

256. Cabantchik ZI. Labile iron in cells and body fluids: physiology, pathology, and pharmacology. Front Pharmacol. 2014;5:45.

257. Desjardins P, Conklin D. NanoDrop Microvolume Quantitation of Nucleic Acids. J Vis Exp JoVE [Internet]. 2010 Nov 22;(45). Available from: https://www.ncbi.nlm.nih.gov/pmc/articles/PMC3346308/

258. Agarose Gel Electrophoresis of RNA [Internet]. [cited 2017 Dec 17]. Available from: https://www.thermofisher.com/in/en/home/references/protocols/nucleic-acid-purification-and-analysis/rna-protocol/agarose-gel-electrophoresis-of-rna.html

259. Torrance JD, Bothwell TH. A simple technique for measuring storage iron concentrations in formalinised liver samples. S Afr J Med Sci. 1968 Apr;33(1):9–11.

260. Sarbassov DD, Guertin DA, Ali SM, Sabatini DM. Phosphorylation and regulation of Akt/PKB by the rictor-mTOR complex. Science. 2005 Feb 18;307(5712):1098–101.

261. Horike N, Sakoda H, Kushiyama A, Ono H, Fujishiro M, Kamata H, et al. AMP-activated protein kinase activation increases phosphorylation of glycogen synthase kinase 3beta and thereby reduces cAMP-responsive element transcriptional activity and phosphoenolpyruvate carboxykinase C gene expression in the liver. J Biol Chem. 2008 Dec 5;283(49):33902–10.

262. Horton JD, Goldstein JL, Brown MS. SREBPs: activators of the complete program of cholesterol and fatty acid synthesis in the liver. J Clin Invest. 2002 May;109(9):1125–31.

263. Li Y, Xu S, Mihaylova MM, Zheng B, Hou X, Jiang B, et al. AMPK phosphorylates and inhibits SREBP activity to attenuate hepatic steatosis and atherosclerosis in diet-induced insulin-resistant mice. Cell Metab. 2011 Apr 6;13(4):376–88.

264. Ide T, Shimano H, Yahagi N, Matsuzaka T, Nakakuki M, Yamamoto T, et al. SREBPs suppress IRS-2-mediated insulin signalling in the liver. Nat Cell Biol. 2004 Apr;6(4):351–7.

265. Seamon KB, Daly JW. Forskolin: its biological and chemical properties. Adv Cyclic Nucleotide Protein Phosphorylation Res. 1986;20:1–150.

266. Guinez C, Filhoulaud G, Rayah-Benhamed F, Marmier S, Dubuquoy C, Dentin R, et al. O-GlcNAcylation Increases ChREBP Protein Content and Transcriptional Activity in the Liver. Diabetes. 2011 May 1;60(5):1399–413.

267. Patitucci C, Couchy G, Bagattin A, Cañeque T, de Reyniès A, Scoazec J-Y, et al. Hepatocyte nuclear factor 1α suppresses steatosis-associated liver cancer by inhibiting PPARγ transcription. J Clin Invest. 2017 May 1;127(5):1873–88.

268. Baker E, Baker SM, Morgan EH. Characterisation of non-transferrin-bound iron (ferric citrate) uptake by rat hepatocytes in culture. Biochim Biophys Acta. 1998 Mar 12;1380(1):21–30.

269. Evans RW, Rafique R, Zarea A, Rapisarda C, Cammack R, Evans PJ, et al. Nature of non-transferrin-bound iron: studies on iron citrate complexes and thalassemic sera. J Biol Inorg Chem JBIC Publ Soc Biol Inorg Chem. 2008 Jan;13(1):57–74.

270. Chopra I, Li HF, Wang H, Webster KA. Phosphorylation of the insulin receptor by AMP-activated protein kinase (AMPK) promotes ligand-independent activation of the insulin signalling pathway in rodent muscle. Diabetologia. 2012 Mar;55(3):783–94.

271. Zheng T, Yang X, Wu D, Xing S, Bian F, Li W, et al. Salidroside ameliorates insulin resistance through activation of a mitochondria-associated AMPK/PI3K/Akt/GSK3β pathway. Br J Pharmacol. 2015 Jul;172(13):3284–301.

272. Nakae J, Kitamura T, Silver DL, Accili D. The forkhead transcription factor Foxo1 (Fkhr) confers insulin sensitivity onto glucose-6-phosphatase expression. J Clin Invest. 2001 Nov 1;108(9):1359–67.

273. Schmoll D, Walker KS, Alessi DR, Grempler R, Burchell A, Guo S, et al. Regulation of glucose-6-phosphatase gene expression by protein kinase Balpha and the forkhead transcription factor FKHR. Evidence for insulin response unit-dependent and -independent effects of insulin on promoter activity. J Biol Chem. 2000 Nov 17;275(46):36324–33.

274. Lee HJ, Choi JS, Lee HJ, Kim W-H, Park SI, Song J. Effect of excess iron on oxidative stress and gluconeogenesis through hepcidin during mitochondrial dysfunction. J Nutr Biochem. 2015 Dec;26(12):1414–23.

275. Aguirre V, Werner ED, Giraud J, Lee YH, Shoelson SE, White MF. Phosphorylation of Ser307 in insulin receptor substrate-1 blocks interactions with the insulin receptor and inhibits insulin action. J Biol Chem. 2002 Jan 11;277(2):1531–7.

276. Aguirre V, Uchida T, Yenush L, Davis R, White MF. The c-Jun NH(2)-terminal kinase promotes insulin resistance during association with insulin receptor substrate-1 and phosphorylation of Ser(307). J Biol Chem. 2000 Mar 24;275(12):9047–54.

277. Carlson CJ, White MF, Rondinone CM. Mammalian target of rapamycin regulates IRS-1 serine 307 phosphorylation. Biochem Biophys Res Commun. 2004 Apr 2;316(2):533–9.

278. Qiao L-Y, Zhande R, Jetton TL, Zhou G, Sun XJ. In vivo phosphorylation of insulin receptor substrate 1 at serine 789 by a novel serine kinase in insulin-resistant rodents. J Biol Chem. 2002 Jul 19;277(29):26530–9.

279. Matsui T, Nagoshi T, Hong E-G, Luptak I, Hartil K, Li L, et al. Effects of chronic Akt activation on glucose uptake in the heart. Am J Physiol Endocrinol Metab. 2006 May;290(5):E789–97.

280. Ni YG, Wang N, Cao DJ, Sachan N, Morris DJ, Gerard RD, et al. FoxO transcription factors activate Akt and attenuate insulin signaling in heart by inhibiting protein phosphatases. Proc Natl Acad Sci U S A. 2007 Dec 18;104(51):20517–22.

281. Messner DJ, Rhieu BH, Kowdley KV. Iron overload causes oxidative stress and impaired insulin signaling in AML-12 hepatocytes. Dig Dis Sci. 2013 Jul;58(7):1899–908.

282. Haap M, Fritsche A, Mensing HJ, Häring H-U, Stumvoll M. Association of high serum ferritin concentration with glucose intolerance and insulin resistance in healthy people. Ann Intern Med. 2003 Nov 18;139(10):869–71.

283. Acton RT, Barton JC, Passmore LV, Adams PC, Speechley MR, Dawkins FW, et al. Relationships of serum ferritin, transferrin saturation, and HFE mutations and self-reported diabetes in the Hemochromatosis and Iron Overload Screening (HEIRS) study. Diabetes Care. 2006 Sep;29(9):2084–9.

284. Forouhi NG, Harding AH, Allison M, Sandhu MS, Welch A, Luben R, et al. Elevated serum ferritin levels predict new-onset type 2 diabetes: results from the EPIC-Norfolk prospective study. Diabetologia. 2007 May;50(5):949–56.

285. Baynes R, Bezwoda W, Bothwell T, Khan Q, Mansoor N. The non-immune inflammatory response: serial changes in plasma iron, iron-binding capacity, lactoferrin, ferritin and C-reactive protein. Scand J Clin Lab Invest. 1986 Nov;46(7):695–704.

286. Brailsford S, Lunec J, Winyard P, Blake DR. A possible role for ferritin during inflammation. Free Radic Res Commun. 1985;1(2):101–9.

287. Dandona P, Aljada A, Bandyopadhyay A. Inflammation: the link between insulin resistance, obesity and diabetes. Trends Immunol. 2004 Jan;25(1):4–7.

288. Corradini E, Meynard D, Wu Q, Chen S, Ventura P, Pietrangelo A, et al. Serum and liver iron differently regulate the bone morphogenetic protein 6 (BMP6)-SMAD signaling pathway in mice. Hepatol Baltim Md. 2011 Jul;54(1):273–84.

289. Gao J, Chen J, Kramer M, Tsukamoto H, Zhang A-S, Enns CA. Interaction of the hereditary hemochromatosis protein HFE with transferrin receptor 2 is required for transferrin-induced hepcidin expression. Cell Metab. 2009 Mar;9(3):217–27.

290. Chung J, Kim MS, Han SN. Diet-induced obesity leads to decreased hepatic iron storage in mice. Nutr Res N Y N. 2011 Dec;31(12):915–21.

291. Park CY, Chung J, Koo K-O, Kim MS, Han SN. Hepatic iron storage is related to body adiposity and hepatic inflammation. Nutr Metab. 2017;14:14.

292. Orr JS, Kennedy A, Anderson-Baucum EK, Webb CD, Fordahl SC, Erikson KM, et al. Obesity alters adipose tissue macrophage iron content and tissue iron distribution. Diabetes. 2014 Feb;63(2):421–32.

293. Rosen ED, Spiegelman BM. Adipocytes as regulators of energy balance and glucose homeostasis. Nature. 2006 Dec 14;444(7121):847–53.

294. Reilly SM, Saltiel AR. Adapting to obesity with adipose tissue inflammation. Nat Rev Endocrinol. 2017 Nov;13(11):633–43.

295. Winzell MS, Ahrén B. The high-fat diet-fed mouse: a model for studying mechanisms and treatment of impaired glucose tolerance and type 2 diabetes. Diabetes. 2004 Dec;53 Suppl 3:S215–9.

296. OpenSource Diets - Stock Diets - DIO Series Diets - Research Diets, Inc [Internet]. [cited 2017 Oct 20]. Available from: http://www.researchdiets.com/opensource-diets/stock-diets/dio-series-diets

297. Diets [Internet]. SAFE DIETS. [cited 2017 Nov 3]. Available from: http://www.safe-diets.com/en/products/diets/

298. Andrikopoulos S, Blair AR, Deluca N, Fam BC, Proietto J. Evaluating the glucose tolerance test in mice. Am J Physiol Endocrinol Metab. 2008 Dec;295(6):E1323–32.

299. Ayala JE, Samuel VT, Morton GJ, Obici S, Croniger CM, Shulman GI, et al. Standard operating procedures for describing and performing metabolic tests of glucose homeostasis in mice. Dis Model Mech. 2010 Oct;3(9-10):525–34.

300. Romero-Calvo I, Ocón B, Martínez-Moya P, Suárez MD, Zarzuelo A, Martínez-Augustin O, et al. Reversible Ponceau staining as a loading control alternative to actin in Western blots. Anal Biochem. 2010 Jun 15;401(2):318–20.

301. Kohyama M, Ise W, Edelson BT, Wilker PR, Hildner K, Mejia C, et al. Role for Spi-C in the development of red pulp macrophages and splenic iron homeostasis. Nature. 2009 Jan 15;457(7227):318–21.

302. Varghese J, James JV, Sagi S, Chakraborty S, Sukumaran A, Ramakrishna B, et al. Decreased hepatic iron in response to alcohol may contribute to alcohol-induced suppression of hepcidin. Br J Nutr. 2016 Jun;115(11):1978–86.

303. Pitman JL, Bonnet DJ, Curtiss LK, Gekakis N. Reduced cholesterol and triglycerides in mice with a mutation in Mia2, a liver protein that localizes to ER exit sites. J Lipid Res. 2011 Oct;52(10):1775–86.

304. Sanyal AJ, American Gastroenterological Association. AGA technical review on nonalcoholic fatty liver disease. Gastroenterology. 2002 Nov;123(5):1705–25.

305. Sarvas JL, Otis JS, Khaper N, Lees SJ. Voluntary physical activity prevents insulin resistance in a tissue specific manner. Physiol Rep. 2015 Feb 1;3(2).

306. Matsumoto M, Ogawa W, Teshigawara K, Inoue H, Miyake K, Sakaue H, et al. Role of the insulin receptor substrate 1 and phosphatidylinositol 3-kinase signaling pathway in insulin-induced expression of sterol regulatory element binding protein 1c and glucokinase genes in rat hepatocytes. Diabetes. 2002 Jun;51(6):1672–80.

307. Chu DT, Stumpo DJ, Blackshear PJ, Granner DK. The inhibition of phosphoenolpyruvate carboxykinase (guanosine triphosphate) gene expression by insulin is not mediated by protein kinase C. Mol Endocrinol Baltim Md. 1987 Jan;1(1):53–9.

308. Yoon JC, Puigserver P, Chen G, Donovan J, Wu Z, Rhee J, et al. Control of hepatic gluconeogenesis through the transcriptional coactivator PGC-1. Nature. 2001 Sep 13;413(6852):131–8.

309. Collins S, Martin TL, Surwit RS, Robidoux J. Genetic vulnerability to diet-induced obesity in the C57BL/6J mouse: physiological and molecular characteristics. Physiol Behav. 2004 Apr;81(2):243–8.

310. Petro AE, Cotter J, Cooper DA, Peters JC, Surwit SJ, Surwit RS. Fat, carbohydrate, and calories in the development of diabetes and obesity in the C57BL/6J mouse. Metabolism. 2004 Apr;53(4):454–7.

311. Rossmeisl M, Rim JS, Koza RA, Kozak LP. Variation in type 2 diabetes--related traits in mouse strains susceptible to diet-induced obesity. Diabetes. 2003 Aug;52(8):1958–66.

312. Lee YS, Li P, Huh JY, Hwang IJ, Lu M, Kim JI, et al. Inflammation is necessary for long-term but not short-term high-fat diet-induced insulin resistance. Diabetes. 2011 Oct;60(10):2474–83.

313. Kraegen EW, Clark PW, Jenkins AB, Daley EA, Chisholm DJ, Storlien LH. Development of muscle insulin resistance after liver insulin resistance in high-fat-fed rats. Diabetes. 1991 Nov;40(11):1397–403.

314. Park S-Y, Cho Y-R, Kim H-J, Higashimori T, Danton C, Lee M-K, et al. Unraveling the temporal pattern of diet-induced insulin resistance in individual organs and cardiac dysfunction in C57BL/6 mice. Diabetes. 2005 Dec;54(12):3530–40.

315. Samuel VT, Liu Z-X, Qu X, Elder BD, Bilz S, Befroy D, et al. Mechanism of hepatic insulin resistance in non-alcoholic fatty liver disease. J Biol Chem. 2004 Jul 30;279(31):32345–53.

316. Turner N, Kowalski GM, Leslie SJ, Risis S, Yang C, Lee-Young RS, et al. Distinct patterns of tissue-specific lipid accumulation during the induction of insulin resistance in mice by high-fat feeding. Diabetologia. 2013 Jul;56(7):1638–48.

317. van Beek L, van Klinken JB, Pronk ACM, van Dam AD, Dirven E, Rensen PCN, et al. The limited storage capacity of gonadal adipose tissue directs the development of metabolic disorders in male C57Bl/6J mice. Diabetologia. 2015 Jul;58(7):1601–9.

318. Itani SI, Ruderman NB, Schmieder F, Boden G. Lipid-induced insulin resistance in human muscle is associated with changes in diacylglycerol, protein kinase C, and IkappaB-alpha. Diabetes. 2002 Jul;51(7):2005–11.

319. Schmitz-Peiffer C, Craig DL, Biden TJ. Ceramide generation is sufficient to account for the inhibition of the insulin-stimulated PKB pathway in C2C12 skeletal muscle cells pretreated with palmitate. J Biol Chem. 1999 Aug 20;274(34):24202–10.

320. Bruce CR, Risis S, Babb JR, Yang C, Kowalski GM, Selathurai A, et al. Overexpression of sphingosine kinase 1 prevents ceramide accumulation and ameliorates muscle insulin resistance in high-fat diet-fed mice. Diabetes. 2012 Dec;61(12):3148–55.

321. Meng R, Zhu D, Bi Y, Yang D, Wang Y. Erythropoietin Inhibits Gluconeogenesis and Inflammation in the Liver and Improves Glucose Intolerance in High-Fat Diet-Fed Mice. PLOS ONE. 2013 Jan 10;8(1):e53557.

322. Guo T, Jou W, Chanturiya T, Portas J, Gavrilova O, McPherron AC. Myostatin inhibition in muscle, but not adipose tissue, decreases fat mass and improves insulin sensitivity. PloS One. 2009;4(3):e4937.

323. Fu T, Seok S, Choi S, Huang Z, Suino-Powell K, Xu HE, et al. MicroRNA 34a inhibits beige and brown fat formation in obesity in part by suppressing adipocyte fibroblast growth factor 21 signaling and SIRT1 function. Mol Cell Biol. 2014 Nov 15;34(22):4130–42.

324. Chartoumpekis DV, Ziros PG, Psyrogiannis AI, Papavassiliou AG, Kyriazopoulou VE, Sykiotis GP, et al. Nrf2 Represses FGF21 During Long-Term High-Fat Diet–Induced Obesity in Mice. Diabetes. 2011 Oct 1;60(10):2465–73.

325. Sajan MP, Standaert ML, Nimal S, Varanasi U, Pastoor T, Mastorides S, et al. The critical role of atypical protein kinase C in activating hepatic SREBP-1c and NFkappaB in obesity. J Lipid Res. 2009 Jun;50(6):1133–45.

326. Xu J, Lloyd DJ, Hale C, Stanislaus S, Chen M, Sivits G, et al. Fibroblast Growth Factor 21 Reverses Hepatic Steatosis, Increases Energy Expenditure, and Improves Insulin Sensitivity in Diet-Induced Obese Mice. Diabetes. 2009 Jan 1;58(1):250–9.

327. Puigserver P, Rhee J, Donovan J, Walkey CJ, Yoon JC, Oriente F, et al. Insulin-regulated hepatic gluconeogenesis through FOXO1–PGC-1α interaction. Nature. 2003 May 29;423(6939):550–5.

328. Kersten S. Mechanisms of nutritional and hormonal regulation of lipogenesis. EMBO Rep. 2001 Apr 15;2(4):282.

329. Ahmed U, Latham PS, Oates PS. Interactions between hepatic iron and lipid metabolism with possible relevance to steatohepatitis. World J Gastroenterol WJG. 2012 Sep 14;18(34):4651–8.

330. Fujita N, Takei Y. Iron overload in nonalcoholic steatohepatitis. Adv Clin Chem. 2011;55:105–32.

331. Czaja MJ. Function of Autophagy in Nonalcoholic Fatty Liver Disease. Dig Dis Sci. 2016 May;61(5):1304–13.

332. Latunde-Dada GO. Ferroptosis: Role of lipid peroxidation, iron and ferritinophagy. Biochim Biophys Acta. 2017;1861(8):1893–900.

333. Sumida Y, Niki E, Naito Y, Yoshikawa T. Involvement of free radicals and oxidative stress in NAFLD/NASH. Free Radic Res. 2013 Nov;47(11):869–80.

334. Matsuzawa-Nagata N, Takamura T, Ando H, Nakamura S, Kurita S, Misu H, et al. Increased oxidative stress precedes the onset of high-fat diet-induced insulin resistance and obesity. Metabolism. 2008 Aug;57(8):1071–7.

335. Torti FM, Torti SV. Regulation of ferritin genes and protein. Blood. 2002 May 15;99(10):3505–16.

336. Altamura S, Kopf S, Schmidt J, Müdder K, da Silva AR, Nawroth P, et al. Uncoupled iron homeostasis in type 2 diabetes mellitus. J Mol Med Berl Ger. 2017 Oct 3;

337. Wahedi M, Wortham AW, Kleven MD, Zhao N, Jue S, Enns CA, et al. Matriptase-2 Suppresses Hepcidin Expression by Cleaving Multiple Components of the Hepcidin Induction Pathway. J Biol Chem. 2017 Sep 18;

338. Zhang A-S, Anderson SA, Wang J, Yang F, DeMaster K, Ahmed R, et al. Suppression of hepatic hepcidin expression in response to acute iron deprivation is associated with an increase of matriptase-2 protein. Blood. 2011 Feb 3;117(5):1687–99.

339. Zhao N, Nizzi CP, Anderson SA, Wang J, Ueno A, Tsukamoto H, et al. Low intracellular iron increases the stability of matriptase-2. J Biol Chem. 2015 Feb 13;290(7):4432–46.

340. Robb A, Wessling-Resnick M. Regulation of transferrin receptor 2 protein levels by transferrin. Blood. 2004 Dec 15;104(13):4294–9.

341. van der Heijden RA, Sheedfar F, Morrison MC, Hommelberg PPH, Kor D, Kloosterhuis NJ, et al. High-fat diet induced obesity primes inflammation in adipose tissue prior to liver in C57BL/6j mice. Aging. 2015 Apr;7(4):256–68.

342. Wang H, Li H, Jiang X, Shi W, Shen Z, Li M. Hepcidin is directly regulated by insulin and plays an important role in iron overload in streptozotocin-induced diabetic rats. Diabetes. 2014 May;63(5):1506–18.

343. Pasricha S-R, Lim PJ, Duarte TL, Casu C, Oosterhuis D, Mleczko-Sanecka K, et al. Hepcidin is regulated by promoter-associated histone acetylation and HDAC3. Nat Commun. 2017 Sep 1;8(1):403.

344. Duval C, Thissen U, Keshtkar S, Accart B, Stienstra R, Boekschoten MV, et al. Adipose tissue dysfunction signals progression of hepatic steatosis towards nonalcoholic steatohepatitis in C57BL/6 mice. Diabetes. 2010 Dec;59(12):3181–91.

345. Mottillo EP, Balasubramanian P, Lee Y-H, Weng C, Kershaw EE, Granneman JG. Coupling of lipolysis and de novo lipogenesis in brown, beige, and white adipose tissues during chronic β3-adrenergic receptor activation. J Lipid Res. 2014 Nov;55(11):2276–86.

346. Schoiswohl G, Stefanovic-Racic M, Menke MN, Wills RC, Surlow BA, Basantani MK, et al. Impact of Reduced ATGL-Mediated Adipocyte Lipolysis on Obesity-Associated Insulin Resistance and Inflammation in Male Mice. Endocrinology. 2015 Oct;156(10):3610–24.

347. Bertinato J, Aroche C, Plouffe LJ, Lee M, Murtaza Z, Kenney L, et al. Diet-induced obese rats have higher iron requirements and are more vulnerable to iron deficiency. Eur J Nutr. 2014 Apr;53(3):885–95.

348. Fernández-Real JM, Blasco G, Puig J, Moreno M, Xifra G, Sánchez-Gonzalez J, et al. Adipose tissue R2* signal is increased in subjects with obesity: A preliminary MRI study. Obes Silver Spring Md. 2016 Feb;24(2):352–8.

349. Moreno-Navarrete JM, Novelle MG, Catalán V, Ortega F, Moreno M, Gomez-Ambrosi J, et al. Insulin resistance modulates iron-related proteins in adipose tissue. Diabetes Care. 2014 Apr;37(4):1092–100.

350. Ma X, Pham VT, Mori H, MacDougald OA, Shah YM, Bodary PF. Iron elevation and adipose tissue remodeling in the epididymal depot of a mouse model of polygenic obesity. PloS One. 2017;12(6):e0179889.

351. Canonne-Hergaux F, Donovan A, Delaby C, Wang H, Gros P. Comparative studies of duodenal and macrophage ferroportin proteins. Am J Physiol Gastrointest Liver Physiol. 2006 Jan;290(1):G156–63.

352. Li Y, Booth GR, Feng Q, Fleming RE. Hypoferremia of Fasting in Mice Is Associated with Increased Hepcidin and Decreased Erythroferrone Expression. Blood. 2014 Dec 6;124(21):4026–4026.

353. Paulson RF, Shi L, Wu D-C. Stress erythropoiesis: new signals and new stress progenitor cells. Curr Opin Hematol. 2011 May;18(3):139–45.

354. Gregory CJ, Eaves AC. Three stages of erythropoietic progenitor cell differentiation distinguished by a number of physical and biologic properties. Blood. 1978 Mar;51(3):527–37.

355. Chen K, Liu J, Heck S, Chasis JA, An X, Mohandas N. Resolving the distinct stages in erythroid differentiation based on dynamic changes in membrane protein expression during erythropoiesis. Proc Natl Acad Sci U S A. 2009 Oct 13;106(41):17413–8.

356. Liu J, Zhang J, Ginzburg Y, Li H, Xue F, De Franceschi L, et al. Quantitative analysis of murine terminal erythroid differentiation in vivo: novel method to study normal and disordered erythropoiesis. Blood. 2013 Feb 21;121(8):e43–9.

357. Griffiths RE, Kupzig S, Cogan N, Mankelow TJ, Betin VMS, Trakarnsanga K, et al. The ins and outs of human reticulocyte maturation. Autophagy. 2012 Jul 1;8(7):1150–1.

358. Chiabrando D, Mercurio S, Tolosano E. Heme and erythropoieis: more than a structural role. Haematologica. 2014 Jun;99(6):973–83.

359. Finch C. Regulators of iron balance in humans. Blood. 1994 Sep 15;84(6):1697–702.

360. Barbieri M, Ragno E, Benvenuti E, Zito GA, Corsi A, Ferrucci L, et al. New aspects of the insulin resistance syndrome: impact on haematological parameters. Diabetologia. 2001 Oct;44(10):1232–7.

361. Tulloch-Reid MK, Hanson RL, Saremi A, Looker HC, Williams DE, Krakoff J, et al. Hematocrit and the incidence of type 2 diabetes in the pima indians. Diabetes Care. 2004 Sep;27(9):2245–6.

362. Nebeck K, Gelaye B, Lemma S, Berhane Y, Bekele T, Khali A, et al. Hematological parameters and metabolic syndrome: findings from an occupational cohort in Ethiopia. Diabetes Metab Syndr. 2012 Mar;6(1):22–7.

363. Kawamoto R, Tabara Y, Kohara K, Miki T, Kusunoki T, Abe M, et al. Hematological parameters are associated with metabolic syndrome in Japanese community-dwelling persons. Endocrine. 2013 Apr;43(2):334–41.

364. Lohsoonthorn V, Jiamjarasrungsi W, Williams MA. Association of Hematological Parameters with Clustered Components of Metabolic Syndrome among Professional and Office Workers in Bangkok, Thailand. Diabetes Metab Syndr. 2007 Sep;1(3):143–9.

365. Wang Y-Y, Lin S-Y, Liu P-H, Cheung BMH, Lai W-A. Association between hematological parameters and metabolic syndrome components in a Chinese population. J Diabetes Complications. 2004 Dec;18(6):322–7.

366. Choi KM, Lee J, Kim YH, Kim KB, Kim DL, Kim SG, et al. Relation between insulin resistance and hematological parameters in elderly Koreans-Southwest Seoul (SWS) Study. Diabetes Res Clin Pract. 2003 Jun;60(3):205–12.

367. Kim SH, Reaven GM. Insulin Resistance and Hyperinsulinemia. Diabetes Care. 2008 Jul;31(7):1433–8.

368. Aoki I, Taniyama M, Toyama K, Homori M, Ishikawa K. Stimulatory effect of human insulin on erythroid progenitors (CFU-E and BFU-E) in human CD34+ separated bone marrow cells and the relationship between insulin and erythropoietin. Stem Cells Dayt Ohio. 1994 May;12(3):329–38.

369. Ratajczak J, Zhang Q, Pertusini E, Wojczyk BS, Wasik MA, Ratajczak MZ. The role of insulin (INS) and insulin-like growth factor-I (IGF-I) in regulating human erythropoiesis. Studies in vitro under serum-free conditions--comparison to other cytokines and growth factors. Leukemia. 1998 Mar;12(3):371–81.

370. Sawada K, Krantz SB, Dessypris EN, Koury ST, Sawyer ST. Human colony-forming units-erythroid do not require accessory cells, but do require direct interaction with insulin-like growth factor I and/or insulin for erythroid development. J Clin Invest. 1989 May;83(5):1701–9.

371. Grigorescu F, White MF, Kahn CR. Insulin binding and insulin-dependent phosphorylation of the insulin receptor solubilized from human erythrocytes. J Biol Chem. 1983 Nov 25;258(22):13708–16.

372. Wang LM, Myers MG, Sun XJ, Aaronson SA, White M, Pierce JH. IRS-1: essential for insulin- and IL-4-stimulated mitogenesis in hematopoietic cells. Science. 1993 Sep 17;261(5128):1591–4.

373. Trottier MD, Naaz A, Li Y, Fraker PJ. Enhancement of hematopoiesis and lymphopoiesis in diet-induced obese mice. Proc Natl Acad Sci U S A. 2012 May 15;109(20):7622–9.

374. Doucette CR, Horowitz MC, Berry R, MacDougald OA, Anunciado-Koza R, Koza RA, et al. A High Fat Diet Increases Bone Marrow Adipose Tissue (MAT) But Does Not Alter Trabecular or Cortical Bone Mass in C57BL/6J Mice. J Cell Physiol. 2015 Sep;230(9):2032–7.

375. Yue R, Zhou BO, Shimada IS, Zhao Z, Morrison SJ. Leptin Receptor Promotes Adipogenesis and Reduces Osteogenesis by Regulating Mesenchymal Stromal Cells in Adult Bone Marrow. Cell Stem Cell. 2016 Jun 2;18(6):782–96.

376. Scheller EL, Cawthorn WP, Burr AA, Horowitz MC, MacDougald OA. Marrow Adipose Tissue: Trimming the Fat. Trends Endocrinol Metab TEM. 2016 Jun;27(6):392–403.

377. Naveiras O, Nardi V, Wenzel PL, Hauschka PV, Fahey F, Daley GQ. Bone-marrow adipocytes as negative regulators of the haematopoietic microenvironment. Nature. 2009 Jul 9;460(7252):259–63.

378. Libregts SF, Gutiérrez L, de Bruin AM, Wensveen FM, Papadopoulos P, van Ijcken W, et al. Chronic IFN-γ production in mice induces anemia by reducing erythrocyte life span and inhibiting erythropoiesis through an IRF-1/PU.1 axis. Blood. 2011 Sep 1;118(9):2578–88.

379. Prince OD, Langdon JM, Layman AJ, Prince IC, Sabogal M, Mak HH, et al. Late stage erythroid precursor production is impaired in mice with chronic inflammation. Haematologica. 2012 Nov;97(11):1648–56.

380. Koulnis M, Pop R, Porpiglia E, Shearstone JR, Hidalgo D, Socolovsky M. Identification and analysis of mouse erythroid progenitors using the CD71/TER119 flow-cytometric assay. J Vis Exp JoVE. 2011;(54).

381. Liu Y, Pop R, Sadegh C, Brugnara C, Haase VH, Socolovsky M. Suppression of Fas-FasL coexpression by erythropoietin mediates erythroblast expansion during the erythropoietic stress response in vivo. Blood. 2006 Jul 1;108(1):123–33.

382. Kina T, Ikuta K, Takayama E, Wada K, Majumdar AS, Weissman IL, et al. The monoclonal antibody TER-119 recognizes a molecule associated with glycophorin A and specifically marks the late stages of murine erythroid lineage. Br J Haematol. 2000 May;109(2):280–7.

383. Ogawa M, Matsuzaki Y, Nishikawa S, Hayashi S, Kunisada T, Sudo T, et al. Expression and function of c-kit in hemopoietic progenitor cells. J Exp Med. 1991 Jul 1;174(1):63–71.

384. Drabkin DL, Austin JH. Spectrophotometric Studies I. Spectrophotometric Constants for Common Hemoglobin Derivatives in Human, Dog, and Rabbit Blood. J Biol Chem. 1932 Nov 1;98(2):719–33.

385. Beutler E. Red cell metabolism: a manual of biochemical methods. Grune & Stratton; 1971. 166 p.

386. Itano HA, Fogarty WM, Alford WC. The molar extinction coefficient of cyanmethemoglobin as determined by carbon analysis. Am J Clin Pathol. 1971 Feb;55(2):135–40.

387. Iacopetta BJ, Morgan EH, Yeoh GC. Transferrin receptors and iron uptake during erythroid cell development. Biochim Biophys Acta. 1982 May 7;687(2):204–10.

388. Socolovsky M, Nam H, Fleming MD, Haase VH, Brugnara C, Lodish HF. Ineffective erythropoiesis in Stat5a(-/-)5b(-/-) mice due to decreased survival of early erythroblasts. Blood. 2001 Dec 1;98(12):3261–73.

389. Aruffo A, Stamenkovic I, Melnick M, Underhill CB, Seed B. CD44 is the principal cell surface receptor for hyaluronate. Cell. 1990 Jun 29;61(7):1303–13.

390. Keel SB, Doty R, Liu L, Nemeth E, Cherian S, Ganz T, et al. Evidence that the expression of transferrin receptor 1 on erythroid marrow cells mediates hepcidin suppression in the liver. Exp Hematol. 2015 Jun;43(6):469–78.e6.

391. Forejtnikovà H, Vieillevoye M, Zermati Y, Lambert M, Pellegrino RM, Guihard S, et al. Transferrin receptor 2 is a component of the erythropoietin receptor complex and is required for efficient erythropoiesis. Blood [Internet]. 2010 Sep 8 [cited 2010 Oct 5]; Available from: http://www.ncbi.nlm.nih.gov/pubmed/20826723

392. Seldin MM, Peterson JM, Byerly MS, Wei Z, Wong GW. Myonectin (CTRP15), a novel myokine that links skeletal muscle to systemic lipid homeostasis. J Biol Chem. 2012 Apr 6;287(15):11968–80.

393. Mankelow TJ, Griffiths RE, Trompeter S, Flatt JF, Cogan NM, Massey EJ, et al. The ins and outs of reticulocyte maturation revisited: The role of autophagy in sickle cell disease. Autophagy. 2016 Apr 5;12(3):590–1.

394. Waugh RE. Reticulocyte rigidity and passage through endothelial-like pores. Blood. 1991 Dec 1;78(11):3037–42.

395. Chasis JA, Prenant M, Leung A, Mohandas N. Membrane assembly and remodeling during reticulocyte maturation. Blood. 1989 Aug 15;74(3):1112–20.

396. Leblond PF, Lacelle PL, Weed RI. Cellular Deformability: A Possible Determinant of the Normal Release of Maturing Erythrocytes From the Bone Marrow. Blood. 1971 Jan 1;37(1):40–6.

397. McMillan DE, Utterback NG, La Puma J. Reduced erythrocyte deformability in diabetes. Diabetes. 1978 Sep;27(9):895–901.

398. Engström KG, Grankvist K, Täljedal IB. Insulin-driven erythropoiesis may underlie impairment of erythrocyte deformability in hyperinsulinaemic, hyperglycaemic ob/ob-mice. Diabetologia. 1990 Mar;33(3):127–30.

399. Linderkamp O, Ruef P, Zilow EP, Hoffmann GF. Impaired deformability of erythrocytes and neutrophils in children with newly diagnosed insulin-dependent diabetes mellitus. Diabetologia. 1999 Jun 1;42(7):865–9.

400. Unruh D, Srinivasan R, Benson T, Haigh S, Coyle D, Batra N, et al. Red Blood Cell Dysfunction Induced by High-Fat Diet. Circulation. 2015 Nov 17;132(20):1898–908.

401. Schwartz RS, Madsen JW, Rybicki AC, Nagel RL. Oxidation of Spectrin and Deformability Defects in Diabetic Erythrocytes. Diabetes. 1991 Jun 1;40(6):701–8.

402. Sailaja YR, Baskar R, Srinivas Rao CS, Saralakumari D. Membrane lipids and protein-bound carbohydrates status during the maturation of reticulocytes to erythrocytes in type 2 diabetics. Clin Chim Acta. 2004 Mar 1;341(1):185–92.

403. Chung HK, Ryu D, Kim KS, Chang JY, Kim YK, Yi H-S, et al. Growth differentiation factor 15 is a myomitokine governing systemic energy homeostasis. J Cell Biol. 2017 Jan 2;216(1):149–65.

404. Rapisarda C, Puppi J, Hughes RD, Dhawan A, Farnaud S, Evans RW, et al. Transferrin receptor 2 is crucial for iron sensing in human hepatocytes. Am J Physiol Gastrointest Liver Physiol. 2010 Sep;299(3):G778–83.

405. Nai A, Lidonnici MR, Rausa M, Mandelli G, Pagani A, Silvestri L, et al. The second transferrin receptor regulates red blood cell production in mice. Blood. 2015 Feb 12;125(7):1170–9.

406. Forouhi NG, Harding AH, Allison M, Sandhu MS, Welch A, Luben R, et al. Elevated serum ferritin levels predict new-onset type 2 diabetes: results from the EPIC-Norfolk prospective study. Diabetologia. 2007 May;50(5):949–56.

407. Pechlaner R, Weiss G, Bansal S, Mayr M, Santer P, Pallhuber B, et al. Inadequate hepcidin serum concentrations predict incident type 2 diabetes mellitus. Diabetes Metab Res Rev. 2016 Feb;32(2):187–92.

408. Kim I, Yetley EA, Calvo MS. Variations in iron-status measures during the menstrual cycle. Am J Clin Nutr. 1993 Nov;58(5):705–9.

409. Harvey LJ, Armah CN, Dainty JR, Foxall RJ, John Lewis D, Langford NJ, et al. Impact of menstrual blood loss and diet on iron deficiency among women in the UK. Br J Nutr. 2005 Oct;94(4):557–64.

410. Lee E, Choi HS, Hwang JH, Hoh JK, Cho Y-H, Baek EJ. The RNA in reticulocytes is not just debris: it is necessary for the final stages of erythrocyte formation. Blood Cells Mol Dis. 2014 Aug;53(1-2):1–10.

411. American Diabetes Association. (2) Classification and diagnosis of diabetes. Diabetes Care. 2015 Jan;38 Suppl:S8–16.

412. Matthews DR, Hosker JP, Rudenski AS, Naylor BA, Treacher DF, Turner RC. Homeostasis model assessment: insulin resistance and beta-cell function from fasting plasma glucose and insulin concentrations in man. Diabetologia. 1985 Jul;28(7):412–9.

413. Pal S, Nemeth MJ, Bodine D, Miller JL, Svaren J, Thein SL, et al. Neurokinin-B transcription in erythroid cells: direct activation by the hematopoietic transcription factor GATA-1. J Biol Chem. 2004 Jul 23;279(30):31348–56.

414. Silver N, Best S, Jiang J, Thein SL. Selection of housekeeping genes for gene expression studies in human reticulocytes using real-time PCR. BMC Mol Biol. 2006;7:33.

415. Pearson TA, Mensah GA, Alexander RW, Anderson JL, Cannon RO, Criqui M, et al. Markers of inflammation and cardiovascular disease: application to clinical and public health practice: A statement for healthcare professionals from the Centers for Disease Control and Prevention and the American Heart Association. Circulation. 2003 Jan 28;107(3):499–511.

416. Burtis CA, Ashwood ER, Bruns DE. Tietz Textbook of Clinical Chemistry and Molecular Diagnostics - E-Book. Elsevier Health Sciences; 2012. 2259 p.

417. Ganz T. Hepcidin, a key regulator of iron metabolism and mediator of anemia of inflammation. Blood. 2003 Aug 1;102(3):783–8.

418. Nicolas G, Chauvet C, Viatte L, Danan JL, Bigard X, Devaux I, et al. The gene encoding the iron regulatory peptide hepcidin is regulated by anemia, hypoxia, and inflammation. J Clin Invest. 2002 Oct;110(7):1037–44.

419. Moreno-Navarrete JM, Blasco G, Xifra G, Karczewska-Kupczewska M, Stefanowicz M, Matulewicz N, et al. Obesity Is Associated With Gene Expression and Imaging Markers of Iron Accumulation in Skeletal Muscle. J Clin Endocrinol Metab. 2016 Mar;101(3):1282–9.

420. Guglielmi V, D'Adamo M, Bellia A, Ciotto RT, Federici M, Lauro D, et al. Iron status in obesity: An independent association with metabolic parameters and effect of weight loss. Nutr Metab Cardiovasc Dis NMCD. 2015 Jun;25(6):541–7.

421. Nikonorov AA, Skalnaya MG, Tinkov AA, Skalny AV. Mutual interaction between iron homeostasis and obesity pathogenesis. J Trace Elem Med Biol Organ Soc Miner Trace Elem GMS. 2015 Apr;30:207–14.

422. WHO | Haemoglobin concentrations for the diagnosis of anaemia and assessment of severity [Internet]. WHO. [cited 2017 Dec 14]. Available from: http://www.who.int/vmnis/indicators/haemoglobin/en/

423. WHO | Obesity [Internet]. [cited 2015 Jun 27]. Available from: http://www.who.int/gho/ncd/risk_factors/obesity_text/en/

424. Kasuga M. Insulin resistance and pancreatic β cell failure. J Clin Invest. 2006 Jul 3;116(7):1756–60.

425. Unnikrishnan R, Pradeepa R, Joshi SR, Mohan V. Type 2 Diabetes: Demystifying the Global Epidemic. Diabetes. 2017 Jun 1;66(6):1432–42.

426. Ikehara S, Tabák AG, Akbaraly TN, Hulmán A, Kivimäki M, Forouhi NG, et al. Age trajectories of glycaemic traits in non-diabetic South Asian and white individuals: the Whitehall II cohort study. Diabetologia. 2015 Mar;58(3):534–42.

427. Jainandunsing S, Özcan B, Rietveld T, van Miert JNI, Isaacs AJ, Langendonk JG, et al. Failing beta-cell adaptation in South Asian families with a high risk of type 2 diabetes. Acta Diabetol. 2015 Feb;52(1):11–9.

428. Narayan KMV. Type 2 Diabetes: Why We Are Winning the Battle but Losing the War? 2015 Kelly West Award Lecture. Diabetes Care. 2016;39(5):653–63.

429. Staimez LR, Weber MB, Ranjani H, Ali MK, Echouffo-Tcheugui JB, Phillips LS, et al. Evidence of reduced β-cell function in Asian Indians with mild dysglycemia. Diabetes Care. 2013 Sep;36(9):2772–8.

430. Søgaard KL, Ellervik C, Svensson J, Thorsen SU. The Role of Iron in Type 1 Diabetes Etiology: A Systematic Review of New Evidence on a Long-Standing Mystery. Rev Diabet Stud RDS. 2017 Summer-Fall;14(2-3):269–78.

431. Lipschitz DA, Cook JD, Finch CA. A clinical evaluation of serum ferritin as an index of iron stores. N Engl J Med. 1974 May 30;290(22):1213–6.

432. Wang W, Knovich MA, Coffman LG, Torti FM, Torti SV. Serum ferritin: Past, present and future. Biochim Biophys Acta. 2010 Aug;1800(8):760–9.

433. Bekri S, Gual P, Anty R, Luciani N, Dahman M, Ramesh B, et al. Increased adipose tissue expression of hepcidin in severe obesity is independent from diabetes and NASH. Gastroenterology. 2006 Sep;131(3):788–96.

434. Zheng X, Jiang T, Wu H, Zhu D, Wang L, Qi R, et al. Hepatic iron stores are increased as assessed by magnetic resonance imaging in a Chinese population with altered glucose homeostasis. Am J Clin Nutr. 2011 Oct;94(4):1012–9.

11. APPENDIX

APPENDIX I

Minimum Information for Publication of Quantitative Real-Time PCR Experiments (MIQE) checklist

Item to check	Importance*	Response
EXPERIMENTAL DESIGN		
Definition of experimental and control groups	E	Details provided in methods section of each study.
Number within each group	E	Details provided in methods section of each study.
Assay carried out by core lab or investigator's lab?	D	All assays were carried out in the investigators' lab
SAMPLE		
Description	E	Details provided in methods section of each study.
Volume/mass of sample processed	D	Details provided in methods section of each study.
Microdissection or macrodissection	E	Not applicable
Processing procedure	E	Details provided in methods section of each study.
If frozen - how and how quickly?	E	All samples were snap-frozen in liquid nitrogen and immediately transferred to a -70°C freezer
If fixed - with what, how quickly?	E	Not applicable
Sample storage conditions and duration (especially for FFPE samples)	E	All samples were stored at - 70°C until processed for RNA isolation
NUCLEIC ACID EXTRACTION		
Procedure and/or instrumentation	E	Guanidinium thiocyanate-phenol-chloroform extraction method using Tri-reagent (Sigma)
Name of kit and details of any modifications	E	Not applicable
Source of additional reagents used	D	Chloroform and isopropanol used for RNA isolation were of molecular biology grade obtained from Sigma.

Details of DNase or RNAse treatment	E	DNAase treatment using the Ambion TURBO DNA-free kit was done.
Contamination assessment (DNA or RNA)	E	All samples were run on 1% agarose gel to look for DNA contamination and RNA integrity.
Nucleic acid quantification	E	Done using a NanoDrop spectrophotometer
Instrument and method	E	NanoDrop2000c from Thermo Fischer
Purity (A260/A280)	D	A260/A280 for all samples were > 1.80
RNA integrity method/instrument	E	All samples were run on a 1% agarose gel. Only those samples that showed clear and distinct bands corresponding to 18s and 28s rRNA were used for cDNA construction
RIN/RQI or Cq of 3' and 5' transcripts	E	Not done
REVERSE TRANSCRIPTION		
Complete reaction conditions	E	Reaction buffer containing 5mM MgCl2, 500µM dNTPs, 2.5µM random nonamers, 0.4U/µL RNAase inhibitor, 1.25U/µL reverse transcriptase (final concentration)
Amount of RNA and reaction volume	E	One microgram of total RNA was added to a total volume of 20µL
Priming oligonucleotide (if using GSP) and concentration	E	Oligo dT 2.5µM (final conc.)
Reverse transcriptase and concentration	E	Moloney Murine leukemia virus reverse transcriptase 1.25U/µL (final conc.)
Temperature and time	E	25°C for 10 min, 48°C for 30 min, 95°C for 5 min
Manufacturer of reagents and catalogue numbers	D	Reverse Transcriptase Core kit from Eurogentec, Belgium (Catalogue no. RT-RTCK-05)
Storage conditions of cDNA	D	-20°C
qPCR TARGET INFORMATION		
If multiplex, efficiency and LOD of each assay	E	Not applicable
Sequence accession number	D	Information provided in methodology section of each study.
Amplicon length	E	Information provided in methodology section of each study
In silico specificity screen (BLAST, etc)	E	Primer BLAST (http://www.ncbi.nlm.nih.gov/tools/primer-blast/) was used to check the specificity of each primer-pair used.

Pseudogenes, retropseudogenes or other homologs?	D	No
Location of each primer by exon or intron (if applicable)	E	Not applicable
What splice variants are targeted?	E	Primers were designed to amplify all splice variants of the target genes
qPCR OLIGONUCLEOTIDES		
Primer sequences	E	Information provided in methodology section of each study.
RTPrimerDB Identification Number	D	Not applicable
Probe sequences	D	Not applicable
Location and identity of any modifications	E	Not applicable
Manufacturer of oligonucleotides	D	Sigma, India
qPCR PROTOCOL		
Reaction volume and amount of cDNA/DNA	E	10 µL reaction volume containing 2 µL cDNA diluted 1:10
Primer, (probe), Mg++ and dNTP concentrations	E	Final concentrations were: Primer: 250nM Mg^{2+} : 2.5mM dNTPs: not specified by the kit manufacturer
Polymerase identity and concentration	E	Takyon™ DNA polymerase (concentration not specified by the kit manufacturer)
Buffer/kit identity and manufacturer	E	Takyon™ No Rox SYBR MasterMix dTTP Blue (Catalogue number: UF-NSMT-B0701)
Exact chemical constitution of the buffer	D	Information not provided by the kit manufacturer
Additives (SYBR Green I, DMSO, etc.)	E	Not applicable
Manufacturer of plates/tubes and catalog number	D	96-well plates from Axygen Scientific (catalogue number: PCR-96-FS-C)
Complete thermocycling parameters	E	95°C for 5 min, followed by 40 cycles of 95°C for 10 sec and 60°C for 60 sec)
Reaction setup (manual/robotic)	D	Manual
Manufacturer of qPCR instrument	E	BioRad Chromo4 real-time PCR machine

qPCR VALIDATION		
Specificity (gel, sequence, melt, or digest)	E	Melt curve analysis was done for all PCR runs for all the genes. Single peaks were detected. No primer dimers were seen in any of reaction wells.
For SYBR Green I, Cq of the NTC	E	Information provided in Appendix II
Standard curves with slope and y-intercept	E	Information provided in Appendix II
PCR efficiency calculated from slope	E	Information provided in Appendix II
r2 of standard curve	E	Information provided in Appendix II
Linear dynamic range	E	Information provided in Appendix II
Cq variation at lower limit	E	Information provided in Appendix II
If multiplex, efficiency and LOD of each assay.	E	Not applicable
DATA ANALYSIS		
qPCR analysis program (source, version)	E	MJ Opticon Monitor Analysis Software Version 3.1 (BioRad)
Cq method determination	E	Manual
Outlier identification and disposition	E	Not applicable
Results of NTCs	E	Information provided in Appendix II
Justification of number and choice of reference genes	E	The reference gene used was RPL19. The choice was based on previous publications which have used RPL19 as the reference gene.
Description of normalisation method	E	The delta Ct method was used for normalization
Number and stage (RT or qPCR) of technical replicates	E	All reactions were conducted in duplicate when qPCR was carried out.
Repeatability (intra-assay variation)	E	Average of Cq values for duplicates was taken for calculation. Runs were repeated in samples where the Cq SD exceeded 0.2
Statistical methods for result significance	E	The Kruskal Wallis test was used to detect statistically significant changes occurring in the different groups of mice. Mann Whitney test was used for all pair-wise comparisons.
Software (source, version)	E	SPSS version 16.0

* E – essential, D - desirable

APPENDIX II

QUANTITATIVE POLYMERASE CHAIN REACTION (qPCR) VALIDATION DATA

Sl. No	Gene	Standard curve slope	R^2 of standard curve	Linear dynamic range (cDNA dilution)	Standard deviation of Ct at lower limit of dynamic range	Primer dimer (melting curve analysis)	Ct of amplification (if any) in the NTC
Mouse							
1	*Fasn*	-3.061	0.998	1:5 to 1:625	0.14	In NTC	32
2	*Pck1*	-3.677	0.998	1:5 to 1:625	0.14	None	-
3	*Irs1*	-3.435	0.993	1:5 to 1:625	0.09	In NTC	36
4	*Irs2*	-3.149	0.999	1:5 to 1:625	0.11	In NTC	38
5	*Tfrc*	-3.689	0.999	1:5 to 1:625	0.06	None	-
6	*Hamp1*	-3.332	0.996	1:5 to 1:625	0.16	None	-
7	*Gck1*	-3.668	0.999	1:5 to 1:625	0.13	None	-
8	*Slc40a1*	-3.485	0.998	1:5 to 1:625	0.01	None	-
9	*G6pc*	-3.397	0.999	1:10 to 1:10000	0.49	In NTC	33
10	*FtL*	-3.631	0.997	1:5 to 1:625	0.05	In NTC	36
11	*Rpl19*	-3.638	0.997	1:5 to 1:625	0.26	In NTC	32

Sl. No	Gene	Standard curve slope	R^2 of standard curve	Linear dynamic range (cDNA dilution)	Standard deviation of Ct at lower limit of dynamic range	Primer dimer (melting curve analysis)	Ct of amplification (if any) in the NTC
12	*Acaca*	-3.158	0.998	1:10 to 1:10000	0.02	In NTC	31
13	*Bmp6*	-3.155	0.997	1:10 to 1:10000	0.02	In NTC	35
14	*Tmprss6*	-3.609	0.996	1:5 to 1:3125	0.1	None	-
15	*Tfr2*	-3.541	0.997	1:10 - 1:10000	0.02	None	-
16	*Efre*	-3.229	0.997	1:5 to 1:625	0.1	None	-
17	*Gdf15*	-3.516	0.999	1:5 to 1:625	0.15	In NTC	34
18	*Twsg1*	-3.479	0.997	1:5 to 1:625	0.12	None	-
19	*Ppargc1a*	-3.551	0.999	1:5 to 1:3125	0.07	None	-
20	*Pparg2*	-3.253	0.998	1:5 to 1:625	0.09	In NTC	34
21	*Adipoq*	-3.205	0.999	1:5 to 1:625	0.12	None	-
22	*Pnpla2*	-2.970	1	1:5 to 1:625	0.11	In NTC	36
23	*Lipe*	-3.189	1	1:5 to 1:625	0.04	In NTC	32
24	*Ftl*	-3.631	0.996	1:10 to 1:10000	0.34	None	-
25	*Fth*	-3.722	0.997	1:10 to 1:10000	0.24	None	-

Sl. No	Gene	Standard curve slope	R^2 of standard curve	Linear dynamic range (cDNA dilution)	Standard deviation of Ct at lower limit of dynamic range	Primer dimer (melting curve analysis)	Ct of amplification (if any) in the NTC
Human							
26	*ERFE*	-3.201	0.996	1:1 to 1:125	0.1	None	-
29	*TFRC*	-3.238	0.999	1:5 to 1:625	0.06	None	-
30	*TFR2*	-3.209	0.995	1:5 to 1:625	0.07	None	-
31	*GAPDH*	-3.32	0.996	1:5 to 1:625	0.1	In NTC	35

APPENDIX III - COMPOSITION OF CONTROL DIET (CD) – D12450J

Formula

Product #D12450J		gm%	kcal%
Protein		19.2	20
Carbohydrate		67.3	70
Fat		4.3	10
	Total		100
	kcal/gm	3.85	

Ingredient	gm	kcal
Casein, 30 Mesh	200	800
L-Cystine	3	12
Corn Starch	506.2	2024.8
Maltodextrin 10	125	500
Sucrose	68.8	275.2
Cellulose, BW200	50	0
Soybean Oil	25	225
Lard*	20	180
Mineral Mix S10026	10	0
DiCalcium Phosphate	13	0
Calcium Carbonate	5.5	0
Potassium Citrate, 1 H2O	16.5	0
Vitamin Mix V10001	10	40
Choline Bitartrate	2	0
FD&C Yellow Dye #5	0.04	0
FD&C Blue Dye #1	0.01	0
Total	1055.05	4057

*Typical analysis of cholesterol in lard = 0.72 mg/gram.
Cholesterol (mg)/4057 kcal = 14.4
Cholesterol (mg)/kg = 13.6

Source: http://www.researchdiets.com/opensource-diets/custom-diets/control-diets

APPENDIX IV – COMPOSITION OF HIGH-FAT DIET (HFD) – D12492

Formula

Product #D12492		gm%	kcal%
Protein		26.2	20
Carbohydrate		26.3	20
Fat		34.9	60
	Total		100
	kcal/gm	5.24	

Ingredient	gm	kcal
Casein, 30 Mesh	200	800
L-Cystine	3	12
Corn Starch	0	0
Maltodextrin 10	125	500
Sucrose	68.8	275.2
Cellulose, BW200	50	0
Soybean Oil	25	225
Lard*	245	2205
Mineral Mix S10026	10	0
DiCalcium Phosphate	13	0
Calcium Carbonate	5.5	0
Potassium Citrate, 1 H2O	16.5	0
Vitamin Mix V10001	10	40
Choline Bitartrate	2	0
FD&C Blue Dye #1	0.05	0
Total	**773.85**	**4057**

Formulated by E. A. Ulman, Ph.D., Research Diets, Inc., 8/26/98 and 3/11/99.

*Typical analysis of cholesterol in lard = 0.72 mg/gram.
Cholesterol (mg)/4057 kcal = 216.4
Cholesterol (mg)/kg = 279.6

Source: http://www.researchdiets.com/opensource-diets/stock-diets/dio-series-diets

APPENDIX V

PATIENT INFORMATION SHEET

Title of the study: Why does iron overload associated with insulin resistance occur?

The Department of Biochemistry, in association with the Department of Community Health, is carrying out research to understand changes in the way iron is handled in the body in patients who have diabetes mellitus. Iron levels in the body are often higher than normal in this situation and may worsen the disease. We do not fully understand why iron accumulates in the body in this condition. We would like to study this problem to understand it better. For this, we would like to ask if you would be willing to donate 15 ml of your blood to help us study this. You may not benefit directly from this study. However, if you are willing to allow us to take this sample, it will help us try to understand why iron accumulates in the body in patients with diabetes mellitus and may help improve treatment for the disease.

The blood sample that we request will be used purely for scientific research and any remaining sample will be discarded. The collection of the 15 ml of blood sample will not cause harm to your health in any foreseeable manner. All your personal information obtained by us from you will be kept completely confidential.

If you do not wish to give the blood sample requested, you are free to say so. It will not affect the treatment that you will receive in the hospital.

APPENDIX VI

INFORMED CONSENT

---------- has explained the details of the study proposed and what it involves to me. I have understood what has been said including the following:

1. A sample of blood amounting to 15 ml in quantity will be collected from me.
2. It will not affect my health in any foreseeable manner.
3. The sample will be used to study what happens to the process by which iron is handled in the body in patients with diabetes mellitus. It will be used only for research purposes.

I am willing to donate 15 ml of blood voluntarily and without any coercion from the investigators of this project.

Signature of donor Signature of investigator

Name of Donor

Signature of witness

Date:

In case you have additional queries, please feel free to contact me:

Dr. Joe Varghese
Assistant Professor,
Department of Biochemistry,
Christian Medical College,
Bagayam, Vellore, Tamil Nadu - 632002
INDIA
Phone: +91-416-2284267 (office), +91 – 9843243682 (mobile)
E-mail: joevarghese@cmcvellore.ac.in

APPENDIX VII

PATIENT INFORMATION SHEET (TAMIL)

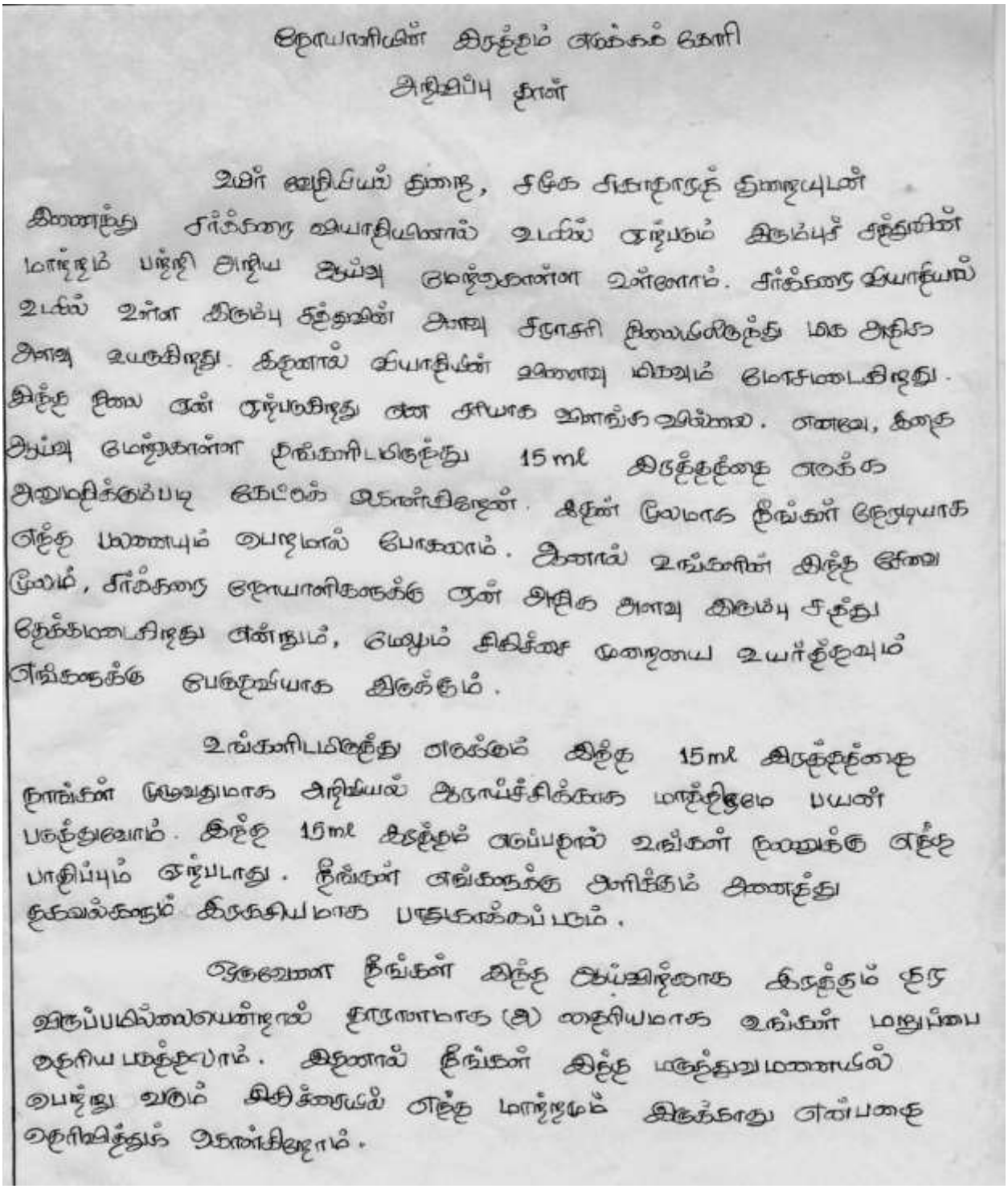

நோயாளியின் இரத்தம் எடுக்கும் கோரி

அறிவிப்பு தாள்

உயிர் வாழியல் துறை, சிறுநீரகவியல் துறையுடன் இணைந்து சர்க்கரை வியாதியினால் உடலில் ஏற்படும் இரும்புச் சத்துவின் மாற்றும் பற்றி அறிய ஆய்வு மேற்கொள்ள உள்ளோம். சர்க்கரை வியாதியால் உடலில் உள்ள இரும்பு சத்துவின் அளவு சீராகச் நிலையிலிருந்து மிக அதிக அளவு உயருகிறது. இதனால் வியாதியின் வீரியமும் மோசமடைகிறது. இந்த நிலை ஏன் ஏற்படுகிறது என சரியாக இனங்கா இல்லை. எனவே, இதை ஆய்வு மேற்கொள்ள நீங்களிடமிருந்து 15 ml இரத்தத்தை எடுக்க அனுமதிக்கும்படி கேட்டுக் கொள்கிறோம். இதன் மூலமாக நீங்கள் நேரடியாக எந்த பலனையும் பெறமால் போகலாம். ஆனால் உங்களின் இந்த இவை மூலம், சர்க்கரை நோயாளிகளுக்கு ஏன் அதிக அளவு இரும்பு சத்து தேங்கமடைகிறது என்றும், மேலும் சிகிச்சை முறையை உயர்த்தவும் எங்களுக்கு பெருதவியாக இருக்கும்.

உங்களிடமிருந்து எடுக்கும் இந்த 15 ml இரத்தத்தை நாங்கள் முழுவதுமாக அறிவியல் ஆராய்ச்சிக்காக மட்டுமே பயன் படுத்துவோம். இந்த 15 ml இரத்தம் எடுப்பதால் உங்கள் உடலுக்கு எந்த பாதிப்பும் ஏற்படாது. நீங்கள் எங்களுக்கு அளித்தும் அனைத்து தகவல்களும் இரகசியமாக பாதுகாக்கப்படும்.

ஒருவேளை நீங்கள் இந்த ஆய்வுக்காக இரத்தம் தர விருப்பமில்லையென்றால் தாராளமாக (அ) தைரியமாக உங்கள் மறுப்பை தெரிய படுத்தலாம். இதனால் நீங்கள் இந்த மருத்துவமனையில் பெற்று வரும் சிகிச்சையில் எந்த மாற்றமும் இருக்காது என்பதை தெரிவித்துக் கொள்கிறோம்.

APPENDIX VIII

INFORMED CONSENT (TAMIL)

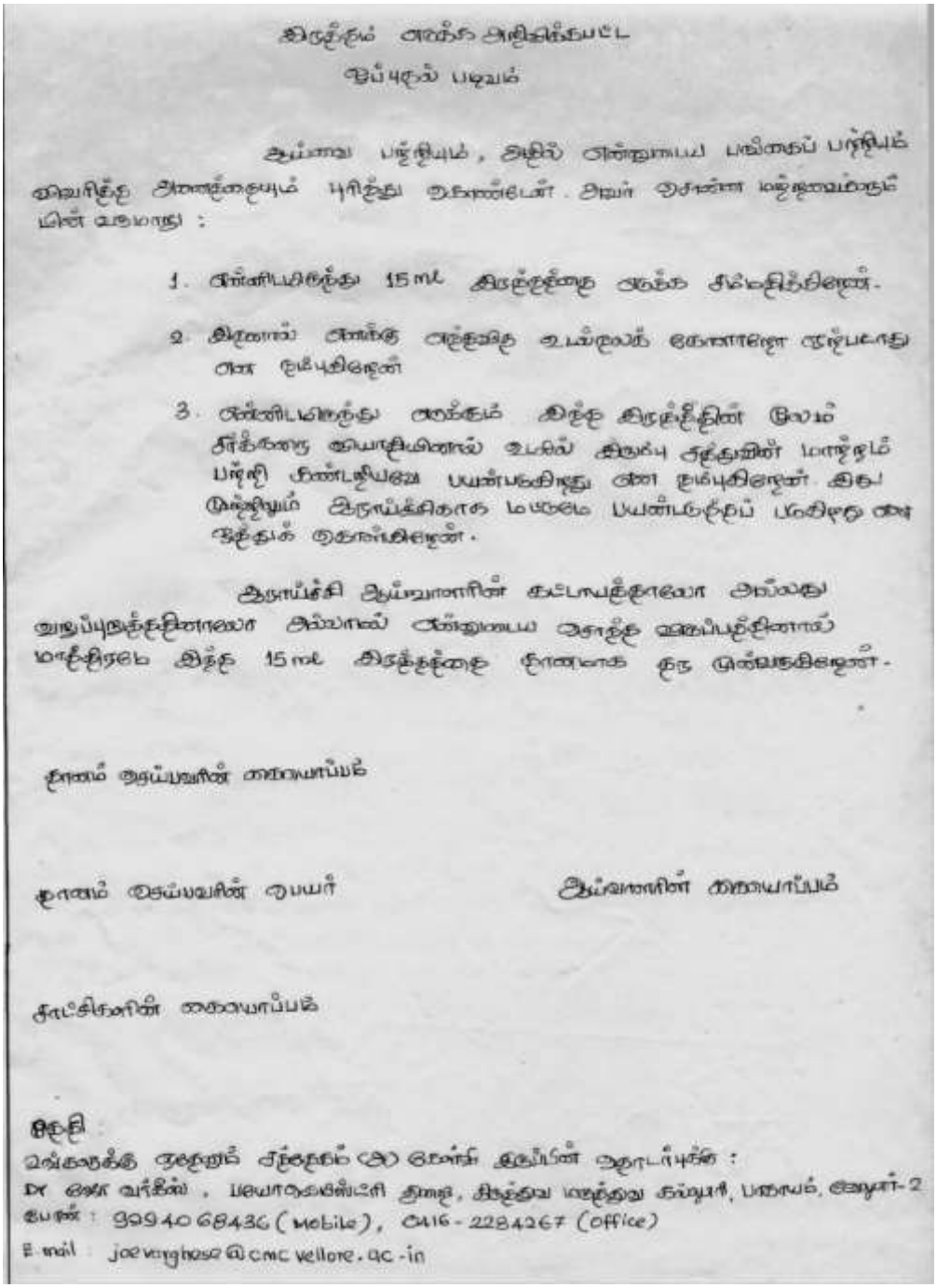

இருதீரும் எனக்கு அளிக்கப்பட்ட

ஒப்புதல் படிவம்

ஆய்வை பற்றியும், அதில் என்னுடைய பங்கைப் பற்றியும் விவரித்து அனைத்தையும் புரிந்து கொண்டேன். அவர் சொன்ன மற்றவைகளும் பின் வருமாறு :

1. என்னிடமிருந்து 15 மி.லி இரத்தத்தை எடுக்க சம்மதித்தேன்.
2. இதனால் எனக்கு ஏற்படுகின்ற உபத்திரவங்கள் ஏதாவது ஏற்படாது என நம்புகிறேன்
3. என்னிடமிருந்து எடுக்கும் இந்த இரத்தத்தின் மூலம் சீர்க்கேடு ஏதேனும் உயிரினால் உடலில் இருப்பு தெரிந்தால் மாதிரி பற்றி கண்டறியவே பயன்படுகிறது என நம்புகிறேன். இது மற்றும் இதனால் எனக்கு மட்டுமே பயன்படுத்தப் படுகிறது என தெரிந்துக் கொள்கிறேன்.

ஆராய்ச்சி ஆய்வாளரின் கட்டாயத்தாலோ அல்லது மிரட்டுதலினாலோ அவ்வாறு என்னுடைய சொந்த விருப்பத்தினால் மனதிருந்தே இந்த 15 மி.லி இரத்தத்தை தானமாக தர முன்வருகிறேன்.

தானம் அளிப்பவரின் கையொப்பம்

தானம் செய்பவரின் பெயர் ஆய்வாளரின் கையொப்பம்

சாட்சிகளின் கையொப்பம்

குறிப்பு :
மேற்கொண்டு ஏதேனும் சந்தேகம் ஏ தொடர்பு இருப்பின் தொடர்புக்கு :
Dr ஜோ வர்கீஸ், பேராசிரியர், நிரந்தர மருத்துவ கல்வியர், பாலாம், வேலூர்-2
தொலை : 99940 68436 (Mobile), 0416-2284267 (office)
E-mail : joevarghese@cmcvellore.ac.in

APPENDIX IX

PROFORMA FOR COLLECTION OF DEMOGRAPHIC AND OTHER DETAILS REGARDING THE PATIENT

Date:

Name				**Age (years)**	
Sex		**Hospital No**		**DOB**	
Address			**Phone Number**		
			Education/ Occupation		

1. **Medical history:**

Reason for current visit/presenting complaint:
History of previous diagnosis of diabetes/prediabetes:

2. **Final diagnosis:**

3. **Family history:**

Diabetes: Hypertension: Any other:

4. **Personal history:**

Diet: Veg/non-veg Alcohol use: Smoking:

Any other:

5. **Clinical examination:**

Acanthosis nigricans: Pallor: BP:

Any other significant finding:

6. **Anthropometric measurements:**

Height: Weight: BMI:

Waist circumference: Hip circumference:

7. Laboratory investigations:

Haemoglobin		CRP		Any other analytes measured as part of clinical management	
Fasting glucose		Post prandial glucose			

12. PUBLICATIONS

Manuscript under review for publication

1. Varghese J, James JV, Vaulont S, Mckie AT, Jacob M. Increased intracellular iron in mouse primary hepatocytes increases basal activation of the Akt pathway but decreases its response to insulin. *Biochimica et Biophysica Acta – General Subjects* (Manuscript under revision)

Manuscripts under preparation

1. Varghese J, James JV, Nellickal AJ, Anand R, Jacob M High-fat feeding-induced insulin resistance in C57Bl/6 mice is associated with reduced hepcidin and liver iron, but elevated adipose tissue iron content. *Manuscript in preparation.*
2. Varghese J, James JV, Jacob M. High-fat feeding-induced insulin resistance does not affect maturation of erythroid precursors in the bone marrow or expression of erythroid regulators of hepcidin in erythroid precursor cells. *Manuscript in preparation*
3. Varghese J, Venkatesan P, James, JV, Jacob M. Iron homeostasis is dysregulated in patient newly diagnosed with diabetes mellitus but not in pre-diabetes. *Manuscript in preparation*

Conference abstracts

Varghese J, Mckie AT, Jacob M. Does Insulin Affect Expression Of Proteins Involved In Iron Homeostasis? Preliminary Results From Hepg2 Cells And Primary Mouse Hepatocytes (2013). *American Journal of Hematology.* 88 (5), E235. (Poster presentation at the Fifth Congress of the International BioIron Society (IBIS) Biennial World Meeting (BioIron 2017) April 14 – 18, 2013 at London, United Kingdom)

Varghese J, McKie AT, Voulont S, Jacob M. Insulin signaling in primary hepatocytes from wild-type and hepcidin knock-out mice. (Oral presentation at European Iron Club Meeting 2014 at Verona, Italy (Sep 12 – 14th, 2014))

Varghese J, James JV, Mckie AT, Jacob M. Insulin Resistance In Diet-induced Obese Mice Is Associated With Dysregulation Of Iron Homeostasis. *American Journal of Hematology*. 91 (3), E104. (Poster presentation at the Sixth Congress of the International BioIron Society (IBIS) Biennial World Meeting (BioIron 2015) Sep 6 – 10, 2015 at Hangzhou, China)

Varghese J, James JV, Jacob M. Diet-induced insulin resistance in mice is associated with decreased levels of liver iron and serum hepcidin. *American Journal of Hematology*. 92 (8), E304-E304 (Poster presentation at the Seventh Congress of the International BioIron Society (IBIS) Biennial World Meeting (BioIron 2017) May 7 – 11, 2017 at Los Angeles, USA)

Jacob M, Venkatesan P, Varghese J James JV, Prasad J. Hepcidin-ferritin ratio is decreased in diabetes mellitus. (Poster presentation at the Seventh Congress of the International BioIron Society (IBIS) Biennial World Meeting (BioIron 2017) May 7 – 11, 2017 at Los Angeles, USA)

Formatting techniques used in preparation of Compact Disc (CD)

- Microsoft Office 2010 software was used to prepare the contents of this CD
- The sources of the figures, when obtained from published literature, have been acknowledged in the figure legends.
- The figures were downloaded from PDF documents and incorporated in to the Microsoft Word (MS Word) document at their appropriate places.
- Images of western blots in the results section were captured using a gel documentation system (Alpha Innotech, USA).
- All figures in the results section were prepared using Microsoft PowerPoint 2010 software and the images were incorporated into the MS Word document.
- References were incorporated into the text using Zotero reference management software.
- After the final formatting of the document was done, the MS Word file was converted to a Portable Document Format (PDF) file using the conversion option available in the MS Word 2010.
- The softcopy of the completed thesis work was copied on compact disc (CD).